ABC MIKTOARM STAR TERPOLYMERS AND THEIR SPHERICAL CAPSULES BEARING PH-RESPONSIVE NANOCHANNELS

by

Heng Hu

A thesis submitted to the Department of Chemistry

In conformity with the requirements for

the degree of Doctor of Philosophy

Queen's University

Kingston, Ontario, Canada

(September, 2014)

Dedicated to my Wife, Daughter and Coming Son.

Abstract

This thesis reports the preparation of several ABC and ABC_x miktoarm star terpolymers using a novel "assembly-and-reaction" strategy. Some of the prepared polymers were used to undergo another level of self-assembly to form vesicles. After chemical derivations, the vesicles were converted to capsules bearing regularly packed nano-scale channels, which were pH-responsive. This thesis is about the "double assembly" of linear block copolymer precursors and "double chemical processing" to yield functional nanostructures

Triblock copolymers containing a short central carboxyl-bearing block and a diblock copolymer containing a short amine-bearing block were synthesized. One triblock and one diblock copolymer precursor was subsequently associated via electrostatic interactions between their amine- and carboxyl-bearing blocks and were covalently linked via amidization to yield ABC miktoarm copolymers. In particular, this "assembly-and-reaction" strategy was used to prepare μ-($PtBA_{100}$)($PSMA_{66/200}$)($PCEMA_{120}$) copolymers, where $PtBA$, $PSMA$, and $PCEMA$ respectively denote poly(*tert*-butyl acrylate), poly(2,2-dimethyl-1,3-dioxolan-4-yl)methyl methacrylate (also called poly(solketal methacrylate)), and poly(2-cinnamoyloxyethyl methacrylate). These copolymers were ideal candidates for functional nanostructures, because all three of their arms could be derivatised. PSMA was hydrophobic but could be hydrolyzed into PGMA (poly(glyceryl methacrylate)), which contained hydroxyl groups and was soluble in water, $PtBA$ could be hydrolyzed into PAA (poly acrylic acid), and PCEMA was photocrosslinkable.

ABC_x miktoarm copolymers were synthesized through the same "assembly and reaction" strategy but using different precursor feed ratios. These copolymers were pseudo-miktoarm structures because two short reactive blocks rather than a traditional trivalent functional group were used to link the long blocks. Moreover, the average number x of diblock copolymer chains

that were attached to each triblock copolymer chain was not 1, but 1.14 and 1.58 for the two μ-(PtBA)(PCEMA)(PEO)$_x$ copolymers that we have prepared. Since only the poly(ethylene oxide) (PEO) block was soluble in a tetrahydrofuran/water mixture containing 80 vol% water, the two μ-(PtBA)(PCEMA)(PEO)$_x$ samples formed vesicles with PtBA and PCEMA as the wall. Using appropriate lengths for the PtBA and PCEMA blocks, we also ensured that PtBA formed cylinders that permeated across the PCEMA wall. Photocrosslinking the PCEMA wall and hydrolyzing the PtBA chains in the cylindrical domains yielded permanent capsules permeated by regularly-packed poly(acrylic acid)-gated nanochannels. These capsules were loaded with various cargoes and exhibited pH-responsive reagent release in water, releasing reagents faster and more completely at higher pH's.

Acknowledgements

I would like to express my special appreciation and thanks to my supervisor Dr. Guojun Liu, you have been a tremendous mentor for me. I would like to thank you for encouraging my research and for allowing me to grow as a research scientist. Your advice on both research as well as on my career have been priceless.

I wish to extend many thanks to Dr. Ian Wyman for proof-reading my thesis and manuscripts. I would also like to thank Dr. Dehui Han and Dr. Liangzhi Hong for teaching me many laboratory techniques, including anionic polymerization and ATRP. I also wish to extend many thanks to Dr. Zhihan Zhou for sharing with me many theories and knowledge.

I have had the privilege to work with the many talented chemists, including post-docs and graduate students that have helped contribute to my development over the years, including: Dr. Hongjing Dou, Dr. Ronghua Zheng, Dr. Gabriel Njikang, Dr. Nan Wang, Dr. Ganwei Zhang, Dr. Muhammad Rabnawaz, Dr. Dean Xiong, Dr. Claudia Grozea, Dr. Xu Wu, Qiliang Peng, Yu Wang, Weijie Jiang, Bolu Peng, Danielle Macoretta, and Prashant Agrawal. I would also like to thank them all. I would like to also express my special appreciation for my lab benchmate John Dupont for sharing with me not only his clean glassware and lab bench, but also for his attention to detail in keeping everything tidy and well organized.

I also would like to express my appreciation for Jian Wang and Dr. Xiaohu Yan for their AFM and TEM technique support. In my mind, Dr. Françoise Sauriol who trained me NMR technique is one of the best people in the world, and is the world's best NMR manager. The work

Last, but certainly not least, I sincerely appreciate the love and support from my wife Tian Fang, my two year old daughter Pan Hu, my parents and my parent-in-law. Tian and Pan are the sunshine of my life and make me feel happy and rich. All of my family's support for me was what sustained me thus far.

Statement of Originality

All the results presented in this thesis, *Synthesis of ABC Miktoarm Star Terpolymers and Their Spherical Capsules Bearing pH-Responsive Nanochannels*, were conducted by the author under the supervision of Professor Guojun Liu. All results are the product of original research.

I hereby certify that all of the work described within this thesis is the original work of the author. Any published (or unpublished) ideas and/or techniques from the work of others are fully acknowledged in accordance with the standard referencing practices.

(Heng Hu)

(June, 2014)

Table of Contents

List of Figures

xiii

List of Schemes

List of Tables

List of Abbreviations

μ	(mu) in Greek, means mikto
μ-(PEO)(PEE)(PFP)	μ-(poly(ethylene oxide))(poly(ethyl ethylene))(poly(perfluoropropylene oxide))
μ-1	μ-(PtBA$_{100}$)(PGMA$_{200}$)(PCEMA$_{120}$)
μ-2	μ-(PtBA$_{100}$)(PSMA$_{66}$)(PCEMA$_{120}$)
μ-AB(CD)	a tri-arm miktoarm polymer containing A, B and (C-b-D) arms
μ-ABCD	a four-arm miktoarm polymer containing one A, one B, one C and one D arms
μL	microlitre
^{1}H NMR	proton nuclear magnetic resonance
A	area of a SEC peak
Å	angstrom (1 Å = 10^{-10} m)
AFM	atomic force microscopy
ATRP	atom transfer radical polymerization
ATRP	atom transfer radical polymerization
-b-	-$block$-
Br	bromide
CaH$_2$	calcium hydride
Cbz or Z	carbobenzyloxyl group
CDCl$_3$	deuterated chloroform
CH$_2$Cl$_2$	dichloromethane
CHCl$_3$	chloroform

CL	ε-caprolactone
CMC	critical micellization concentration
CMPI	2-chloro-1-methylpyridinium iodide
COOH	carboxylic acid group
c_p	total polymer concentration in mg/mL
CuBr	cuprous bromide
$CuBr_2$	cupric bromide
d	day(s)
d	diameter
DCC	N,N'-dicyclohexylcarbodiimide
DCM	dichloromethane
d_h	hydrodynamic diameter
Di	diblock copolymer precursor
DLS	dynamic light scattering
DMAP	4-dimethylaminopyridine
DMF	N,N-dimethylformamide
dn/dc	refractive index increments
DPE	diphenylethylene
EDC(I)	1-ethyl-3-(3-dimethylaminopropyl)carbodiimide
Et_3Al	triethyl aluminium
f	volume fraction
Gly	glycine
GPC	gel permeation chromatography
h	hour(s)

HCl	hydrochloric acid
HEA	hydroxylethyl acrylate
HEA-TMS	trimethylsiloxyethyl acrylate
HEMA	hydroxylethyl methacrylate
HEMA-tBDMS	2-($tert$-butyldimethylsiloxy)ethyl methacrylate
HEMA-TMS	trimethylsiloxyethyl methacrylate
I	intensity
$I(t)$	fluorescence intensity as a function of time
IUPAC	International Union of Pure and Applied Chemistry chemical nomenclature
$I_xS_yP_z$	μ-(polyisoprene)(polystyrene)(poly(2-vinyl-pyridine))
j/k or $m/n/l$	number of repeating units
k	rate constant
L	fully stretched chain length
LiCl	lithium chloride
M	mol/litre
M	mass
MeOH	methanol
mg	milligram(s)
min	minute(s)
mL	millilitre
MMA	methyl methacrylate
M_n	number average molecular weight

M_w	weight average molecular weight
N	number of the C-C bonds in the main chain
nm	nanometer(s)
NMR	nuclear magnetic resonance
NMRP	nitroxide-mediated radical polymerization
OsO_4	osmium tetraoxide
P(HEA-TMS)	poly(trimethylsiloxyethyl acrylate)
P(HEMA-tBDMS)	poly(2-(*tert*-butyldimethylsiloxy)ethyl methacrylate)
P(HEMA-TMS)	poly(trimethylsiloxyethyl methacrylate)
P(NH_2-Cbz)	poly[2-(carbobenzyloxy-glycyl)ethyl methacrylate]
P_2O_5	diphosphorus pentoxide
PAA	poly(acrylic acid)
PB	polybutadiene
PBMA	poly(*n*-butyl methacrylate)
PCL	poly(ε-caprolactone)
PCMEA	poly(2-cinnamoyloxyethyl methacrylate)
PCOOH	succinic acid-labeled stitching block bearing carboxylic acid groups
PDI or M_w/M_n	polydispersity index
PDMAEMA	poly(2-(dimethylamino)ethyl acrylate)
PEO	poly(ethylene oxide)
PEO_{45}-Py	poly(ethylene oxide) with a pyrene end
PEO-Br	poly(ethylene oxide) with a bromide end

PEO-OH	poly(ethylene oxide) with a hydroxyl end
PGMA	poly(glyceryl methacrylate)
PHEA	poly(hydroxylethyl acrylate)
PHEMA	poly(hydroxylethyl methacrylate)
PI	polyisoprene
pI	isoelectric point
pK_a	acid dissociation constant
PMCL	poly(γ-methyl-ε-caprolactone)
PMMA	polymethyl methacrylate
PNH_2	glycine-labeled stitching block bearing amino groups
PS	polystyrene
PSMA	poly(solketal methacrylate)
PtBA	poly(t-butyl acrylate)
Py	pyrene
Pyridine-d_5	fully deuterated pyridine
r.t.	room temperature
R_g	radius of gyration
RI	refractive index
ROP	ring-opening polymerization
RuO_4	ruthenium tetraoxide
s	second(s)
SBS	polystyrene-b-polybutadiene-b-polystyrene
SEC	size exclusion chromatography

SIM	μ-(polystyrene)(polyisoprene)(poly(methyl methacrylate))
SMA	solketal methacrylate
SSSR	superstrong segregation regime
*t*BA	*tert*-butyl acrylate
TBC	triblock copolymer precursor(s)
TEA	triethylamine
TEM	transmission electron microscopy
TFA	trifluoroacetic acid
THF	tetrahydrofuran
Tri	triblock copolymer
TSA	*p*-toluenesulfonic acid monohydrate
UO_2Ac	uranium acetate
UV	ultraviolet
vs.	versus
w	weight fractions
W/2	half-width of a reating domain
Z-glycine	*N*-carbobenzyloxyglycine
γ	relative interfacial tension
μ-(PCL)(PMMA)(PS)	μ-(poly(ε-caprolactone))(poly(methyl methacrylate))(polystyrene)
μ-(PI)(PS)(PBd)	μ-(polyisoprene)(polystyrene)(polybutadiene)
μ-(PS)(PB)(PMMA)	μ-(polystyrene)(polybutadiene)(poly(methyl methacrylate))

xxiii

μ-ABC	a tri-arm miktoarm polymer containing A, B and C arms
μ-ABC$_2$	a four-arm miktoarm polymer containing one A, one B, and two C arms
μ-EOC	μ-poly(ethyl ethylene)(poly(ethylene oxide))(poly(γ-methyl-ε-caprolactone))
μ-E$_x$O$_y$F$_z$	μ-(poly(ethyl ethylene))(poly(ethylene oxide))(poly(perfluoropropylene oxide))
μ-SODA	μ-(polystyrene)(poly(ethylene oxide))(poly(2-(dimethylamino)ethyl acrylate))

Chapter 1

Introduction

The research described in this thesis focuses on the synthesis of ABC and ABC$_x$ miktoarm star terpolymers, and the preparation of nanostructures exhibiting fascinating morphologies from these copolymers via self-assembly in selective solvents. This thesis is written in manuscript format, following the guidelines of Queen's School of Graduate Studies. Chapters 2 and 3 represent two individual manuscripts that have recently been submitted for publication in peer-reviewed journals. Chapter 2 will cover the synthesis of a series of μ-ABC miktoarm star terpolymers by a novel "assembly-and-reaction" method. That chapter will describe factors that affect the yield and can cause mismatching between reagents (side products), along with the optimized conditions for the synthesis and the purification methods. Chapter 3 will describe a modified strategy for the synthesis of μ-ABC$_x$ miktoarm terpolymers and the preparation of pH-responsive capsules. In addition, the loading of an oligomer into these capsules will be described, and the release kinetics at different pH values will be compared. In that chapter, the fluorescence quenching effect between pyrene and CEMA will also be studied. Appendix A-C will cover the preliminary investigations on the self-assembly of the miktoarm polymers reported in Chapter 2, in solution and solid state.

Chapter 1 will provide an introduction to the polymers involved in this thesis as well as the general principles involved in their synthesis and self-assembly. In particular, this chapter will initially provide an introduction to the general structures of linear block copolymers and miktoarm star copolymers, as well as the specific structures of the

1

copolymers described in this thesis. This chapter will describe the general principles that govern linear block copolymer and miktoarm star copolymer self-assembly behavior in bulk and in selective solvents. Finally, this chapter will also describe the strategies involved in the synthesis of miktoarm copolymers.

1.1 Structures of Linear Block Copolymers, Miktoarm Copolymers, and the Copolymers Investigated in this Thesis

Linear block copolymers are copolymers that are formed when more than one monomer cluster together and form 'blocks' of repeating units by sequence. [1] For example, an ABC block copolymer made up of A, B and C monomers that are joined together in the manner shown below:

$$-A-A-A-A-B-B-B-B-C-C-C-C-$$

is a linear block copolymer where A-A-A-A-, -B-B-B-B-, and -C-C-C-C- repeating units correspond to the blocks. As defined by the number of blocks, common examples include diblock, triblock, and tetrablock copolymers, and examples incorporating even more blocks have also been reported. [1]

Miktoarm (μικτός means mixed in Greek) or μ- copolymers are a family of star polymers containing three or more chemically distinct arms that are linked together at one junction point.[2] There have been many types of miktoarm polymers reported, such as $A_m B_n$ ($m + n > 3$), ABC, AB_2C_2, and ABCD copolymers in which "A, B, C and D" denote chemically distinct polymers forming the arms, and "m and n" denote the number of the arm(s) in one miktoarm copolymer molecule. The generic structure of an ABC miktoarm star copolymer is shown in Figure 1.1.

-A-A-A-A-B-B-B-B-
        C
        C
        C
        C-
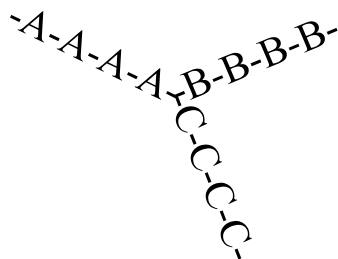
Figure 1.1 Illustration of an ABC miktoarm star terpolymer.

The final forms of all of the linear block copolymer, miktoarm copolymers and of a fluorescent dye-labelled homopolymer described in this thesis are listed in Table 1.1. In addition, the chemical structures of these polymers are provided in Scheme 1.1. Further details on the synthesis of these copolymers are described in Chapters 2 and 3.

Table 1.1 Names of the linear block copolymers, miktoarm copolymers and the fluorescent dye-labeled polymer described in this thesis, as well as their general function.

Sample	Function
P(NH$_2$)$_5$-b-PCEMA$_{120}$ ^{a}	diblock precursor
PEO$_{113}$-b-P(GNH$_2$)$_5$	diblock precursor
PtBA$_{100}$-b-PSCOOH$_5$-b-PSMA$_{200}$	triblock precursor
PtBA$_{100}$-b-PSCOOH$_5$-b-PSMA$_{66}$	triblock precursor
PtBA$_{100}$-b-PSCOOH$_5$-b-PCEMA$_{130}$	triblock precursor
μ-(PtBA$_{100}$)(PSMA$_{66}$)(PCEMA$_{120}$)	miktoarm polymer product
μ-(PtBA$_{100}$)(PGMA$_{200}$)(PCEMA$_{120}$)	miktoarm polymer product
μ-(PtBA$_{100}$)(PCEMA$_{130}$)(PEO$_{113}$)$_{1.14}$ ^{b}	miktoarm polymer product
μ-(PtBA$_{100}$)(PCEMA$_{130}$)(PEO$_{113}$)$_{1.58}$	miktoarm polymer product
PEO$_{45}$-Pyrene	fluorescent dye-labeled polymer for investigating release kinetics

^{a}: The subscripts denote the numbers of repeat units.

^{b}: The number outside of the bracket denotes the average number of PEO chains per mikto-arm copolymer.

P(NH₂)₅-*b*-PCEMA₁₂₀   **PEO₁₁₄-*b*-P(NH₂)₅**   **P*t*BA₁₀₀-*b*-PCOOH₅-*b*-PSMA₂₀₀/₆₆**

PtBA₁₀₀-*b*-PCOOH₅-*b*-PCEMA₁₃₀   **mu-(PtBA₁₀₀)(PCEMA₁₂₀)(PGMA₂₀₀)**

mu-(PtBA₁₀₀)(PCEMA₁₂₀)(PSMA₆₆)   **mu-(PtBA₁₀₀)(PCEMA₁₃₀)(PEO₁₁₄)ₓ**

PEO₄₅-Pyrene
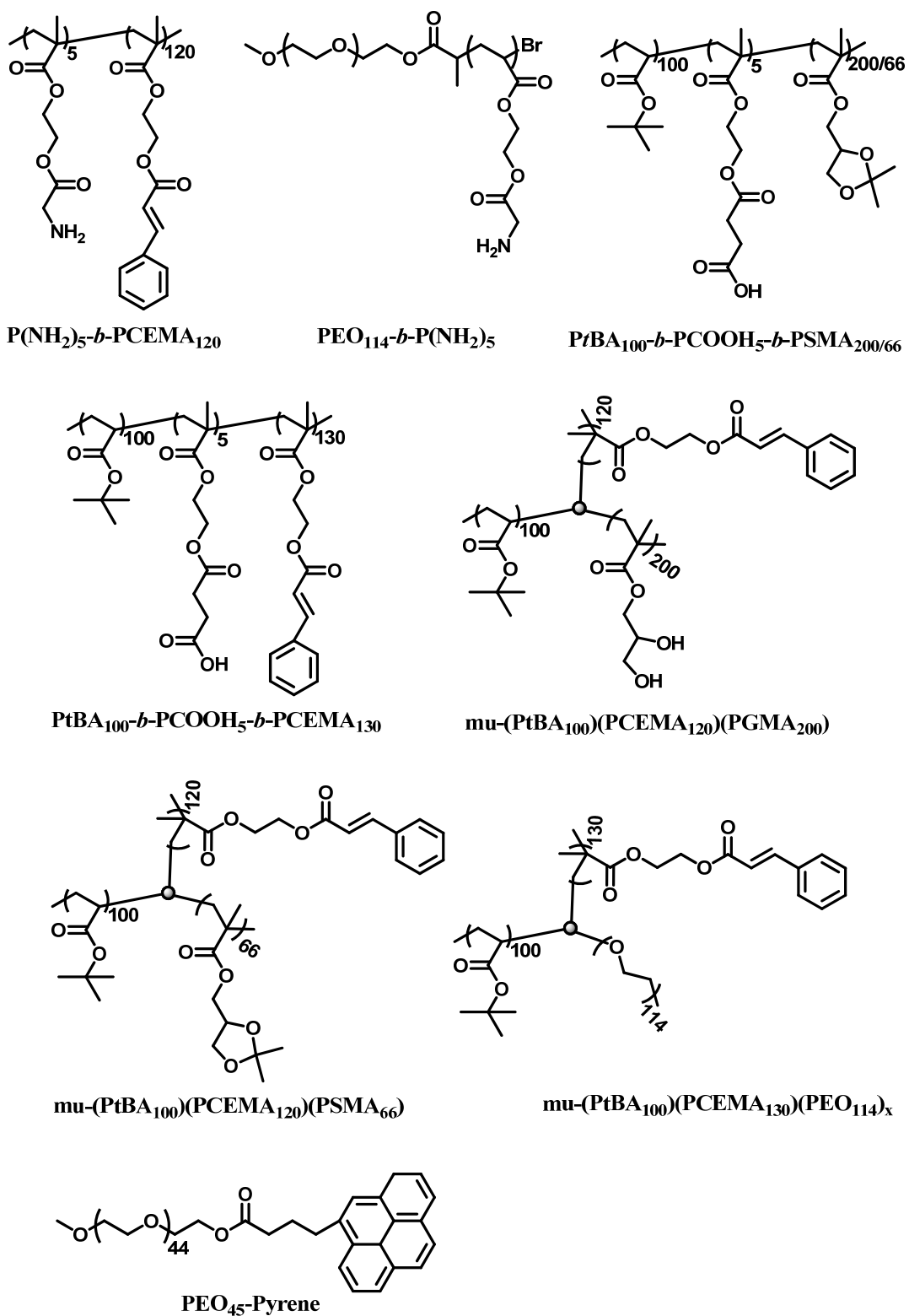
Figure 1.2 Chemical structures of the copolymers listed in Table 1.1.

5

1.2 Self-Assembly of Linear Block Copolymer

1.2.1 Linear Block Copolymers in Bulk

Self-assembly represents one of the key strategies for the fabrication of functional nanostructured materials and is a cornerstone of nanotechnology. The self-assembly of block copolymers has attracted much attention over the past decade. Since most polymers are incompatible with one another, the different blocks of a block copolymer tend to segregate into well-defined morphologies. In the case of a coil-coil diblock copolymer in the bulk state, if one block length is fixed and the length of the other block is varied, a diverse range of morphologies, such as spheres, cylinders, gyroids and lamellae structures may be formed (Figure 1.3).[3, 4] When the volume fraction of one block of a diblock copolymer is ~30%, this block forms a hexagonally-packed phase that is dispersed in the other block, as shown in Figure 1.3b. A-B-A coil-coil-coil triblock copolymers behave in a similar manner as diblock copolymers.
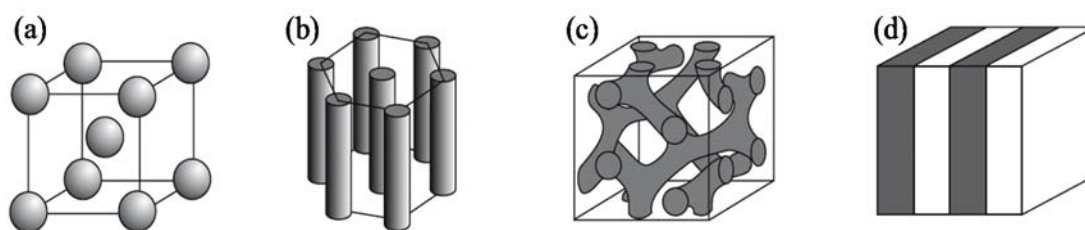
Figure 1.3 Morphologies of AB coil-coil diblock copolymers: (a) $f_A \leq 25\%$ (the A block forms cubic packed spheres), (b) $f_A \approx 30\%$ (the A block forms hexagonally packed cylinders), (c) $f_A \approx 38\%$ (the A block forms a double gyroid), and (d) $f_A \approx 50\%$ (the A block forms lamellae). Inverse phases are not shown. Reprinted from Ref.[3]

The gyroidal morphology (Figure 1.3 c) is a bicontinuous structure, meaning that both the minority block forming the gyroidal domain and the matrix polymer forming the

surrounding regions are continuous and permeate throughout the entire thickness of the film. Films with this morphology are the ideal precursors of making membranes,eg. for ultrafiltraion, since they are orientation-independent. Unfortunately, only a narrow composition window yields this morphology.[4] Furthermore, this morphology occurs only when the two blocks are moderately incompatible. At sufficiently high molecular weights, most polymers are incompatible and this morphology is replaced by another morphology (perforated lamellae). Consequently, it is difficult to obtain the gyroidal morphology. Thus, films exhibiting a cylindrical morphology are often employed as precursors toward membranes.

In industry, linear block copolymers are used to tune the properties of product, by introducing different blocks and forming different micro phase separation. For example, polystyrene and polybutadiene are copolymerized to make polystyrene-*b*-polybutadiene-*b*-polystyrene (or SBS). In SBS, the polystyrene and polybutadiene are microly phase separately. Polybutadiene is rubbery, which gives SBS its rubber-like properties; polystyrene is a plastic, and the chains tend to tie different polybutadiene domains together and retain the shape after being stretched. Due to combination of properties from both polystyrene and polybutadiene, SBS is a hard rubber which is used to make products with durability, like the soles of shoes and tire treads.

1.2.2 Linear Block Copolymers in Selective Solvents

As defined by IUPAC, a selective solvent is "A medium that is a solvent for at least one component of a mixture of polymers, or for at least one block of a block or graft polymer, but a non-solvent for the other component(s) or block(s)".[5] As an example, consider an AB diblock copolymer that is initially dissolved in a good solvent for both the

A and B blocks. Let us then imagine that another solvent that is a good solvent for the A block but a poor solvent for B is gradually added into this solution under vigorous stirring. At a critical point, the B block would begin to collapse, while the A block will remain soluble in this given solvent mixture. If more of the second solvent is added, the chains of B block would form dispersed aggregates, which are stabilized by the soluble A chains. This solvent mixture is a selective solvent for this A. In a selective solvent, an AB block copolymer will undergo micellization. The insoluble B block will form the micellar core, and the soluble A chains will extend into solution and form the corona and help keep the micelles dispersed and stabilized in the solvent. The micellization of AB block copolymers and the various morphologies observed in solution have been studied extensively since the 1990s. One of the most widely investigated amphiphilic copolymers in selective solvents system is poly(styrene)-*block*-poly(acrylic acid) (PS-*b*-PAA), which bears a hydrophilic PAA block and a hydrophobic PS block. This system has been studied systematically by Eisenberg and coworkers,[6-10] who found that by tuning the chain length/volume fraction in PS-*b*-PAA as well as the solvent composition, they could obtain various thermodynamically controlled morphologies. As shown in Figure 1.4, these morphologies included spheres, rods, bicontinuous rods, bilayers (lamellae and vesicles), inverse rods (hexagonally packed hollow hoops, HHHs) and large compound micelles (LCMs).
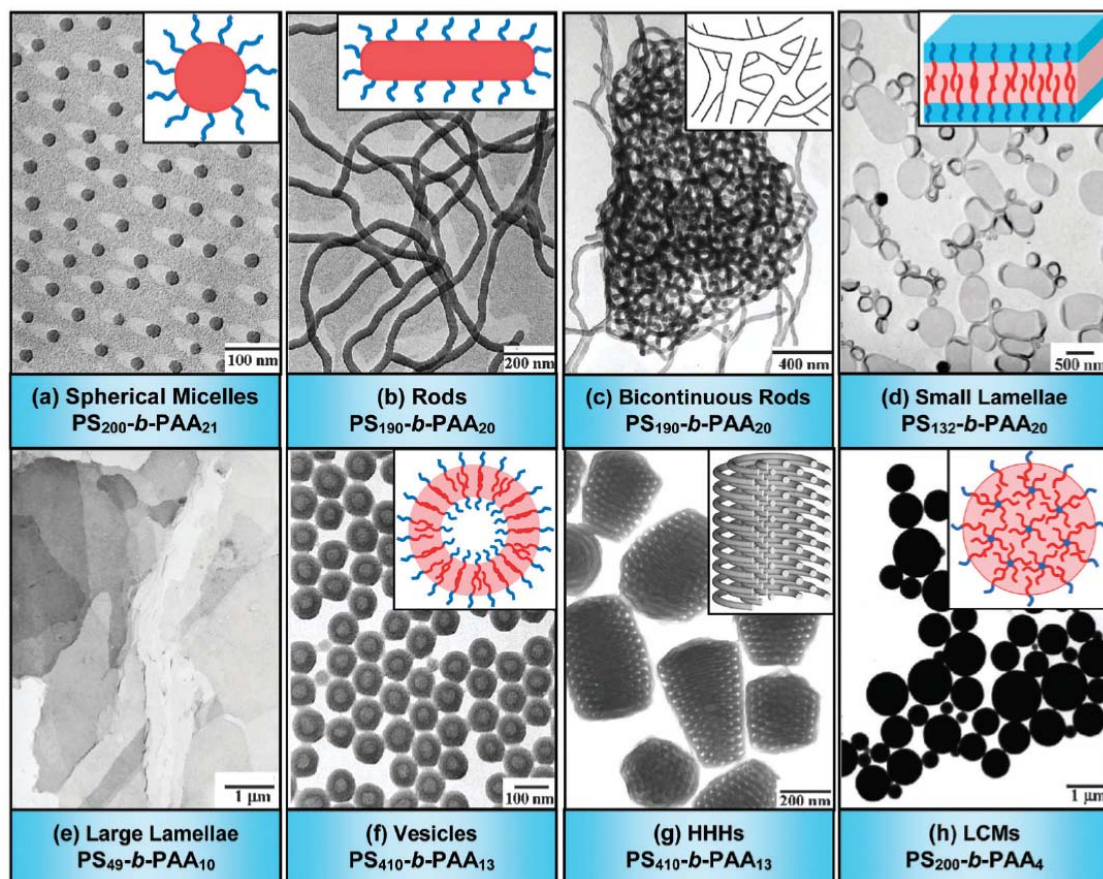
Figure 1.4 Transmission electron microscopy (TEM) images and corresponding schematic diagrams (shown in the insets) of various morphologies formed from amphiphilic PS$_m$-b-PAA$_n$ copolymers.[11, 12] Note: m and n denote the degrees of polymerization of PS and PAA, respectively. In the schematic diagrams, red represents hydrophobic PS domains, while blue denotes hydrophilic PAA domains. Reprinted from ref.[12]

The trends governing the self-assembly behaviour of amphiphilic diblock copolymers have also been summarized and have also been theoretically explained.[4, 13,14] These amphiphilic copolymers undergo self-assembly in selective solvents in order to minimize energetically unfavourable insoluble block–solvent interactions. The inherent molecular curvature influences the packing of the copolymer chains, and thus yields the various reported morphologies. In other words, one can selectively target a specific self-

assembled nanostructure, according to a dimensionless 'packing parameter', denoted as p. This parameter was developed by Israelachvili[15] for the prediction of micellar morphologies and sizes among small molecule surfactants, but also applies as a general rule for amphiphilic block copolymers. The theory is defined by Equation 1.1:

$$p = \frac{v}{a_o l_c}$$
Equation 1.1

where v is the volume of the solvent-phobic chains, a_o is the optimal cross-sectional area of the solvent-phobic core of the aggregate expressed per molecule in the aggregate, and l_c is the length of the solvent-phobic tail. Spherical micelles are favoured when $p \leq 1/3$, while cylindrical micelles are favoured, when $1/3 \leq p \leq 1/2$, and vesicles (also known as polymersomes or enclosed membrane structures) are generally observed when $1/2 \leq p \leq 1$ (Figure 1.5).
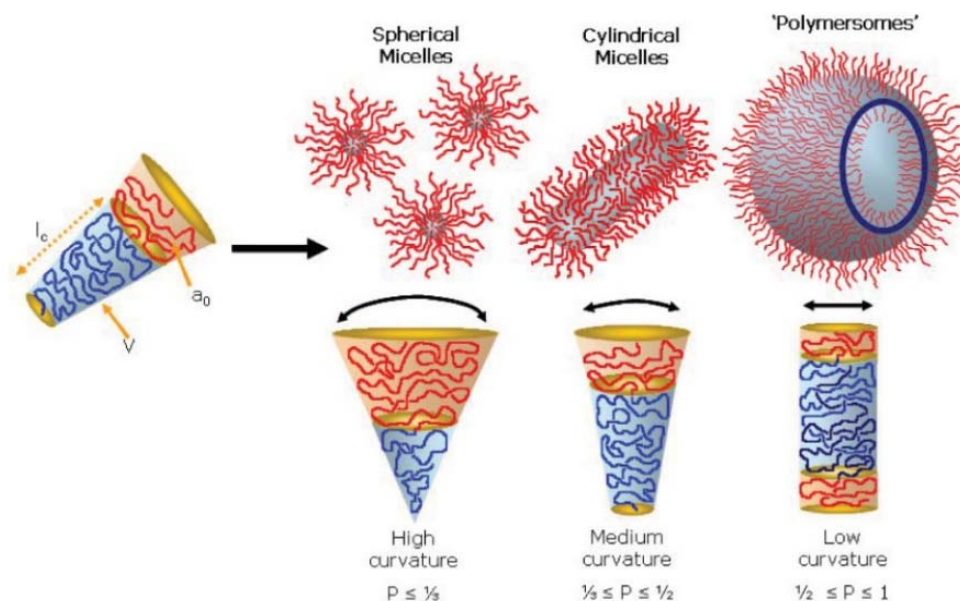
Figure 1.5 Various self-assembled structures formed by amphiphilic block copolymers in a block-selective solvent. The morphology of the structure is governed by the inherent curvature of the molecule, which can be estimated through calculation of its dimensionless packing parameter, p. Reprinted from Ref.[14]

An amphiphilic block copolymer only undergoes micellization in a selective solvent when it reaches a critical concentration. This concentration is known as the critical micellization concentration (CMC).[5] When the polymer concentration is below the CMC in a selective solvent, it forms individual unimer chains instead of aggregating to form micelles. Several factors can influence the CMC, including the nature of the polymer itself, the volume fraction of each block, the molecular weight, as well as the solvent composition.[13,16] Figure 1.6 illustrates a typical micellization process of an AB diblock copolymer that occurs when a non-solvent is added into a good solvent system containing the copolymer. Taking PS-*b*-PAA as an example, this copolymer could be initially dissolved in a good solvent such as THF or DMF, in which both the PS and PAA blocks are soluble. Let us imagine that water, which is a good solvent for PAA but a non-solvent for PS, is gradually added into the solution under vigorous stirring. The PS block would collapse at a certain water volume fraction. However, at this moment, the copolymer is still somewhat soluble in this solvent mixture, and the CMC of the polymer in this mixed solvent is still higher than the polymer concentration. The copolymer thus forms unimers, also known as single chain micelles.[17] Upon the addition of more water, the solvent system gradually becomes worse for the PS block, and the CMC decreases below copolymer concentration. The PS blocks of different unimers aggregate together to form a solid core in order to minimize the interaction with water. Meanwhile, the soluble PAA chains remain outside to stabilize the structure and form the corona. This assembly thus yields micelles consisting of a PS core and a PAA corona.

Add Non-solvent → **Add Non-solvent** →

AB block copolymer
in good solvent

Unimer
Below CMC
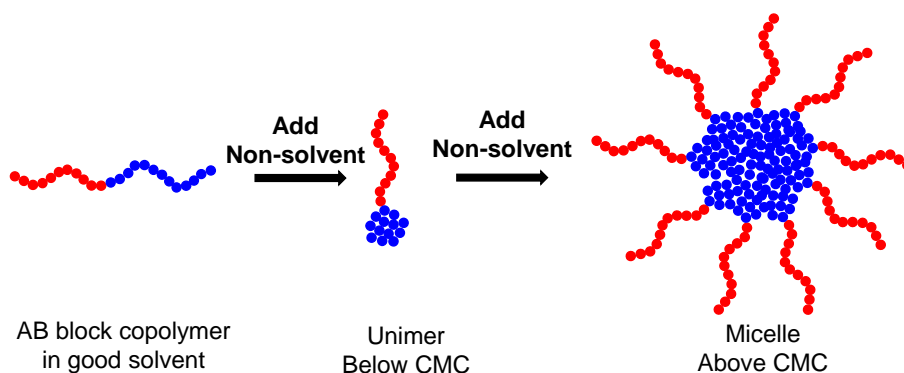
Micelle
Above CMC

Figure 1.6 Illustration of an AB block copolymer forming unimers and micelles upon the gradual addition of a non-solvent to a good solvent.

In a selective solvent system containing an AB diblock copolymer, such as the example mentioned above, six Flory Huggins parameters (χ-parameters) are involved,[13] including χ_{AB}, χ_{AS}, χ_{AN}, χ_{BS}, χ_{BN} and χ_{SN}. Here A and B represent the two blocks, S denotes the good solvent for both blocks, and N denotes the non-solvent for one of the blocks. Increasing the number of components in the solution will increase the complexity of the self-assembly process, and provide a wider and more elaborate range of morphologie. Take ABC triblock copolymers as an example, which only incorporate one more block than AB diblock copolymers, but the range and complexity of their nanostructures are far more diverse than those of diblock copolymers. One can manipulate the solubility of each block to prepare different morphologies. For example, Liu *et al.* prepared double and triple helices (Figure 1.7) in solvents which were good for the central block, selective for one terminal block, and marginal for the other terminal block.[18, 19] The polymer they investigated was poly(*n*-butyl methacrylate)-*b*-poly(2-cinnamoyloxyethyl methacrylate)-*b*-poly(*tert*-butyl acrylate) (PBMA-*b*-PCEMA-*b*-P*t*BA). This terpolymer was initially dissolved in a good solvent and a selective solvent was added to reduce the overall solvent quality for the PCEMA block, and to a lesser extent for the PBMA block. Finally, the

solvent was tuned so that it was selective for PCEMA and marginally selective for PBMA. The polymer initially formed spherical micelles in which PCEMA formed the core, and PBMA and P*t*BA formed the corona. These spherical micelles gradually self-assembled into cylinders, and eventually into double or triple helices, in order to minimize the interaction between PBMA and solvent. Similarly, twisted cylinders were prepared in a selective solvent for the terminal blocks.[20]
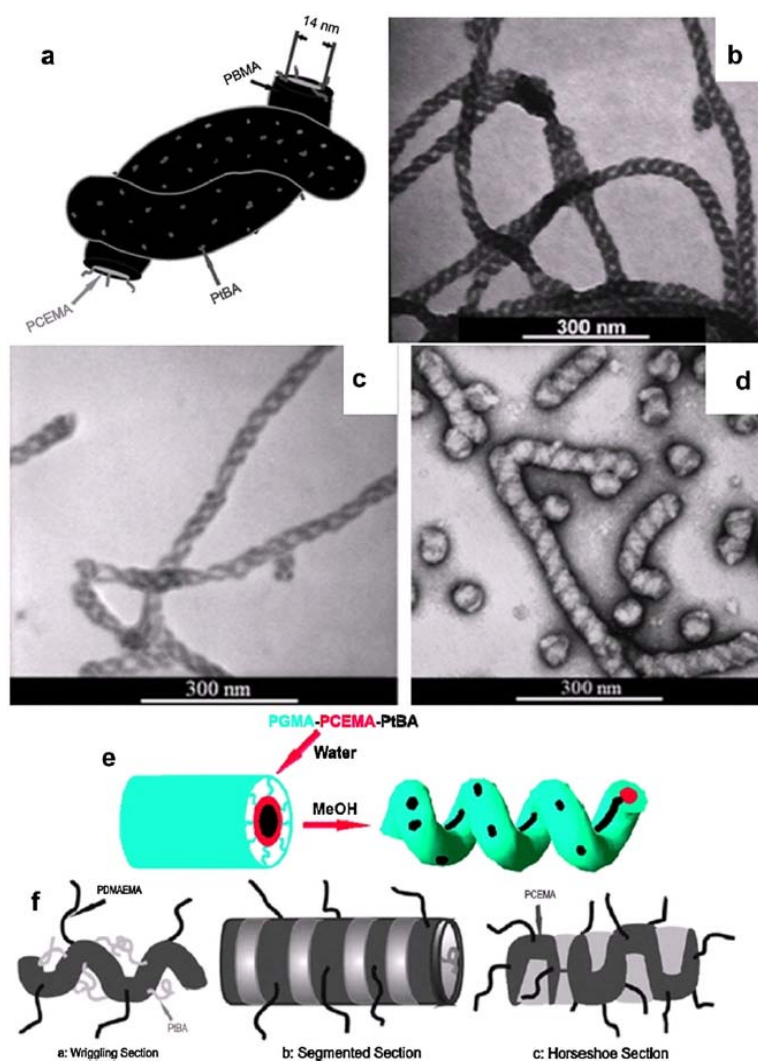
Figure 1.7 Schematic and TEM (stained with OsO$_4$) images of double helical assemblies of PBMA-*b*-PCEMA-*b*-P*t*BA are shown in (a) and (b), respectively.[18] TEM images of

PBMA-*b*-PCEMA-*b*-PAA helices (derivatized via P*t*BA hydrolysis) that were stained with OsO$_4$ and uranyl acetate, respectively, are shown in (c) and (d). OsO$_4$ was used to selectively stain the PCEMA domains, while uranyl acetate was applied to selectively stain the PAA domains. A schematic diagram depicting the formation of twisted cylinders from PGMA-*b*-PCEMA-*b*-P*t*BA cylinders upon the addition of water is shown in image (e).[20] The green, red, and black regions correspond to PGMA, PCEMA, and P*t*BA domains, respectively. The formation of twisted cylinders, segmented cylinders, and "horseshoe section" segmented cylinders are shown schematically in image (f).[21] Among the twisted cylinders PCEMA forms the core, while the P*t*BA and PDMAEMA corona chains respectively favour the sheltered concave and exposed convex sides of the curves. The segmented cylinders consist of alternating PCEMA and P*t*BA disks forming the core, while PDMAEMA forms the corona. In the case of the "horseshoe section" the PCEMA domains form horseshoe-like structures, with P*t*BA filling the gaps in the core between the horseshoes as PDMAEMA forms the corona. These images are reprinted from Ref.[22]

So far, many morphologies have been reported experimentally from ABC triblock copolymers, including multicompartment micelles, micelles bearing mixed coronas, core-shell micelles, micelles with anisotropic or patchy surfaces, and Janus particles

1.3 Self-Assembly of ABC Miktoarm Copolymers

ABC Miktoarm polymers are a family of nonlinear copolymers bearing three chemically distinct blocks (also called arms), which are linked together at one central junction point. In contrast to linear block copolymers, their arms have mutual intersections from the junction point. Since they only have one junction point, their chain packing behaviour during self-assembly is quite different from that of ABC linear block terpolymers, which have two junction pointes. Their self-assembly behaviour is so interesting, that some scientists have even called ABC miktoarm polymers a "Jewellery

Box of Morphologies".[23] Further details on the assembly of these copolymers in both bulk and solution will be provided below.

1.3.1 ABC Miktoarm Polymer Self-Assembly in Bulk

In the bulk state, in a certain volume fraction range, ABC miktoarm polymers form various tiling structures. In these structures, their common block junction occurs on a line, as shown in Figure 1.8. The different arms segregate into domains around the block junction line. Viewing the cross section of the domains cut perpendicular to the block junction line, one sees two-dimensional tiling structures or periodic and regular polygons. The polygons are divided into sub-regions where the three arms are located. The 12 types of possible tile structures have been summarized by Grunbaum and Shephard and have been called "Archimedean Tilings." after the ancient work of Archimedes, [24] These 12 Archimedean tilings are shown in Figure 1.9. By tuning the volume fractions of the arms, one can obtain a wide range of tiling structures.
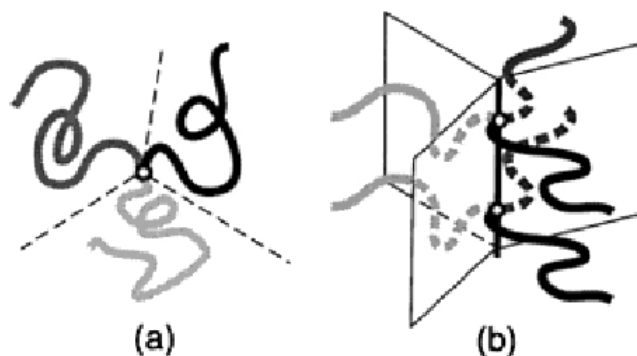
Figure 1.8 Illustration of the chain packing of an ABC miktoarm polymer in the solid state. Reprinted from Ref.[25]
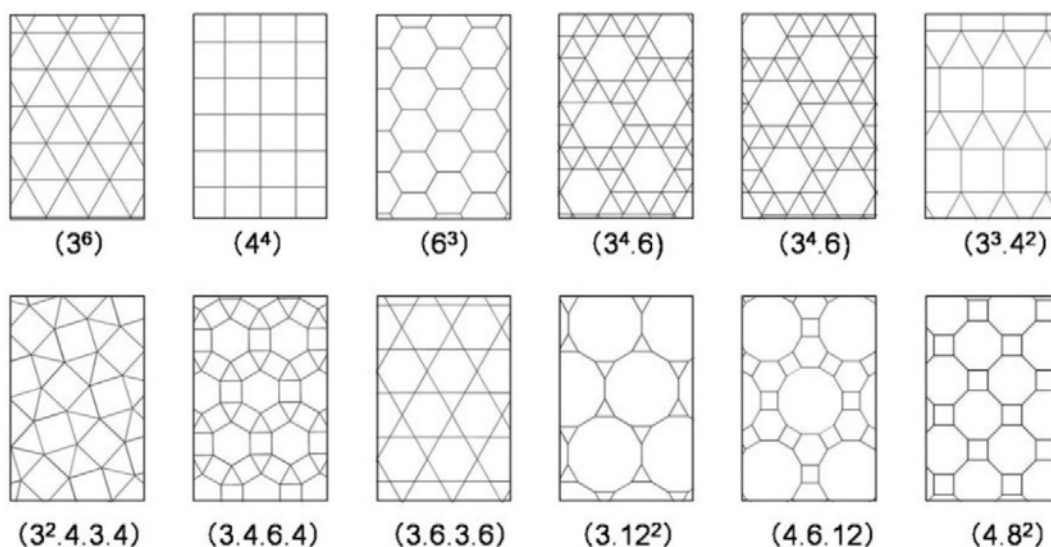
Figure 1.9 Twelve Archimedean tilings. Reprinted from Ref. [23]

Fujimoto and coworkers reported the first tiling pattern formed by a μ-ABC miktoarm polymer.[26] They obtained a structure with three-fold symmetry from a μ-(polystyrene)(poly(dimethylsiloxane))(poly(*tert*-butyl methacrylate)) miktoarm polymer system. Subsequently, Hadjichristidis *et al.* reported a six-fold symmetry tiling pattern from a μ-(polystyrene)(polyisoprene)(poly(methyl methacrylate)) (SIM) miktoarm copolymer.[27]

In the bulk state, if the volume fraction of one arm of a μ-ABC miktoarm polymer increases beyond the tiling zone, hierarchical morphologies begin to form. Matsushita *et al.* performed systematic studies on a μ-(polyisoprene)(polystyrene)(poly(2-vinyl-pyridine)) (or $I_x S_y P_z$) miktoarm polymer system, where x, y and z denote the relative volume fractions.[28] They fixed the x and y values at 1.0 and 1.0 respectively, and tuned the z values from 0.2 to 53. As shown in Figure 1.11, they found that when z ranged between 0.2 and 1.9, the ISP copolymers still formed 2-D tilings. However, when z was increased from 3.0

to 10, different hierarchical "lamella + cylinder" and "columnar piled disk cylinder" structures were observed. With further increases of z to 22, the lamellar-base structures became a cylinder-base structure, which consisted of alternating I and S lamellae aligned within a cylinder embedded in a P matrix (Figure 1.12c). If z was increased further to a very high value, 53, isolated spheres composed of internal phase separation were observed as shown in Figure 1.12k. They also tuned the y values and the obtained various morphologies, as summarized in Ref.[23].
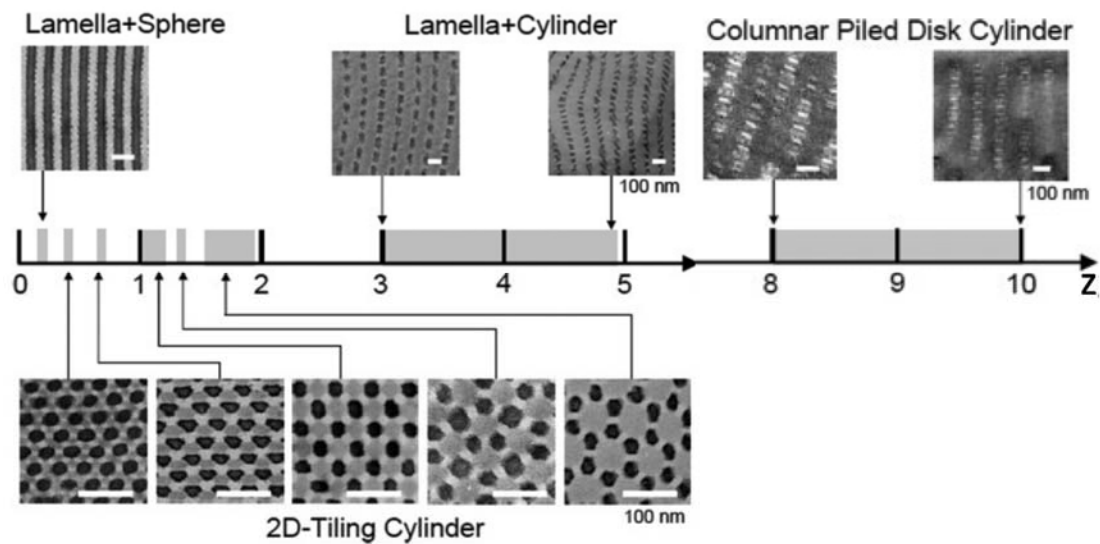
Figure 1.10 The phase diagram of $I_{1.0} S_{1.0} P_x$ star-shaped terpolymers and related blends against x ($0.2 \leq x \leq 10$). The white scale bars in each TEM of the images correspond to 100 nm. Adapted from Ref.[28]

17
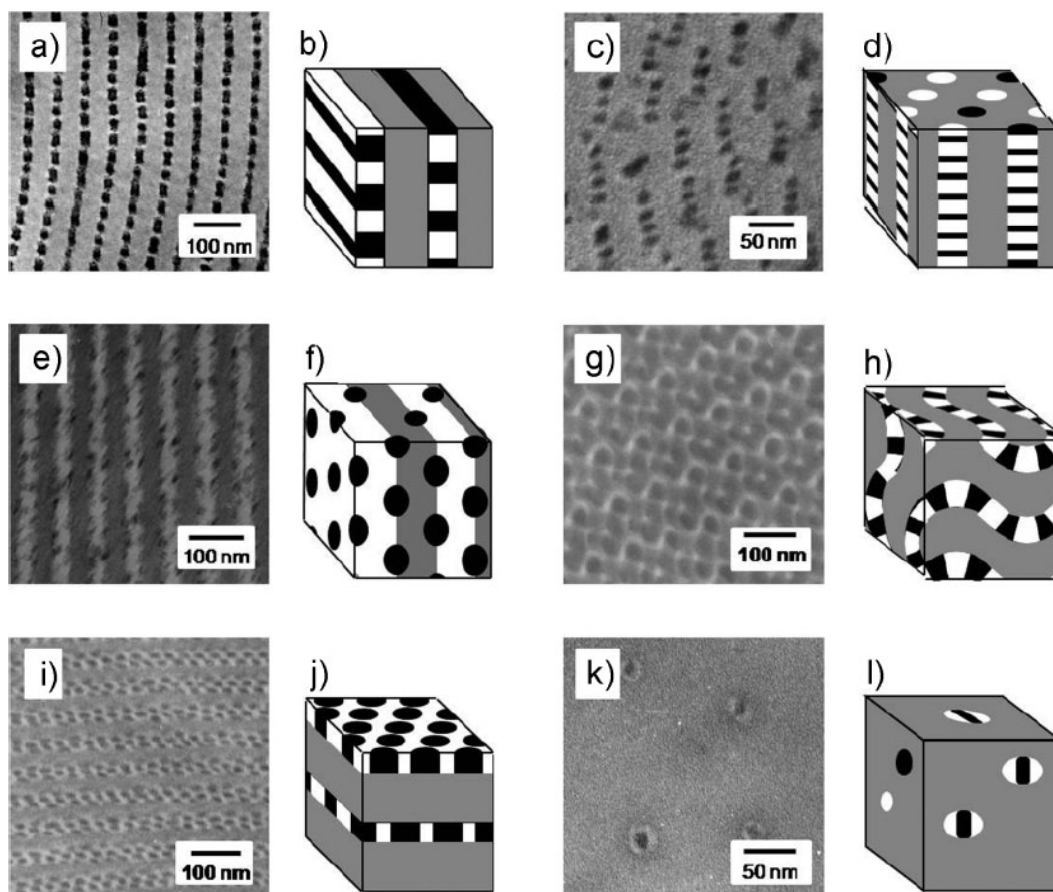
Figure 1.11 Hierarchical three phase structures observed via TEM for various star-shaped terpolymers: a)$I_{1.0} S_{1.0} P_{3.0}$, c) $I_{1.0} S_{1.0} P_{22}$, e) $I_{1.0} S_{1.0} P_{0.2}$, g) $I_{1.0} S_{1.8} P_{3.2}$, i) $I_{1.0} S_{1.8} P_{6.4}$, and k) $I_{1.0} S_{1.0} P_{53}$. The corresponding schematic of these structures are shown in b), d), f), h), j), and l), respectively. Reprinted from Ref.[23]

1.3.2 Self-Assembly of ABC Miktoarm Copolymers in Solution

ABC miktoarm polymers that bear mutually immiscible components, can form exotic compartmentalized micelles in block-selective solvents. Hillmyer and Lodge *et al.* initially found that this type of miktoarm polymer would form a basic structure illustrated in Figure 1.13. In addition, they observed that these basic units tended to stack together to form more complex multicompartment structures.[29] They investigated the morphological formation

18

of an triphilic μ-(poly(ethyl ethylene))(poly(ethylene oxide))(poly(perfluoropropylene oxide)) miktoarm copolymer (μ-E$_x$O$_y$F$_z$) in water, where x, y, and z represent the molecular weights of the E, O, and F blocks, respectively, in units of kg/mol. Consequently, they reported a family of multicompartment micelles exhibiting intricate structures, such as hamburger micelles (Figure 1.14d), three- or four-lobed micelles, segmented wormlike micelles (Figure 1.14e), laterally nanostructured vesicles (Figure 1.14f), and polygonal bilayer sheets, etc.[29-35] As mentioned earlier, AB block copolymers can typically yield classical morphologies (such as spheres, cylinders, and bilayer vesicles which are shown in Figure 1.14a-c) that can be adjusted by tuning the corona block volume fraction or by increasing the interfacial tension. Similarly, as the length of the soluble O block is gradually decreased, μ-EOF polymers sequentially form hamburger micelles, segmented wormlike micelles, and nanostructured vesicles.[32] This trend is shown in Figure 1.14, in which images d-f show the corresponding chain-packing motifs of these morphologies, and images g-i show the respective cryo-TEM images of these structures. The cryo-TEM images exhibit dark and grey domains, which correspond to the F and E domains, respectively. As shown in Figure 1.14, the cores of these micelles are subdivided into nanoscopic E and F domains, because of high compatibility between the fluorinated (F) and the hydrophobic blocks(E).

Figure 1.12 Illustration of the chain packing observed in a basic structure of an ABC miktoarm polymer. The red and green colors represent insoluble chains, and the blue color represents the soluble corona chains. Reprinted from Ref.[29]
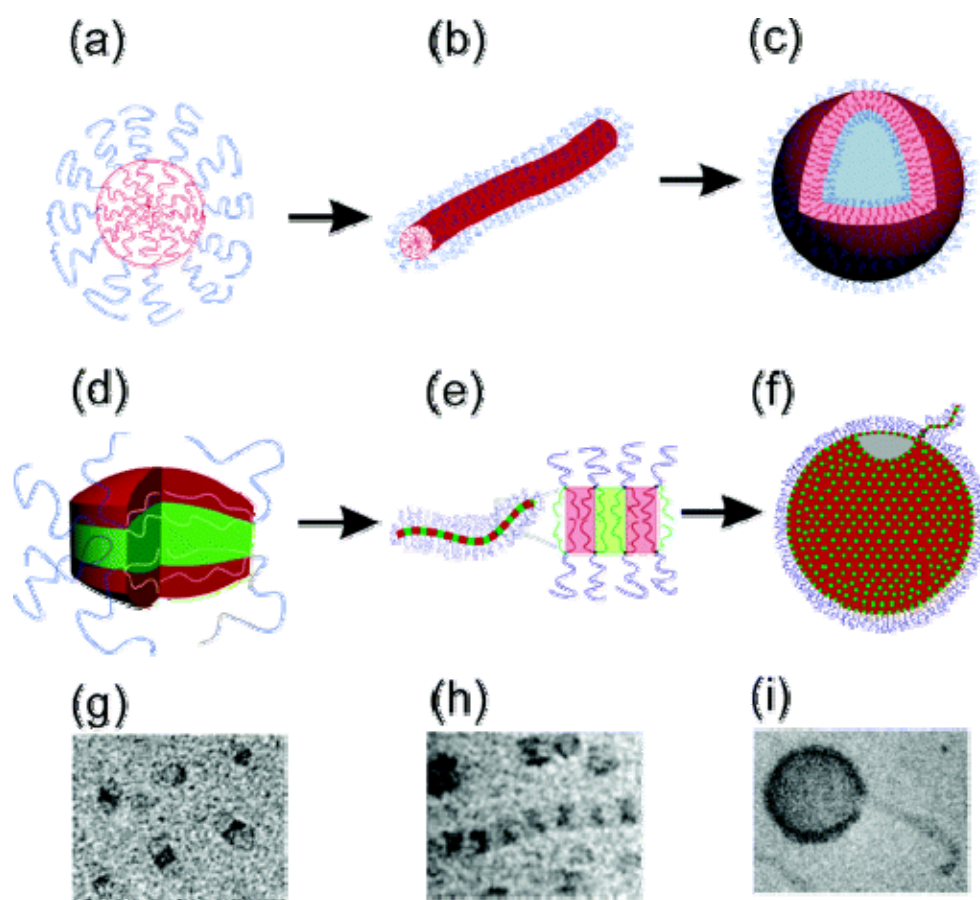
Figure 1.13 Schematic representation of micellar self-assemblies of AB diblock copolymers and ABC star terpolymers: (a) a spherical micelle, (b) a wormlike micelle, and (c) a bilayer vesicle formed from an AB diblock copolymer; (d) a hamburger micelle, (e) a segmented wormlike micelle, and (f) a nanostructured bilayer vesicle formed from an ABC miktoarm star terpolymers. Representative cryo-TEM images showing (g) hamburger micelles, (h) segmented wormlike micelles, and (i) nanostructured vesicles formed from μ-EOF terpolymers. Reprinted from Ref.[32]

The range of intricate structures that are formed by ABC miktoarm copolymers are not limited to the three examples mentioned above. A diverse range of complex nanostructures have been experimentally observed, and are summarized as a function of the copolymer composition in the morphology-composition diagram shown in Figure 1.15.

This helps demonstrate the wide range of intricate nanostructures that are available, and one can envision that this diverse range of nanostructures will continue to grow as researchers begin to devote more attention to the assembly behavior of these fascinating copolymers.
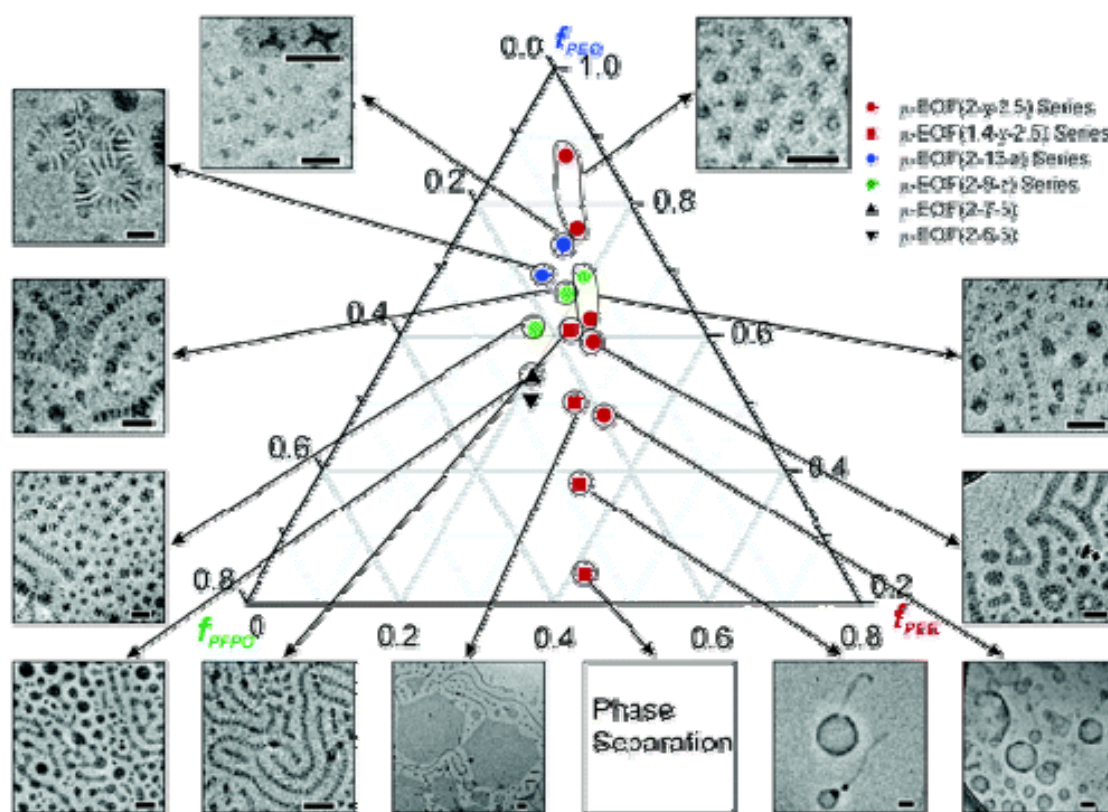
Figure 1.14 Morphological diagram showing TEM images of various multicompartment micelles formed from μ-EOF miktoarm star terpolymers in dilute aqueous solution as a function of the copolymer composition. The terms f_{PEE}, f_{PEO}, and f_{PFPO} denote the volume fractions of the E, O, and F blocks, respectively. The inset in the upper left image represents the three- and four-lobed multicompartment micelles formed from μ-EOF (2−13−3.5). The numbers denote molecular weights of arms in the unit of kg/mol. The scale bars correspond to 50 nm. Reprinted from Ref.[32]

Researchers have also introduced functional groups into miktoarm polymers and their assembly structures in order to prepare novel morphologies that may have various potential applications. For example, μ-(polystyrene)(poly(ethylene oxide))(poly(2-(dimethylamino)ethyl acrylate)) (μ-SODA) were synthesized,[33] which contains a pH-responsive poly(2-(dimethylamino)ethyl acrylate) (PDMAEA) block. PDMAEA is soluble in acidic media, but becomes insoluble in alkaline media, and this stimuli-responsive behaviour was thus employed to tune the morphologies of multicompartment micelles formed by this copolymer. In another example, μ-poly(ethyl ethylene)(poly(ethylene oxide))(poly(γ-methyl-ε-caprolactone)) (μ-EOC) (Figure 1.16a) was reported, which incorporated a poly(γ-methyl-ε-caprolactone) (PMCL) block that underwent pH-responsive degradation.[35] As shown in Figure 1.16b, this polymer initially formed segmented wormlike structures in pH=7 water. Subsequently, when the copolymer was placed in a pH = 12 aqueous buffer at 50 °C, PMCL underwent hydrolytic degradation. After four weeks, the majority of the μ-EOC copolymers had degraded into EO diblock copolymers and PMCL homopolymers. During this process, the segmented wormlike structures gradually "evolved" into raspberry-like vesicle structures composed of spherical PMCL subdomains embedded within an E matrix, as shown in Figure1.16b.

Despite the variety of novel morphologies that have been reported, miktoarm copolymers have received relatively little attention in comparison with linear block copolymers. Aside from these experimental findings, computational simulations have been performed and predicted that ABC copolymers can form an even greater range of fascinating nanostructures via self-assembly in both solution[36, 37] and in the bulk state.[25] It is apparent that a diverse range of nanostructures remain to be observed experimentally.
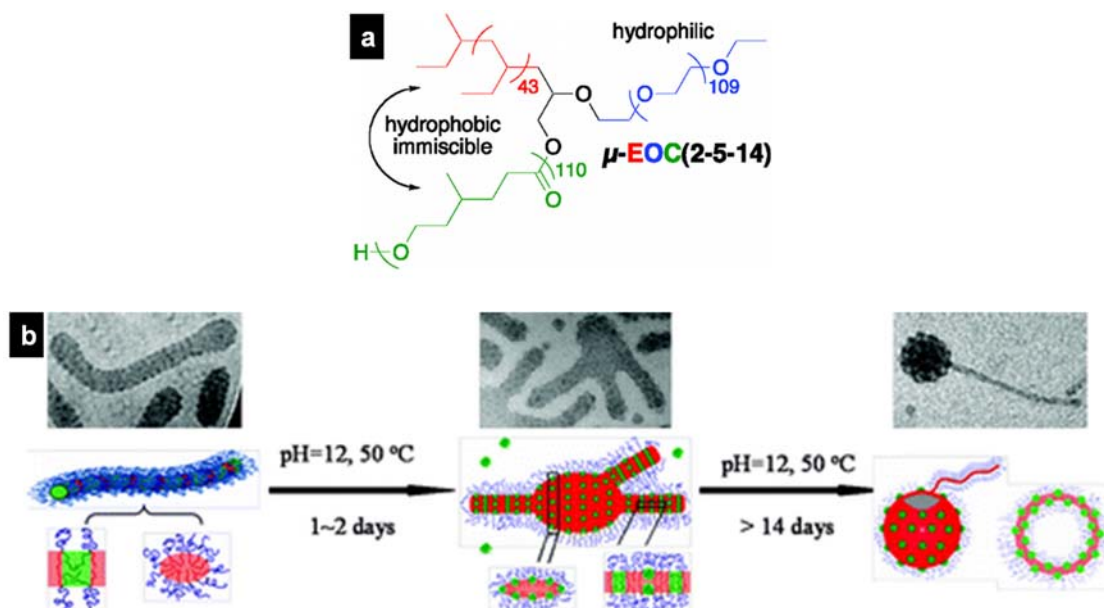
Figure 1.15 (a) Chemical structure of μ-EOC, (b) Schematic diagrams illustrating the morphological transition of μ-EOC micelles during the hydrolytic degradation at pH = 12 and at 50 °C. Adapted from Ref. [35]

1.4 Synthesis of Miktoarm Star Terpolymers

The synthesis of miktoarm star polymers is much more challenging than the preparation of linear block copolymers. The preparation of miktoarm copolymers possessing low polydispersity and elaborate functionality is especially challenging.[38] These synthetic challenges may represent the main reason why morphological studies of miktoarm polymers have not been as extensive as those of linear chain block copolymers. Traditionally, miktoarm polymers have been synthesized by three types of general strategies, including the "arm-first", the "grafting-from", and a "hybrid" approach. These strategies will be described in the following paragraphs.

The first strategy for preparing miktoarm copolymers is known as the "arm-first" approach.[39, 40] The different arms are prepared via living or controlled polymerizations first and then linked together to form a miktoarm star polymer. Taking the synthesis of μ-(polyisoprene)(polystyrene)(polybutadiene) (μ-(PI)(PS)(PBd))[40] as an example, PI, PS and PBd were individually prepared via anionic polymerizations, and kept separately in their polyisoprenyllithium, polystyrillithium and polybutadienyllithium forms, respectively. As shown in Figure 1.17, the polyisoprenyllithium was firstly terminated with an excess of methyltrichlorosilane. After the excess of methyltrichlorosilane had been removed, a stoichiometric addition (titration) of polystyrillithium was performed before a small excess of polybutadienyllithium was finally added. The by-product was removed after three fractionations, thus yielding an ABC miktoarm terpolymer with a very low PDI of 1.03 (Figure 1.18). The entire process took a few days to complete, and it is extremely challenging to ensure that these very sensitive anions remain alive for so long.

$$\text{PILi} + \text{excess } CH_3SiCl_3 \longrightarrow PISi(Cl_2)CH_3 + LiCl + CH_3SiCl_3\uparrow$$

$$PISi(Cl_2)CH_3 + \text{PSLi} \longrightarrow (PI)(PS)SiClCH_3 + LiCl$$

$$(PI)(PS)SiClCH_3 + \text{excess PBdLi} \longrightarrow (PI)(PS)(PBd)SiCH_3 + LiCl$$
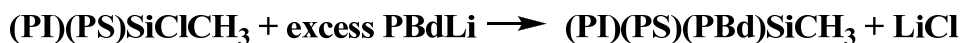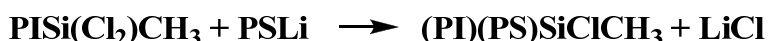
Figure 1.16 Synthetic pathway toward μ-(PI)(PS)(PBd) via the "arm-first" approach. Reproduced from Ref.[40]
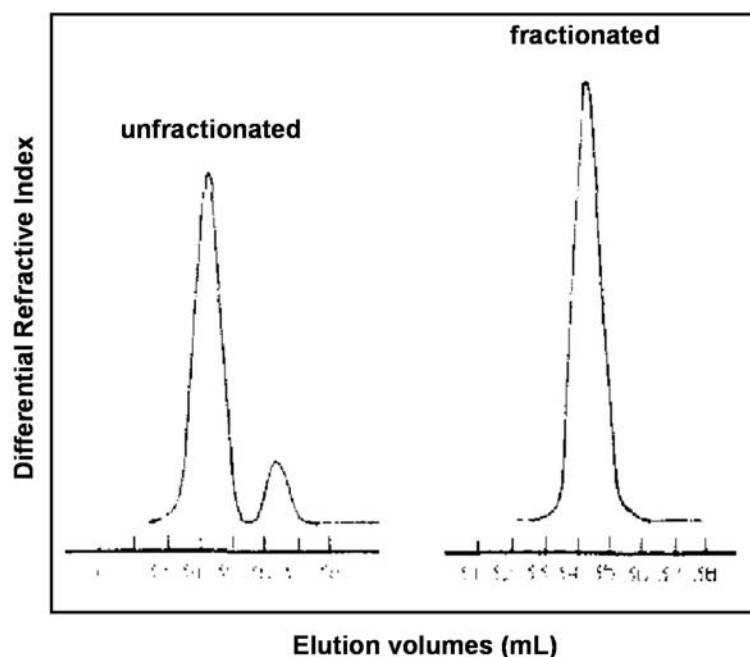
Figure 1.17 SEC traces of the μ-(PI)(PS)(PBd) star terpolymer prior to and after three fractionations. Adapted from Ref. [40]

The second strategy is known as the "grafting-from" approach, which involves a multifunctional initiator. The polymerization of different monomers by different controlled/"living" mechanisms is performed in sequence.[41-43] The preparation of μ-(poly(ε-caprolactone))(poly(methyl methacrylate))(polystyrene) (μ-(PCL)(PMMA)(PS)) via ring-opening polymerization (ROP), atom transfer radical polymerization (ATRP), and nitroxide-mediated radical polymerization (NMRP) is shown in Figure 1.19 as an example.[43] A trifunctional initiator bearing a hydroxyl group, an ATRP-initiating center and an NMRP-initiating center was synthesized. This initiator was used to initiate the CL, MMA and styrene monomers in a stepwise manner so that they can undergo ROP, ATRP, and NMRP polymerization, respectively. This "grafting-from" strategy is much easier to execute than the "arm-first" strategy. However, since the monomers must be "selective"

25

to the different initiation centers, the types of miktoarm polymers that can be prepared through this strategy are very limited. In addition, due to the numerous steps and controlled mechanisms involved, this strategy does not facilitate the preparation of copolymers that bear numerous arms and exhibit a low polydispersities (such as those with PDI $\leq$ 1.05).
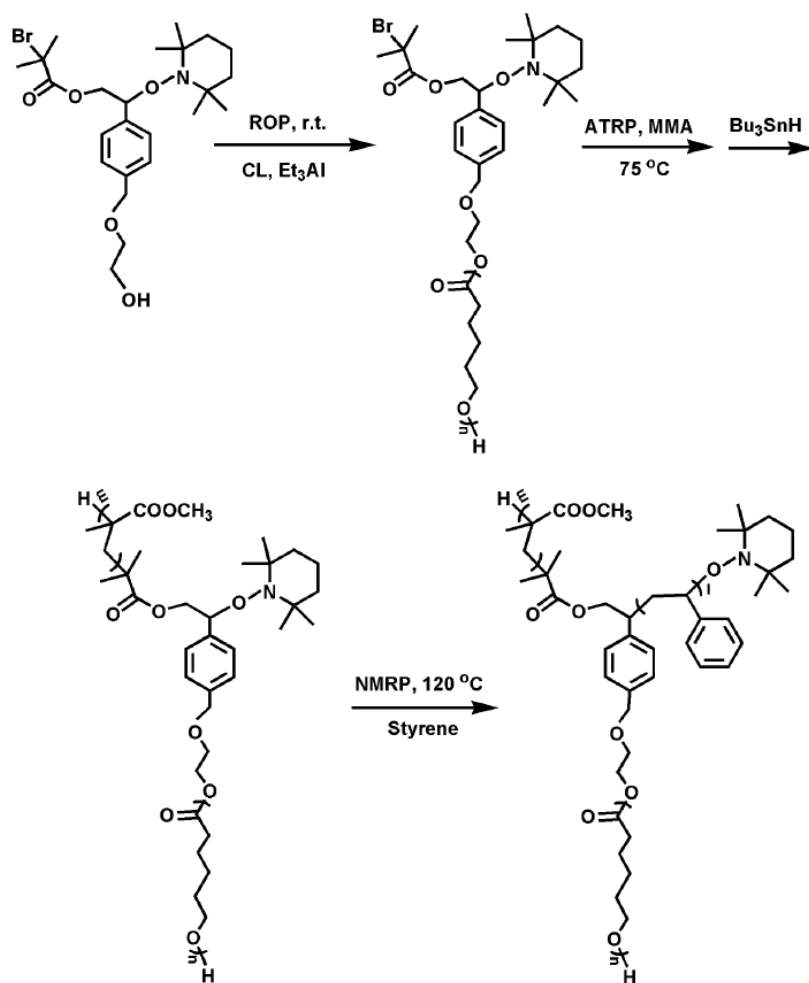
Figure 1.18 Synthesis of miktoarm terpolymers via the "grafting-from" strategy. The example that is shown above combines ring-opening polymerization (ROP), atom transfer radical polymerization (ATRP), and nitroxide-mediated radical polymerization (NMRP) techniques to grow the different polymer chains from a trifunctional initiator. Reprinted from Ref.[43]

The third strategy is known as the "hybrid" approach, which combines features of the first two strategies.[38, 44-47] A core molecule containing a mixture of terminating and initiating sites can be used to prepare miktoarm polymers.[38] For example, to prepare μ-(polystyrene)(polybutadiene)(poly(methyl methacrylate)) (μ-(PS)(PB)(PMMA))[48], a polystyrene macromonomer bearing a terminal 1,1-diphenylethylene (DPE) unit was prepared first (Figure 1.20). A living polybutadienyllithium was initially prepared as well, and was added to the macromonomer to form a (PS)(DPE$^-$)(PB) diblock copolymer with a living anionic center in the center, which initiated the polymerization of the MMA monomer. This polymerization was subsequently terminated with acetic acid to yield μ-(PS)(PB)(PMMA) as the final product. This strategy was not limited to living polymerizations, and controlled polymerizations have also been used.[44] Since the second arm was grafted onto the macromonomer and formed a new initiating center for the growth of the third block, this strategy has also been called the "in-out" method as well.[44]
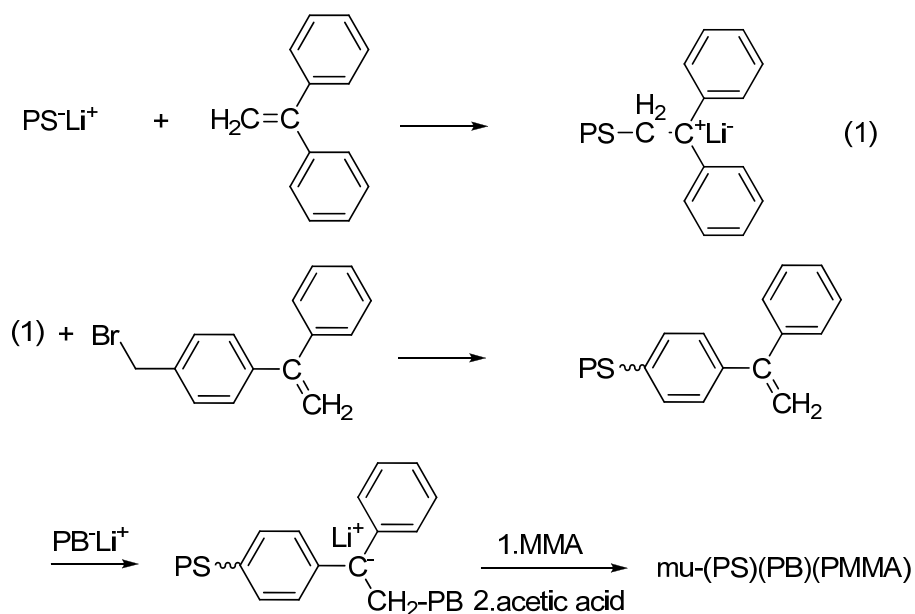
Figure 1.19 Synthetic route toward μ-(PS)(PB)(PMMA) via the "hybrid approach". Reproduced from Ref.[38]

1.5 Scope of this Thesis

As mentioned in the previous sections, the morphologies of μ-ABC miktoarm terpolymer are fascinating. However, the experimental studies focusing on the morphologies of these copolymers have traditionally been limited by the challenges encountered with their synthesis. Therefore, the research described in this thesis has focuses on the development of a relatively facile and general methodology for preparation of functional μ-ABC/μ-ABC$_x$ miktoarm terpolymers with narrow molecular weight distributions. Meanwhile, the preparation of capsules and the encapsulation of various cargoes have been long practiced in industry and are a hallmark of biological systems. The work described herein will also cover the preparation of nanocapsules bearing walls that are perforated by regularly-packed and pH-responsive channels from our μ-ABC$_x$ miktoarm terpolymers.

Chapter 2 describes the development of a "assembly-and-reaction" method to prepare μ-(PtBA$_{100}$)(PSMA$_{66/200}$)(PCEMA$_{120}$) miktoarm polymers. Two types of linear block copolymers were initially firstly synthesized as precursors. These precursors included triblock copolymers bearing a short (five units in length) central complementary stitching block (PtBA$_{100}$-b-PCOOH$_5$-b-PSMA$_{66/200}$), and a diblock copolymer that also possessed a short complementary stitching block (P(NH$_2$)$_5$-b-PCEMA$_{120}$) with a similar length. The short complementary blocks of the triblock and diblock copolymer precursor chains contained carboxyl and amino groups, respectively. These short PCOOH and PNH$_2$ blocks were subsequently associated together via hydrogen bonding in solution, thus merging a triblock terpolymer chain and a diblock copolymer chain together. A coupling reagent was then added to allow the amidization reaction to permanently "stitch" the

28

polymer chains together. This protocol yielded functional μ-$(PtBA_{100})(PSMA_{66/200})(PCEMA_{120})$ miktoarm terpolymers, in which the $PtBA$ block can be hydrolyzed to yield a pH-responsive PAA chain, the hydrophobic PSMA block could be hydrolyzed into a hydrophilic PGMA block, while the PCEMA block could become structurally locked via photocrosslinking. This synthetic strategy may provide a facile and versatile gateway for the preparation of novel miktoarm copolymers and thus also expand the library of nanostructures based on these copolymers.

Chapter 3 describes the preparation of μ-$(PtBA_{100})(PCEMA_{130})(PEO_{114})_x$ ($x = 1.14$ and 1.58) terpolymers, which are also prepared via the "assembly-and-reaction" method. In this case, only the poly(ethylene oxide) (PEO) block was soluble in a tetrahydrofuran/water mixture containing 80 vol% water, so that the two μ-$(PtBA)(PCEMA)(PEO)_x$ samples formed vesicles with the $PtBA$ and PCEMA domains forming the wall. It was found that a $PtBA$/PCEMA volume ratio of 3/7 yielded vesicular walls consisting of a PCEMA matrix that was perforated by regularly-packed $PtBA$ cylinders. In addition, the subsequent photocrosslinking of the PCEMA wall and hydrolysis of the cylindrical $PtBA$ domains yielded permanent capsules that were permeated by regularly-packed poly(acrylic acid)-gated nanochannels. These intricate block copolymer nanostructures were unprecedented. We also loaded dyes into these capsules and investigated the release kinetics of the dyes from these capsules. The kinetic data suggested that the channels were pH-responsive, and released reagents both more rapidly and more completely at elevated pH values. Thus, future generations of these capsules may provide promising candidates for controlled release applications. In addition, we discovered that the fluorescence of pyrene monomers and excimers were quenched by PCEMA. This discovery helped enrich the photochemistry of PCEMA.

29

1.6 References

1. Hamley, I. W. *Block Copolymers*. Oxford University Press: Oxford, **1999**.

2. Hadjichristidis, N.; Iatrou, H.; Pitsikalis, M.; Mays, J. Macromolecular architectures by living and controlled/living polymerizations. *Progress In Polymer Science* **2006**, *31*, 1068-1132.

3. Abetz, V.; Goldacker, T. Formation of superlattices via blending of block copolymers. *Macromolecular Rapid Communications* **2000**, *21*, 16-34.

4. Bates, F. S.; Fredrickson, G. H. Block copolymers - Designer soft materials. *Physics Today* **1999**, *52*, 32-38.

5. A. D. McNaught, A. W. *IUPAC. Compendium of Chemical Terminology*. Blackwell Scientific Publications: Oxford, **1997**.

6. Zhang, L. F.; Eisenberg, A. Multiple morphologies and characteristics of "crew-cut" micelle-like aggregates of polystyrene-*b*-poly(acrylic acid) diblock copolymers in aqueous solutions. *Journal of the American Chemical Society* **1996**, *118*, 3168-3181.

7. Zhang, L. F.; Yu, K.; Eisenberg, A. Ion-induced morphological changes in "crew-cut" aggregates of amphiphilic block copolymers. *Science* **1996**, *272*, 1777-1779.

8. Discher, D. E.; Eisenberg, A. Polymer vesicles. *Science* **2002**, *297*, 967-973.

9. Shen, H. W.; Zhang, L. F.; Eisenberg, A. Thermodynamics of crew-cut micelle formation of polystyrene-*b*-poly(acrylic acid) diblock copolymers in DMF/H_2O mixtures. *Journal of Physical Chemistry B* **1997**, *101*, 4697-4708.

10. Shen, H. W.; Eisenberg, A. Morphological phase diagram for a ternary system of block copolymer PS310-*b*-PAA(52)/dioxane/H2O. *Journal Of Physical Chemistry B* **1999**, *103*, 9473-9487.

11.   Cameron, N. S.; Corbierre, M. K.; Eisenberg, A. 1998 E.W.R. Steacie Award Lecture Asymmetric amphiphilic block copolymers in solution: a morphological wonderland. *Canadian Journal Of Chemistry-Revue Canadienne De Chimie* **1999**, *77*, 1311-1326.

12.   Mai, Y.; Eisenberg, A. Self-assembly of block copolymers. *Chemical Society Reviews* **2012**, *41*, 5969-5985.

13.   Mai, Y. Y.; Eisenberg, A. Self-assembly of block copolymers. *Chemical Society Reviews* **2012**, *41*, 5969-5985.

14.   Blanazs, A.; Armes, S. P.; Ryan, A. J. Self-Assembled Block Copolymer Aggregates: From Micelles to Vesicles and their Biological Applications. *Macromolecular Rapid Communications* **2009**, *30*, 267-277.

15.   Israelachvili, J. N.; Mitchell, D. J.; Ninham, B. W. Theory of self-assembly of hydrocarbon amphiphiles into micelles and bilayers. *J. Chem. Soc., Faraday Trans. 2* **1976**, *72*, 1525-1568.

16.   Allen, C.; Eisenberg, A.; Maysinger, D. Copolymer drug carriers: conjugates, micelles and microspheres. *Stp Pharma Sciences* **1999**, *9*, 139-151.

17.   Njikang, G.; Liu, G. J.; Hong, L. Z. Chiral Imprinting of Diblock Copolymer Single-Chain Particles. *Langmuir* **2011**, *27*, 7176-7184.

18.   Dupont, J.; Liu, G. J.; Niihara, K.; Kimoto, R.; Jinnai, H. Self-Assembled ABC Triblock Copolymer Double and Triple Helices. *Angewandte Chemie-International Edition* **2009**, *48*, 6144-6147.

19.   Dou, H.; Liu, G.; Dupont, J.; Hong, L. Triblock terpolymer helices self-assembled under special solvation conditions. *Soft Matter* **2010**, *6*, 4214-4222.

20.   Hu, J. W.; Njikang, G.; Liu, G. J. Twisted ABC Triblock Copolymer Cylinders with Segregated A and C Coronal Chains. *Macromolecules* **2008**, *41*, 7993-7999.

21.   Han, D. H.; Li, X. Y.; Hong, S.; Jinnai, H.; Liu, G. J. Morphological transition of triblock copolymer cylindrical micelles responding to solvent change. *Soft Matter* **2012**, *8*, 2144-2151.

22.   Wyman, I. W.; Liu, G. J. Micellar structures of linear triblock terpolymers: Three blocks but many possibilities. *Polymer* **2013**, *54*, 1950-1978.

23.   Matsushita, Y.; Hayashida, K.; Takano, A. Jewelry Box of Morphologies with Mesoscopic Length Scales - ABC Star-shaped Terpolymers. *Macromolecular Rapid Communications* **2010**, *31*, 1579-1587.

24.   Branko Grünbaum, G. C. S. *Tilings and Patterns*. Freeman: New York, **1986**.

25.   Gemma, T.; Hatano, A.; Dotera, T. Monte Carlo simulations of the morphology of ABC star polymers using the diagonal bond method. *Macromolecules* **2002**, *35*, 3225-3237.

26.   Okamoto, S.; Hasegawa, H.; Hashimoto, T.; Fujimoto, T.; Zhang, H. M.; Kazama, T.; Takano, A.; Isono, Y. Morphology of model three-component three-arm star-shaped copolymers. *Polymer* **1997**, *38*, 5275-5281.

27.   Sioula, S.; Hadjichristidis, N.; Thomas, E. L. Direct evidence for confinement of junctions to lines in an 3 miktoarm star terpolymer microdomain structure. *Macromolecules* **1998**, *31*, 8429-8432.

28.   Takano, A.; Kawashima, W.; Wada, S.; Hayashida, K.; Sato, S.; Kawahara, S.; Isono, Y.; Makihara, M.; Tanaka, N.; Kawaguchi, D.; Matsushita, Y. Composition dependence of nanophase-separated structures formed by star-shaped terpolymers of the

A(1.0)B(1.0)C(x) type. *Journal of Polymer Science Part B-Polymer Physics* **2007**, *45*, 2277-2283.

29.   Li, Z. B.; Kesselman, E.; Talmon, Y.; Hillmyer, M. A.; Lodge, T. P. Multicompartment micelles from ABC miktoarm stars in water. *Science* **2004**, *306*, 98-101.

30.   Li, Z. B.; Hillmyer, M. A.; Lodge, T. P. Control of structure in multicompartment micelles by blending mu-ABC star terpolymers with AB diblock copolymers. *Macromolecules* **2006**, *39*, 765-771.

31.   Li, Z. B.; Hillmyer, M. A.; Lodge, T. P. Laterally nanostructured vesicles, polygonal bilayer sheets, and segmented wormlike micelles. *Nano Letters* **2006**, *6*, 1245-1249.

32.   Li, Z. B.; Hillmyer, M. A.; Lodge, T. P. Morphologies of multicompartment micelles formed by ABC miktoarm star terpolymers. *Langmuir* **2006**, *22*, 9409-9417.

33.   Liu, C.; Hillmyer, M. A.; Lodge, T. P. Multicompartment Micelles from pH-Responsive Miktoarm Star Block Terpolymers. *Langmuir* **2009**, *25*, 13718-13725.

34.   Saito, N.; Liu, C.; Lodge, T. P.; Hillmyer, M. A. Multicompartment Micelles from Polyester-Containing ABC Miktoarm Star Terpolymers. *Macromolecules* **2008**, *41*, 8815-8822.

35.   Saito, N.; Liu, C.; Lodge, T. P.; Hillmyer, M. A. Multicompartment Micelle Morphology Evolution in Degradable Miktoarm Star Terpolymers. *Acs Nano* **2010**, *4*, 1907-1912.

36.   Kong, W. X.; Li, B. H.; Jin, Q. H.; Ding, D. T.; Shi, A. C. Helical Vesicles, Segmented Semivesicles, and Noncircular Bilayer Sheets from Solution-State Self-

Assembly of ABC Miktoarm Star Terpolymers. *Journal of the American Chemical Society* **2009**, *131*, 8503-8512.

37.   Jiang, T.; Wang, L.; Lin, S.; Lin, J.; Li, Y. Structural Evolution of Multicompartment Micelles Self-Assembled from Linear ABC Triblock Copolymer in Selective Solvents. *Langmuir* **2011**, *27*, 6440-6448.

38.   Hadjichristidis, N. Synthesis of miktoarm star (mu-star) polymers. *Journal of Polymer Science Part a-Polymer Chemistry* **1999**, *37*, 857-871.

39.   Pennisi, R. W.; Fetters, L. J. Preparation of Asymmetric 3-Arm Polybutadiene and Polystyrene Stars. *Macromolecules* **1988**, *21*, 1094-1099.

40.   Iatrou, H.; Hadjichristidis, N. Synthesis of a Model 3-Miktoarm Star Terpolymer. *Macromolecules* **1992**, *25*, 4649-4651.

41.   Heise, A.; Trollsas, M.; Magbitang, T.; Hedrick, J. L.; Frank, C. W.; Miller, R. D. Star polymers with alternating,arms from miktofunctional mu-initiators using consecutive atom transfer radical polymerization and ring-opening polymerization. *Macromolecules* **2001**, *34*, 2798-2804.

42.   Celik, C.; Hizal, G.; Tunca, U. Synthesis of miktoarm star and miktoarm star block copolymers via a combination of atom transfer radical polymerization and stable free-radical polymerization. *Journal of Polymer Science Part a-Polymer Chemistry* **2003**, *41*, 2542-2548.

43.   He, T.; Li, D. J.; Sheng, X.; Zhao, B. Synthesis of ABC 3-miktoarm star terpolymers from a trifunctional initiator by combining ring-opening polymerization, atom transfer radical polymerization, and nitroxide-mediated radical polymerization. *Macromolecules* **2004**, *37*, 3128-3135.

44.   Gao, H. F.; Matyjaszewski, K. Synthesis of miktoarm star polymers via ATRP using the "in-out" method: Determination of initiation efficiency of star macroinitiators. *Macromolecules* **2006**, *39*, 7216-7223.

45.   Fragouli, P.; Iatrou, H.; Hadichristidis, N.; Sakurai, T.; Matsunaga, Y.; Hirao, A. Synthesis of well-defined miktoarm star polymers of poly(dimethylsiloxane) by the combination of chlorosilane and benzyl chloride linking chemistry. *Journal of Polymer Science Part a-Polymer Chemistry* **2006**, *44*, 6587-6599.

46.   Li, C.; Ge, Z.; Liu, H.; Liu, S. Synthesis of Amphiphilic and Thermo responsive ABC Miktoarm Star Terpolymer via a Combination of Consecutive Click Reactions and Atom Transfer Radical Polymerization. *Journal of Polymer Science Part a-Polymer Chemistry* **2009**, *47*, 4001-4013.

47.   Iskin, B.; Yilmaz, G.; Yagci, Y. ABC Type Miktoarm Star Copolymers Through Combination of Controlled Polymerization Techniques with Thiol-ene and Azide-Alkyne Click Reactions. *Journal of Polymer Science Part a-Polymer Chemistry* **2011**, *49*, 2417-2422.

48.   Huckstadt, H.; Abetz, V.; Stadler, R. Synthesis of a polystyrene-arm-polybutadiene-arm-poly(methyl methacrylate) triarm star copolymer. *Macromolecular Rapid Communications* **1996**, *17*, 599-606.

Chapter 2

Functional Miktoarm Star Terpolymers by an Association-and-Reaction Strategy
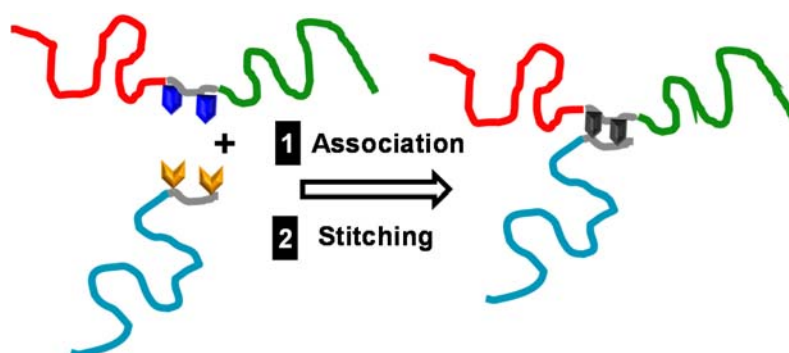
Abstract. Two functional miktoarm star terpolymers μ-(PtBA)(PSMA)(PCEMA) have been prepared by a modular approach, where PtBA, PCEMA, and PSMA denote poly($tert$-butyl acrylate), poly[2-(cinnamoyloxy)ethyl methacrylate], and poly(solketal methacrylate), respectively. In this approach, two PtBA-b-PCOOH-b-PSMA triblock copolymers containing a carboxyl group-bearing PCOOH block of five repeating units and a PNH$_2$-b-PCEMA diblock copolymer incorporating an amino group-bearing PNH$_2$ block of five repeating units were first prepared. The PCOOH and PNH$_2$ blocks then associated in solution, bringing a triblock copolymer chain and a diblock copolymer chain together. Functional μ-(PtBA)(PSMA)(PCEMA) copolymers were obtained after amidization reactions between the associated PCOOH and PNH$_2$ blocks. The effect of varying the reactant concentration on the yield and selectivity of μ-the (PtBA)(PSMA)(PCEMA) synthesis was examined. In addition, we developed fractional precipitation protocols for the purification of the resultant crude reacted mixtures to yield essentially pure μ-(PtBA)(PSMA)(PCEMA) samples.

2.1 Introduction

Tying together three different polymer chains (denoted as A, B, and C) by one end yields a μ-ABC miktoarm star terpolymer. μ-ABC terpolymers may self-assemble into various nanostructures with exotic morphologies, in a selective solvent or in bulk, depending on the copolymer composition and/or the solvent selectivity.[1-6] While some of these morphologies have been observed experimentally in the laboratories of Hillmyer and Lodge,[7-11] Hadjichristidis,[12-15] Hirao,[16] and Matsushita,[17-21] other theoretically-predicted morphologies [22-27] remain undiscovered. In order to gain an improved understanding of the micellization or solid-state block segregation behaviour of μ-ABC terpolymers, polymers with chemical compositions that differ from those that have been previously studied are needed. In addition, micellar chemical processing techniques involving the selective crosslinking[28, 29] and/or degradation[30-33] of particular domains (blocks) of copolymer micelles is an effective post-self-assembly strategy to create novel nanostructures. However, this strategy has rarely been used on μ-ABC micelles.[34] Thus, the synthesis of μ-ABC bearing readily crosslinkable or degradable blocks is required to facilitate the chemical processing of μ-ABC micelles. This chapter describes the synthesis of a novel family of two μ-ABC copolymers via a modular approach.

The μ-ABC samples that we have synthesized are μ-(PtBA)(PSMA)(PCEMA) terpolymers (Scheme 2.1), where PtBA, PSMA, and PCEMA denote poly($tert$-butyl acrylate), poly(solketal methacrylate), and poly[2-(cinnamoyloxy)ethyl methacrylate], respectively. In this modular approach, two PtBA-b-PCOOH-b-PSMA triblock copolymers containing a carboxyl group-bearing PCOOH block of five units and a PNH$_2$-b-PCEMA diblock copolymer containing an amino group-bearing PNH$_2$ block of five units

were first prepared. The PCOOH and PNH$_2$ blocks were then associated together in solution, thus merging a triblock terpolymer chain and a diblock copolymer chain together. Functional μ-(P*t*BA)(PSMA)(PCEMA) copolymers were eventually obtained after some groups of the associated PCOOH and PNH$_2$ blocks had underwent amidization reactions (Scheme 2.2).
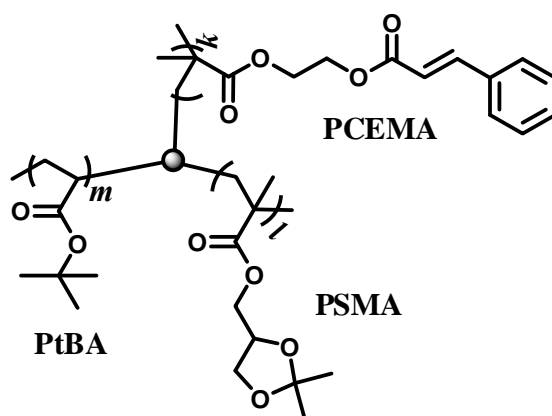
Scheme 2.1 Chemical structure of μ-(P*t*BA)(PSMA)(PCEMA).
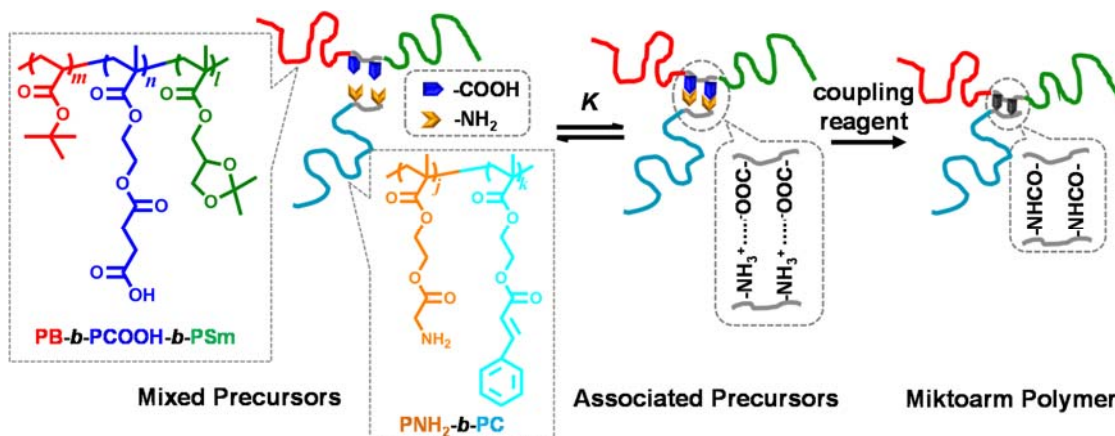
Scheme 2.2 Illustration of the steps involved in the preparation of μ-(P*t*BA)(PSMA)(PCEMA).

We have used this new strategy to prepare the μ-(PtBA)(PSMA)(PCEMA) samples because the synthesis of μ-ABC copolymers is generally challenging. The preparation of μ-ABC with arms possessing low polydispersity and functionality is especially challenging.[35] As mentioned in Chapter 1, miktoarm copolymers have traditionally been prepared through three general strategies. The first method is known as the "arms-first" approach.[36, 37] The different arms are prepared via living or controlled polymerizations first and then linked together to yield the star polymers. For instance, different polymer chains bearing a terminal anion can be linked by molecules containing multiple terminating sites (such as chloromethylphenylethyl)methyl dichlorosilane).[38] These linkage reactions can take days to reach completion and one can imagine the challenge of ensuring that the anions (and especially the anions of polymethacrylates) remain alive for so long. The second strategy is called the "grafting-from" approach, which involves the use of a trifunctional initiator and different monomers that are polymerized through different mechanisms in sequence.[39-41] Meanwhile, the third strategy is known as the "hybrid" approach, which combines features of the first two approaches.[35, 42-45] For example, a core molecule containing a mixture of terminating and initiating sites can be used to prepare μ-ABC.[35] Our approach differs from the previous approaches and our chain coupling chemistry can be performed under very mild conditions.

2.2 Experimental Section

2.2.1 Materials

Cinnamoyl chloride (98%), Z-glycine (99%), succinic anhydride (99%), hexamethylenediamine (98%), trifluoroacetic acid (TFA, 99%), 2-chloro-1-

methylpyridinium iodide (CMPI, 97%), *N,N'*-dicyclohexylcarbodiimide (DCC, 99%)，

tetrabutylammonium bromide (99%), 2-hydroxyethyl methacrylate (HEMA, 97%),

hexamethyldisilazane (98%), chlorotrimethylsilane (99%), *tert*-butyldimethylsilyl chloride

(97%), *D,L*-1,2-isopropylideneglycerol (98%), methacryloyl chloride (97%), *n*-butylamine

(99.5%), triethyl aluminum (1 M solution in hexanes), and *N,N*-dimethylformamide

(anhydrous, DMF) were purchased from Aldrich and used as received. Pyridine (Fisher

Scientific) was refluxed and distilled over CaH_2 under argon. Tetrahydrofuran (Fisher

Scientific) was refluxed and distilled over sodium under nitrogen with benzophenone as

indicator. *p*-Toluenesulfonic acid monohydrate (TSA, 98%) was dehydrated at 110 ^{o}C

under vacuum for 4 h and was then recrystallized in chloroform prior to use. Triethylamine

(TEA, Aldrich, 99.5%) was refluxed with *p*-toluensulfonyl chloride for 8 h and then

distilled. 1,1-Diphenylethylene was sequentially distilled over calcium hydride and *n*-butyl

lithium. *tert*-Butyl acrylate (Aldrich) was initially distilled over CaH_2, and was then freshly

titrated and redistilled over triethyl aluminum before polymerization. The monomers 2-

(trimethylsilyloxy)ethyl   methacrylate   (HEMA-TMS),[46]   2-(*tert*-

butyldimethylsilyloxy)ethyl methacrylate (HEMA-*t*BDMS)[47] and solketal methacrylate

(SMA)[47] were prepared and purified according to literature methods.

2.2.2 P(HEMA-tBDMS)-*b*-PHEMA

P(HEMA-*t*BDMS)-*b*-P(HEMA-TMS) was a precursor to PNH2-*b*-PCEMA and was

synthesized via sequential anionic polymerization in THF at -78 ^{o}C.[48] To a three-neck 1 L

round-bottom flask connected to a vacuum line was added 0.5624 g of LiCl. The flask

containing this salt was then vacuum-pumped and flamed-dried with a propane torch.

Approximately 600 mL of THF was then distilled into this flask. After the addition of 0.20

mL of 1,1-diphenylethylene (1.14 mmol, excess), *sec*-butyl lithium (1.4 M in cyclohexane) was added in a dropwise manner to titrate the impurities. After a persistent faint pink color developed, 0.56 mL (0.78 mmol) of the *sec*-butyl lithium solution was added. Subsequently, HEMA-*t*BDMS (0.99 mL, 3.9 mmol) was added dropwise and 2 h was allowed for the monomer to fully polymerize. This polymerization was followed by the slow addition of HEMA-TMS (20.6 mL, 94.5 mmol) and another 2 h polymerization period. The polymerization was terminated by adding 5.0 mL of degassed methanol/H_2O at v/v = 1/1.

In order to remove the trimethylsilyl group from the P(HEMA-TMS) block to yield poly(2-hydroxyethyl methacrylate) or PHEMA, another 100 mL of methanol/H_2O at v/v = 5/2 was added into the polymerization flask. The resultant mixture was stirred overnight at room temperature. Subsequently, the solution was rotary-evaporated to ~100 mL, and the condensate was sprayed onto crushed ice crystals that were added between different layers of the added condensate. After the ice melted, the polymer was collected via filtration and dried under vacuum overnight to yield 12.67 g of product in a 96% yield.

2.2.3 P(HEMA-*t*BDMS)-*b*-PCEMA

To prepare P(HEMA-*t*BDMS)-*b*-PCEMA, both P(HEMA-*t*BDMS)-*b*-PHEMA (5.10 g containing 36.5 mmol of hydroxyl groups) and cinnamoyl chloride (12.2 g, 73.2 mmol) were dissolved into freshly distilled pyridine (50 mL). This mixture was stirred overnight before the pyridinium chloride salt that had formed was settled by centrifugation and separated. The supernatant was added to 300 mL of methanol/H_2O (v/v = 9/1) in order to precipitate P(HEMA-*t*BDMS)-*b*-PCEMA.[49] The polymer was re-dissolved into 40 mL of THF and added into 300 mL of methanol/H_2O (v/v = 9/1) to precipitate the polymer.

After the precipitate had been dried under vacuum at room temperature overnight, 9.45 g of the product was obtained in a 96% yield.

2.2.4 PHEMA-*b*-PCEMA

To remove the *t*-butyldimethylsiloxy groups from the P(HEMA-*t*BDMS) block and thus yield a PHEMA block, 9.00 g of P(HEMA-*t*BDMS)-*b*-PCEMA was dissolved into 50 mL of THF. To this solution was then added 12.5 mL of a 1.0 M aqueous HCl solution. The mixture was stirred for 2 h before it was added into 300 mL of water in order to precipitate the polymer. After the precipitate was dried under vacuum at room temperature overnight, 8.61 g of PHEMA-*b*-PCEMA was obtained in a 97% yield.

2.2.5 PNH$_2$-*b*-PCEMA

In order to prepare P(NH$_2$-Cbz)-*b*-PCEMA, where P(NH$_2$-Cbz) denotes poly[2-(carbobenzyloxy-glycyl)ethyl methacrylate], 2.000 g of PHEMA-*b*-PCEMA (containing 0.31 mmol of hydroxyl groups) was dissolved into 12 mL of dry pyridine. To this solution under vigorous stirring were then added 0.130 g (0.62 mmol) of carbobenzyloxyglycine, 0.014 g (0.08 mmol) of TSA, and 0.150 g (0.74 mmol) of DCC (dispersed in 2 mL of dry pyridine). After the reaction mixture had been stirred for 12 h at room temperature, it was centrifuged and then the supernatant was diluted to 25 mL with THF before it was added into excess methanol to precipitate the polymer. After the precipitate was re-dissolved into 25 mL of THF, the polymer solution was added into excess methanol to precipitate the polymer again. This procedure was repeated another time. After the precipitate was dried under vacuum, 1.938 g of P(GNH$_2$-Cbz)-*b*-PCEMA was obtained in a 94% yield.

To remove the carbobenzyloxy protecting group, 1.800 g of P(GNH$_2$-Cbz)-*b*-PCEMA was dissolved into 10 mL of trifluoroacetic acid (TFA), and the resultant solution

was refluxed at 70 °C for 4 h. The TFA was then evaporated under vacuum. The resulting solid was then dissolved into 25 mL of pyridine, and this solution was added into excess methanol in order to precipitate the polymer. The polymer was subsequently re-dissolved in 25 mL of THF, and then added into methanol to precipitate the polymer. This procedure was repeated twice. After the precipitate was dried under vacuum, 1.622 g of PNH2-*b*-PCEMA was obtained in a 92% yield.

2.2.6 PtBA-*b*-PHEMA-*b*-PSMA

Two P*t*BA-*b*-PCOOH-*b*-PSMA samples were used to prepare μ-(P*t*BA)(PSMA)(PCEMA). The respective targeted repeat units were 100 and 5 for the P*t*BA and PCOOH blocks of both copolymers. Meanwhile, the targeted PSMA repeat unit numbers were 66 and 200 for the P*t*BA-*b*-PCOOH-*b*-PSMA$_{66}$ and P*t*BA-*b*-PCOOH-*b*-PSMA$_{200}$ copolymers, respectively. The P*t*BA-*b*-PCOOH-*b*-PSMA samples were derived from P*t*BA-*b*-P(HEMA-TMS)-*b*-PSMA copolymers that were prepared via anionic polymerization.

The P*t*BA-*b*-P(HEMA-TMS)-*b*-PSMA samples were prepared at -78 °C in the same manner as P(HEMA-*t*BDMS)-*b*-P(HEMA-TMS) using THF as the solvent. The polymerization time for each block was 2 h. To prepare P*t*BA-*b*-P(HEMA-TMS)-*b*-PSMA$_{200}$, the following reagents were used: LiCl (0.079 g), THF (6×10^2 mL), 1,1-diphenylethylene (0.20 mL or 1.14 mmol), *sec*-butyl lithium (0.265 mL at 1.4 M, or 0.37 mmol), B (5.39 mL, 37.2 mmol), HEMA-TMS (0.40 mL, 1.86 mmol), and Sm (14.4 mL, 74.3 mmol). Meanwhile, the procedure used to prepare P*t*BA-*b*-P(HEMA-TMS)-*b*-PSMA$_{66}$ utilized LiCl (0.147 g), THF (6×10^2 mL), 1,1-diphenylethylene (0.30 mL or 1.71

mmol), *sec*-butyl lithium (0.496 mL at 1.4 M or 0.69 mmol), B (10.1 mL, 69.4 mmol), HEMA-TMS (0.76 mL, 3.47 mmol), and Sm (10.1 mL, 46.2 mmol).

The trimethylsilyl groups were removed from the P(HEMA-TMS) blocks of the triblock copolymers via overnight hydrolysis reactions in methanol/water mixtures. The resultant polymers were concentrated and sprayed onto ice crystal layers to yield solid polymers. After they had been dried under vacuum, 19.210 g of P*t*BA-*b*-PHEMA-*b*-PSMA$_{200}$ and 18.230 g of P*t*BA-*b*-PHEMA-*b*-PSMA$_{66}$ were obtained at yields of 97% and 93%, respectively.

2.2.7 PtBA-*b*-PCOOH-*b*-PSMA

Excess succinic anhydride was reacted with P*t*BA-*b*-PHEMA-*b*-PSMA$_{200}$ and P*t*BA-*b*-PHEMA-*b*-PSMA$_{66}$ in order to produce P*t*BA-*b*-PCOOH-*b*-PSMA$_{200}$ (triblock copolymer **1**, or TBC**1**) and P*t*BA-*b*-PCOOH-*b*-PSMA$_{66}$ (TBC**2**). To produce TBC**1**, P*t*BA-*b*-PHEMA-*b*-PSMA$_{200}$ (4.00 g containing 0.35 mmol of hydroxyl groups) and 0.50 g (5.0 mmol) of succinic anhydride were dissolved into 30 mL of dry pyridine. After the mixture had been stirred for 12 h at room temperature, it was added into 300 mL of methanol/water (v/v = 8/2) to precipitate the polymer. The polymer was subsequently re-dissolved into 40 mL of THF and acetic acid was then added until the pH 5 was reached as measured by pH paper. This acidified solution was subsequently added into methanol/water (v/v = 8/2) to precipitate the polymer. The polymer was subsequently re-dissolved into 40 mL of THF and precipitated from methanol/water (v/v = 8/2). This procedure was repeated once. After the precipitate had been dried under vacuum, 3.645 g of P*t*BA-*b*-PCOOH-*b*-PSMA$_{200}$ was obtained in a 91% yield. P*t*BA-*b*-PHEMA-*b*-PSMA$_{66}$ was succinated and purified analogously.

2.2.8 μ-(PtBA)(PSMA)(PCEMA)

In a typical run, PNH$_2$-b-PCEMA (0.375 g or 1.17×10^{-2} mmol of chains) and TBC1 (0.629 g or 1.17×10^{-2} mmol of polymer chains) were mixed together and stirred in 200 mL of THF. After 2 h had passed, 5.0 mL of THF containing 17.9 mg of CMPI (7.02×10^{-2} mmol) and 19.5 μL of TEA (14.1×10^{-1} mmol) were added. The mixture was stirred for 6 h at room temperature before 4.6 μL of n-butylamine was added and the mixture was stirred for another 2 h to deactivate un-reacted carboxyl groups. A crude product was obtained by removing the THF via rotary-evaporation.

2.2.9 Purification of μ-(PtBA)(PSMA)(PCEMA)

The μ-(PtBA)(PSMA)(PCEMA) copolymers that were derived from TBC**1** and TBC**2** are denoted as μ-**1** and μ-**2**, respectively. To purify μ-**2**, water was added to 20 mL of THF containing 500 mg of crude μ-**2** until cloudiness developed. This cloudy solution was left standing in a fridge at 4 $^{\circ}$C overnight before it was centrifuged at 450 g for 5 min to settle the dense layer. Our size-exclusion chromatography (SEC) analysis indicated that the dense layer consisted mostly of μ-(PtBA)(PSMA)(PCEMA)$_2$. The supernatant was subsequently condensed under reduced pressure, and the solid was re-dissolved into ~20 mL of THF. This fractionation-precipitation protocol was repeated for this sample. SEC analysis of the new dense layer indicated that it consisted mostly of μ-**2** as well as PNH$_2$-b-PCEMA. Thus, the dense layer was re-dissolved into ~20 mL of THF and the fractionation was repeated another time. SEC analysis revealed that the dense layer essentially consisted of pure μ-**2**. This dense layer was subsequently diluted to ~2 mL with THF and added into 100 mL of water to precipitate the polymer. The copolymer was subsequently dried under vacuum to yield 120 mg of μ-**2**.

To purify μ-1, a THF solution containing the crude product was fractionated using the protocol mentioned above by adding water to mainly remove μ-(PtBA)(PSMA)(PCEMA)$_2$ side product. The sample was then fractionated again to obtain a mixture of μ-**1** and PNH$_2$-b-PCEMA as the dense layer. To separate the two copolymers, the mixture was re-dissolved into ~10 mL of a pre-made 0.2 M HCl solution (in THF) to hydrolyze PSMA into poly(monoglyceryl methacrylate) or PGMA. The solvent was subsequently removed via rotary-evaporation. The solid residue (without being fully dried) was dissolved in pyridine and added into excess nitromethane in order to precipitate μ-**1**.

2.2.10 ^{1}H NMR Analyses

^{1}H NMR spectra were recorded using a Bruker 300 MHz spectrometer. Depending on the solubility of the sample, either deuterated chloroform (CDCl$_3$) or deuterated pyridine (pyridine-d_5) were used as the solvents.

2.2.11 Size Exclusion Chromatography

The number-average molecular weight (M_n) and polydispersity index (M_w/M_n) of each polymer were determined using a Waters size exclusion chromatograph (SEC) system that was equipped with a Waters 2410 refractive index (RI) detector. A DMF solution containing tetrabutylammonium bromide (5 mg/mL) was heated at 70 ^{o}C and used as the eluent at a flow rate of 0.90 mL/min. The SEC columns were packed with ultra-styragel with the pore diameters of 1 000, 10 000, and 100 000 Å. The system was calibrated with narrowly-dispersed PS standards.

2.3 Results and Discussion

As mentioned in the Introduction, two μ-(PtBA)(PSMA)(PCEMA) samples (μ-**1** and μ-**2**) were synthesized by a modular approach involving first the preparation of a PNH$_2$-b-PCEMA diblock copolymer and two PtBA-b-PCOOH-b-PSMA triblock copolymers (TBC**1** and TBC**2**). While the targeted repeat unit numbers for PNH$_2$ and PCOOH blocks were five, the targeted lengths for the PCEMA and PtBA blocks were 120 and 100 units, respectively. The PSMA blocks of TBC**1** and TBC**2** were targeted at 200 and 66 repeat units, respectively. TBC**1** or TBC**2** was reacted individually with PNH$_2$-b-PCEMA to yield μ-**1** or μ-**2**.

Short PCOOH and PNH$_2$ blocks of five units were used, because we failed to produce a miktoarm copolymer when we reacted TBC**1** with a 120-unit-long poly(methyl methacrylate) (PMMA) polymer bearing only one terminal amino group. This was presumably due to the weak attraction between only one amino group and a PCOOH block as well as the strong repulsion between the PMMA chain and both the PtBA and PSMA blocks of TBC**1**.

2.3.1 PNH$_2$-b-PCEMA preparation

PNH$_2$-b-PCEMA was prepared in six steps (Scheme 2.3). First, P(HEMA-tBDMS)-b-P(HEMA-TMS) was prepared via anionic polymerization.[46, 47] Since P(HEMA-tBDMS) was more stable than P(HEMA-TMS), the TMS protecting groups were selectively removed in step 2 to yield P(HEMA-tBDMS)-b-PHEMA.[3] The PHEMA block was then reacted with cinnamoyl chloride in step 3 to yield a PCEMA block. This was followed by the cleavage of the tBDMS protecting groups in step 4 to yield PHEMA-b-PCEMA. During step 5, the PHEMA block was reacted with N-carbobenzyloxyglycine (Z-glycine)

to yield P(HEMA-GlyCbz)-*b*-PCEMA. Finally, the removal of the carbobenzyl protection

group by trifluoroacetic acid yielded PNH$_2$-*b*-PCEMA.
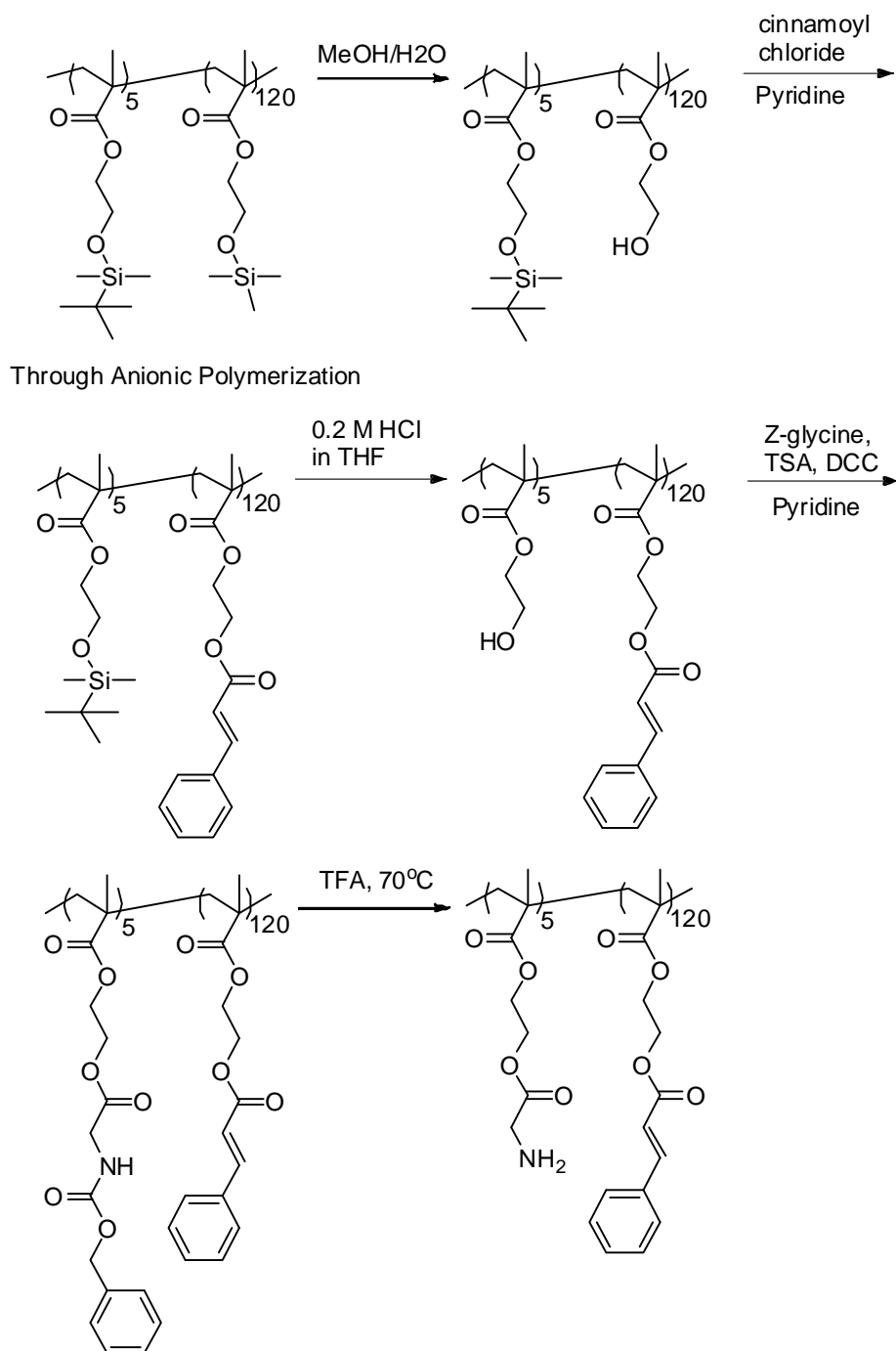
Scheme 2.3 Synthetic pathway toward PNH$_2$-*b*-PCEMA.

49
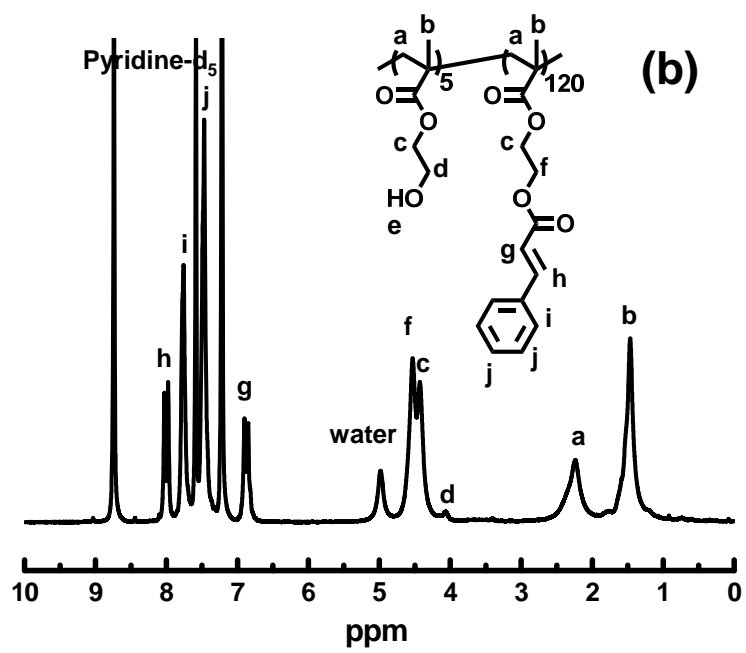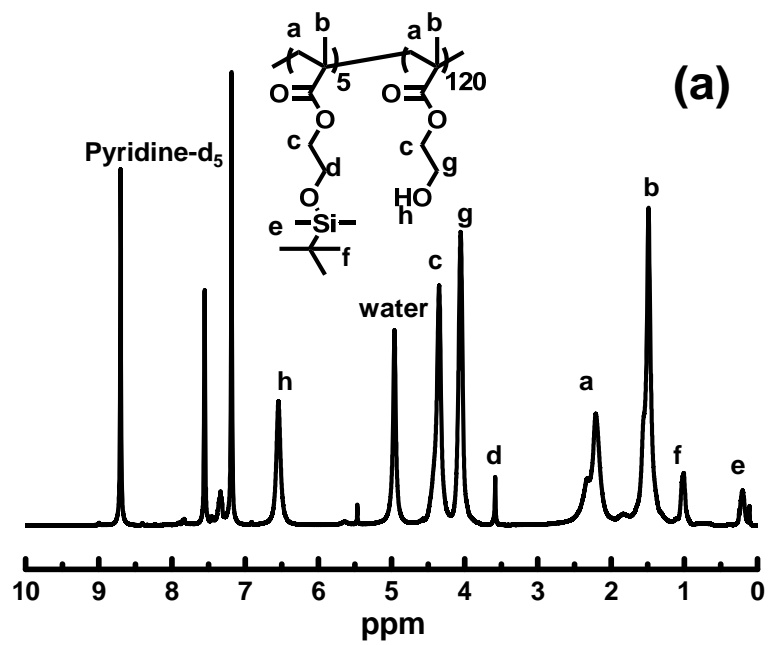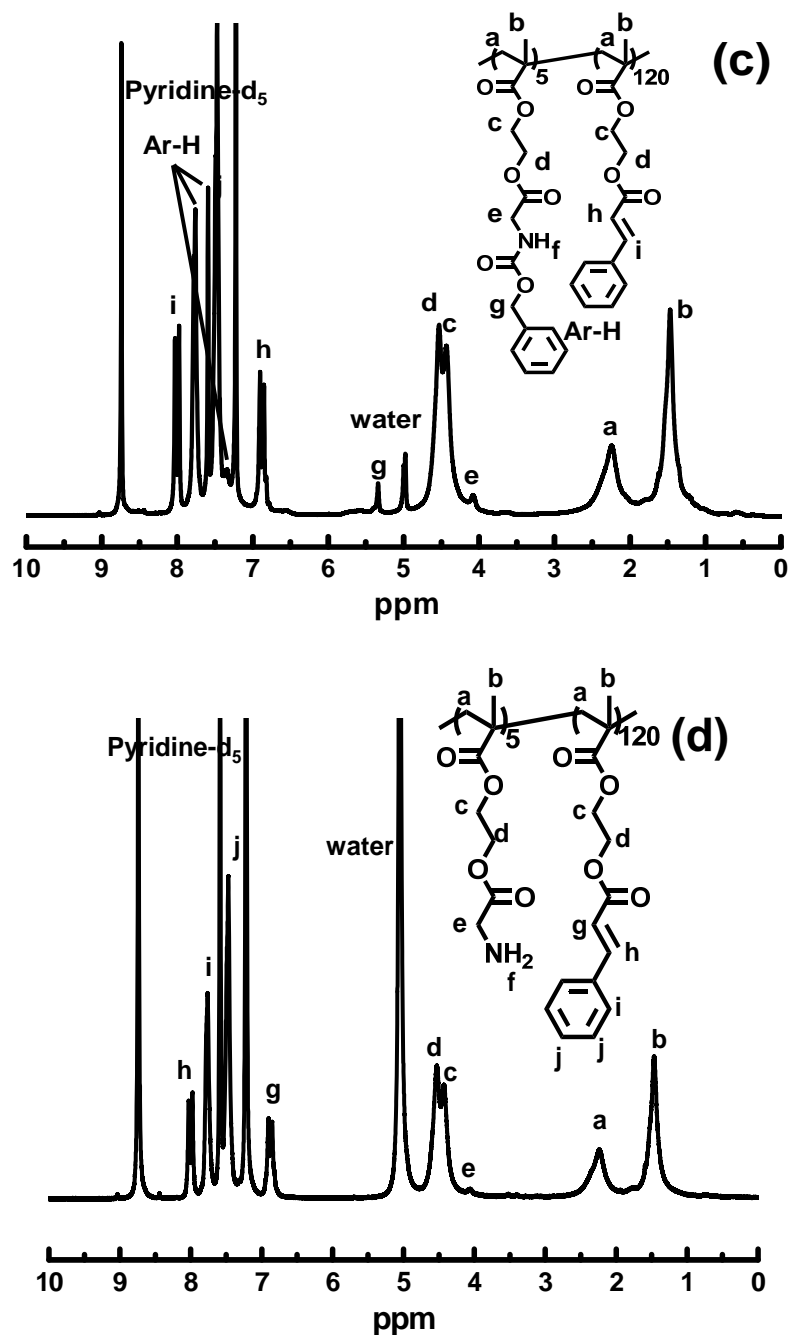
Figure 2.1 ¹H NMR spectra of (a) P(HEMA-*t*BDMS)-*b*-PHEMA, (b) PHEMA-*b*-PCEMA, (c) P(NH₂-Cbz)-*b*-PCEMA, and (d) PNH₂-*b*-PCEMA. Pyridine-*d₅* was used as the solvent in each case.

PNH$_2$-b-PCEMA and its precursors were characterized by ^{1}H NMR spectroscopy using pyridine-d_5 as the solvent. Figure 2.1 compares the ^{1}H NMR spectra of P(HEMA-tBDMS)-b-PHEMA, PHEMA-b-PCEMA, P(NH$_2$-Cbz)-b-PCEMA, and PNH$_2$-b-PCEMA together with their peak assignments. The data suggests that each derivatization was successful. In addition, the ratios between the repeat unit numbers of the first and second blocks were determined from their characteristic peak integrations. For example, we determined at the P(HEMA-tBDMS)-b-PHEMA stage an integration ratio of 45/490 between the f signal and the ($c + g$) peaks. This value allowed us to calculate a repeat unit ratio of 22/1 for the PHEMA and P(HEMA-tBDMS) blocks. The value was consistent within experimental error with the value of 24 expected for the targeted polymer consisting of 120 HEMA and five HEMA-tBDMS units.

PNH$_2$-b-PCEMA and some of its precursors such as P(HEMA-tBDMS)-b-PCEMA, PHEMA-b-PCEMA, and P(NH$_2$-Cbz)-b-PCEMA were also characterized by size-exclusion chromatography (SEC). Figure 2.2 shows the SEC traces of these samples. The key observation was that all of the peaks had a similar shape and were narrow, possessing polydispersity indices of less than 1.05 in terms of PS standards. The similar shapes suggested that the derivatization did not change the backbone structure of the polymer, but only the targeted pendant groups. The low polydispersity indices confirmed that the anionic polymerization had proceeded smoothly.
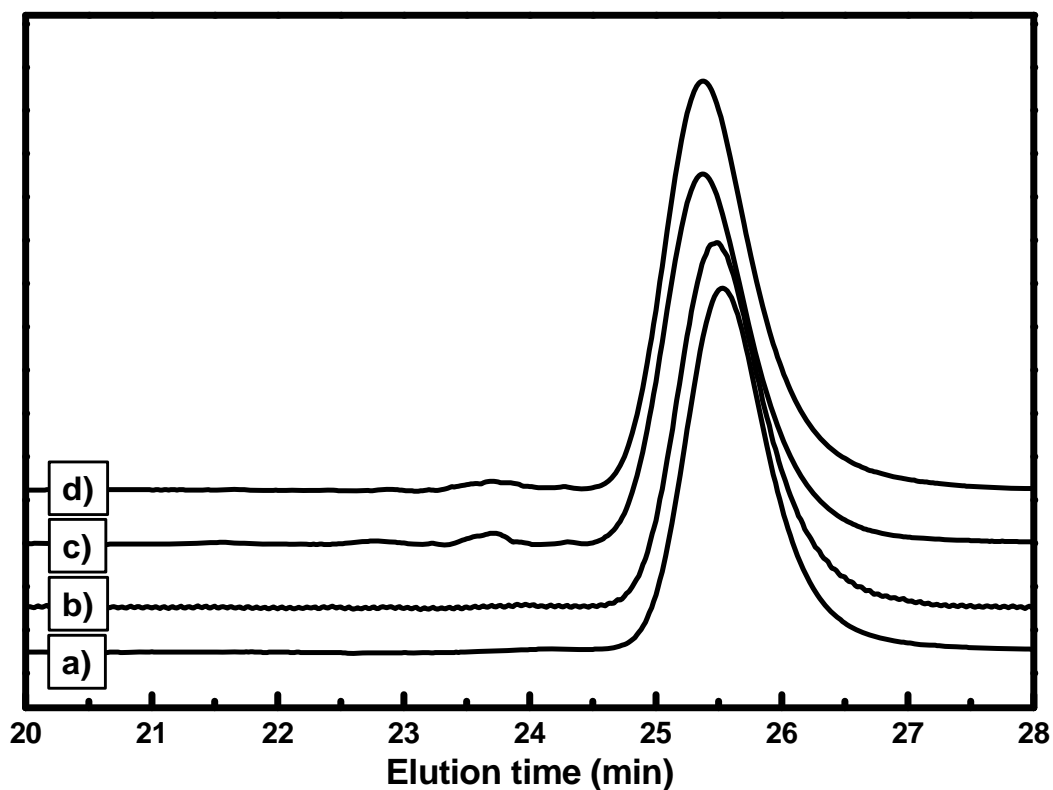
Figure 2.2 SEC traces of (a) P(HEMA-*t*BDMS)-*b*-PCEMA, (b) PHEMA-*b*-PCEMA, (c) P(NH$_2$-Cbz)-*b*-PCEMA, and (d) PNH$_2$-*b*-PCEMA.

We did not determine the absolute molecular weight of PNH$_2$-*b*-PCEMA because the main objective of this work was to prepare the novel functional *μ*-(P*t*BA)(PSMA)(PCEMA) copolymer. Furthermore, the molecular weight of PNH$_2$-*b*-PCEMA should be close to the targeted value of 32 kg/mol for PNH$_2$-*b*-PCEMA consisting of 5 amino-bearing units and 120 C units since the precursor P(HEMA-*t*BDMS)-*b*-P(HEMA-TMS) was prepared via anionic polymerization. Incidentally, the targeted molecular weight of 32 kg/mol was in reasonably close agreement with the value of 40 kg/mol determined via SEC using columns that had been calibrated using PS standards (Table 2.1).

Table 2.1 SEC and NMR characteristics of the precursors.

Sample	SEC M_n (kg/mol)	SEC M_w/M_n	NMR j/k or $m/n/l$
PHEMA-*b*-PCEMA	38	1.02	5/122
P(NH$_2$-Cbz)-*b*-PCEMA	40	1.02	5/121
PNH$_2$-*b*-PCEMA	40	1.02	
P*t*BA-*b*-PHEMA-*b*-PSMA$_{200}$	60	1.05	
P*t*BA-*b*-PCOOH-*b*-PSMA$_{200}$	61	1.05	102/5/201
P*t*BA-*b*-PHEMA-*b*-PSMA$_{66}$	37	1.03	
P*t*BA-*b*-PCOOH-*b*-PSMA$_{66}$	38	1.03	101/5/66

2.3.2 Synthesis of PtBA-*b*-PCOOH-*b*-PSMA

While the respective targeted repeat units were 100 and 5 for the P*t*BA and PCOOH blocks of both TBC**1** and TBC**2**, the PSMA repeat unit numbers were 66 and 200 for these respective copolymers. TBC**1** and TBC**2** were prepared via the synthetic pathways depicted in Scheme 2.4. First, the P*t*BA-*b*-P(HEMA-TMS)-*b*-PSMA copolymers were prepared via anionic polymerization. The TMS protecting groups were then selectively removed during step 2.[3] The resultant hydroxyl groups of the central PHEMA block were then reacted with excess succinic anhydride to yield P*t*BA-*b*-PCOOH-*b*-PSMA.
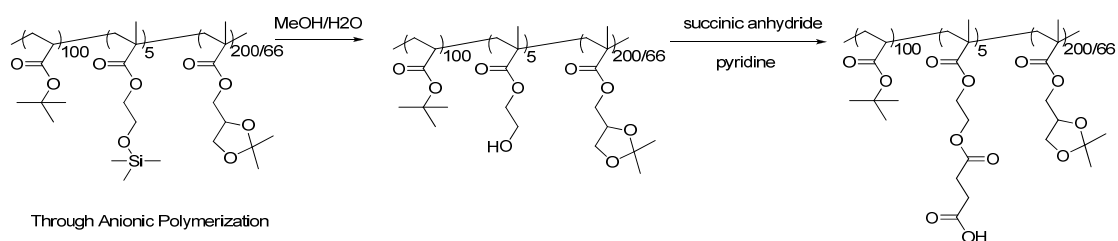
Scheme 2.4 Synthetic pathway toward P*t*BA-*b*-PCOOH-*b*-PSMA.

The PHEMA block was reacted with succinic anhydride in pyridine. To ensure that the pendant carboxyl groups were mostly in their acidic form, the precipitated crude P*t*BA-*b*-PCOOH-*b*-PSMA copolymer was re-dissolved into a THF solution containing acetic acid before it was re-precipitated out from a water/methanol mixture. The weak acetic acid was used because PSMA readily undergoes hydrolysis when it is treated with a strong acid such as hydrochloric acid.

The P*t*BA-*b*-PCOOH-*b*-PSMA samples and their precursor P*t*BA-*b*-PHEMA-*b*-PSMA samples were characterized by ^{1}H NMR spectroscopy in pyridine-d_5. Figure 2.3 shows the spectra of these samples along with their peak assignments. The signals labeled as *g* in Figure 2.3b and 2.3d clearly demonstrate our success at the targeted reactions. Our quantitative analysis yielded the integration ratios of 910/20/1060 and 900/20/350 among the *c*+*g*, and the *e*+*f*+*i* signals for TBC**1** and TBC**2**, respectively. Based on the targeted repeat unit ratio of 100/5/200 for the *b*, COOH, and *c* signals of TBC**1**, the integration ratio should be 900/20/1020. Meanwhile, this ratio should be 900/20/350 for TBC**2**. The experimental values were consistent with the experimental values.

54
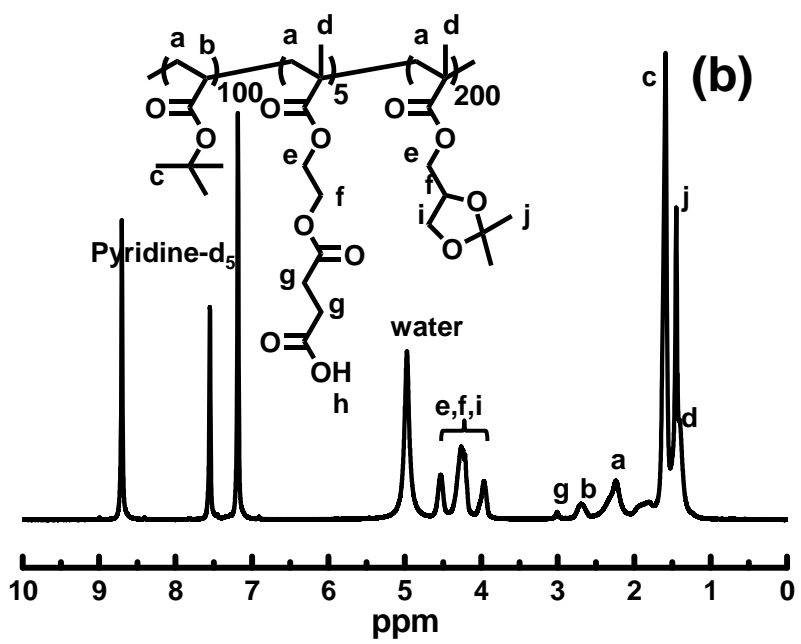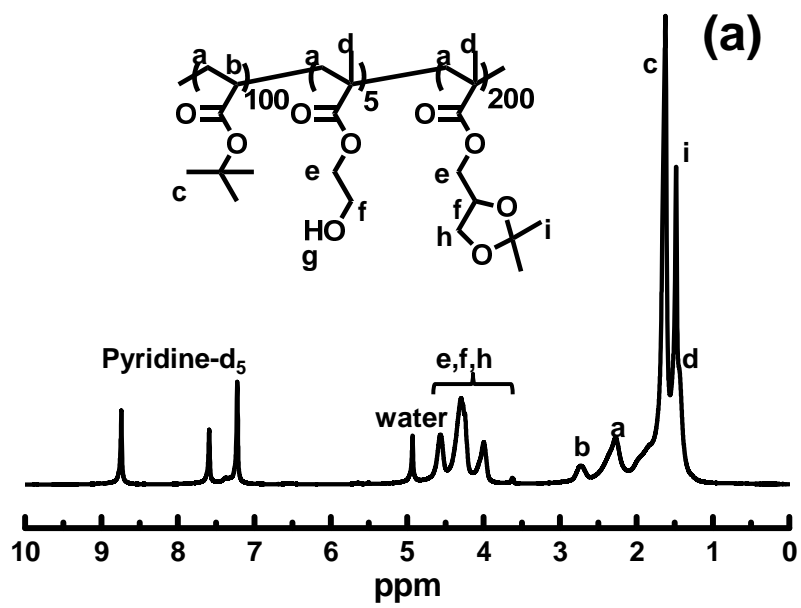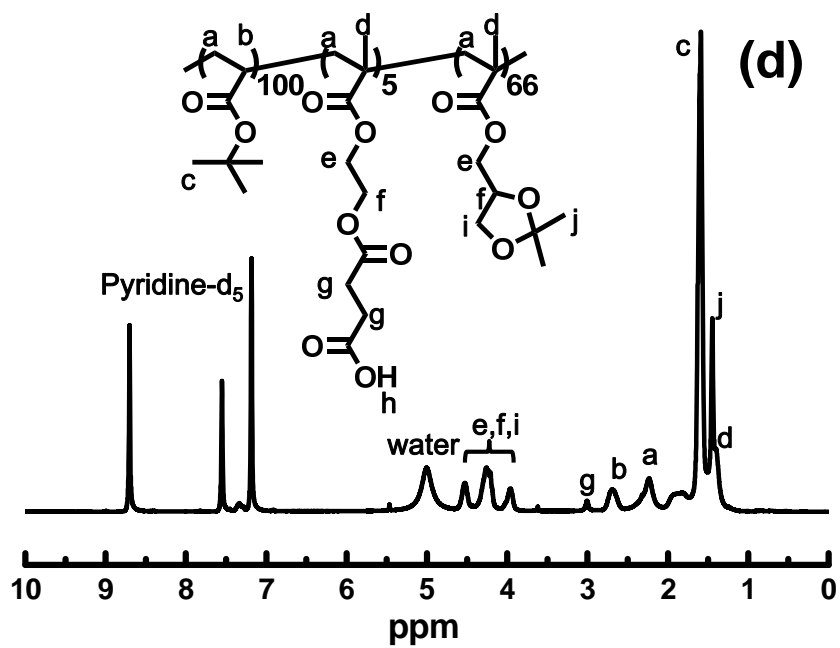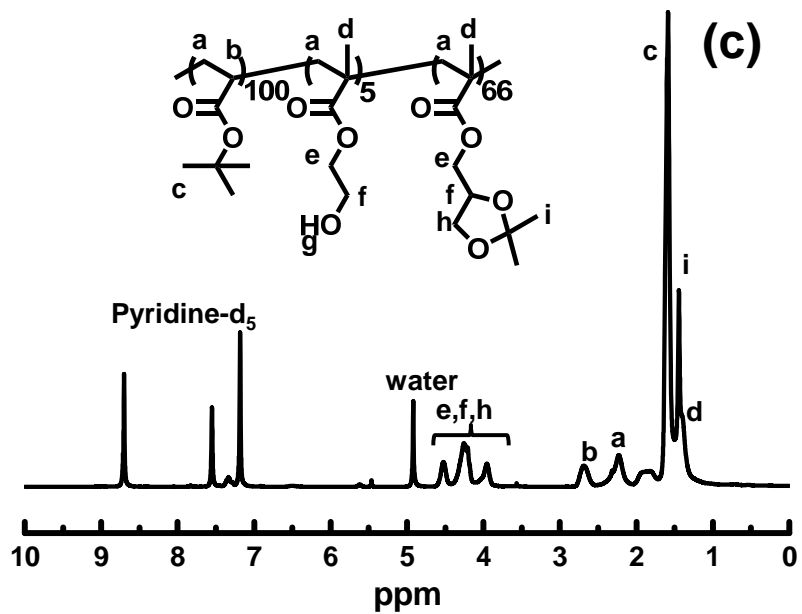
Figure 2.3 Comparison of ^{1}H NMR spectra of (a) P*t*BA-*b*-PHEMA-*b*-PSMA$_{200}$, (b) TBC**1**, (c) P*t*BA-*b*-PHEMA-*b*-PSMA$_{66}$, and (d) TBC**2**.

The samples were also analyzed by SEC and the results are shown in Figure 2.4. As expected, TBC**1** had a shorter retention time than TBC**2**. In terms of PS standards, the M_n values of TBC**1** and TBC**2** were 61 and 38 kg/mol, respectively (see Table 2.1). These values were reasonably consistent with the respective targeted molecular weights of 54 and 27 kg/mol for TBC**1** and TBC**2**. The two sets of data were not in exact agreement because the PS standards used for SEC calibration bear no structural resemblance to the triblock copolymers. The low polydispersity indices of the polymers (Table 2.1) suggested again that our synthesis and derivatization of the polymers was successful.
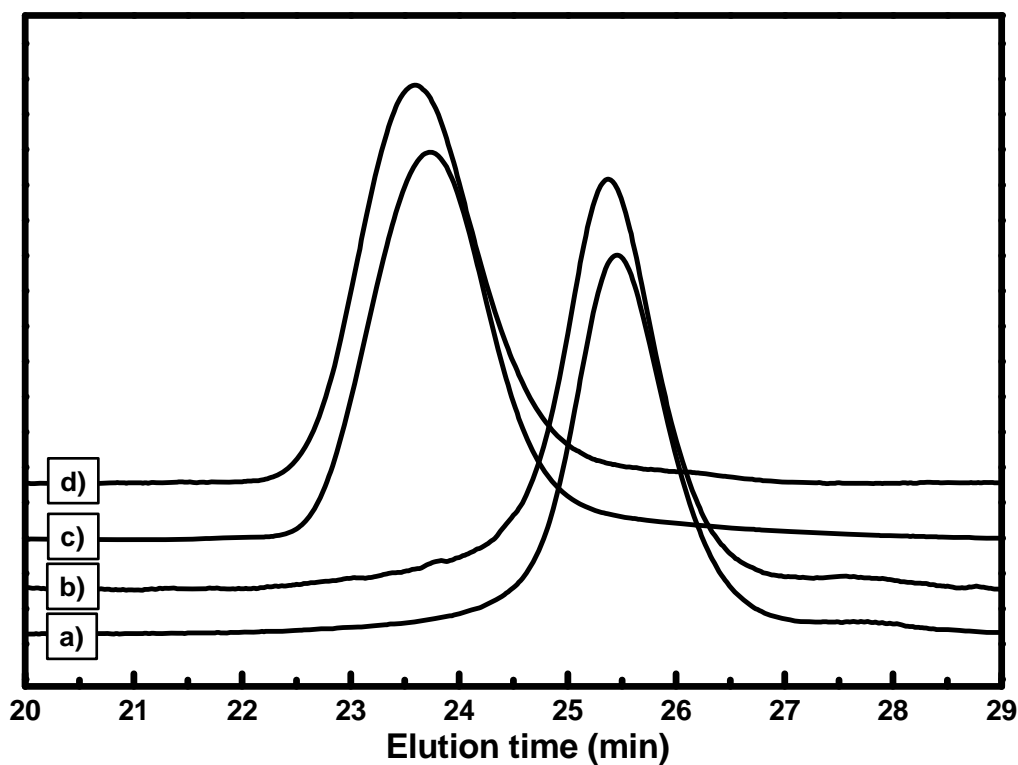
Figure 2.4 SEC traces of (a) P*t*BA-*b*-PHEMA-*b*-PSMA$_{66}$, (b) TBC**2**, (c) P*t*BA-*b*-PHEMA-*b*-PSMA$_{200}$, and (d) TBC**1**.

2.3.3 Synthesis of *μ*-(P*t*BA)(PSMA)(PCEMA)

The *μ*-(P*t*BA)(PSMA)(PCEMA) miktoarm star copolymers were prepared in two steps. In step 1, PNH$_2$-*b*-PCEMA and either TBC**1** or TBC**2** were stirred together in THF in order to establish an association equilibrium between these precursors. During step 2, a coupling agent 2-chloro-1-methylpyridinium iodide (CMPI) was added along with triethylamine to stitch the associated chains together. Triethylamine was added during this step to neutralize the HCl and HI that were generated from the stitching reaction (Scheme 2.5). This method has previously been used to prepare a *μ*-AB$_2$ miktoarm copolymer.[50] The PNH$_2$ and PCOOH blocks used in that case were longer than 22 repeat units. Our polymers have much shorter PNH$_2$ and PCOOH blocks at only 5 repeat units and thus the coupled products obtained here better resembled miktoarm copolymers.
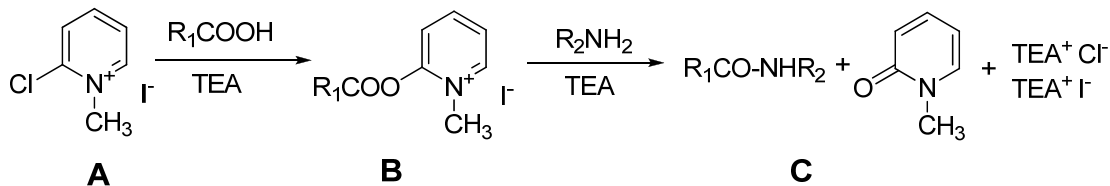
Scheme 2.5 Amidization reaction facilitated by the coupling agent CMPI.
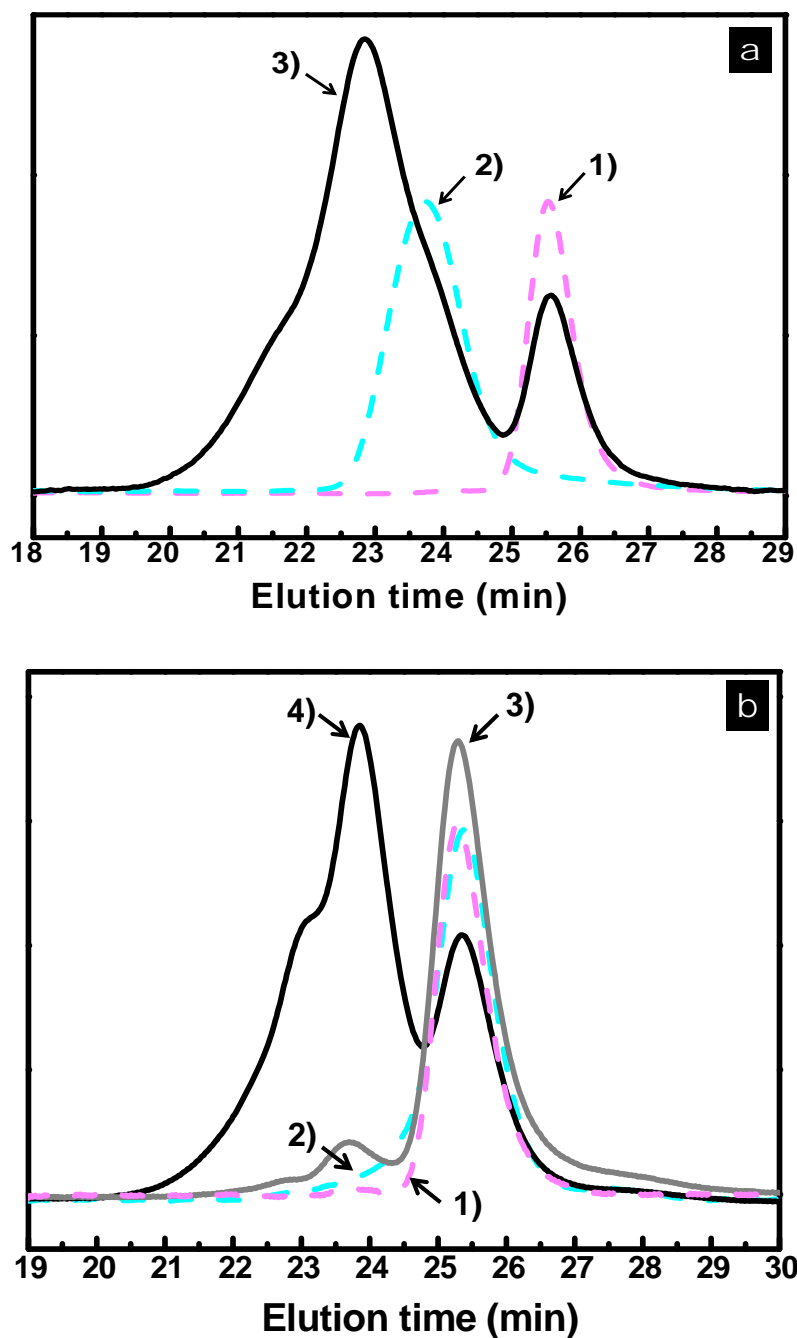
Figure 2.5 (a) SEC traces of 1) PNH$_2$-*b*-PCEMA, 2) TBC**1**, and 3) a crude reaction mixture of PNH$_2$-*b*-PCEMA and TBC**1** at a molar ratio of 1.00/1.00. (b) SEC traces of 1) PNH$_2$-*b*-PCEMA, 2) TBC**2**, 3) a physical mixture of PNH$_2$-*b*-PCEMA and TBC**2** at a molar ratio of 1.00/1.00, and 4) a crude reaction mixture of PNH$_2$-*b*-PCEMA and TBC**2** at a molar ratio of 1.00/1.00.

The μ-**1** or μ-**2** miktoarm copolymers were prepared by reacting PNH$_2$-b-PCEMA with either TBC**1** or TBC**2** at a molar ratio of 1.00/1.00. In order to calculate the molar concentrations, the number-average molecular weights M_n of the polymers were evaluated based on their targeted repeat unit numbers for the individual blocks. The crude products were then analyzed via SEC. Figure 2.5 shows the SEC traces of crude products obtained from trials that used a total polymer concentration of 10.0 mg/mL. Also shown are SEC traces that were measured using a refractive index detector to characterize their precursors. In the case of μ-**2**, the SEC trace of a physical mixture consisting of PNH$_2$-b-PCEMA and TBC**2** at the molar ratio of 1/1 is also provided.

In both cases, a peak with a shorter retention time or a higher molecular weight was seen for the crude reaction mixture, suggesting the formation of μ-**1** and μ-**2**. Based on PS standards, the molecular weights corresponding to the μ-**1** and μ-**2** peaks were 95 and 59 kg/mol, respectively. However, unreacted precursors were also present in the crude products, although they were observed in lower amounts. In addition, a shoulder peak with a PS-equivalent peak molecular weight of 120 or 90 kg/mol was observed for the μ-**1** or μ-**2** crude product, respectively.

These shoulders peaks are likely due to formation of μ-(PtBA)(PSMA)(PCEMA)$_2$ through the linkage of two PNH$_2$-b-PCEMA chains by one TBC chain. This was possible because of the distributions in the number of amino and carboxyl groups in the PNH$_2$ and PCOOH blocks. The shoulders arose due to μ-(PtBA)(PSMA)(PCEMA)$_2$ rather than from the formation of μ-(PtBA)$_2$(PSMA)$_2$(PCEMA) by the linkage of two TBC chains with one PNH$_2$-b-PCEMA chain. The latter formation would be less likely because the steric hindrance associated with clustering of two TBC chains around the same PNH$_2$ block of a

PNH$_2$-*b*-PCEMA chain would be much higher than that encountered as bring two PNH$_2$-*b*-PCEMA chains would be brought closer to a TBC chain. Furthermore, we have previously used this technique to prepare μ-AB$_2$ samples and a shoulder peak was also observed in that case.[50] We fractionated the polymer that corresponded to the shoulder peak and our ^{1}H NMR analysis of the shoulder component confirmed that it consisted of a product derived from the reaction between two diblock copolymer chains and one triblock copolymer chain.

Another notable observation was that a weak peak at the μ-**2** peak position was detected for the physical mixture of PNH$_2$-*b*-PCEMA and TBC**2** before the coupling agent CMPI was added. This provided direct evidence for the association of the PNH$_2$-*b*-PCEMA and TBC**2** precursors even when the sample was highly diluted by the SEC eluent that consisted of a DMF solution containing tetrabutylammonium bromide.

2.3.4 SEC Peak Deconvolution

In order to determine the amounts of μ-(P*t*BA)(PSMA)(PCEMA) and μ-(P*t*BA)(PSMA)(PCEMA)$_2$ formed, the SEC traces of the crude products were resolved using a commercial program, Peakfit, into peaks corresponding to μ-ABC, μ-ABC$_2$ and their block copolymer precursors.[50] Figure 2.6 shows an example of how a SEC trace was resolved by the Peakfit program into individual peaks corresponding to μ-ABC, μ-ABC$_2$, and their precursors.
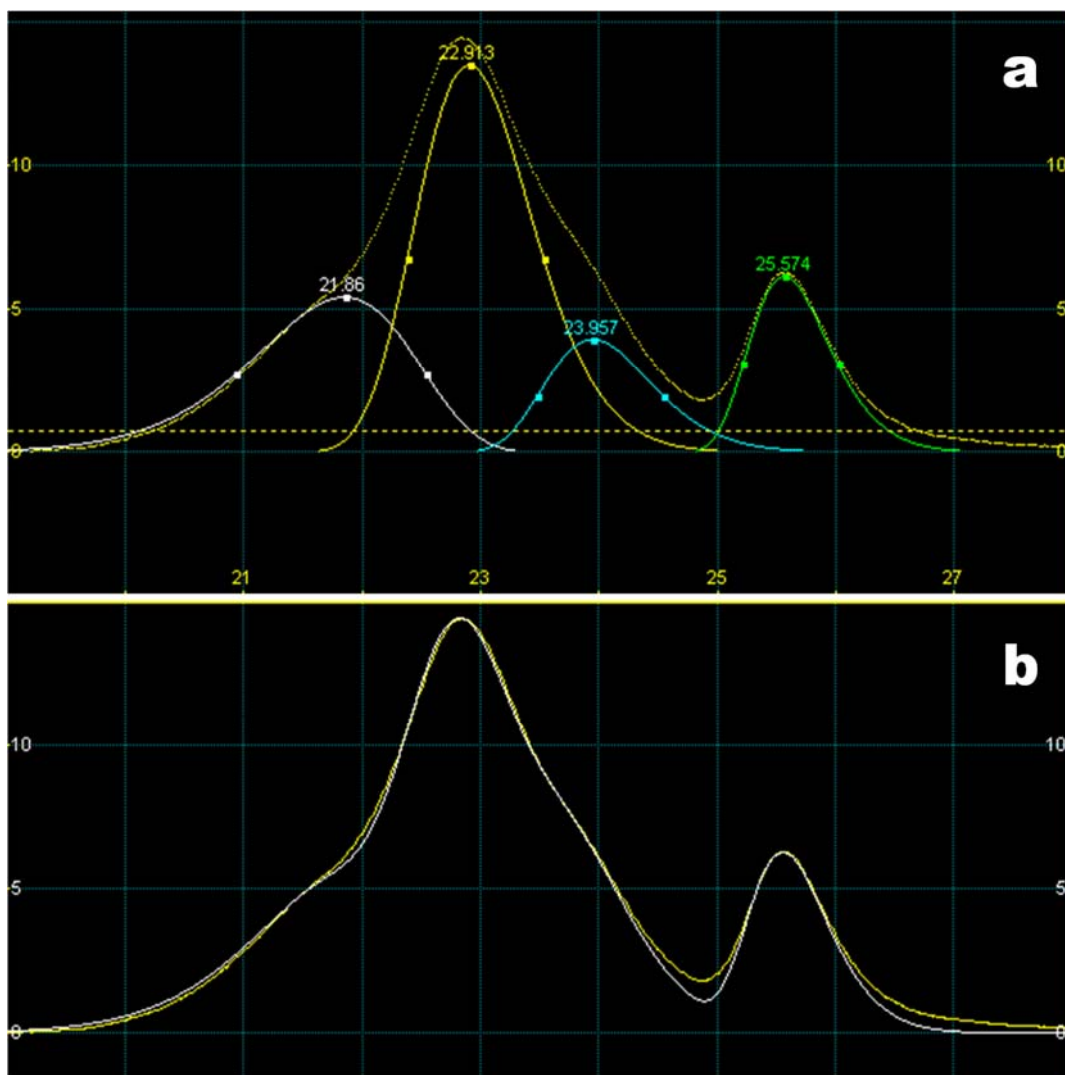
Figure 2.6 (a) Comparison of the original SEC trace of a crude μ-**1** product (dotted curve shown in light yellow) with de-convoluted peaks corresponding to μ-ABC$_2$, μ-ABC, TBC**1**, and PNH$_2$-b-PCEMA (colored curves from left to right). (b) Comparison between the SEC trace of the above-mentioned crude μ-**1** product (dotted yellow curve) and the fitting curve (white solid curve), whose intensity at a given retention time is the sum of intensities corresponding to the μ-ABC$_2$, μ-ABC, TBC**1**, and PNH$_2$-b-PCEMA curves.

2.3.5 Relationship Between the Mass Amount and the Peak Area

When a trace generated by a refractive index detector is analyzed, its area A is related to the sample's component mass amount M and its specific refractive index increment dn/dc by eq. 2.1:

$$A \propto M \left(\frac{dn}{dc}\right)$$

Equation 2.1

Another form of this equation allows us to compare the mass corresponding to each sub-peak resolved from the crude product SEC trace as expressed by eq. 2.2:

$$M \propto \frac{A}{\frac{dn}{dc}}$$

Equation 2.2

Here, the A value of each sub-peak is given by the Peakfit program.

The dn/dc values of all the precursors in the SEC eluent were determined using a Wyatt Optilab rEX instrument. The dn/dc values of the μ-ABC and μ-ABC$_2$ miktoarm polymers were subsequently calculated from the dn/dc values of their constituent copolymers using eq. 2.3:

$$\left(\frac{dn}{dc}\right) = w_1 \left(\frac{dn}{dc}\right)_1 + w_2 \left(\frac{dn}{dc}\right)_2$$

Equation 2.3

where the subscripts 1 and 2 denote PNH$_2$-b-PCEMA and TBC**1/2**, respectively. Meanwhile, w_1 and w_2 correspond to their respective weight fractions, while $(dn/dc)_1$ and $(dn/dc)_2$ are the respective dn/dc values of the precursors. Table 2.2 summarizes the experimental and calculated dn/dc values corresponding to all the sub-peaks.

Table 2.2 dn/dc values of the precursors and miktoarm polymers as observed via SEC.[a]

Sample	dn/dc (mL/g)
P(GNH$_2$)$_5$-b-PCEMA$_{120}$	0.1365 ± 0.0004
PtBA$_{100}$-b-PCOOH$_5$-b-PSMA$_{200}$	0.0514 ± 0.0002
PtBA$_{100}$-b-PCOOH$_5$-b-PSMA$_{66}$	0.0445 ± 0.0005
μ-(PSMA$_{66}$)(PtBA$_{100}$)(PCEMA$_{120}$)	0.0943 ± 0.0004[b]
μ-(PSMA$_{66}$)(PtBA$_{100}$)(PCEMA$_{120}$)$_2$	0.1091 ± 0.0004[2]
μ-(PGMA$_{200}$)(PtBA$_{100}$)(PCEMA$_{120}$)	0.0832 ± 0.0003[2]
μ-(PGMA$_{200}$)(PtBA$_{100}$)(PCEMA$_{120}$)$_2$	0.0977 ± 0.0003[2]

[a] SEC measurements were performed using a DMF solution containing 5 mg/mL of tetrabutylammonium bromide as the eluent at a flow rate of 0.9 mL/min.

[b] Calculated from the experimental results of precursors based on Equation 2.3.

2.3.6 Effect of Varying the Reactant Concentration.

The SEC traces of the crude μ-**1** and μ-**2** products were de-convoluted using the PeakFit program. In the case of the crude μ-**1** products, the SEC trace was de-convoluted into four peaks belonging to μ-(PtBA)(PSMA)(PCEMA)$_2$, μ-**1**, TBC**1**, and PNH$_2$-b-PCEMA. The area of each peak was then integrated. Dividing each area by the dn/dc value yielded the component mass for a particular constituent of a crude product. The total component mass present in a sample was calculated from sum of the dn/dc-corrected areas of all peaks. The yield of a product was then obtained from the ratio of its dn/dc-corrected area with respect to the total dn/dc-corrected area. Dividing the dn/dc-corrected area of a particular product by its molar mass yielded the number of moles of that component that was present and the molar quantities of μ-(PtBA)(PSMA)(PCEMA)$_2$ and μ-**1** produced

were thus used to calculate the molar ratio for these two components in a given sample. In these calculations, we used the dn/dc values determined experimentally for TBC**1** and PNH$_2$-b-PCEMA. The dn/dc values for μ-(PtBA)(PSMA)(PCEMA)$_2$ and μ-**1** were calculated from those of TBC**1** and PNH$_2$-b-PCEMA and their known polymer compositions.

The above data analysis method allowed us to examine the SEC traces of samples prepared at different total polymer concentrations c_p. Shown in Figure 2.7 are results that we obtained from a series of coupling experiments performed in THF at room temperature for 6 h after CMPI addition. In these experiments, the total precursor concentration c_p was changed but the molar concentration ratio between PNH$_2$-b-PCEMA and TBC**1** was kept fixed at 1.00/1.00. The yields of μ-(PtBA)(PSMA)(PCEMA)$_2$ and μ-**1** as well as the total yield of μ-ABC$_2$ and μ-**1** increased initially as c_p increased. The yields plateaued at high c_p values.

Figure 2.7a further suggests that the yield of μ-**1** increased more sharply with c_P before reaching a plateau, than that of μ-(PtBA)(PSMA)(PCEMA)$_2$. Thus, the targeted product μ-**1** was preferentially formed at low c_P values This trend was more apparent in Figure 2.7b where the molar concentration ratios of μ-(PtBA)(PSMA)(PCEMA)$_2$ and μ-**1** formed at different c_P's were plotted as a function of c_P. [μ-(PtBA)(PSMA)(PCEMA)$_2$]/[μ-**1**] increased almost linearly with c_p. Thus, data shown in Figure 2.7 suggest that μ-**1** should have been prepared at c_P ~2.5 mg/mL, where the overall product yield and the selectivity for μ-**1** were reasonably high. For large-scale preparations, we normally used $c_P = 5$ mg/mL in order to reduce solvent consumption.
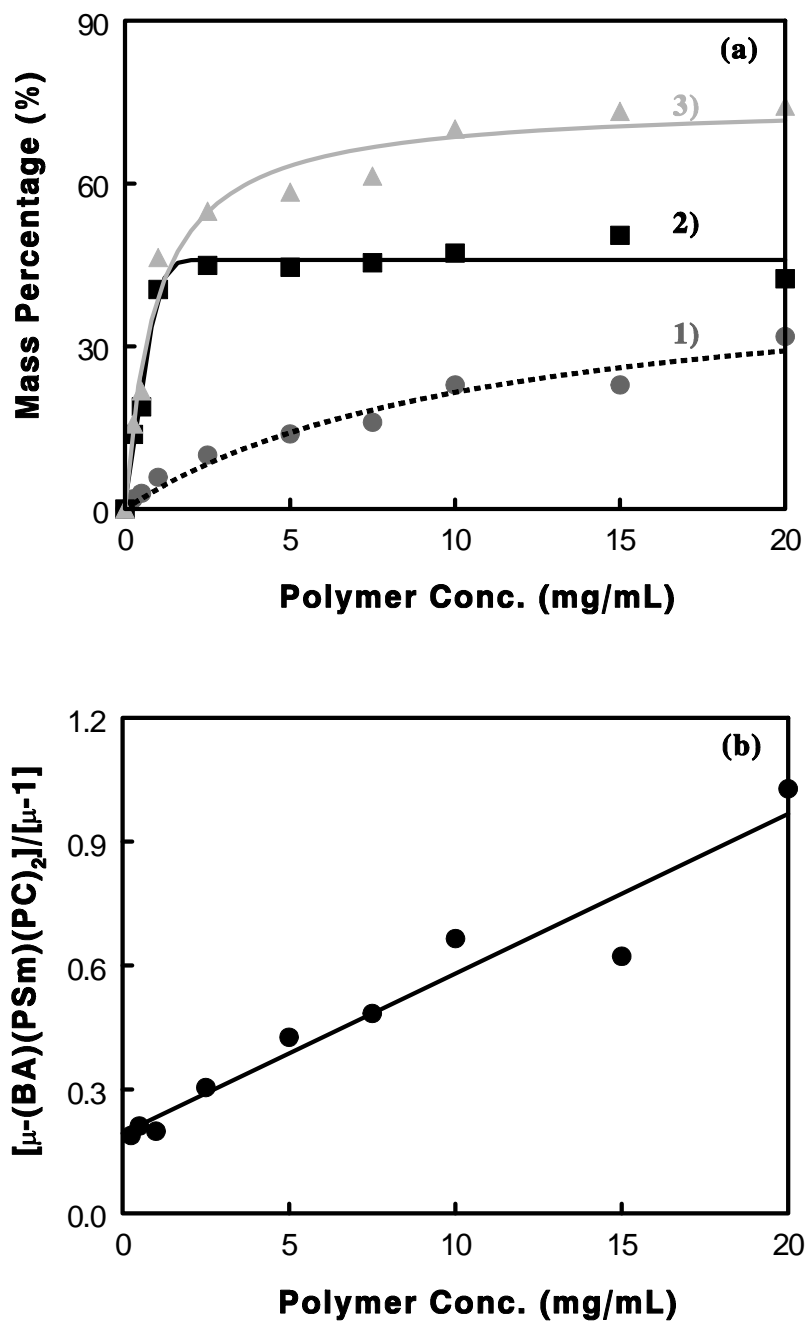
Figure 2.7 (a) Variations in the yields of 1) μ-(PtBA)(PSMA)(PCEMA)$_2$ plus μ-**1**, 2) μ-**1**, and 3) μ-(PtBA)(PSMA)(PCEMA)$_2$ as a function of the total concentration c_P for TBC**1** and PNH$_2$-b-PCEMA used during μ-**1** preparation. (b) Variation in [μ-(PtBA)(PSMA)(PCEMA)$_2$]/[μ-**1**] as a function of c_P.

2.3.7 Miktoarm Copolymer Purification.

Crude products of μ-**1** and μ-**2** were purified via fractional precipitation. The polymers were each dissolved in THF and enough water was added to induce first the separation of μ-(PtBA)(PSMA)(PCEMA)$_2$ as a dense layer at the bottom of the mixture. The fractionation was continued until μ-**1** or μ-**2** was separated as the dense phase. While μ-**2** could be purified by this method alone, the μ-**1** fraction always contained a significant amount of PNH$_2$-b-PCEMA. Thus, the PSMA block in μ-**1** was hydrolyzed to yield a PGMA block. The resultant μ-(PtBA)(PGMA)$_{200}$(PCEMA) copolymer precipitated from nitromethane and was thus readily separated from PNH$_2$-b-PCEMA, which was soluble in nitromethane.

The purified μ-**2** and μ-(PtBA)(PGMA$_{200}$)(PCEMA) copolymers were analyzed by SEC and their traces are shown in Figure 2.8. While the μ-**2** peak showed some tailing on its low-molecular weight side (suggesting the presence of unreacted precursors), a shoulder corresponding to μ-(PtBA)(PGMA$_{200}$)(PCEMA)$_2$ was seen for the μ-(PtBA)(PGMA$_{200}$)(PCEMA) trace. Despite the impurities, the purified μ-**2** and μ-(PtBA)(PGMA$_{200}$)(PCEMA) samples had low polydispersity indices of 1.04 and 1.08, respectively. Their PS-equivalent M_n values were 59 and 95 kg/mol, respectively.
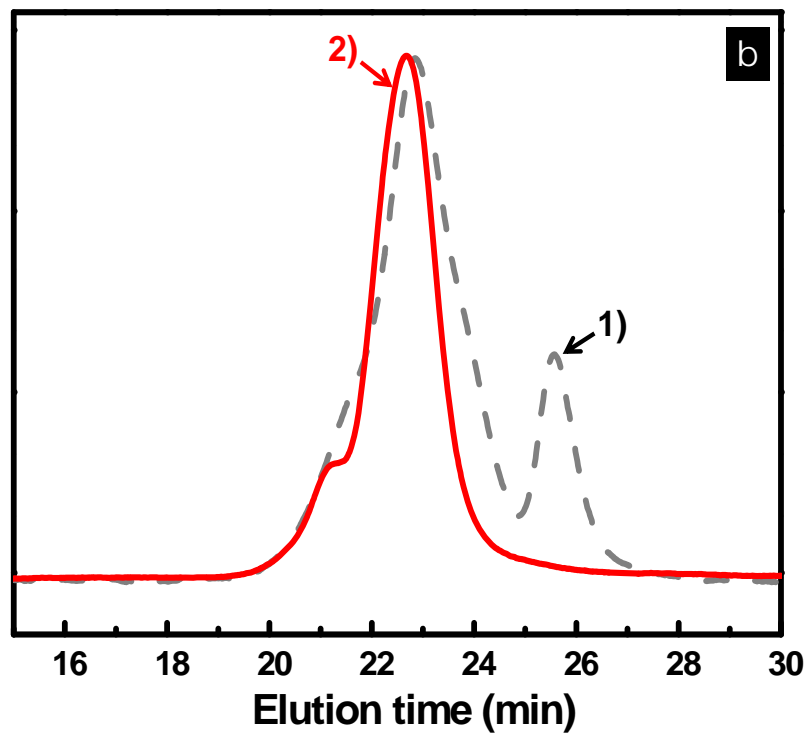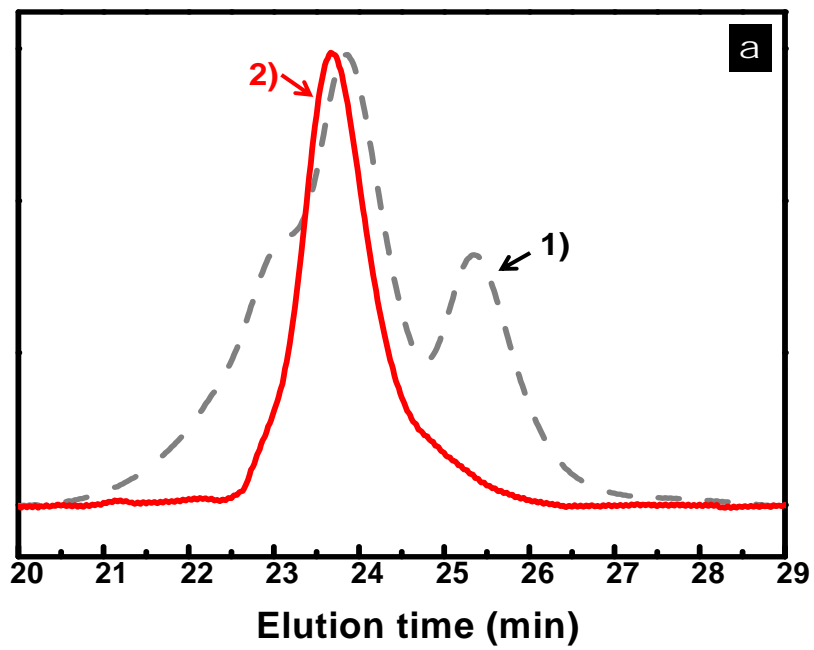
Figure 2.8 (a) SEC traces of μ-**2** 1) before and 2) after purification. (b) SEC traces of 1) crude μ-**1** and 2) purified μ-(PtBA)(PGMA$_{200}$)(PCEMA).

A ^{1}H NMR spectrum of μ-**2** was recorded in CDCl$_3$ and is shown in Figure 2.9. Our quantitative analysis yielded an integration ratio of 600/1268 between the ($k + l$) peaks (phenyl ring protons of PCEMA) and the ($c + h$) peaks for PtBA and PSMA. This ratio was consistent with the ratio of 600/1296 that was expected for μ-**2**. We did not obtain a ^{1}H NMR spectrum of μ-(PtBA)(PGMA$_{200}$)(PCEMA) because this polymer did not re-dissolve fully after it was fully dried, presumably due to the condensation of the PGMA chains.
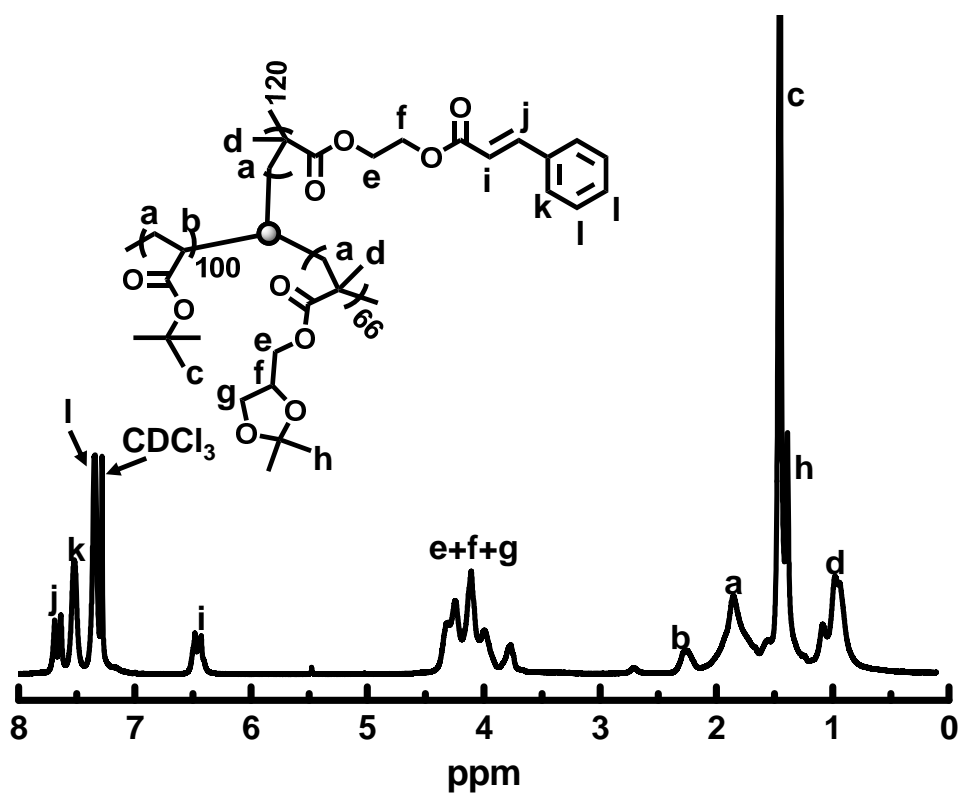
Figure 2.9 ^{1}H NMR spectrum of μ-**2** recorded in CDCl$_3$.

2.4 Conclusions

Anionic polymerization was used to prepare two novel P*t*BA-*b*-P(HEMA-TMS)-*b*-PSMA triblock copolymers. The selective removal of the TMS groups and the reaction of the resultant PHEMA blocks with succinic anhydride yielded P*t*BA-*b*-PCOOH-*b*-PSMA, where the PCOOH block was only five units long. Anionic polymerization was also used to prepare P(HEMA-*t*BDMS)-*b*-P(HEMA-TMS). After the TMS groups had been selectively removed to yield P(HEMA-*t*BDMS)-*b*-PHEMA, the sample was cinnamated to produce P(HEMA-*t*BDMS)-*b*-PCEMA. Further derivatization eventually yielded PNH$_2$-*b*-PCEMA, where the PNH$_2$ block was five units in length.

The P*t*BA-*b*-PCOOH-*b*-PSMA and PNH$_2$-*b*-PCEMA copolymers were coupled together using an association-and-reaction strategy to yield a functional miktoarm copolymer μ-(P*t*BA)(PSMA)(PCEMA). The μ-(P*t*BA)(PSMA)(PCEMA) terpolymer was produced in its highest yield and selectivity when it was synthesized using a total precursors concentration of ~2.5 mg/mL in THF. We also discovered methods for the purification of the miktoarm copolymers of different compositions. These copolymers are likely to exhibit fascinating micellization behaviour in selective solvents and the subsequent chemical processing of the resultant micelles should yield a fascinating array of novel functional nanostructures.

2.5 References

1.   Hanisch, A.; Groeschel, A. H.; Foertsch, M.; Loebling, T. I.; Schacher, F. H.; Mueller, A. H. E. Hierarchical self-assembly of miktoarm star polymers containing a polycationic segment: A general concept. *Polymer* **2013**, *54*, 4528-4537.

2.   Hanisch, A.; Groeschel, A. H.; Foertsch, M.; Drechsler, M.; Jinnai, H.; Ruhland, T. M.; Schacher, F. H.; Mueller, A. H. E. Counterion-Mediated Hierarchical Self-Assembly of an ABC Miktoarm Star Terpolymer. *ACS Nano* **2013**, *7*, 4030-4041.

3.   Choi, H. K.; Nunns, A.; Sun, X. Y.; Manners, I.; Ross, C. A. Thin Film Knitting Pattern Morphology from a Miktoarm Star Terpolymer. *Advanced Materials* **2014**, *26*, 2474-2479.

4.   Birshtein, T. M.; Polotsky, A. A.; Abetz, V. Theory of the lamellar superstructure of an ABC 3-miktoarm star-terpolymer. *Macromolecular Theory and Simulations* **2004**, *13*, 512-519.

5.   Huckstadt, H.; Gopfert, A.; Abetz, V. Synthesis and morphology of ABC heteroarm star terpolymers of polystyrene, polybutadiene and poly(2-vinylpyridine). *Macromolecular Chemistry and Physics* **2000**, *201*, 296-307.

6.   Aissou, K.; Choi, H. K.; Nunns, A.; Manners, I.; Ross, C. A. Ordered Nanoscale Archimedean Tilings of a Templated 3-Miktoarm Star Terpolymer. *Nano Letters* **2013**, *13*, 835-839.

7.   Li, Z. B.; Kesselman, E.; Talmon, Y.; Hillmyer, M. A.; Lodge, T. P. Multicompartment micelles from ABC miktoarm stars in water. *Science* **2004**, *306*, 98-101.

8.   Li, Z. B.; Hillmyer, M. A.; Lodge, T. P. Control of structure in multicompartment micelles by blending mu-ABC star terpolymers with AB diblock copolymers. *Macromolecules* **2006**, *39*, 765-771.

9.   Li, Z. B.; Hillmyer, M. A.; Lodge, T. P. Laterally nanostructured vesicles, polygonal bilayer sheets, and segmented wormlike micelles. *Nano Letters* **2006**, *6*, 1245-1249.

10.   Li, Z. B.; Hillmyer, M. A.; Lodge, T. P. Morphologies of multicompartment micelles formed by ABC miktoarm star terpolymers. *Langmuir* **2006**, *22*, 9409-9417.

11.   Liu, C.; Hillmyer, M. A.; Lodge, T. P. Multicompartment Micelles from pH-Responsive Miktoarm Star Block Terpolymers. *Langmuir* **2009**, *25*, 13718-13725.

12.   Sioula, S.; Hadjichristidis, N.; Thomas, E. L. Direct evidence for confinement of junctions to lines in an 3 miktoarm star terpolymer microdomain structure. *Macromolecules* **1998**, *31*, 8429-8432.

13.   Pavlopoulou, E.; Anastasiadis, S. H.; Iatrou, H.; Moshakou, M.; Hadjichristidis, N.; Portale, G.; Bras, W. Micellization of Miktoarm Star SnIn Copolymers in Block Copolymer/Homopolymer Blends. *Macromolecules* **2009**, *42*, 5285-5295.

14.   Yamauchi, K.; Takahashi, K.; Hasegawa, H.; Iatrou, H.; Hadjichristidis, N.; Kaneko, T.; Nishikawa, Y.; Jinnai, H.; Matsui, T.; Nishioka, H.; Shimizu, M.; Fukukawa, H. Microdomain morphology in an ABC 3-miktoarm star terpolymer: A study by energy-filtering TEM and 3D electron tomography. *Macromolecules* **2003**, *36*, 6962-6966.

15.   Yamauchi, K.; Akasaka, S.; Hasegawa, H.; Iatrou, H.; Hadjichristidis, N. Blends of a 3-miktoarm star terpolymer (3 mu-ISD) of isoprene (I), styrene (S), and dimethylsiloxane

(D) with PS and PDMS. Effect on microdomain morphology and grain size. *Macromolecules* **2005**, *38*, 8022-8027.

16.   Junnila, S.; Houbenov, N.; Hanski, S.; Iatrou, H.; Hirao, A.; Hadjichristidis, N.; Ikkala, O. Hierarchical Smectic Self-Assembly of an ABC Miktoarm Star Terpolymer with a Helical Polypeptide Arm. *Macromolecules* **2010**, *43*, 9071-9076.

17.   Matsushita, Y.; Hayashida, K.; Takano, A. Jewelry Box of Morphologies with Mesoscopic Length Scales - ABC Star-shaped Terpolymers. *Macromolecular Rapid Communications* **2010**, *31*, 1579-1587.

18.   Hayashida, K.; Takano, A.; Dotera, T.; Matsushita, Y. Giant zincblende structures formed by an ABC star-shaped terpolymer/homopolymer blend system. *Macromolecules* **2008**, *41*, 6269-6271.

19.   Takano, A.; Kawashima, W.; Wada, S.; Hayashida, K.; Sato, S.; Kawahara, S.; Isono, Y.; Makihara, M.; Tanaka, N.; Kawaguchi, D.; Matsushita, Y. Composition dependence of nanophase-separated structures formed by star-shaped terpolymers of the A(1.0)B(1.0)C(x) type. *Journal of Polymer Science Part B-Polymer Physics* **2007**, *45*, 2277-2283.

20.   Hayashida, K.; Saito, N.; Arai, S.; Takano, A.; Tanaka, N.; Matsushita, Y. Hierarchical morphologies formed by ABC star-shaped terpolymers. *Macromolecules* **2007**, *40*, 3695-3699.

21.   Hayashida, K.; Kawashima, W.; Takano, A.; Shinohara, Y.; Amemiya, Y.; Nozue, Y.; Matsushita, Y. Archimedean tiling patterns of ABC star-shaped terpolymers studied by microbeam small-angle X-ray scattering. *Macromolecules* **2006**, *39*, 4869-4872.

22.   Kong, W. X.; Li, B. H.; Jin, Q. H.; Ding, D. T.; Shi, A. C. Helical Vesicles, Segmented Semivesicles, and Noncircular Bilayer Sheets from Solution-State Self-Assembly of ABC Miktoarm Star Terpolymers. *Journal of the American Chemical Society* **2009**, *131*, 8503-8512.

23.   Jiang, T.; Wang, L.; Lin, S.; Lin, J.; Li, Y. Structural Evolution of Multicompartment Micelles Self-Assembled from Linear ABC Triblock Copolymer in Selective Solvents. *Langmuir* **2011**, *27*, 6440-6448.

24.   Zhu, Y.; Yu, H.; Wang, Y.; Cui, J.; Kong, W.; Jiang, W. Multicompartment micellar aggregates of linear ABC amphiphiles in solvents selective for the C block: a Monte Carlo simulation. *Soft Matter* **2012**, *8*, 4695-4707.

25.   Zhu, Y.; Li, R. K. Y.; Jiang, W. A Monte Carlo simulation for the micellization of ABC 3-miktoarm star terpolymers in a selective solvent. *Chemical Physics* **2006**, *327*, 137-143.

26.   Gemma, T.; Hatano, A.; Dotera, T. Monte Carlo simulations of the morphology of ABC star polymers using the diagonal bond method. *Macromolecules* **2002**, *35*, 3225-3237.

27.   Lin, B.; Zhang, H. D.; Qiu, F.; Yang, Y. L. Self-Assembly of ABC Star Triblock Copolymer Thin Films Confined with a Preferential Surface: A Self-Consistent Mean Field Theory. *Langmuir* **2010**, *26*, 19033-19044.

28.   Yan, X. H.; Liu, G. J.; Li, Z. Preparation and phase segregation of block copolymer nanotube multiblocks. *Journal of the American Chemical Society* **2004**, *126*, 10059-10066.

29.   Liu, G.; Qiao, L.; Guo, A. Diblock Copolymer Nanofibers. *Macromolecules* **1996**, *29*, 5508-5510.

30.   Ahmed, F.; Pakunlu, R. I.; Brannan, A.; Bates, F.; Minko, T.; Discher, D. E. Biodegradable polymersomes loaded with both paclitaxel and doxorubicin permeate and shrink tumors, inducing apoptosis in proportion to accumulated drug. *Journal of Controlled Release* **2006**, *116*, 150-158.

31.   Zhang, Q.; Remsen, E. E.; Wooley, K. L. Shell cross-linked nanoparticles containing hydrolytically degradable, crystalline core domains. *Journal of the American Chemical Society* **2000**, *122*, 3642-3651.

32.   Ahmed, F.; Discher, D. E. Self-porating polymersomes of PEG-PLA and PEG-PCL: hydrolysis-triggered controlled release vesicles. *Journal of Controlled Release* **2004**, *96*, 37-53.

33.   Ahmed, F.; Pakunlu, R. I.; Srinivas, G.; Brannan, A.; Bates, F.; Klein, M. L.; Minko, T.; Discher, D. E. Shrinkage of a rapidly growing tumor by drug-loaded polymersomes: pH-triggered release through copolymer degradation. *Mol Pharm* **2006**, *3*, 340-50.

34.   Saito, N.; Liu, C.; Lodge, T. P.; Hillmyer, M. A. Multicompartment Micelle Morphology Evolution in Degradable Miktoarm Star Terpolymers. *Acs Nano* **2010**, *4*, 1907-1912.

35.   Hadjichristidis, N. Synthesis of miktoarm star (mu-star) polymers. *Journal of Polymer Science Part a-Polymer Chemistry* **1999**, *37*, 857-871.

36.   Pennisi, R. W.; Fetters, L. J. Preparation of Asymmetric 3-Arm Polybutadiene and Polystyrene Stars. *Macromolecules* **1988**, *21*, 1094-1099.

37.   Iatrou, H.; Hadjichristidis, N. Synthesis of a Meodel 3-Miktoarm Star Terpolymer. *Macromolecules* **1992**, *25*, 4649-4651.

38.   Fragouli, P. G.; Iatrou, H.; Hadjichristidis, N.; Sakurai, T.; Hirao, A. Synthesis and characterization of model 3-miktoarm star copolymers of poly(dimethylsiloxane) and poly(2-vinylpyridine). *Journal of Polymer Science Part a-Polymer Chemistry* **2006**, *44*, 614-619.

39.   Heise, A.; Trollsas, M.; Magbitang, T.; Hedrick, J. L.; Frank, C. W.; Miller, R. D. Star polymers with alternating,arms from miktofunctional mu-initiators using consecutive atom transfer radical polymerization and ring-opening polymerization. *Macromolecules* **2001**, *34*, 2798-2804.

40.   Celik, C.; Hizal, G.; Tunca, U. Synthesis of miktoarm star and miktoarm star block copolymers via a combination of atom transfer radical polymerization and stable free-radical polymerization. *Journal of Polymer Science Part a-Polymer Chemistry* **2003**, *41*, 2542-2548.

41.   He, T.; Li, D. J.; Sheng, X.; Zhao, B. Synthesis of ABC 3-miktoarm star terpolymers from a trifunctional initiator by combining ring-opening polymerization, atom transfer radical polymerization, and nitroxide-mediated radical polymerization. *Macromolecules* **2004**, *37*, 3128-3135.

42.   Gao, H. F.; Matyjaszewski, K. Synthesis of miktoarm star polymers via ATRP using the "in-out" method: Determination of initiation efficiency of star macroinitiators. *Macromolecules* **2006**, *39*, 7216-7223.

43.   Fragouli, P.; Iatrou, H.; Hadichristidis, N.; Sakurai, T.; Matsunaga, Y.; Hirao, A. Synthesis of well-defined miktoarm star polymers of poly(dimethylsiloxane) by the combination of chlorosilane and benzyl chloride linking chemistry. *Journal of Polymer Science Part a-Polymer Chemistry* **2006**, *44*, 6587-6599.

44.   Li, C.; Ge, Z.; Liu, H.; Liu, S. Synthesis of Amphiphilic and Thermo responsive ABC Miktoarm Star Terpolymer via a Combination of Consecutive Click Reactions and Atom Transfer Radical Polymerization. *Journal of Polymer Science Part a-Polymer Chemistry* **2009**, *47*, 4001-4013.

45.   Iskin, B.; Yilmaz, G.; Yagci, Y. ABC Type Miktoarm Star Copolymers Through Combination of Controlled Polymerization Techniques with Thiol-ene and Azide-Alkyne Click Reactions. *Journal of Polymer Science Part a-Polymer Chemistry* **2011**, *49*, 2417-2422.

46.   Hirao, A.; Kato, H.; Yamaguchi, K.; Nakahama, S. Polyerization of Monomers Containing Functional-Groups Protected By Trialkylsilyl Groups 5. Syntheisi of Poly(2-Hydroxyethyl Methacrylate) with a Narrow Molecular-Weight Distribution by Means of Anionic Living Polymerization. *Macromolecules* **1986**, *19*, 1294-1299.

47.   Mori, H.; Hirao, A.; Nakahama, S. Protection and Polymeriztion of Funtional Monomers - Anionic Living Polymerization of (2,2-Dimethyl-1,3-Dioxolan-4-yl)Methyl Methacrylate. *Macromolecules* **1994**, *27*, 35-39.

48.   Simon, R. H. M. Anioic-Polymerization.-.Principles and Practice *American Scientist* **1984**, *72*, 413-414.

49.   Chung, J. E.; Yokoyama, M.; Suzuki, K.; Aoyagi, T.; Sakurai, Y.; Okano, T. Reversibly thermo-responsive alkyl-terminated poly(N-isopropylacrylamide) core-shell micellar structures. *Colloids and Surfaces B-Biointerfaces* **1997**, *9*, 37-48.

50.   Dou, H. J.; Hong, L. Z.; Liu, G. J. Miktoarm Star Copolymers from the Chemical Stitching of Associating Block Copolymers. *Macromolecules* **2010**, *43*, 4629-4637.

2.6 Appendix: Further Discussion of Chapter 2

The main portion of Chapter 2 was written in the manuscript format. However, the following sections have not been submitted with this manuscript, but are included in this Chapter to provide further discussion on other factors that affect the synthesis of these miktoarm copolymers. Further investigations will be required in order to gain more insight into the mechanism that underlies this "assembly-and-reaction" process.

2.6.1 Effect of the Total Precursor Concentration on the Yield

In one series of experiments, PNH$_2$-*b*-PCEMA and TBC**1** were reacted together in THF at equal molar ratio (1:1), but at different total polymer concentrations (c_p). The variations of the SEC yields of μ-ABC and μ-ABC$_2$, as well as the total yields of μ-ABC and μ-ABC$_2$, are plotted as functions of c_p in Figure 2.7a. As c_p increased, the yield of μ-ABC$_2$, as well as the total yields of μ-ABC and μ-ABC$_2$, increased. The yield of μ-ABC initially increased with increasing c_P, but subsequently decreased as c_p continued to increase. This model is described by Equations 2.4-2.6:

According to Scheme 2.2, both μ-ABC and μ-ABC$_2$ may have formed clusters prior to the chemical stitching treatment

$$[\mu\text{-ABC}] \propto K_1[\text{TBC}\mathbf{1}]_0[\text{PNH}_2\text{-}b\text{-PCEMA}]_0 \qquad \text{Equation 2.4}$$

$$[\mu\text{-ABC}_2] \propto K_2[\text{TBC}\mathbf{1}]_0[\text{PNH}_2\text{-}b\text{-PCEMA}]_0^2 \qquad \text{Equation 2.5}$$

Where K$_1$ and K$_2$ are constants. Equation 2.5 divided by Equation 2.4 gives:

$$[\mu\text{-ABC}_2]/[\mu\text{-ABC}] \propto (K_1/K_2)[\text{PNH}_2\text{-}b\text{-PCEMA}]_0 \qquad \text{Equation 2.6}$$

which indicates that based on this proposed mechanism, the by-product/product molar ratio (μ-ABC$_2$/μ-ABC) is a function of the initial concentration of PNH$_2$-*b*-PCEMA ([PNH$_2$-*b*-

PCEMA]$_0$). Therefore, we derived the data of Figure 2.7a, and prepared a plot of the by-product/product molar ratio *versus* PNH$_2$-*b*-PCEMA molar feeding concentration in Figure 2.7b. All of the data points except for one provided a linear fit, which supports our proposed cluster-forming mechanism of the miktoarm synthesis. This behaviour is also consisted with the predictions of Equation 2.6, that μ-ABC$_2$ /μ-ABC molar ratio in the crude product, is a function of feeding molar concentration of PNH$_2$-*b*-PCEMA.

2.6.2 Influence of the Precursor Feed Ratio on the Yield

We also investigated the effect of varying [PNH$_2$-*b*-PCEMA]/[TBC**1**] on the yields of the product μ-**1**. For this set of experiments, c_p was fixed at 10.0 mg/mL, and THF was used as the solvent. Figure 2.10 demonstrates how the [μ-(P*t*BA)(PSMA)(PCEMA)$_2$]/[μ-**1**] ratio observed in the crude product varied with [PNH$_2$-*b*-PCEMA]/[TBC**1**]. A minimum seemed to occur (indicating that μ-**1** was prepared at the highest purity) at [PNH$_2$-*b*-PCEMA]/[TBC**1**] $\approx$ 1.67. This value appears unreasonable, but can be explained by considering the concept of the "isoelectric point" (pI) encountered among amino acids. A pI value is the pH of an amino acid, at which the amino and carboxylic groups carry the same amount electrical charge, so that the amino acid exhibits no net charge. With this in mind, it should be noted that because the net charge of –COOH and –NH$_2$ varies with the pH value, and that the pH is dominated by PNH$_2$-*b*-PCEMA, TBC**1** and the addition of the coupling agent CMPI as well as triethylamine. A certain ratio (PNH$_2$-*b*-PCEMA/TBC**1** = 1.67/1 (n/n)) will provide a pH at which each PNH$_2$-*b*-PCEMA and TBC**1** chain contains the same net charge, and minimizes the mismatch between the reagents. Unfortunately, we did not find the pK_a value of the glycine amino labled PHEMA or the pK_{a1} of succinic

acid labled PHEMA in THF from literatures. Moreover, CMPI and TEA are also present,

which adds to the complexity of our system. Therefore, we do not have experimental

evidence to the support our proposed explanation.
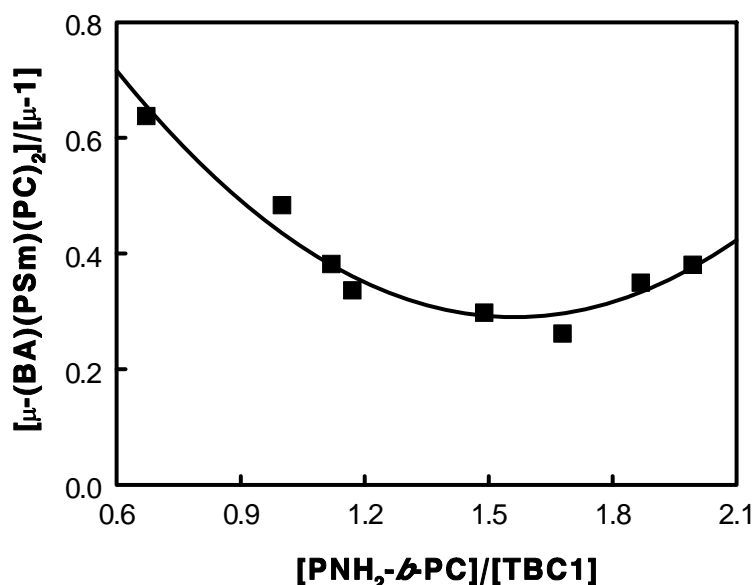
Figure 2.10 Variation in $[\mu\text{-}(PtBA)(PSMA)(PCEMA)_2]/[\mu\text{-}\mathbf{1}]$ as a function of $[PNH_2\text{-}b\text{-}PCEMA]/[TBC\mathbf{1}]$ used for the synthesis of $\mu\text{-}\mathbf{1}$. The total polymer concentration c_P was kept constant at 10.0 mg/mL.

2.6.3 Influence on the Solvents on the Yield

The third factor we investigated was the effect of the solvent. In this series of

experiments, we reacted $PNH_2\text{-}b\text{-}PCEMA$ with TBC**1** at fixed a $PNH_2\text{-}b\text{-}PCEMA/TBC\mathbf{1}$

molar ratio (1:1), but at different total polymer concentrations (c_p) in both THF and CH_2Cl_2,

respectively. The variations of the SEC total yields of μ-ABC and μ-ABC$_2$ in both THF

and CH_2Cl_2, are plotted as functions of c_p in Figure 2.11. At each c_p value, the product

prepared in CH_2Cl_2 had a higher total yield of the miktoarm polymer than the product

80

prepared in THF at the same c_p. These differences were more dramatic at lower concentrations, and became much less distinguishable when c_p was increased above 10.0 mg/mL.

The variations of the mass ratio of μ-ABC to μ-ABC$_2$ in both THF and CH$_2$Cl$_2$, are plotted as functions of c_p in Figure 2.12. Samples prepared in THF, provided higher μ-ABC to μ-ABC$_2$ mass ratios than the samples prepared in CH$_2$Cl$_2$. This trend suggests that increasing the solvent polarity inhibits the yield of μ-ABC$_2$, but enhances the yield of μ-ABC. Hence, a slight degree of polarity provides an ideal balance in promoting this coupling reaction, since we can restrict the drawbacks of a lower total yield by increasing the concentration slightly.
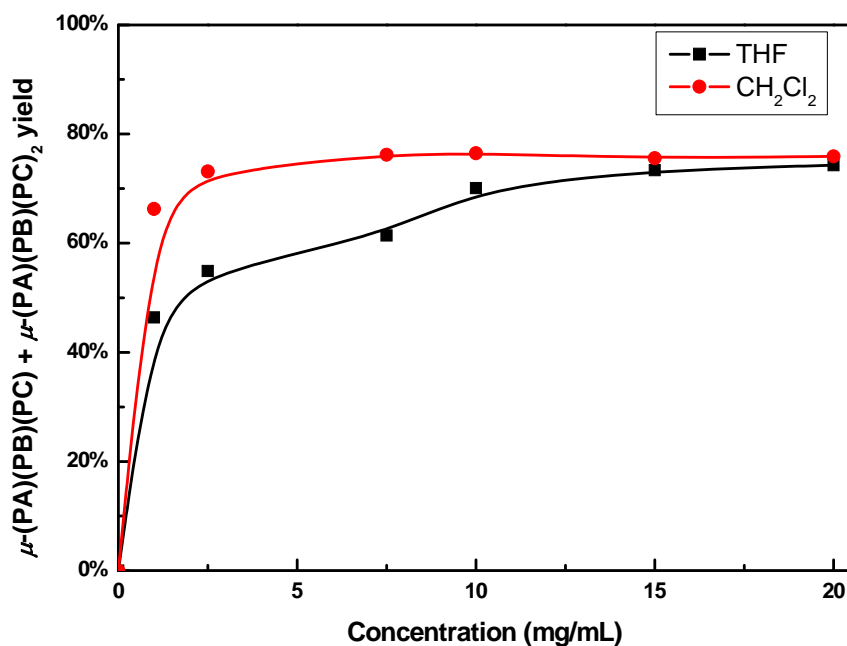
Figure 2.11 Plots of the variations of the SEC total yields of μ-ABC and μ-ABC$_2$ in both THF (black) and CH$_2$Cl$_2$ (red) as functions of c_p.

81
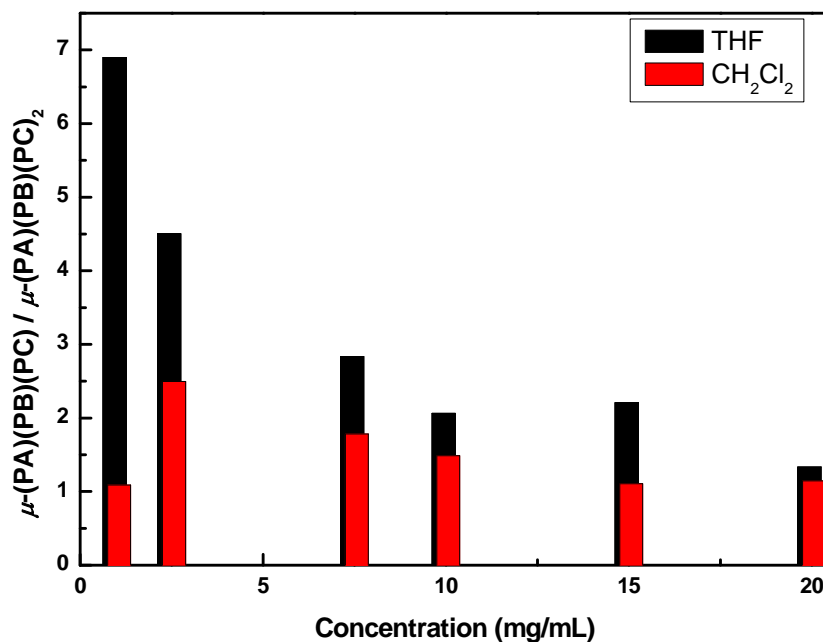
Figure 2.12 Plots of variations of the mass ratio of μ-ABC to μ-ABC$_2$ in both THF (black) and CH$_2$Cl$_2$ (red), are plotted as functions of c_p.

2.6.4 Formation of the μ-ABC$_2$ Side-Product

Based on our experimental results, the yield of the mis-matching product μ-ABC$_2$ can be minimized by optimizing the reaction conditions, but cannot be completely avoided. We believe this side-product is encountered due to a competition between the formation of μ-ABC and μ-ABC$_2$ during the synthesis depicted in Scheme 2.2. The complementary stitching blocks must overcome steric hindrance in order to undergo association with each other, and this steric hindrance is stronger when two PNH$_2$-b-PCEMA chains are attached to one TBC**1** chain. Due to this phenomenon, other mis-matching products such as μA$_2$B$_2$C or μ-ABC$_3$ are theoretically less likely to form due to the very high steric hindrance encountered in these situations. In addition, our SEC traces did not display any mis-matching product peaks other than those corresponding to μ-ABC$_2$.

82

An investigation was performed in an attempt to optimize the conditions for the synthesis of miktoarm copolymers prepared via the "assembly-and-reaction" strategy. In order to inhibit the formation of the side-product while also enhancing the product yield, our investigation indicated that the best results were obtained with c_p = 2.5~5 mg/mL, and PNH$_2$-b-PCEMA/TBC**1** = 1.67/1 (m/m) in THF However, considering the fact that it was more difficult to remove PNH$_2$-b-PCEMA than TBC**1** from the crude product, we typically we kept PNH$_2$-b-PCEMA/TBC**1** at 1/1 (m/m) during large-scale preparations.

2.6.5 Reference of Appendix

1.   Sadek, P. C. *The HPLC Solvent Guide*. 2nd Edition ed.; John Wiley and Sons, Inc.: New York, **2002**; p 664.

Chapter 3

Miktoarm Star Terpolymers and Their Spherical Capsules Bearing pH-Responsive Nanochannels
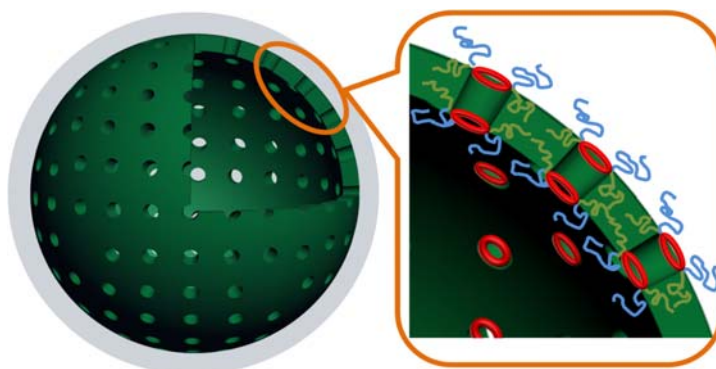
Abstract. Despite the diversity of nanostructures that have been created from block copolymers over the past two decades, the challenging fabrication of polymer nanocapsules bearing regularly-sized nanochannels has not been possible until now. In this study, μ-(PtBA)(PCEMA)(PEO)$_x$ (x = 1.14 and 1.58) pseudo-miktoarm copolymers were prepared. The copolymers consisted of one poly(*tert*-butyl acrylate) (PtBA) chain, one poly(2-cinnamoyloxyethyl methacrylate) (PCEMA) chain, and an average of x poly(ethylene oxide) (PEO) chains. These copolymers formed vesicles in a tetrahydrofuran/water solvent mixture with the soluble PEO block as the corona. At 100 units long, the PtBA chains formed cylinders that permeated the wall formed by the PCEMA chains, which were 130 units in length. Photocrosslinking the PCEMA wall and hydrolyzing the PtBA chains in the cylindrical domains yielded unprecedented capsules bearing walls that were perforated by regularly-packed uniform poly(acrylic acid)-gated nanochannels. These capsules exhibited pH-responsive reagent release in aqueous media.

3.1 Introduction

Capsules are small containers that separate reagents of interest from their surroundings. The preparation of capsules and the encapsulation of various cargoes have been long practiced in industry and are a hallmark of biological systems. For example, enzymes are encapsulated and used in laundry detergent formulations because other enzymes and reagents in a detergent deactivate unprotected enzymes.[1] Drugs, fertilizers, fragrances, and hormones are frequently encapsulated in order to control the time, location, and rate of their release.[2-4] Within cells, important events such as the transcription of DNA to form RNA and the translation of the RNA message for protein synthesis all occur within encapsulated compartments.[5] Encapsulation is used in chemistry field mainly to regulate the rate and outcome of reactions.[5]

Capsules are frequently prepared from polymers.[2] Pre-made polymer particles[6] and inorganic particles[7, 8] can also be used as the capsular walls. Popular methods to prepare polymeric capsules include interfacial polymerization,[9] and mini-emulsion polymerization,[10] the layer-by-layer coating of a sacrificial solid particulate template with polyelectrolytes and subsequently decomposing the template, as well as the dispersion of oil in water by linear triblock terpolymers[11] or ternary graft copolymers.[12] Amphiphilic diblock copolymers that consist of both a hydrophilic and a hydrophobic block can also self-assemble in water to yield capsules in the form of vesicles or polymersomes.[13-16] Polymersomes are bilayer structures with chains of the hydrophobic block forming the wall and chains of the hydrophilic block stretching into the solvent phases from the surfaces of both the inner and outer walls.[17] Compared to the traditional phospholipid liposomes[18] that are used for the delivery of hydrophilic drugs, polymersomes have the advantages of being

mechanically more robust and able to carry more hydrophobic species within their thick hydrophobic wall. Thus, polymersomes are an appealing alternative to the traditional liposomes in controlled drug release and other applications.

Regardless of the applications, the regulation of reagent transport across the walls of polymersomes is critical. For this purpose, Meier and coworkers have, for example, incorporated a trans-membrane protein into the walls of polymersomes.[19,20] More traditional approaches involve preparing polymersomes with walls made of stimuli-responsive polymers[3,21] that change their degree of swelling,[22] integrity,[23] or conformation[24] upon exposure to light, heat, a magnetic field, or a particular chemical. Evidently, the reagent permeation rate increases when the wall-forming block degrades and becomes more soluble or swollen by the solvent.

Using a stimuli-responsive block to regulate traffic across the vesicular wall is convenient and sufficient for many applications. However, it is difficult to produce uniform pores with sizes in the range between one and tens of nanometers. The production of such large pores increases solvent flux, which is known to facilitate the application of encapsulated paramagnetic species in magnetic resonance imaging[25] and should be desirable in certain other applications as well. Aside from the above examples, polymersomes with walls perforated by regularly-sized nanochannels should facilitate size-selective reagent transport in the nanometer range.[7,26]

Tying three different polymer chains PA, PB, and PB together by one end to a central point produces a miktoarm star triblock terpolymer μ-(PA)(PB)(PC).[27,28] In block-selective solvents that solubilize only certain block(s), μ-(PA)(PB)(PC) copolymers form micelles with a diverse range of fascinating shapes depending on the composition of the

copolymer.[27-30] The influence of the copolymer composition on the morphology has been systematically studied by Hillmyer, Lodge and coworkers for a family of μ-(PEO)(PEE)(PFP) samples,[31-33] where PEO, PEE, and PFP respectively denote poly(ethylene oxide), poly(ethyl ethylene), and poly(perfluoropropylene oxide). Of the obtained morphologies, polymersomes that had self-assembled in water were particularly interesting. These vesicles had a wall made of the insoluble PFP and PEE blocks. Additionally, PFP formed a cylindrical phase that permeated the PEE wall at a PFP volume fraction of 38% among the PEE and PFP blocks. PFP formed a wall-permeating cylindrical domain because both the PEE and PFP blocks had to stretch into the bulk of the wall from the wall surfaces due to the miktoarm architecture of the copolymers. Computer simulations performed by Kong et al. have also demonstrated that this morphology is thermodynamically stable.[34]

We imagined that polymersomes bearing walls that were permeated by a cylindrical phase could be used to prepare capsules with permeating nanochannels if we used a functional μ-(PA)(PB)(PC) miktoarm copolymer that could be chemically processed. Chemical processing refers to the performance of chemistry to selective domains of a block copolymer that had formed segregated domains in the solid state or had formed micelles in solution.[35-37] This strategy has previously enabled the Liu group to prepare various novel nanostructured materials including nanofibers,[38, 39] nanotubes,[40, 41] and thin films containing nanochannels.[42, 43] To prepare thin films containing nanochannels from a diblock copolymer, they prepared and used two poly(*tert*-butyl acrylate)-*block*-poly(2-cinnamoyloxyethyl methacrylate) (P*t*BA-*b*-PCEMA) samples consisting of 380 (or 230) *t*BA units and 640 (or 370) CEMA units, which corresponded to a P*t*BA volume fraction

of 26% for both samples.[42, 43] In thin films of these block copolymers, the P*t*BA blocks formed cylinders that were dispersed in the PCEMA matrix. The PCEMA phase was then crosslinked by UV light and the labile *tert*-butyl groups were removed from the cylindrical P*t*BA domains to yield thin films containing uniform poly(acrylic acid)-lined nanochannels. In principle, nanochannels could be obtained in the walls of μ-(PA)(PB)(PC) polymersomes from a similar strategy by derivatizing the cylinder-forming block.

However, capsules with permeating nanochannels have not been reported probably because of the challenges associated with synthesizing functional μ-(PA)(PB)(PC) samples.[44,45] Anionic polymerization can yield well-defined linear block copolymers that possess low polydispersity indices and a wide range of molecular weights. To prepare the miktoarm architecture, a multifunctional terminator is titrated with different polymer chains bearing terminal anions. Since these coupling reactions are slow even at room temperature, their performance at low temperatures at which functional methacrylate-based or acrylate-based polymers are stable toward anionic attack would be extremely challenging. The degree of this challenge increases further as the polymer molecular weight increases and the coupling reactions become slower. Modern controlled radical polymerization techniques can be used prepare miktoarm terpolymers. μ-(PA)(PB)(PC) copolymers prepared through these techniques are, however, less ideal because the individual blocks would normally have polydispersity indices higher than 1.10.

We recently demonstrated a modular approach to synthesize pseudo miktoarm polymers and used this strategy to prepare μ-(PCEMA)(PMMA)$_2$, where PMMA denotes poly(methyl methacrylate).[46] For this current project, we extended our previous method

and used it to prepare pseudo mikoarm copolymers μ-(PtBA)(PCEMA)(PEO). While the PtBA and PCEMA blocks were chosen for their ability to undergo chemical processing, PEO was used for its selective solubility in water. To prepare the pseudo μ-(PtBA)(PCEMA)(PEO), we first prepared a linear triblock copolymer PtBA-b-PCOOH-b-PCEMA and a diblock copolymer PEO-b-PNH$_2$ (Scheme 3.1), where b denotes *block* and PCOOH and PNH$_2$ are individually short carboxyl- and amine-group bearing blocks. The PCOOH and PNH$_2$ blocks were used to bring the two polymers together via electrostatic attractions after proton transfer from PCOOH to PNH$_2$ (Scheme 3.2). The associated dimers were then structurally linked via amidization reactions between PCOOH and PNH$_2$. The bonded dimer was a pseudo miktoarm structure because the PtBA, PCEMA, or PEO blocks were held together by two short PCOOH and PNH$_2$ blocks rather than a traditional trivalent functional group. We used PCOOH and PNH$_2$ blocks rather than single carboxyl and amino groups because the latter strategy was ineffective, probably due to the low probability for the single carboxyl and amino groups to find each other.
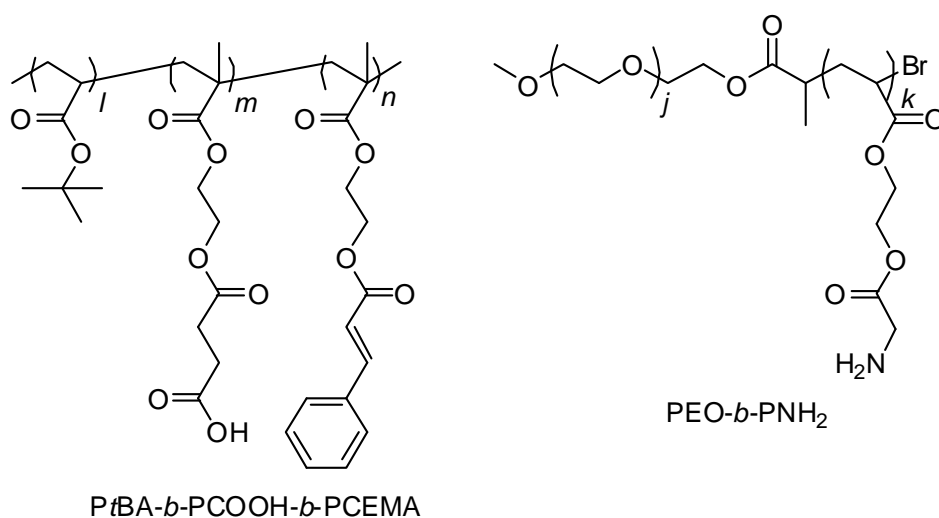
Scheme 3.1 Structures of PtBA-b-PCOOH-b-PCEMA and PEO-b-PNH$_2$.

90
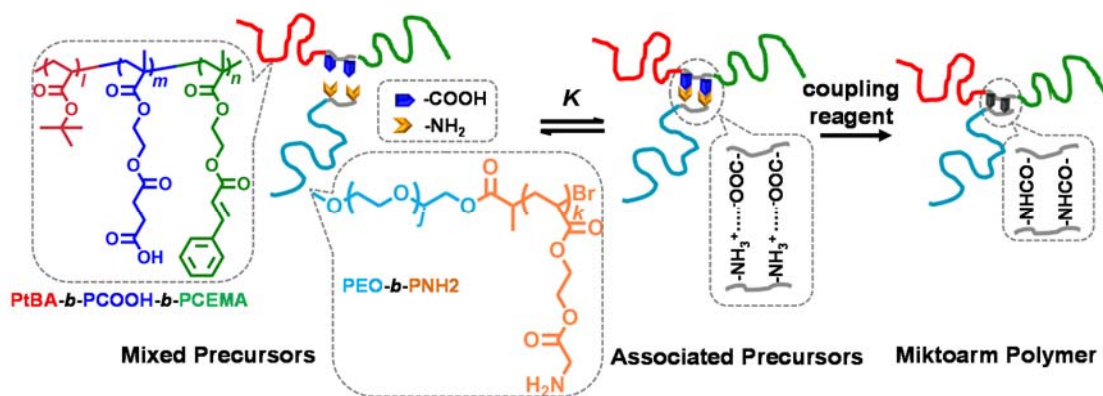
Scheme 3.2 Illustration of the preparation of a μ-(PtBA)(PCEMA)(PEO) molecule by the "association-and-then-reaction strategy".

The samples prepared from our "association-and-then-reaction" approach were also pseudo μ-(PtBA)(PCEMA)(PEO) copolymers because not exactly one PEO-b-PNH$_2$ chain reacted with one PtBA-b-PCOOH-b-PCEMA chain to produce μ-(PtBA)(PCEMA)(PEO). Rather, the pseudo copolymers were of the form μ-(PtBA)(PCEMA)(PEO)$_x$, where the subscript x denotes the average number of PEO-b-PNH$_2$ chains that were linked with each μ-(PtBA)(PCEMA)(PEO) chain for a given sample. Even for a given x, μ-(PtBA)(PCEMA)(PEO)$_x$ is a mixture consisting of μ-(PtBA)(PCEMA)(PEO), μ-(PtBA)(PCEMA)(PEO)$_2$, and probably other species. The coupling reaction did not occur at an exact 1:1 stoichiometry probably because both the PCOOH and PNH$_2$ blocks had a certain distribution in their repeat unit numbers. While the production of μ-(PtBA)(PCEMA)(PEO)$_x$ is non-ideal from a purist point of view, we emphasize that the PtBA-to-PCEMA volume ratio did not change with x. Rather, tuning x by varying the molar feed ratio between PEO-b-PNH$_2$ and PtBA-b-PCOOH-b-PCEMA offered a means to fine-tune the hydrophilic-to-hydrophobic balance of the copolymer to facilitate vesicular micelle formation.
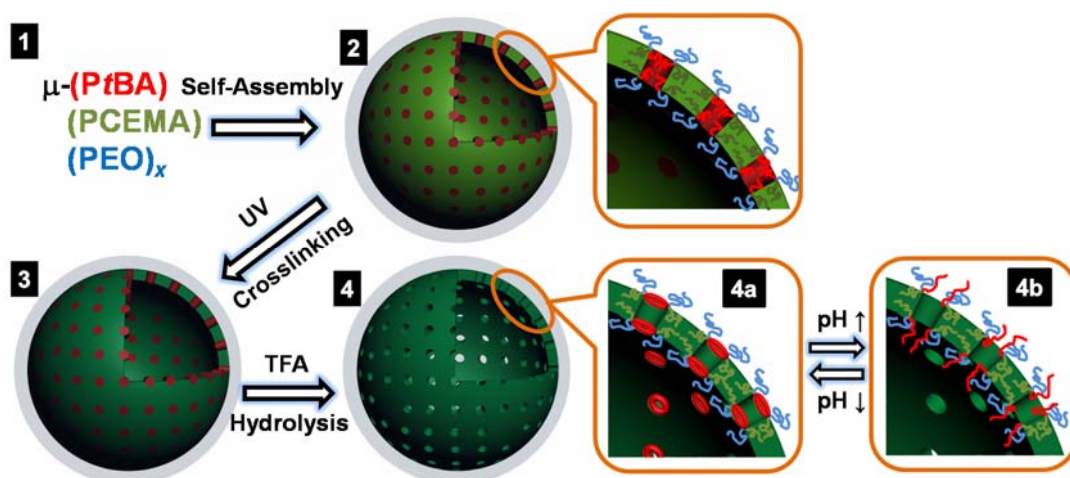
Scheme 3.3 Preparation of polymersomes bearing walls permeated by pH-responsive nanochannels. From 1→2, μ-(PtBA)(PCEMA)(PEO)$_x$ self-assembles into a vesicle with PtBA and PCEMA forming the wall and PEO stretching into the solvent phase. Within the wall, PtBA forms a cylindrical phase that permeates the PCEMA matrix. The PCEMA matrix is then photocrosslinked in step 2→3. The cleavage of the *tert*-butyl groups from the PtBA phase yields nanochannels that are gated by pH-responsive poly(acrylic acid) chains (3→4). In acidic media, the PAA chains undergo hydrogen bonding and assume compact conformations. They may form structures similar to gelled rings gating the nanochannels (4a). In basic media, the PAA chains assume expanded conformations.

Evidently, capsules containing permeating nanochannels were prepared by first forming μ-(PtBA)(PCEMA)(PEO)$_x$ vesicles in a water-rich solvent with the insoluble PtBA and PCEMA blocks forming the vesicular wall (Scheme 3.3, 1→2). By properly adjusting the lengths of the PtBA and PCEMA blocks, PtBA formed permeating cylinders dispersed in the PCEMA matrix. The PCEMA matrix was then crosslinked (2→3), and the *tert*-butyl groups were cleft from the PtBA phase to yield nanochannels that were "gated" by the pH-responsive PAA chains (3→4). These PAA chains would most likely

92

form gates at the entrances rather than become confined within the nanochannels especially under solvated conditions, because of the entropy gain associated with the escape from the channels (Structure 4b).

3.2 Experimental Section

3.2.1 Materials

Cinnamoyl chloride (98%), Z-glycine (99%), succinic anhydride (99%), hexamethylenediamine (98%), 1,3-dicyclohexylcarbodiimide (99%), trifluoroacetic acid (TFA, 99%), 2-chloro-1-methylpyridinium iodide (CMPI, 97%), tetrabutylammonium bromide (99%), 2-hydroxyethyl methacrylate (HEMA, 97%), hexamethyldisilazane (98%), chlorotrimethylsilane (99%), *tert*-butyldimethylsilyl chloride (97%), *sec*-butyl lithium (1.4 M solution in cyclohexane), triethyl aluminum (1 M solution in hexanes), 1-ethyl-3-(3-dimethylaminopropyl)carbodiimide (EDC, 97%), 4-dimethylaminopyridine (DMAP, 98%), 2-bromopropionyl bromide (98%), and dimethylformamide (anhydrous, DMF) were used as received from Aldrich. Pyridine (Fisher Scientific) was refluxed and distilled over CaH_2 under argon. Dichloromethane (DCM, Fisher Scientific) was refluxed and distilled over P_2O_5 under nitrogen. Tetrahydrofuran (THF, Fisher Scientific) was refluxed and distilled over sodium under nitrogen with benzophenone as an indicator. *p*-Toluenesulfonic acid monohydrate (TSA, 98%) was dehydrated at 110 ºC under vacuum for 4 h and was subsequently recrystallized from chloroform before use. For the preparation of μ-(P*t*BA)(PCEMA)(PEO)$_x$, triethylamine (TEA, Aldrich, 99.5%) was refluxed with some *p*-toluensulfonyl chloride for 8 h and subsequently distilled. 1,1-Diphenylethylene was sequentially distilled over calcium hydride and *n*-butyl lithium. *tert*-

Butyl acrylate was purchased from Aldrich, distilled over CaH_2, and immediately titrated and redistilled over triethyl aluminum before use.

3.2.2 P*t*BA-*b*-P(HEMA-*t*BDMS)-*b*-PHEMA

P*t*BA-*b*-P(HEMA-*t*BDMS)-*b*-P(HEMA-TMS) was a precursor to P*t*BA-*b*-PCOOH-*b*-PCEMA and was synthesized via anionic polymerization. Here P(HEMA-*t*BDMS) denotes poly(2-(*tert*-butyldimethylsiloxy)ethyl methacrylate) and P(HEMA-TMS) denotes poly(2-(trimethylsiloxy)ethyl methacrylate). To prepare P*t*BA-*b*-P(HEMA-*t*BDMS)-*b*-P(HEMA-TMS), sequential anionic polymerization was performed according to standard procedures in THF at -78 °C.[47] The monomers HEMA-TMS[48] and HEMA-*t*BDMS[49] used in this preparation were prepared and purified according to literature methods.

The polymerization was performed in a three-neck round-bottom flask that was connected to a vacuum line. Initially, LiCl (0.292 g) was added into the flask. The flask containing this salt was then evacuated and flame-dried. This was followed by the introduction of 600 mL of freshly distilled THF. The initiator was prepared *in situ* by reacting 0.49 mL of 1.4 M *sec*-butyl lithium in cyclohexane (0.69 mmol) with 0.20 mL of 1,1-diphenylethylene (1.14 mmol, excess). Freshly distilled monomers, *t*BA (9.98 mL, 69.0 mmol), HEMA-*t*BDMS (0.91 mL, 3.4 mmol), and HEMA-TMS (19.77 mL, 90.0 mmol) were then added sequentially and 2 h was provided for each monomer to polymerize. Finally, the polymerization was terminated by adding 5.0 mL of degassed methanol/H_2O at v/v = 1/1.

To remove the trimethylsilyl group from the P(HEMA-TMS) block of the synthesized triblock copolymer mentioned above, another 100 mL of methanol/H_2O at v/v

= 5/2 was added into the polymerization flask. The resultant mixture was stirred overnight at room temperature. The next morning, the solution was rotary evaporated to ~100 mL, and the condensate was sprayed onto crushed ice crystals that were added between different layers of added condensate. After the ice had melted, the polymer was collected via filtration and dried under vacuum overnight to yield 20.15 g of the product in a 95% yield.

3.2.3 PtBA-*b*-P(HEMA-*t*BDMS)-*b*-PCEMA

Reacting the PHEMA block of P*t*BA-*b*-P(HEMA-*t*BDMS)-*b*-PHEMA with cinnamoyl chloride yielded the PCEMA block. To prepare P*t*BA-*b*-P(HEMA-*t*BDMS)-*b*-PCEMA, P*t*BA-*b*-P(HEMA-*t*BDMS)-*b*-PHEMA (5.00 g containing 20.1 mmol of hydroxyl groups) was mixed with cinnamoyl chloride (6.94 g, 29.6 mmol) and dissolved in freshly distilled pyridine (40 mL). The mixture was stirred overnight before the pyridinium chloride salt that had formed was settled via centrifugation and separated. The supernatant was added to 250 mL of a methanol/H_2O (v/v = 9/1) solvent mixture to precipitate P*t*BA-*b*-P(HEMA-*t*BDMS)-*b*-PCEMA. The copolymer was re-dissolved in 20 mL of THF and precipitated into 250 mL of methanol/H_2O (v/v = 9/1). After the polymer had been dried under vacuum at room temperature overnight, 7.02 g of the product was obtained in a 91% yield. ^{1}H NMR (CDCl3), δ: 0.06 (s, Si-C**H3**), 0.90 (s, Si-C(C**H3**)3), 0.97 (s, C-C**H3**), 1.44 (s, O- C(C**H3**)3), 1.55-1.85 (br, -C**H2**- groups on the polymer backbone), 2.26 (br, -C**H**(CO)- on the backbone of the P*t*BA block), 3.82 (m, -C**H2**OSi), 4.10-4.24 (br, COOC**H2**C**H2**), 6.45 (d, C**H**=CH-Ph), 7.33-7.53 (m, **Ar-H**), 7.68 (m, CH=C**H**-Ph) ppm.

3.2.4 PtBA-*b*-P(HEMA-*t*BDMS)-*b*-PCEMA

The removal of the *tert*-butyldimethylsiloxy groups from P*t*BA-*b*-P(HEMA-*t*BDMS)-*b*-PCEMA yielded P*t*BA-*b*-PHEMA-*b*-PCEMA. To synthesize this copolymer, 5.00 g of P*t*BA-*b*-P(HEMA-*t*BDMS)-*b*-PCEMA was dissolved in 24 mL of THF. Subsequently, 6.0 mL of a 1.0 M HCl in THF solution was added to this copolymer solution. After this reaction mixture had been stirred at room temperature for 2 h, it was subsequently added into 200 mL of water in order to precipitate the copolymer. This copolymer was subsequently dried under vacuum at room temperature overnight, to provide 4.83 g of P*t*BA-*b*-PHEMA-*b*-PCEMA in a 97% yield. ^{1}H NMR (CDCl$_3$), δ: 0.97 (s, C-C**H$_3$**), 1.44 (s, O- C(C**H$_3$**)$_3$), 1.55-1.85 (br, -C**H$_2$**- on the polymer backbones of all three blocks), 2.26 (br, -C**H**(CO)- on the P*t*BA backbone), 3.76 (m, -C**H$_2$**OH), 4.10-4.24 (br, COOC**H$_2$**C**H$_2$**) , 6.45 (d, C**H**=CH-Ph), 7.33-7.53 (m, **Ar-H**), 7.68 (m, CH=C**H**-Ph) ppm.

3.2.5 PtBA-*b*-PCOOH-*b*-PCEMA

P*t*BA-*b*-PCOOH-*b*-PCEMA was obtained by reacting P*t*BA-*b*-PHEMA-*b*-PCEMA with succinic anhydride. To prepare this copolymer, 2.00 g of P*t*BA-*b*-PHEMA-*b*-PCEMA (containing 0.212 mmol of hydroxyl groups) and 4.23 g of succinic anhydride (4.24 mmol, 20 equiv.) were mixed and dissolved in 12 mL of freshly distilled pyridine. After this mixture had been stirred for 24 h at room temperature, it was subsequently centrifuged. The supernatant was then diluted to 25 mL by THF, before it was added into excess methanol/H$_2$O (v/v = 9/1) in order to precipitate the copolymer.

To neutralize the carboxyl groups, the copolymer was re-dissolved in 25 mL of THF/acetic acid (v/v = 24/1), and the copolymer solution was added into excess methanol/H$_2$O (v/v = 9/1) to precipitate the copolymer again. Subsequently, the copolymer

96

was re-dissolved in 25 mL of THF and precipitated from 250 mL of methanol/H_2O (v/v = 9/1). The last procedure was repeated. After the copolymer had been dried under vacuum at room temperature, 1.84 g of PtBA-b-PCOOH-b-PCEMA was obtained in an 85% yield.

3.2.6 PEO-Br

PEO-Br denotes poly(ethylene oxide), which served as the macroinitiator for the atom transfer radical polymerization (ATRP), and thus served as a precursor to PEO-b-PNH$_2$. PEO-Br was derived from a poly(ethylene oxide) methyl ether precursor (PEO-OH, M_n = 5000 g/mol). To purify PEO-OH, 20 g of this polymer was dissolved in 100 mL of DCM and then precipitated from 500 mL of diethyl ether. A white and loose fine powder was obtained after the precipitate had been dried under vacuum overnight.

To prepare PEO-Br,[50] 10 g (2.0 mmol) of PEO-OH, 1.40 mL (10.0 mmol) of triethylamine, and 100 mL of anhydrous DCM were mixed together and cooled in an ice-water bath. Subsequently, 1.05 mL (10.0 mmol) of 2-bromopropionyl bromide in a 10 mL anhydrous DCM solution was added dropwise into the mixture over 10 min. The solution was warmed to room temperature and stirred for 24 h. The reaction mixture was washed successively with aqueous HCl (0.10 M, 100 mL), aqueous NaOH (0.10 M, 100 mL), saturated brine (100 mL), and de-ionized water (100 mL). The final mixture was dried over magnesium sulfate, and the solvent was removed under reduced pressure. The residue was dissolved in 20 mL of DCM and the resultant solution was added into 200 mL of diethyl ether to precipitate the polymer. PEO-Br was recovered by filtration and dried under vacuum overnight to yield 7.13 g of the product in a 70% yield. ^{1}H NMR (CDCl$_3$), δ: 1.80 (d, CHBr-**CH$_3$**), 3.38 (s, **CH$_3$**O at one end of the polymer chain) 3.63 (m, **CH$_2$CH$_2$**O

in the polymer backbone), 4.30 (m, **CH₂**-OOC at the other chain-end), 4.41 (m, COC**H**BrMe) ppm.

3.2.7 PEO-*b*-PHEA

The monomer HEA-TMS was prepared according to a literature method.[51]   To prepare PEO-*b*-PHEA, 4.0 g of PEO-Br (0.80 mmol) and 0.38 mg of 2,2'-bipyridine (bpy, 2.4 mmol, 3 equiv.) were charged in a dry Schlenk flask. The flask was evacuated and then back-filled with argon. This procedure was repeated thrice. Under a flow of argon, 0.17 g of CuBr (1.2 mmol, 1.5 equiv.), 0.027 g of CuBr₂ (0.12 mmol, 0.15 equiv.), and 20 mL of anhydrous DMF were added to the flask. The mixture was degassed via three freeze-pump-thaw cycles to remove oxygen and the flask was subsequently back-filled with argon before the deoxygenated monomer HEA-TMS (1.0 mL, 5.0 mmol, 6.2 equiv.) was added. The mixture was stirred at room temperature until it became homogeneous before the flask was immersed in an oil bath that had been pre-heated at 65 °C. Samples were periodically withdrawn from the reaction mixture in order to monitor the monomer conversion via ¹H NMR spectroscopy. When the monomer conversion reached 80% after 24 h, which corresponded to a HEA-TMS degree of polymerization of 5, the polymerization was terminated by opening the flask to introduce oxygen. The resulting crude product was filtered with a short silica gel column using THF/DCM (v/v = 1/1) as the eluent to remove ligated copper. The solution was rotary evaporated to 30 mL before 1.0 mL of 1.0 M HCl was slowly added and stirred with the polymer for 2 h to remove the TMS protecting group. The polymer solution was added into an excess of diethyl ether to precipitate the polymer.

After the product had been dried under vacuum, 2.93 g of PEO-*b*-PHEA$_5$ was obtained in a 65% yield.

3.2.8 PEO-*b*-PNH$_2$

To prepare PEO-*b*-PNH$_2$, 2.0 g of PEO-*b*-PHEA (containing 1.79 mmol of hydroxyl groups, 1 equiv.) was dissolved in 5 mL of dry pyridine. To this solution under vigorous stirring were then added an 8 mL dry pyridine solution containing 560 mg of carbobenzyloxyglycine (2.68 mmol, 1.5 equiv), 553 mg of DCC (2.68 mmol, 1.5 equiv), and 55 mg of TSA (0.268 mmol, 0.15 equiv). After the reaction mixture had been stirred for 12 h at room temperature, it was subsequently centrifuged, and the supernatant was then added into excess methanol to precipitate the polymer. This polymer was subsequently dissolved in 25 mL of THF before the polymer solution was added into excess diethyl ether to precipitate the polymer again. This dissolution and precipitation process was repeated another time. After the copolymer had been dried under vacuum, 2.09 g of PEO-*b*-P(NH$_2$-Cbz) was obtained in a 90% yield.

To remove the carbobenzyloxy protective groups, 2.0 g of PEO-*b*-P(GNH$_2$-Cbz) was dissolved in 10 mL of TFA before the solution was refluxed at 70 °C for 4 h. The TFA was then removed via rotary evaporation. The resultant solid was then re-dissolved in 10 mL of pyridine to neutralize the amino groups, and this solution was subsequently added into excess diethyl ether to precipitate the polymer. The polymer was subsequently redissolved in 10 mL of methanol, and then added into excess diethyl ether to precipitate the polymer again. This process was repeated twice. After the copolymer had been dried under vacuum, 1.73 g of PEO-*b*-PNH$_2$ was obtained in a yield of 89%.

3.2.9 μ-(PtBA)(PCEMA)(PEO)$_x$

μ-(PtBA)(PCEMA)(PEO)$_x$ (with x = 1.14 and 1.58) terpolymers were prepared by reacting PtBA-b-PCOOH-b-PCEMA with PEO-b-PNH$_2$ at the molar feed ratios of 1.00/2.00 and 1.00/3.00, respectively. To prepare μ-(PtBA)(PCEMA)(PEO)$_{1.14}$, 0.225 g of PEO-b-PNH$_2$ (3.88 $\times$ 10^{-2} mmol) and 0.900 g of PtBA-b-PCOOH-b-PCEMA (1.94 $\times$ 10^{-2} mmol) were mixed together and stirred in 200 mL of THF for 2 h. This procedure was followed by the addition of 5.0 mL of THF containing 0.059 g of CMPI (2.33 $\times$ 10^{-1} mmol) and 65.2 μL of TEA (4.66 $\times$ 10^{-1} mmol). The mixture was stirred for 6 h at room temperature before the solvent was removed via rotary evaporation. To remove the unreacted PEO-b-PNH$_2$, the solid was vigorously stirred with 10 mL of water for 6 h before the mixture was centrifuged to allow μ-(PtBA)(PCEMA)(PEO)$_{1.14}$ to settle before the supernatant was removed and discarded. This extraction process was repeated until no PEO-b-PNH$_2$ was detected in the aqueous phase. The purified μ-(PtBA)(PCEMA)(PEO)$_{1.14}$ was dried under vacuum overnight to provide a light yellow powder at a yield of 76%. μ-(PtBA)(PCEMA)(PEO)$_{1.58}$ was prepared in a similar manner at a yield of 81%.

3.2.10 Preparation and Chemical Processing of the Vesicles

To prepare vesicles from μ-(PtBA)(PCEMA)(PEO)$_{1.14}$, 20 mg of μ-(PtBA)(PCEMA)(PEO)$_{1.14}$ was stirred in 20 mL of THF for 1 h. Subsequently, 80 mL of deionized water was added to this solution at a rate of 50 mL/h using a syringe pump. Vesicles of μ-(PtBA)(PCEMA)(PEO)$_{1.58}$ were prepared in a similar manner.

The PCEMA domains of the vesicles were crosslinked by a focused beam of UV light that was generated by a 500 W high pressure Hg lamp housed in an Oriel Model No 6128 case. This UV beam was passed through a 270 nm cut-off filter before it reached the vesicle solution. Samples were collected at different times during the UV irradiation treatment and diluted with water to allow the absorbance at 274 nm to be measured in order to monitor the disappearance of the CEMA double bonds. Typically a CEMA conversion 60% was used.

To generate channels in the walls of the photocrosslinked vesicles, PtBA was converted to PAA via hydrolysis. The solvent containing the crosslinked vesicles was initially removed via rotary evaporation. Subsequently, 5 mL of TFA and 7 mL of DCM were added to the dry vesicles (~200 mg). The mixture was stirred for 3 h before the solvent and TFA were removed via rotary evaporation.

3.2.11 PEO$_{45}$-Py

PEO$_{45}$-Py denotes a PEO sample that has a molar mass of 2.0×10^3 g/mol and was labeled at one end with a pyrene group. Its release from a polymersome was accompanied by an increase in the Py fluorescence intensity, and this change was used to monitor the permeability of the polymersome channels under different conditions. To synthesize PEO$_{45}$-Py, 346 mg (1.22 mmol) of 1-pyrenebutyric acid, 372 mg (2.41 mmol) of EDC, and 29 mg (0.24 mmol) of DMAP were pre-mixed in 2 mL of dry dichloromethane. This mixture was subsequently added into an 8 mL dry dichloromethane solution that contained 2.0 g (1.0 mmol) of poly(ethylene glycol) methyl ether (M_w = 2000g/mol). The mixed solution was stirred at room temperature for 48 h, before it was extracted twice with 20 mL

of a saturated aqueous sodium carbonate solution, and the oil phase was kept and concentrated during each extraction. This oil phase was subsequently passed through a silica gel column using chloroform/methanol (v/v = 97/3) as the eluent in order to obtain purified PEO_{45}-Py. After the polymer had been dried under vacuum, 1.87 g of PEO_{45}-Py was obtained in an 88% yield.

3.2.12 Capsule Loading by PEO_{45}-Py

μ-(PtBA)(PCEMA)(PEO)$_{1.14}$ capsules (100 mg), PEO_{45}-Py (500 mg), and methanol (1.0 mL) were placed in a vial and homogenized via vigorous shaking. The cap of the vial was then loosened slightly to allow the slow evaporation of the methanol over 5 d to yield a clay-like mixture.

The clay-like mixture prepared above contained PEO_{45}-Py chains that were not encapsulated within the capsules. To remove these free PEO_{45}-Py chains from the sample before each PEO_{45}-Py release experiment, a small piece of the clay-like sample was collected and then shaken with a Vortex-Genie 2 shaker for ~20 s in 1.2 mL of an aqueous HCl solution (pH = 2.85). Subsequently, the capsules were settled via centrifugation at 17,000 g in an accuSpin Micro 17 centrifuge for 2 min and were separated from the supernatant by decantation. This rinsing procedure was performed five times.

3.2.13 UV-Visible Absorption and Fluorescence Analyses

UV-visible absorption spectra were recorded in 1.00 cm quartz cells using a Varian Cary 300 Bio UV-Visible Spectrophotometer instrument. Since samples that contained capsules scattered light, their baseline did not reach zero. Their spectra were presented

after their background absorbance at 500 nm was deducted from the values at wavelengths shorter than 500 nm.

A PTI ALPHASCAN instrument was used to measure the fluorescence spectra and their intensities. The excitation and emission slit widths used were both 1.0 nm. The emission spectra were obtained by exciting the samples at 342 nm and scanning the emission spectra at 0.25 nm intervals and with an integration time of 0.05 s. The time dependent fluorescence intensity was monitored at an emission wavelength of 375 nm.

All fluorescence and UV-visible absorption measurements were performed in water. The pH of the water was adjusted by adding dilute aqueous NaOH or HCl solutions. The reported pH values were those measured using a pH meter after all of the emission or absorption analyses were complete and the pH values of the solution were stabilized.

3.2.14 Determination of PEO$_{45}$-Py Loading Density

A sample of the clay-like capsule/PEO$_{45}$-Py mixture was rinsed five times with an aqueous HCl solution (pH = 2.85) using the procedure described above. The final settled clay-like solid was dried under vacuum overnight to yield 6.037 mg of the solid. The solid was re-dispersed in 18.0324 g of an aqueous NaOH solution at final pH = 11.23 for 8 h and 0.5202 g of the solution was collected and diluted with an aqueous solution (pH ~ 11.23) to 2.0911 g. A UV-visible absorbance spectrum of the diluted solution was recorded using a 1.00 cm quartz cell and the solution was found to exhibit an absorbance of 0.41 at 342 nm.

3.2.15 Release Kinetics of PEO$_{45}$-Py from the Capsules

Freshly rinsed PEO$_{45}$-Py-loaded capsules were collected with a capillary tube and dispensed into a fluorescence cell containing 2.5 mL of water at a particular pH. After the mixture had been vigorously shaken for ~10 s, it was quickly inserted into the fluorometer for intensity analysis. Since the scanning parameters and monochrometers were already calibrated, the entire process of sample dispersion and mixing prior to data acquisition lasted ~15 s. Subsequently, the instrument was operated in the time-based mode and the changes in the fluorescence at 375 nm were monitored as a function of time while the sample was magnetically stirred. Since the amount of the PEO$_{45}$-Py-loaded capsules used were not accurately weighed, we only used release data obtained for samples that had final PEO$_{45}$-Py concentrations in water of less than 0.02 mg/mL. This low concentration ensured that the released PEO$_{45}$-Py did not aggregate in water and the Py end-groups did not form excimers.

3.2.16 Transmission Electron Microscopy

Samples were aero-sprayed onto nitrocellulose-coated copper grids. After the specimens had been dried at room temperature for 24 h, they were stained with OsO$_4$ for 2-4 h for 0.5 h prior to analysis. Morphologies of the micelles were analyzed using a Hitachi H-7000 transmission electron microscope (TEM) that was operated at 75 kV.

3.2.17 Atomic Force Microscopy

Samples were aero-sprayed onto silicon wafers or freshly-cleft mica plates. Atomic force microscopy (AFM) analysis was performed in the tapping mode using a Veeco multimode instrument that was equipped with a Nanoscope IIIa controller.

3.2.18 Size Exclusion Chromatography

The number-average molecular weight (M_n) and polydispersity index (M_w/M_n) of each polymer were determined at 25 °C using a Wyatt size exclusion chromatograph (SEC) system that was equipped with a Wyatt Optilab rEX refractive index (RI) detector. A DMF solution containing tetrabutylammonium bromide (5 mg/mL) was used as the eluent at a flow rate of 0.80 mL/min. The columns used were of the ultra-styragel type with pore sizes of 1 000 and 10 000 Å and were calibrated with narrowly-dispersed PS standards.

3.2.19 NMR Analyses

^{1}H NMR spectra were recorded using a Bruker 300 MHz spectrometer. Depending on the solubility of the sample, either deuterated chloroform ($CDCl_3$) or deuterated pyridine (pyridine-d_5) were used as the solvents for these characterizations. A relaxation delay of 3 s was used to characterize polymer samples, while a relaxation delay of 1 s was used for the characterization of small-molecule samples.

3.2.20 Dynamic Light Scattering

Dynamic light scattering (DLS) measurements were performed at a scattering angle of 90° and at 20 °C using a Brookhaven 9025 instrument that was equipped with a He-Ne laser operating at 632.8 nm. Before the measurements were performed, the vesicles were photocrosslinked to lock in their structures and then dialyzed against water to change the solvent composition from THF/water to water. The concentrations of the samples were ~0.02 mg/mL and the samples were clarified by passing them through 3.1-μm filters. The data were analyzed by the cumulant method[52] to yield the average hydrodynamic diameter

d_h and polydispersity K_1^2/K_2 where K_1 and K_2 denote the first- and second-order cumulants, respectively.

3.3 Results and Discussion

3.3.1 PtBA-*b*-PCOOH-*b*-PCEMA

As mentioned in the Introduction, P*t*BA-*b*-PCOOH-*b*-PCEMA was required to prepare μ-(P*t*BA)(PCEMA)(PEO)$_x$. Ultimately, μ-(P*t*BA)(PCEMA)(PEO)$_x$ would be used to prepare vesicles in a water-rich solvent with P*t*BA forming a permeating cylindrical phase that was dispersed in a PCEMA wall. The last requirement dictated that the P*t*BA-to-PCEMA volume ratios should be 30/70 according to phase diagrams established for diblock copolymers[53] or 38/62 as established for μ-(PEO)(PEE)(PF) terpolymers by Hillmyer, Lodge, and coworkers.[31] As a first attempt, we targeted the repeat unit numbers of $l = 100$ and $n = 130$ for the P*t*BA and PCEMA blocks, respectively, or a P*t*BA volume fraction of 30% among the two blocks. The PCOOH repeat unit number was 5, which was the same as the PNH2 repeat unit number. This block length was chosen to ensure that the PCOOH and PNH2 blocks could pull the P*t*BA-*b*-PCOOH-*b*-PC and PEO-*b*-PNH2 chains together, but were sufficiently short to allow the formation of a pseudo miktoarm star copolymer.

P*t*BA-*b*-PCOOH-*b*-PCEMA was prepared in five steps (Scheme 3.4). First, P*t*BA-*b*-P(HEMA-*t*BDMS)-*b*-P(HEMA-TMS) was prepared via anionic polymerization. Since P(HEMA-*t*BDMS) was more stable than P(HEMA-TMS),[48,49] the TMS protecting groups were selectively removed during step 2 (Scheme 3.4) to yield P*t*BA-*b*-P(HEMA-*t*BDMS)-*b*-PHEMA. The PHEMA block was then reacted with cinnamoyl chloride in step 3 to yield

a PCEMA block. This was followed by the cleavage of the *t*BDMS protecting groups in step 4 to yield P*t*BA-*b*-PHEMA-*b*-PCEMA. The reaction of the PHEMA block with succinic anhydride during step 5 yielded P*t*BA-*b*-PCOOH-*b*-PCEMA.
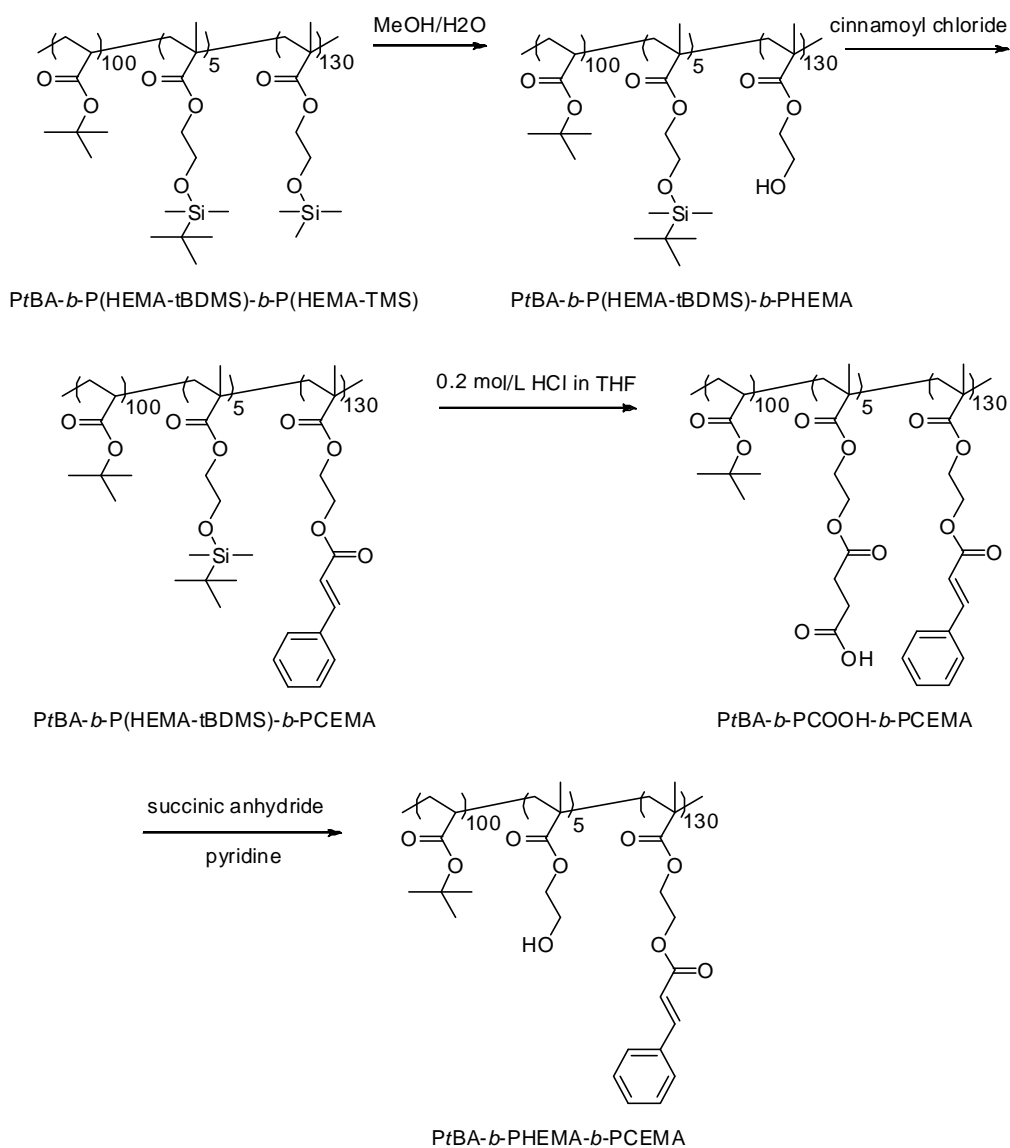
Scheme 3.4 Synthetic pathway for the preparation of P*t*BA-*b*-PCOOH-*b*-PCEMA.

P*t*BA-*b*-PCOOH-*b*-PCEMA and its precursors were carefully characterized via size-exclusion chromatography (SEC) using *N,N*-dimethylformamide (DMF) as the eluent. Figure 3.1 compares the SEC traces obtained for P*t*BA-*b*-P(HEMA-*t*BDMS)-*b*-PHEMA, P*t*BA-*b*-P(HEMA-*t*BDMS)-*b*-PCEMA, P*t*BA-*b*-PHEMA-*b*-PCEMA, and P*t*BA-*b*-PCOOH-*b*-PCEMA. The P*t*BA-*b*-P(HEMA-*t*BDMS)-*b*-PHEMA trace consisted of a main peak at 17.99 min, a shoulder peak at 16.64 min, and a small peak at 20.14 min. The PS-equivalent number-average molar masses M_n for these three peaks were 111, 56, and 20 kg/mol, respectively. The last peak must have corresponded to the deactivated P*t*BA block or the P*t*BA-*b*-P(HEMA-*t*BDMS) diblock copolymer. These species were present because no measure was taken to remove them by this stage. The shoulder peak on the higher molecular weight side should correspond to a P*t*BA-*b*-P(HEMA-*t*BDMS)-*b*-PHEMA dimer. The fact that its content increased as the sample was stored suggested that it formed probably due to nucleophilic attack of the copolymer's ester units by HEMA units. Since this shoulder peak was small, we did not attempt to purify this sample further.
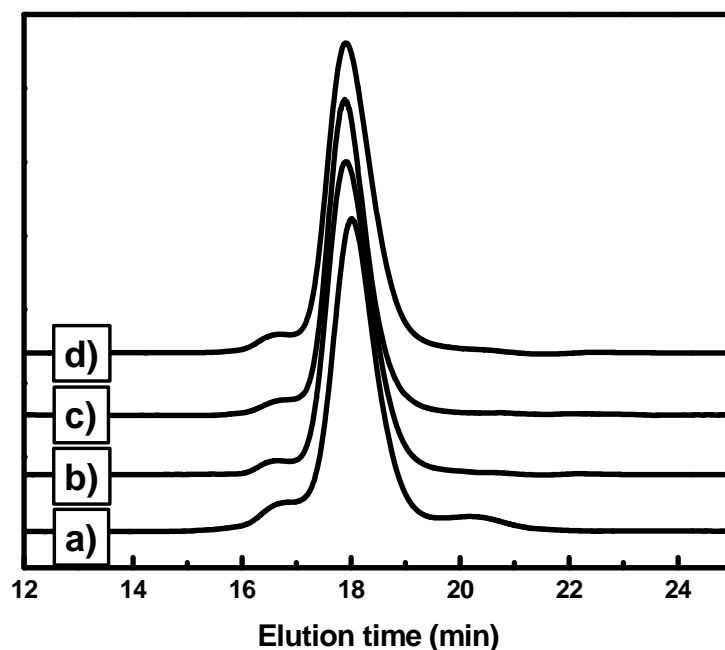
Figure 3.1 Comparison of the SEC traces for (a) P*t*BA-*b*-P(HEMA-*t*BDMS)-*b*-PHEMA, (b) P*t*BA-*b*-P(HEMA-*t*BDMS)-*b*-PCEMA, (c) P*t*BA-*b*-PHEMA-*b*-PCEMA, and (d) P*t*BA-*b*-PCOOH-*b*-PCEMA.

As expected, the main peak shifted to the higher-molecular-weight side after P*t*BA-*b*-P(HEMA-*t*BDMS)-*b*-PHEMA was cinnamated to P*t*BA-*b*-P(HEMA-*t*BDMS)-*b*-PCEMA. The peak corresponding to P*t*BA or P*t*BA-*b*-P(HEMA-*t*BDMS) disappeared because P*t*BA-*b*-P(HEMA-*t*BDMS)-*b*-PCEMA was purified by its repeated precipitation from a methanol/water mixture containing 10 vol% water. In such a solvent mixture also containing residual amounts of pyridine or THF that had been used to dissolve P*t*BA-*b*-P(HEMA-*t*BDMS)-*b*-PCEMA, P*t*BA or P*t*BA-*b*-P(HEMA-*t*BDMS) must have been soluble and thus became separated from P*t*BA-*b*-P(HEMA-*t*BDMS)-*b*-PCEMA.

The SEC traces did not exhibit any significant changes after this cinnamation step because the rest of the steps involved the modification of the central block. Since this block

was short, these modifications contributed little to the size of the overall polymer coil. The invariance of the main SEC peak suggested the structural integrity of the polymer chains was retained during these derivatization steps.

Table 3.1 gives the number-average molecular weights M_n and polydispersity indices M_w/M_n of the samples as evaluated using a size exclusion chromatography (SEC) system that was calibrated using narrowly dispersed polystyrene standards. The M_w/M_n values for the samples even including the shoulder peak on the higher molecular weight side were lower than 1.05, which was expected for samples prepared via anionic polymerization. The absolute M_n values were comparable with those expected and did not agree closely because our SEC M_n values were only apparent.

Table 3.1 Characteristics of PtBA$_l$-b-PCOOH$_m$-b-PCEMA$_n$ and its precursors.

Sample	SEC M_n (kg/mol)	SEC $M_w/M_n{}^a$	NMR $l/m/n{}^b$
PtBA$_l$-b-P(HEMA-tBDMS)$_m$-b-PHEMA$_n$	50	1.05	100/5/134
PtBA$_l$-b-P(HEMA-tBDMS)$_m$-b-PCEMA$_n$	58	1.04	100/5/130
PtBA$_l$-b-PHEMA$_m$-b-PCEMA$_n$	58	1.03	100/5/130
PtBA$_l$-b-PCOOH$_m$-b-PCEMA$_n$	58	1.03	100/5/130

[a]: Calculated without including the peak on the lower-molecular-weight side for PtBA-b-P(HEMA-tBDMS)-b-PHEMA, but including the peak on the higher-molecular-weight side for all samples.

[b]: Repeat unit number ratios for the three different blocks as determined via ^{1}H NMR spectroscopy.

We did not determine the true molecular weights of the samples using another technique such as light scattering for two reasons. First, the molecular weights determined via light scattering are not accurate but are only apparent values for block copolymers.[54] Second, the polymer was prepared via anionic polymerization. For such short chains, the targeted and actual repeat unit numbers should be very similar, e.g. within ± 15%. Thus, the initial precursor should possess 100 tBA units, 5 HEMA-tBDMS units, and 130 HEMA-TMS units.

The precursors were also analyzed at different stages of their preparation by ^{1}H NMR spectroscopy. The resultant spectra and proton peak assignments are given in Figure 3.2. The spectral changes clearly supported our success in each of the derivatization steps.

More interestingly, the ^{1}H NMR spectra allowed the determination of the $l/m/n$ ratios for the repeat unit numbers of the three blocks at different stages of the PtBA-b-P(HEMA-tBDMS)-b-PHEMA derivatization. For example, the integrations of the characteristic signals corresponding to the PtBA, P(HEMA-tBDMS), and PHEMA blocks at 2.75, 0.24, and 3.91-4.52 ppm, respectively, yielded a $l/m/n$ ratio of 100/5/134 for PtBA-b-P(HEMA-tBDMS)-b-PHEMA. This experimental value was in agreement with our targeted ratios of 100/5/130 and thus confirmed that the targeted copolymer with the appropriate block lengths had been successfully prepared via anionic polymerization. These ratios determined at the other stages of PtBA-b-P(HEMA-tBDMS)-b-PHEMA derivatization are listed in Table 3.1 and were all consistent with the targeted block length ratios, as expected.
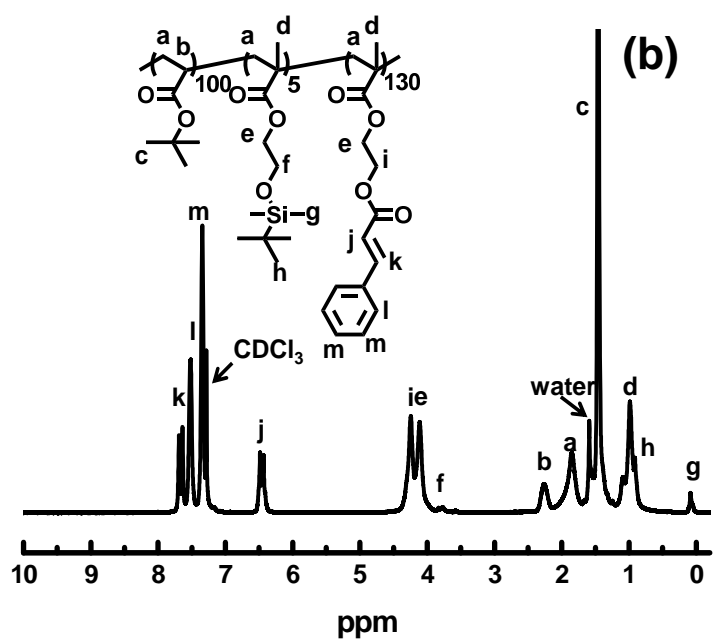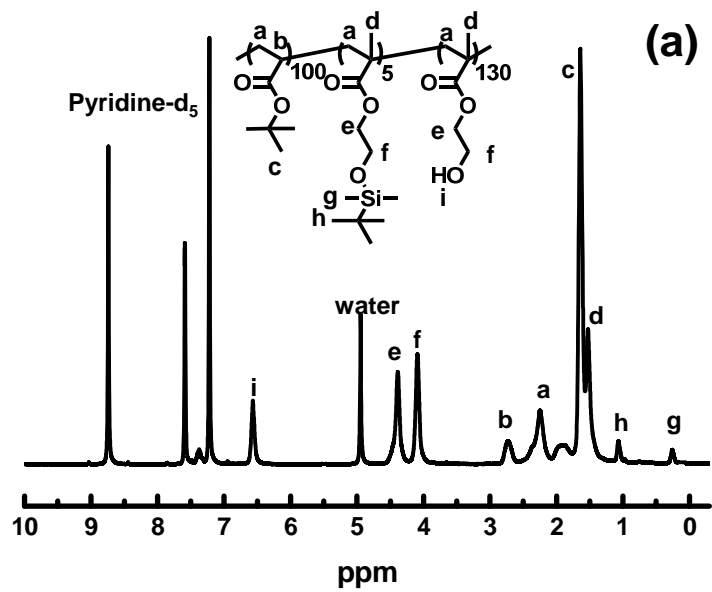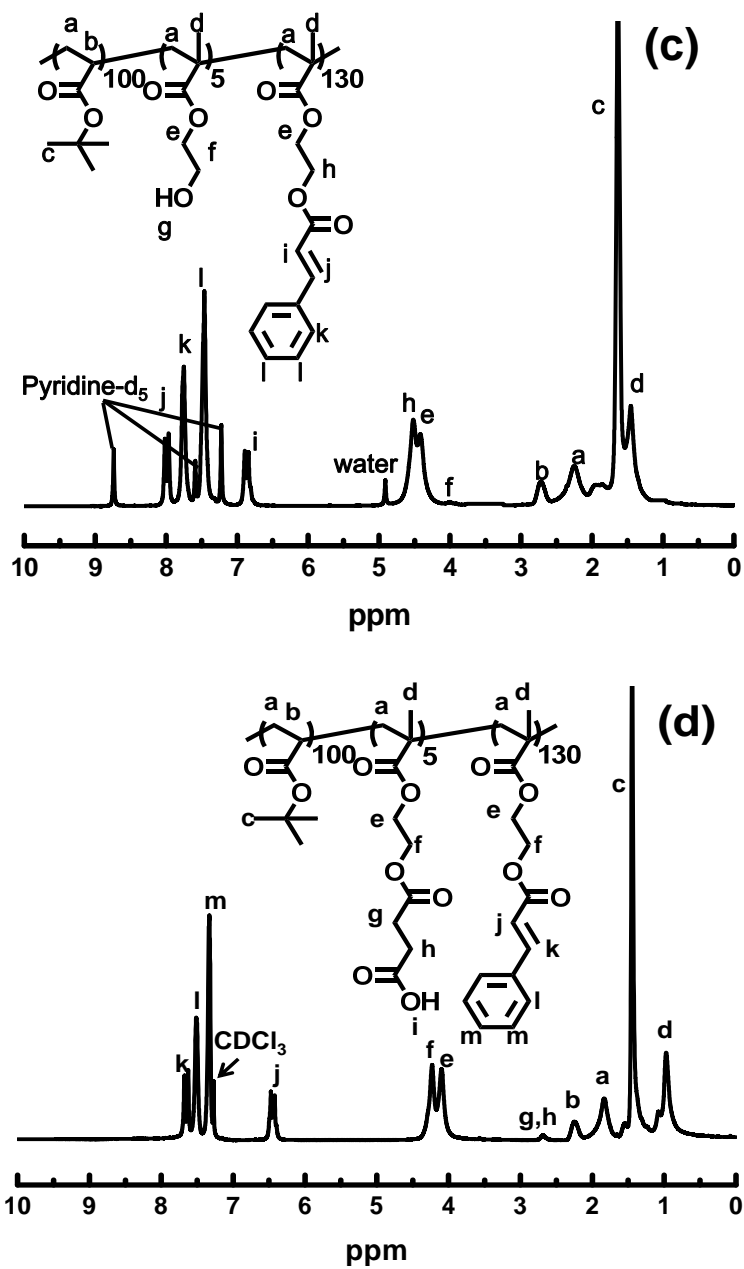
Figure 3.2 ^{1}H NMR spectra of (a) P*t*BA-*b*-P(HEMA-*t*BDMS)-*b*-PHEMA, (b) P*t*BA-*b*-P(HEMA-*t*BDMS)-*b*-PCEMA, (c) P*t*BA-*b*-PHEMA-*b*-PCEMA, and (d) P*t*BA-*b*-PCOOH-*b*-PCEMA.

3.3.2 PEO-*b*-PNH$_2$

The purpose of the PEO block was to stabilize the μ-(P*t*BA)(PCEMA)(PEO)$_x$ vesicles in a water-rich solvent. To ensure vesicle formation, the PEO block length should be appropriately chosen. For convenience, we opted to first try the commercially available poly(ethylene oxide) monomethyl ether, or PEO-OH, with a molar mass of 5.0 kg/mol as the precursor for PEO-*b*-PNH$_2$. If the PEO block in μ-(P*t*BA)(PCEMA)(PEO)$_x$ turned out to be too short, we would try to take advantage of the "pseudo" nature of μ-(P*t*BA)(PCEMA)(PEO)$_x$ and vary x to optimize the hydrophilic-to-hydrophobic balance of the copolymer.

The reactions used to synthesize PEO-*b*-PNH$_2$ are shown in Scheme 3.5. First, PEO-OH was reacted with 2-bromopropionyl bromide to produce a macroinitiator PEO-Br.[50] PEO-Br was then used to grow an average of five HEA-TMS (2-trimethylsiloxyethyl acrylate) units via atom transfer radical polymerization (ATRP).[55] The TMS protecting groups were subsequently removed under acidic conditions, and the resultant hydroxyl groups of the poly(2-hydroxyethyl acrylate) (PHEA) block were further reacted with *N*-carbobenzyloxyglycine (Z-glycine) to yield a P(HEA-GlyCbz) block. The cleavage of the carbobenzyl group yielded PEO-*b*-PNH$_2$.
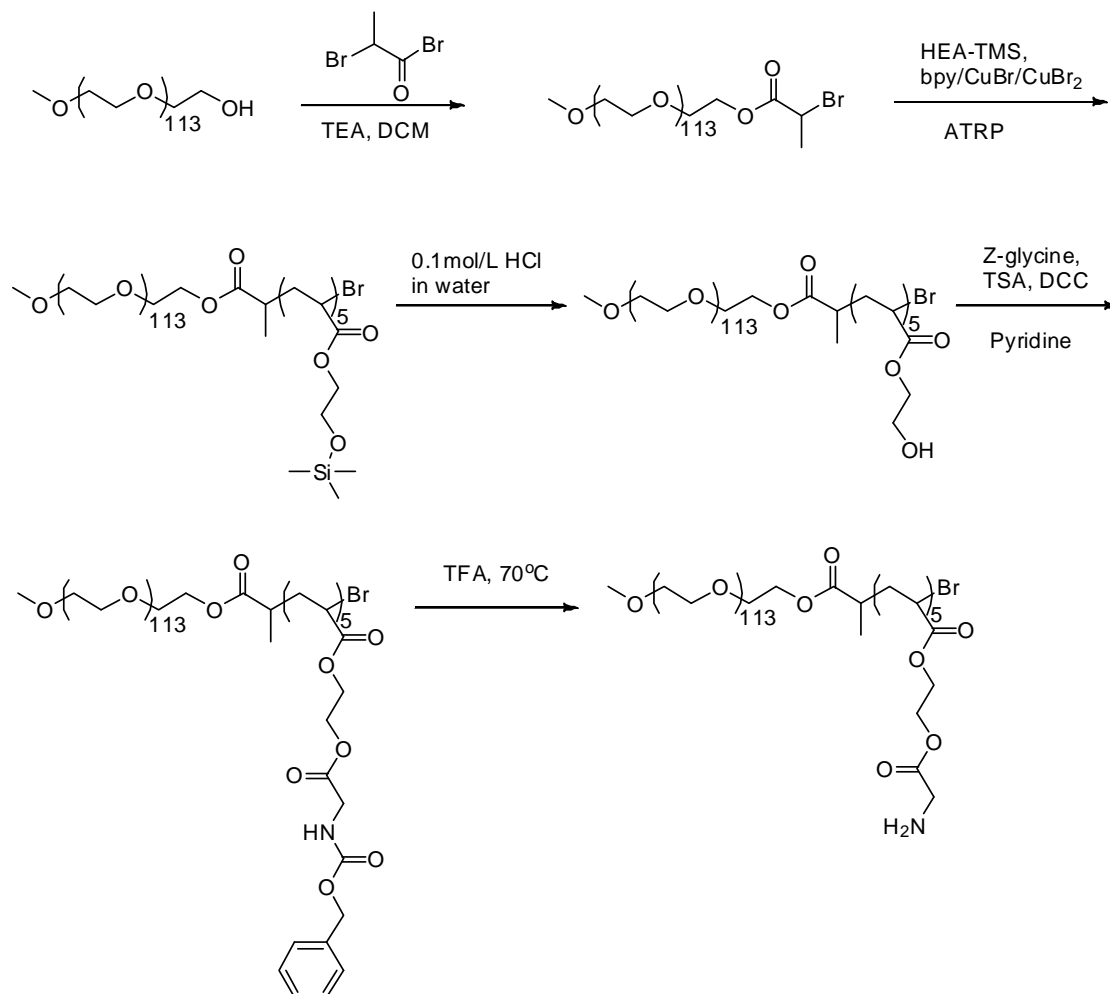
Scheme 3.5 Synthetic pathway toward PEO-*b*-PNH₂.

SEC was used to analyze the polymers that had been prepared at different stages, and the SEC traces of PEO-OH, PEO-Br, PEO-*b*-PHEA, PEO-*b*-P(HEA-GlyCbz), and PEO-*b*-PNH₂ are shown in Figure 3.3. Aside from the main peak, every sample including the commercial PEO-OH precursor contained a weak impurity peak on the high molecular weight side. Since this peak was small, we have not probed into its origin. While the retention time of the main peak changed little between PEO-OH and PEO-Br, it decreased from PEO-Br to PEO-*b*-PHEA. The peak elution time further decreased after PHEA was

115

labelled with Z-glycine and then increased with the cleavage of the carbobenzyl groups. These peak position variations were consistent with the anticipated molecular weight changes accompanying the reaction steps.
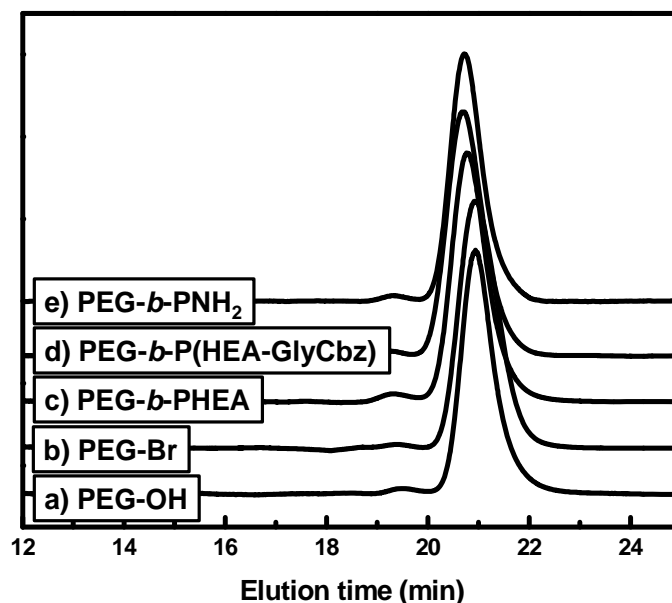
Figure 3.3 SEC traces of (a) PEO-OH, (b) PEO-Br, (c) PEO-*b*-PHEA, (d) PEO-*b*-P(HEA-GlyCbz), and (e) PEO-*b*-PNH2.

The polymers obtained at different derivatization stages were also characterized by ^{1}H NMR spectroscopy. Figure 3.4 shows the spectra of PEO-Br, PEO-*b*-P(HEA-GlyCbz), and PEO-*b*-PNH2 along with the peak assignments. The data clearly show our success with the targeted reactions. For example, the integration ratio between the PEO backbone *b* and *c* protons and the terminal *g* protons of PEO-Br was determined from the data shown in Figure 3.4a to be 150/1, which was consistent with the ratio 152/1 calculated by assuming a molar mass of 5.0 kg/mol for PEO and 100% labeling of the PEO terminal

hydroxyl groups by 2-bromopropionyl bromide. In a similar manner, the repeat unit ratio between the PEO and PNH$_2$ blocks was determined to be 114 to 5.
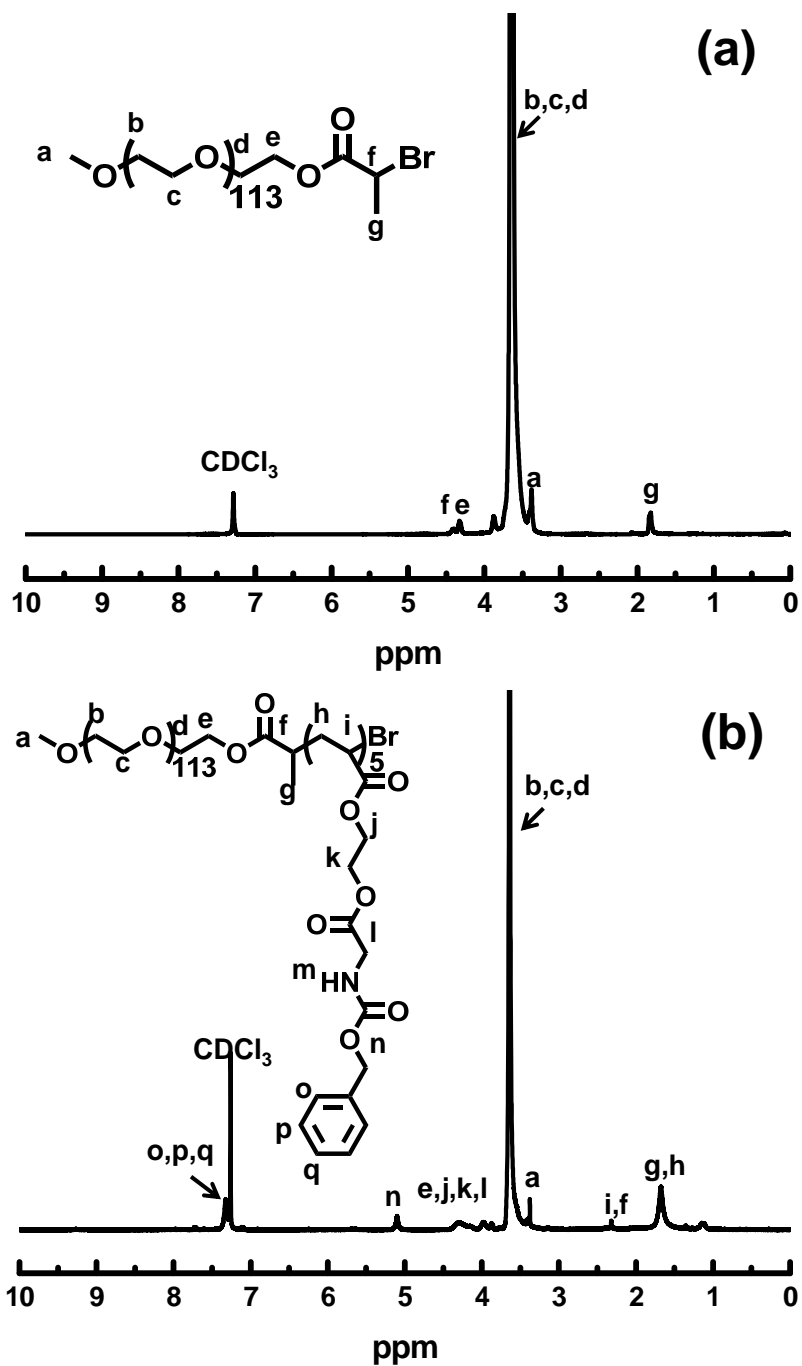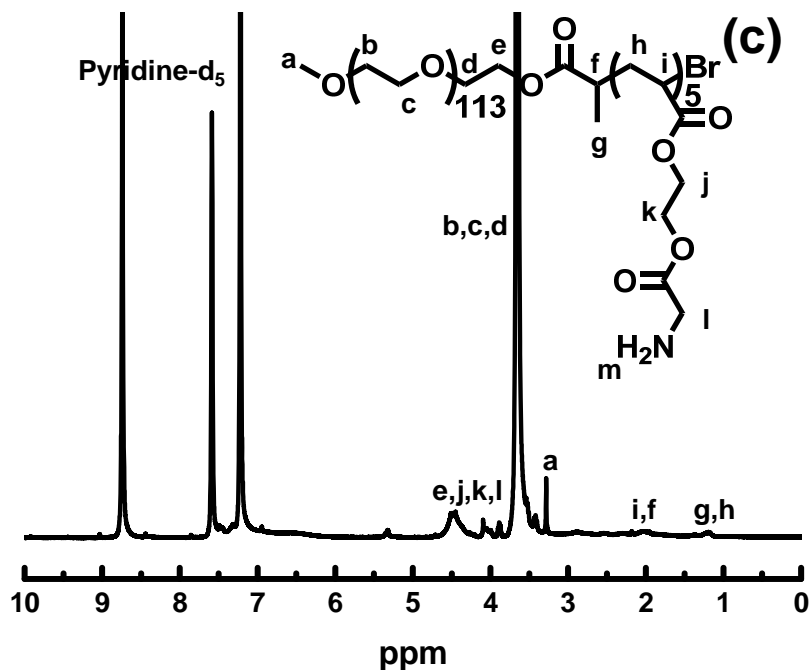
Figure 3.4 Comparison of the ^{1}H NMR spectra of (a) PEO-Br, (b) PEO-*b*-P(NH$_2$-Cbz), and (c) PEO-*b*-PNH$_2$.

3.3.3 *μ*-(PtBA)(PCEMA)(PEO)$_x$

PEO-*b*-PNH$_2$ and P*t*BA-*b*-PCOOH-*b*-PCEMA were stirred in THF for 2 h to associate the polymers[46] before 2-chloro-1-methylpyridinium iodide (CMPI) and triethylamine[56,57] were added to covalently couple the different chains. As shown in Scheme 3.6, the reaction between a carboxyl group and CMPI was performed to produce an activated ester first. This activated ester was then reacted with an amine group to produce an amide.
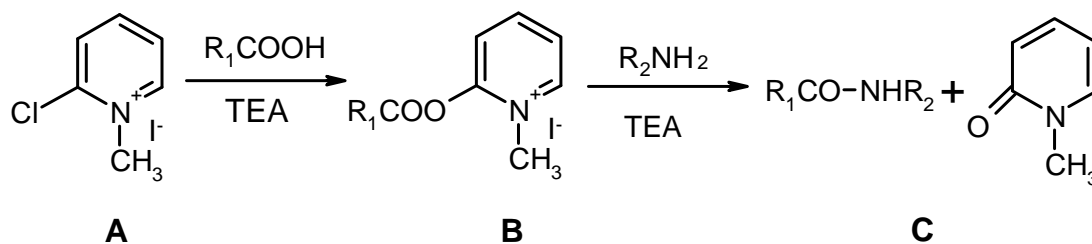
Scheme 3.6 Amidization aided by 2-chloro-1-methylpyridinium iodide and triethylamine.

In order to produce μ-(PtBA)(PCEMA)(PEO)$_x$ with different x values, PEO-b-PNH$_2$ and PtBA-b-PCOOH-b-PCEMA were fed and reacted at the molar ratios of 2.0/1.0 and 3.0/1.0. THF was subsequently evaporated from the reaction mixtures and the resultant solid residues were extracted with water to remove unreacted PEO-b-PNH$_2$. Figure 3.5 compares the SEC traces of PEO-b-PNH$_2$, PtBA-b-PCOOH-b-PCEMA, as well as a coupling product of the former two produced at a molar feed ratio of 2.0/1.0 before and after its purification by water extraction.

The SEC trace of the crude product evidently contained a peak corresponding to PEO-b-PNH$_2$ and its impurity peak at 20.75 min. In comparison with the trace of the precursor PEO-b-PNH$_2$, the PEO-b-PNH$_2$ peak in the crude product was shifted slightly toward the higher molecular weight side. This suggested the preferential reaction of lower-molecular-weight PEO-b-PNH$_2$ with PtBA-b-PCOOH-b-PCEMA. The impurity peak at 20.75 min became more prominent relative to that of the unreacted PEO-b-PNH$_2$, probably because the impurity did not react with PtBA-b-PCOOH-b-PCEMA. As hoped, the peaks corresponding to PEO-b-PNH$_2$ and its impurity disappeared after the crude product was extracted with water. As will be discussed later, our ^{1}H NMR analysis established that the purified sample had the formula of μ-(PtBA)(PCEMA)(PEO)$_{1.14}$.
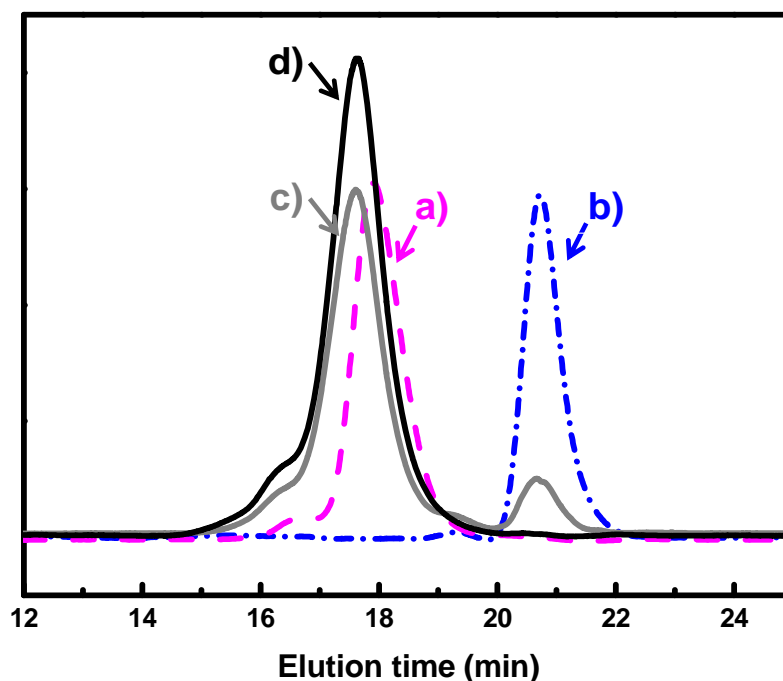
Figure 3.5 SEC traces of (a) PtBA-b-PCOOH-b-PCEMA, (b) PEO-b-PNH$_2$, as well as μ-(PtBA)(PCEMA)(PEO)$_{1.14}$ (c) before and (d) after water extraction.

The purified μ-BCE$_{1.14}$ sample exhibited a main SEC peak and a shoulder peak in Figure 3.5. Both of these peaks shifted to shorter retention times relative to those of PtBA-b-PCOOH-b-PCEMA. Furthermore, the relative intensity between the shoulder and main peak increased from PtBA-b-PCOOH-b-PCEMA to μ-(PtBA)(PCEMA)(PEO)$_{1.14}$. The PS-equivalent peak molar masses for the peak and shoulder were 76 and 156 kg/mol, respectively. The polydispersity index of the main peak including the shoulder was 1.11.

The relative intensity of the shoulder peak for μ-(PtBA)(PCEMA)(PEO)$_{1.14}$ increased probably because some trimers μ-(PtBA)$_2$(PCEMA)$_2$(PEO) were formed from the coupling of two PtBA-b-PCOOH-b-PCEMA chains with one PEO-b-PNH$_2$ chain. This coupling apparently occurred despite the steric hindrance associated with bringing these chains

120

together and the use of excess PEO-*b*-PNH$_2$. The polydispersity index of μ-(P*t*BA)(PCEMA)(PEO)$_{1.14}$ was higher than that of P*t*BA-*b*-PCOOH-*b*-PCEMA, probably because the main peak of this sample contained contributions from P*t*BA-*b*-PCOOH-*b*-PCEMA, μ-(P*t*BA)(PCEMA)(PEO), and μ-(P*t*BA)(PCEMA)(PEO)$_2$, as well as other possible side-products. Despite these impurities, the sample had a very low polydispersity index.

A similar SEC trace was observed for the μ-(P*t*BA)(PCEMA)(PEO)$_{1.58}$ sample that was prepared at the PEO-*b*-PNH$_2$-to-P*t*BA-*b*-PCOOH-*b*-PCEMA feed molar ratio of 3.0/1.0 and then extracted with water. Table 3.2 lists the PS-equivalent number-average molar masses M_n and the polydispersity indices M_w/M_n for these samples. The apparent or PS-based M_n increased with the x value for μ-(P*t*BA)(PCEMA)(PEO)$_x$. However, the 25 kg/mol increase in M_n from 58 kg/mol for P*t*BA-*b*-PCOOH-*b*-PCEMA to 83 kg/mol for μ-(P*t*BA)(PCEMA)(PEO)$_{1.58}$ was substantially larger than the contribution of ~8 kg/mol made by the 1.58 PEO chains grafted onto P*t*BA-*b*-PCOOH-*b*-PCEMA. This large difference in the apparent molecular weight was presumably caused by the grafting of the PEO chains to the middle of the P*t*BA-*b*-PCOOH-*b*-PCEMA chains and thus a large increase in the hydrodynamic volume of the non-linear chains.

Table 3.2 Molecular characteristics of the μ-BCE$_x$ samples used in this study.

Sample	SEC M_n (kg/mol)	SEC M_w/M_n	^{1}H NMR x
μ-BCE$_{1.58}$	83	1.12	1.58
μ-BCE$_{1.14}$	74	1.11	1.14
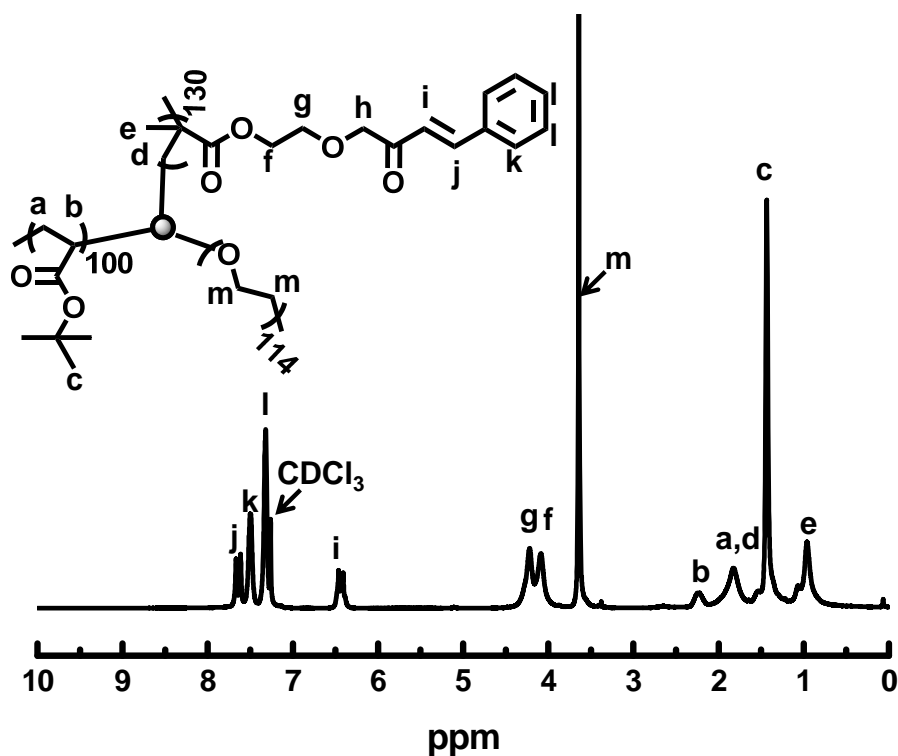
Figure 3.6 ^{1}H NMR spectrum of μ-(PtBA)(PCEMA)(PEO)$_{1.14}$ along with the peak assignments for the different protons.

^{1}H NMR spectroscopy was also used to characterize the purified μ-BCE$_x$ samples dissolved in CDCl$_3$. Figure 3.6 shows a ^{1}H NMR spectrum of the μ-(PtBA)(PCEMA)(PEO)$_x$ sample prepared at the feed molar ratio of 2.0/1.0 for PEO-b-PNH$_2$ and PtBA-b-PCOOH-b-PCEMA. By comparing the integration ratios between the protons m and $g + h$ in Figure 3.6, the x value was calculated to be 1.14. The μ-(PtBA)(PCEMA)(PEO)$_x$ sample prepared at the feed molar ratios of 3.0/1.0 was analogously analyzed to yield a x value of 1.58.

3.3.4 μ-(PtBA)(PCEMA)(PEO)$_x$ Vesicles and Crosslinked Vesicles

To prepare vesicles, we dissolved μ-(PtBA)(PCEMA)(PEO)$_x$ in THF and then slowly added water until the water volume fraction f_{H2O} reached the range of 65% - 95%. At all tested f_{H2O} values, micelles with a similar morphology as revealed by TEM were obtained from the μ-(PtBA)(PCEMA)(PEO)$_x$ samples. Thus, we have focused on the analysis of micelles prepared at $f_{H2O} = 80\%$. These prepared micelles were subsequently aero-sprayed onto nitrocellulose-covered copper grids and stained with OsO_4 vapor for transmission electron microscopy (TEM) analysis. Aero-spraying was used to atomize the solution samples into a fine fog before their collection by TEM grids, mainly to ensure full solvent evaporation within 3 s.[58] Fast solvent evaporation was used to minimize the opportunities for the micelles to undergo morphological transitions during sample preparation. Figures 3.7a-b show TEM images of micellar specimens of μ-(PtBA)(PCEMA)(PEO)$_{1.58}$ and μ-(PtBA)(PCEMA)(PEO)$_{1.14}$.
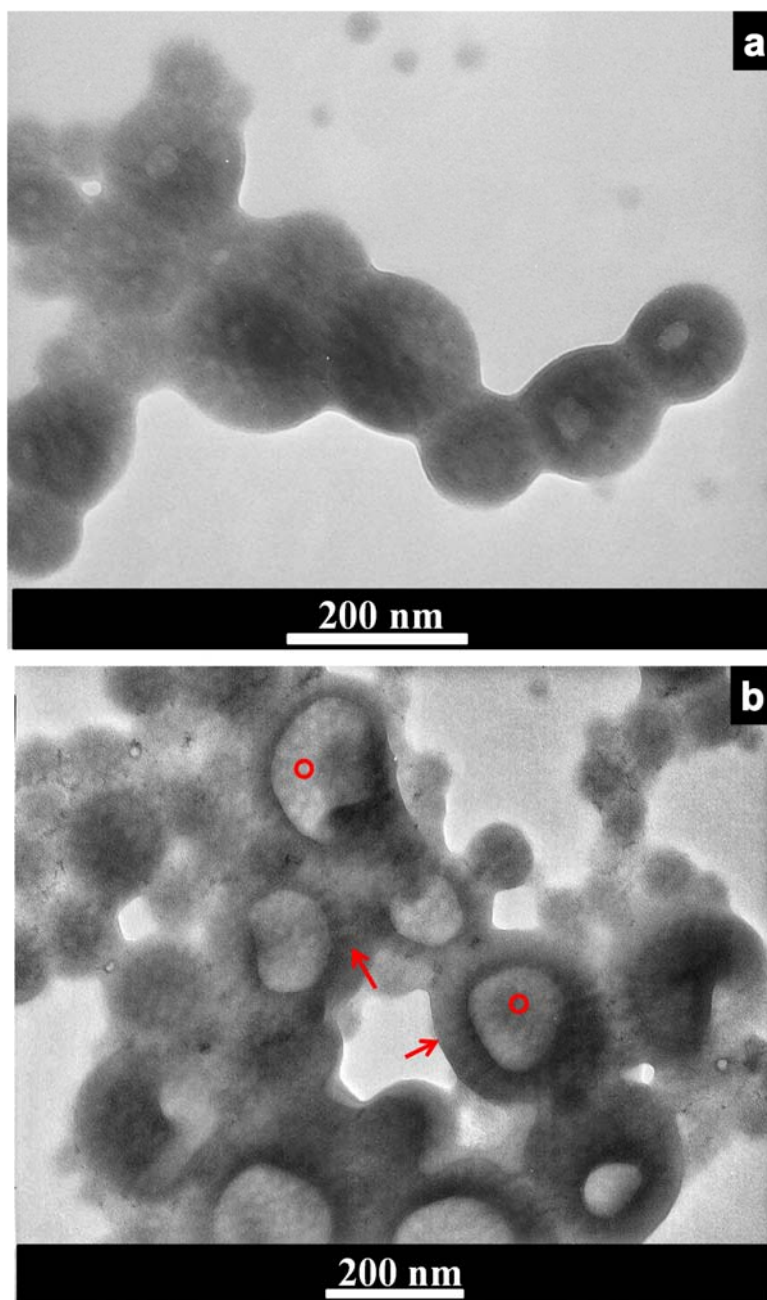
Figure 3.7 TEM images of vesicles of (a) μ-(PtBA)(PCEMA)(PEO)$_{1.58}$ and (b) μ-(PtBA)(PCEMA)(PEO)$_{1.14}$. The samples were aero-sprayed from THF/water at f_{H2O} = 80% and then stained by OsO$_4$.

The TEM images revealed a number of notable features. First, the projections of the particles were approximately circular. Second, the circles were large and possessed moderate size distributions. Our statistical analysis of > 100 particles excluding those smaller than 35 nm yielded average diameters of 90 ± 29 and 122 ± 44 nm for the μ-(PtBA)(PCEMA)(PEO)$_{1.58}$ and μ-(PtBA)(PCEMA)(PEO)$_{1.14}$ micelles, respectively. We excluded the smaller particles because they existed in small numbers and could not possibly correspond to vesicular micelles but may have been spherical micelles. Third, light circular patches with an average diameter of 9 ± 2 nm were observed on many particles in the central regions, such as those marked by the two red circles in Figure 3.7b. These patches were packed densely with some, but not necessarily hexagonal, symmetry. On the peripherals of some particles such as the two regions marked by the red arrows in Figure 3.7b, elongated light stems were visible. The width of these stems was also comparable to the diameter of the white circles in the central regions of the particles. Fourth, the matrix or majority phase in many particles appeared equally gray from the edge to the center of the particles. Only certain particles seemed to possess light "craters" in their central regions, such as those marked by the two red circles. These craters were separated from the outer edge by a dark ridge.

We interpret these particles as vesicles with a chain packing motif illustrated in Structure 2 of Scheme 3.3. The particles had to be hollow vesicles because the PtBA and PCEMA chains had fully-stretched lengths of 33 and 25 nm and were too short to form solid spherical particles with diameters of 90 ± 29 and 122 ± 44 nm, respectively. Moreover, solid particles at these sizes would normally appear much darker under our TEM

125

operation conditions to allow the distinction of their internal structures. In addition, the center of a spherical particle would appear darker than the periphery.

We further propose that the white circular patches close to the center of the vesicles corresponded to projections of the unstained approximately standing P*t*BA cylinders (structures b and c, Scheme 3.7) that were embedded in the stained PCEMA matrix. These P*t*BA cylinders appeared as light patches because they were approximately aligned with the electron beam. The white patches in the TEM images were densely packed and lacked hexagonal symmetry because they were projections of two, rather than one, layer of the P*t*BA cylinders.
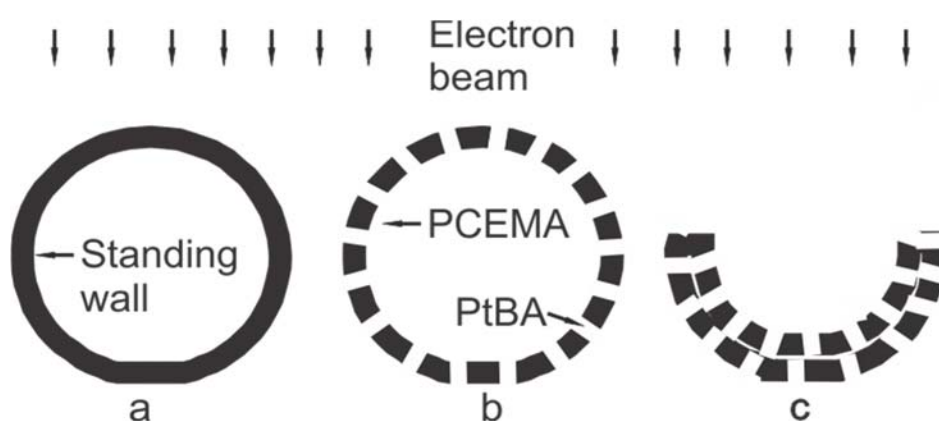
Scheme 3.7 Schematic diagrams of showing the cross-sectional wall structures of (a) a diblock copolymer vesicle, (b) a μ-(P*t*BA)(PCEMA)(PEO)$_x$ vesicle, and (c) a μ-(P*t*BA)(PCEMA)(PEO)$_{1.14}$ vesicle that had collapsed into a hemispherical bilayer. The bottoms of each vesicle are slightly flattened to reflect a possible deformation that may have occurred as the vesicle landed on a TEM grid.

Moreover, we suggest that the white stripes at the edge of the vesicles were projections of P*t*BA cylinders that were oriented along the horizontal direction in the

portion of the standing wall (Scheme 3.7b and c). These white stripes would not appear in particles that were large and had not collapsed (Scheme 3.7b) because the pathlength of the electron beam through the PCEMA domains in the standing wall region would be large. However, the pathlength of the electron beam in this region at the outer edge would be drastically reduced if the particles had collapsed into a structure analogous to the one shown in Scheme 3.7c, which illustrates a perfectly collapsed hemispherical bilayer structure. Thus, the P*t*BA cylinders might appear as short stems, as seen in Figure 3.7b in the regions marked by the red arrows. One can also easily see from Scheme 3.7c that the electron beam pathlength through the PCEMA domains initially increases and then decreases as one moves from the outer edge toward the center of the vesicle. This pathlength variation trend renders a "dark ridge" surrounding the "craters", as observed in the TEM images.

We lastly explain why the PCEMA domains of the intact vesicles would have approximately uniform grayness in the TEM images, which is different from the traditional TEM image of a gray circle encompassed by a dark ring for wall-stained diblock copolymer vesicles. As is evident in Scheme 3.7a, the electron beam pathlength decreases from the edges toward the center for diblock copolymer vesicles, giving rise to the well-known ring-encompassed gray circle that is commonly observed in TEM images of these vesicles. On the other hand, the electron beam pathlength through the stained-PCEMA domains was not necessarily much larger in the standing wall region than through the PCEMA domains in the center of the vesicles because the standing wall contained P*t*BA regions that weakly scattered the electrons. Therefore, the edges of these vesicles may not necessarily appear darker in their TEM images.

The vesicles appeared rather fused in Figure 3.7. This fusion probably occurred during TEM specimen preparation due to the inability of the short coronal PEO chains to prevent the drying vesicles from coming into close contact. In solution or in the solvated state, they most likely appeared as isolated particles. This point was verified by our dynamic light scattering (DLS) analysis. For this analysis, the particles were photocrosslinked to a CEMA double bond conversion > 40% and then dialyzed against water to remove THF. The samples were crosslinked to allow them to withstand changes in the solvent. The DLS measurements were performed in water rather than in THF/water because both the refractive index and viscosity were accurately known for water but not for the THF/water mixture used for vesicle preparation. That the photolysis should only lock in the vesicular structure and not change either the morphology or the aggregation number of the vesicles has been demonstrated previously among other analogous systems.[59] At a scattering angle of 90°, the measured hydrodynamic diameter d_h and polydispersity K_2^2/K_4 values were found to be 169 nm and 0.149, respectively, for the μ-(PtBA)(PCEMA)(PEO)$_{1.58}$ vesicles while these respective values were 188 nm and 0.169 for the μ-(PtBA)(PCEMA)(PEO)$_{1.14}$ vesicles. While the polydispersity K_2^2/K_4 values confirmed the moderate size distributions of the particles, the fact that the d_h values were only slight larger than the d_{TEM} values suggests that the vesicles were not or at least not extensively fused in the solvated state.

In fact, it was anticipated that the dh values would be larger than the dTEM values for several reasons. First, DLS and TEM probed the particles in their solvated and dry states, respectively. The particles and, in particular, the coronal chains should shrink after solvent removal. Second, TEM and DLS respectively yielded the number-average and z-

average diameters of the particles. Since the latter emphasized contributions from the larger particles, it should be larger than the former (Table 3.3).

Table 3.3 Sizes and size distributions of the vesicles or PCEMA-crosslinked vesicles probed by different techniques.

Sample	d_{TEM} (nm)	d_h (nm) [a]	DLS K_2^2/K_4 [1]	d_{AFM} (nm)	AFM d_B (nm) [b]
μ-BCE$_{1.58}$	90 ± 29	169 ± 2	0.149 ± 0.009	122 ± 44	10 ± 2
μ-BCE$_{1.14}$	122 ± 44	188 ± 4	0.169 ± 0.016	140 ± 46	10 ± 2

[a]: Averages and deviations from five separate DLS measurements for a given sample.

[b]: Average diameter with spread for the PtBA domains obtained via AFM.

On can further argue that the craters seen in Figures 3.7a and b were the openings of "semi-vesicles" or un-sealed vesicles, which had been shown by Hillmyer, Lodge, and coworkers to form from μ-(PEO)(PEE)(PFP).[31,33] However, we do not believe this to be a possibility in this case because semi-vesicles were not detected in specimens analyzed by atomic force microscopy (AFM). For AFM analysis, the vesicles were first photocrosslinked and were then aero-sprayed onto freshly-cleft mica plates. Photocrosslinking was used mainly to ensure the structural integrity of the vesicles during AFM specimen preparation. Figure 3.8 shows AFM phase and topography images of the μ-(PtBA)(PCEMA)(PEO)$_{1.14}$ and μ-(PtBA)(PCEMA)(PEO)$_{1.58}$ vesicles. The topography images show that the vesicls were mostly intact, sealed, and approximately round in shape.
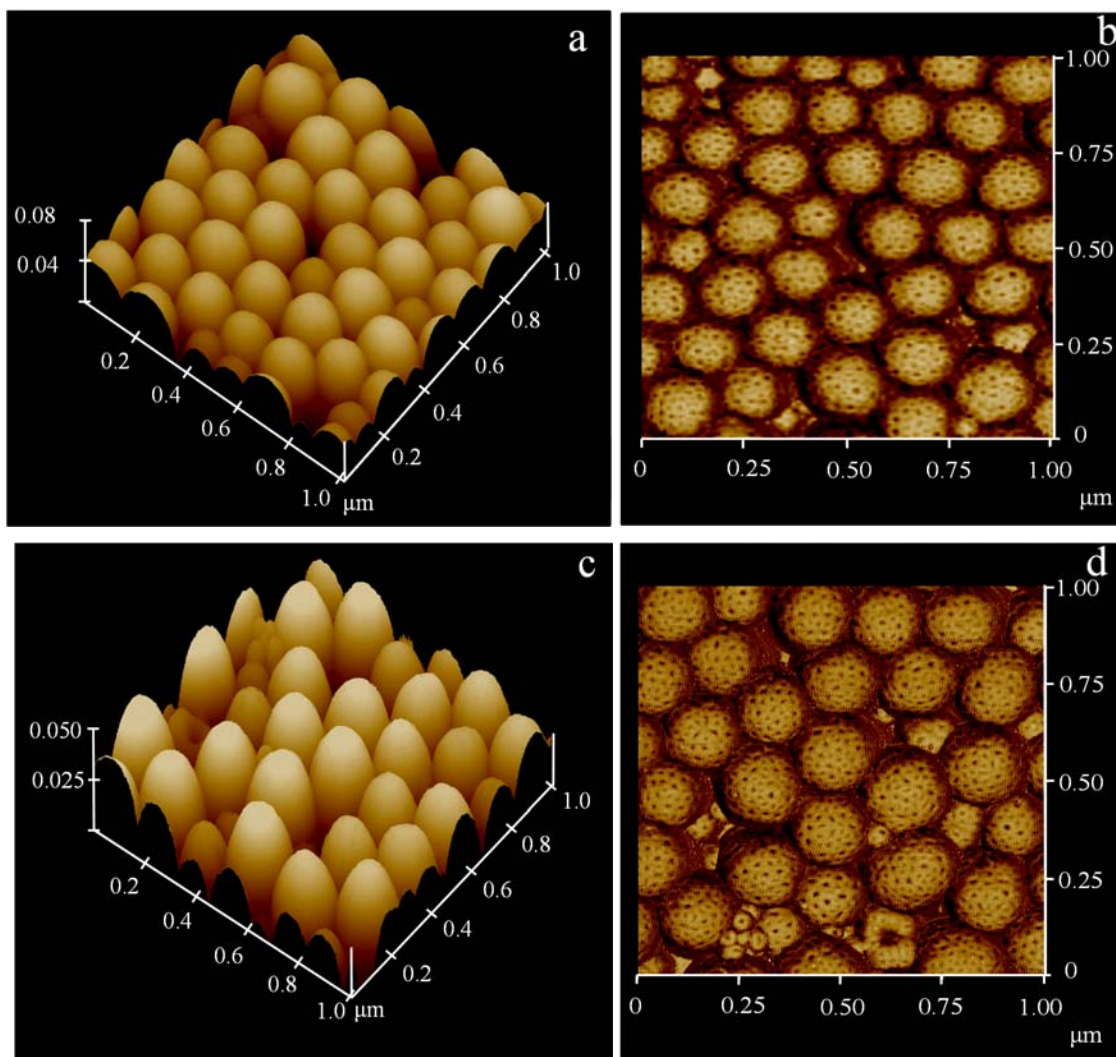
Figure 3.8 AFM (a and c) topography and (b and d) phase images of lightly crosslinked vesicles of (a and b) μ-(P*t*BA)(PCEMA)(PEO)$_{1.58}$ and (c and d) μ-(P*t*BA)(PCEMA)(PEO)$_{1.14}$.

The phase images were particularly interesting because they revealed at least two types of domains on the vesicular surfaces. The minority phase mostly appeared as hexagonally-packed dark circles with diameters of ~10 nm. These circles must have corresponded to one terminal end of the permeating P*t*BA cylinders. The visibility of these P*t*BA cylinders may be attributed to the thinness of the PEO layer. Therefore, the AFM images provided

further evidence that we had prepared vesicles with the chain packing motif shown in Structure 2 of Scheme 3.3.

The TEM, DLS, and AFM results shown in Table 3.3 suggest that the μ-(PtBA)(PCEMA)(PEO)$_{1.58}$ vesicles were smaller than the μ-(PtBA)(PCEMA)(PEO)$_{1.14}$ vesicles. This trend was reasonable, since the interfacial tension between the vesicular wall and the water-swollen PEO corona would have increased as the PEO content decreased. The system adjusted to this change by increasing the size of the vesicles to decrease the total interfacial areas between these two phases.[60]

Since the vesicles did not exhibit the traditional TEM image of a gray circle encapsulated by a dark ring, the determination of the wall thickness was difficult. We imagined that particles with the largest collapsed central craters would exhibit the thinnest edges in their TEM images (Scheme 3.7c). The thickness of the layer measured from the outermost edge to the dark ridge should provide an estimate of the upper bound for the wall thickness. Based on the top structure marked with a red circle in Figure 3.7b, we estimated that the wall thickness should be < 20 nm. This value was reasonable, since it would be substantially smaller than the fully stretched lengths for the PtBA and PCEMA chains.

3.3.5 Capsules Bearing Permeating PAA-Gated Nanochannels

Only vesicles of μ-(PtBA)(PCEMA)(PEO)$_{1.14}$ were used to prepare capsules with permeating PAA-gated nanochannels. This task involved photocrosslinking the PCEMA matrix and then hydrolyzing the PtBA cylindrical domains. The wall was crosslinked due to the dimerization of the double bonds of the CEMA units from different copolymer chains.[61,62] According to the decrease in the CEMA absorbance at 274 nm, the CEMA

double bond conversion was controlled to be ~60% in this study. The locking of the vesicular structure at this CEMA conversion was also qualitatively judged by the stability and thus the retention of the scattering power of the photolyzed vesicles in THF, which solubilized both P*t*BA and uncrosslinked PCEMA chains. Therefore, uncrosslinked vesicles that were suspended in this solvent would have disassembled into weakly scattering individual polymer chains, while crosslinked vesicles would remain intact.

Treating the crosslinked vesicles with trifluoroacetic acid hydrolyzed the P*t*BA domains.[63] We are not presenting further spectroscopic evidence here to demonstrate the occurrence of this reaction because this reaction has again been extensively used by our group in the past. Since the PAA chains produced after P*t*BA hydrolysis were soluble in water under basic conditions, they should have migrated from the space originally occupied by the P*t*BA chains. Thus, the chemical processing of the vesicles should have yielded nanocapsules bearing permeating nanochannels that were gated by PAA chains.

The PCEMA-crosslinked and P*t*BA-hydrolyzed capsules were aero-sprayed onto a freshly-cleft mica plate from water and then characterized via AFM. Figure 3.9 shows an AFM height image of the capsules. While the P*t*BA domains were barely noticeable in the height image of the μ-(P*t*BA)(PCEMA)(PEO)$_{1.14}$ vesicles, dimples were clearly observed on the capsules and especially on the capsules marked by the red arrows in Figure 3.9. These dimples had size and packing comparable to the ends of the original P*t*BA cylinders that were revealed in the AFM phase image (Figure 3.8d) and suggest that they were derived from the hydrolysis of the P*t*BA chains. We further note that the capsules shown in Figure 3.9 were not as round as the crosslinked vesicles seen in Figure 3.8c. This

difference suggested that the nanochannel-bearing capsules were more readily deformed during AFM specimen preparation than the crosslinked vesicles that had solid walls.
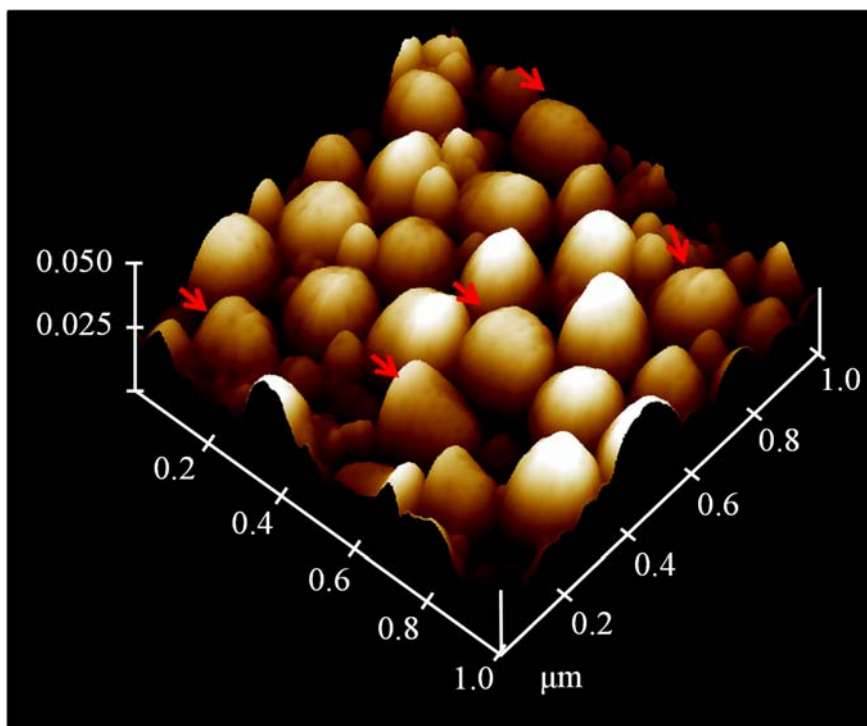
Figure 3.9 AFM topography image of μ-(PtBA)(PCEMA)(PEO)$_{1.14}$ capsules that had been aero-sprayed onto mica from water.

3.3.6 PEO$_{45}$-Py

To demonstrate the stimuli-responsive flow of the PAA-gated nanochannels of the polymersomes, PEO was functionalized with a terminal pyrene unit and used as a fluorescent probe. To prepare this probe, a solution of PEO$_{45}$-OH was reacted with 4-pyrenyl butyric acid to attach a pyrenyl group to the end of the PEO chain and thus prepare PEO$_{45}$-Py. PEO$_{45}$-Py was then loaded into the polymersomes and its release under

different pH conditions was subsequently monitored by monitoring the change in the fluorescence intensity exhibited the PEO$_{45}$-Py probe.

Figure 3.10 compares the SEC traces of PEO$_{45}$-OH and PEO$_{45}$-Py. The identical shape of the polymer peaks suggests the integrity of the PEO backbone was retained after the pyrene labelling. The slight increase in the size of the PEO$_{45}$-Py chain relative to that of the PEO$_{45}$-OH chain is reflected by a shift of the SEC trace corresponding to PEO$_{45}$-Py to a shorter retention time.
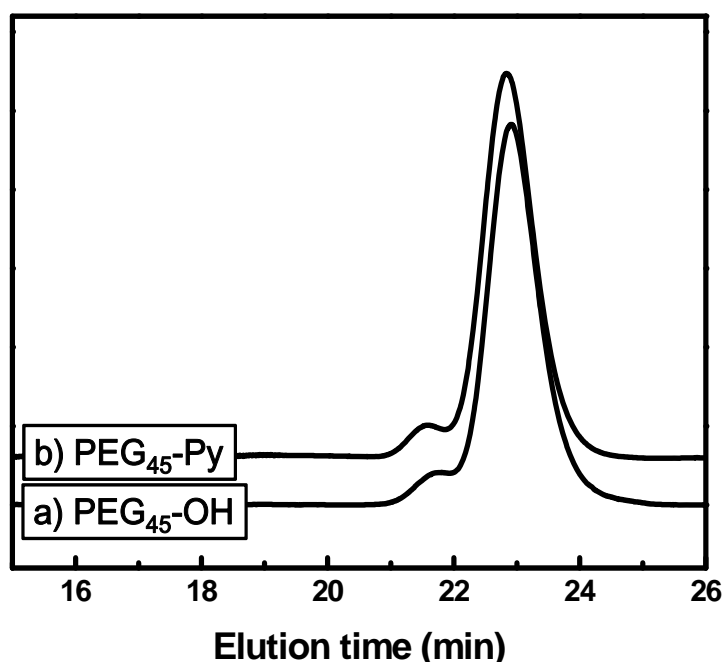
Figure 3.10 Comparison for the SEC traces of (a) PEO$_{45}$-OH and (b) PEO$_{45}$-Py.

The prepared PEO$_{45}$-Py probe was also characterized via ^{1}H NMR spectroscopy in CDCl$_3$. Figure 3.11 shows a ^{1}H NMR spectrum of PEO$_{45}$-Py together with the peak assignment for all of its protons. Integration analysis yielded a signal integration ratio of 20:1, when the integration of the protons on the PEO$_{45}$ backbone chain was compared with the integration of the Ar-H protons. By comparing the determined number of repeating

134

units with that provided by the supplier, we conclude that the pyrene labeling was quantitative within experimental error.
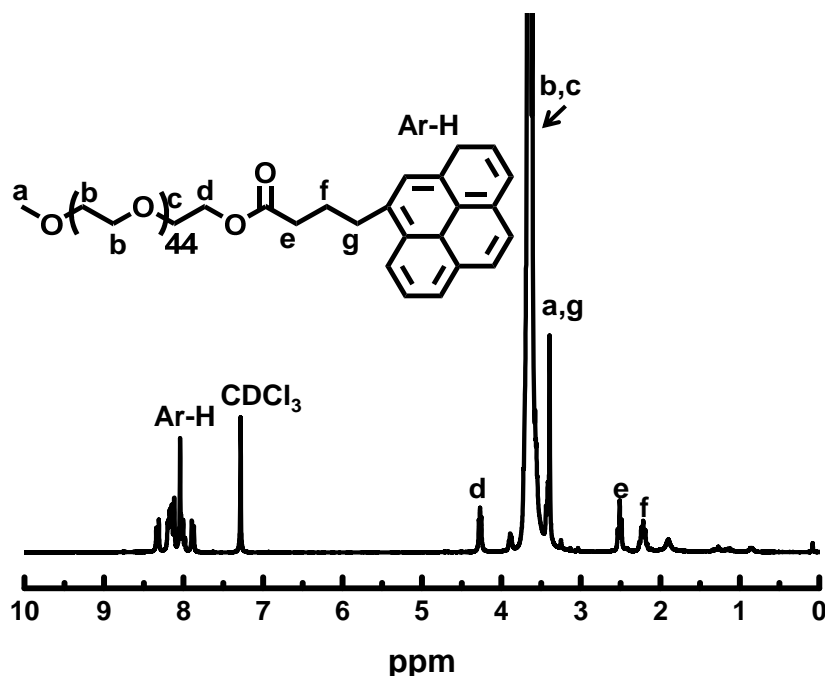
Figure 3.11 ^{1}H NMR spectrum PEO$_{45}$-Py and its signal assignments.

3.3.7 Dependence of Fluorescence Intensity on [PEO$_{45}$-Py]

As mentioned earlier, the fluorescence intensity of PEO$_{45}$-Py would not increase in a linear fashion with [PEO$_{45}$-Py] due to the inner filter effect and also because of PEO$_{45}$-Py aggregation at high [PEO$_{45}$-Py]'s. This was confirmed by us experimentally. Figure 3.12 plots changes in measured PEO$_{45}$-Py monomeric fluorescence intensity at 375 nm as a function of [PEO$_{45}$-Py]. A linear relationship was observed only at [PEO$_{45}$-Py] < 0.02 mg/mL. In all of our PEO$_{45}$-Py release experiments, the final [PEO$_{45}$-Py] in water never exceeded 0.02 mg/mL.
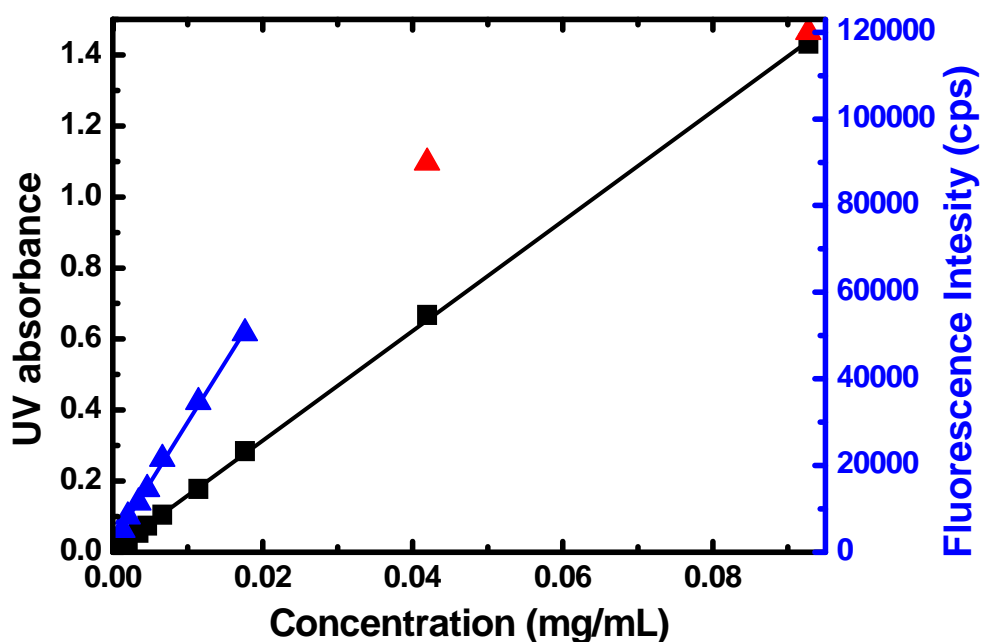
Figure 3.12 Plots of variations in pyrene dye fluorescence emission intensity (▲ and ▲) and UV absorbance (■) *versus* concentration. The solid lines show the linear fitting for the linear regions. The fluorescence intensities were measured at a wavelength of 375 nm with an excitation wavelength of 342 nm. The UV absorbance was measured at 342 nm.

3.3.8 Capsule Loading

Rhodamine B and PEO chains that were end-tagged with pyrene (PEO$_{45}$-Py, with a molar mass of 2000 g/mol or 45 repeat units) were loaded into the μ-(P*t*BA)(PCEMA)(PEO)$_{1.14}$ capsules to allow the examination of their release kinetics. While rhodamine B was commercially available, PEO$_{45}$-Py was synthesized by reacting pyrene butyric acid with PEO$_{45}$-OH. To load the dyes, a concentrated dye solution in methanol was equilibrated with the capsules before the methanol was evaporated very slowly over 5 d. Over this time, the concentration of the dye solution increased gradually

and this concentration gradient between the exterior and the capsular core was presumed to force some of the dye into the cavities of the capsules.

The dried dye/capsule mixture should have contained rhodamine B or PEO_{45}-Py molecules that had not been loaded into the capsules. We suspected that these unloaded dye molecules could be readily removed by stirring the clay-like dye/capsule mixture with a small volume of an aqueous HCl solution and then separating the supernatant from the capsules via centrifugation and decantation. A mildly acidic solution at a final pH of 2.85 after capsule dispersion was used for this separation. This pH was chosen because our previous study of reagent transport across thin PCEMA films permeated by PAA-lined nanochannels established that the channel permeability was the lowest at pH ~3.0 due to the formation, in the nanochannels, of a H-bonded PAA network.[43] We further speculated that the dye concentration in the rinsing liquid would decrease rapidly with the number of rinsing cycles initially. After the external dyes were removed, some fresh dye would still be released from the capsules during each rinsing cycle. Since the volume of the rinsing liquid and the rinsing time were roughly constant for each rinsing cycle, the dye concentration in the rinsing liquid would eventually reach a low steady-state value if the encapsulated dye leached out of the capsules slowly. In one case, we measured the UV absorbance of PEO_{45}-Py in the separated supernatant after each rinsing step. From the first to fourth rinsing liquid, [PEO_{45}-Py] decreased by a factor of 47 (Figure 3.13a). After these rinsing cycles, [PEO_{45}-Py] in the rinsing liquid remained low and constant. This [PEO_{45}-Py] variation trend was in exact agreement with our speculation, thus suggesting that the unloaded PEO_{45}-Py was mostly removed during the initial four rinsing cycles and the loaded PEO_{45}-Py was slowly released at pH = 2.85 under our rinsing conditions.
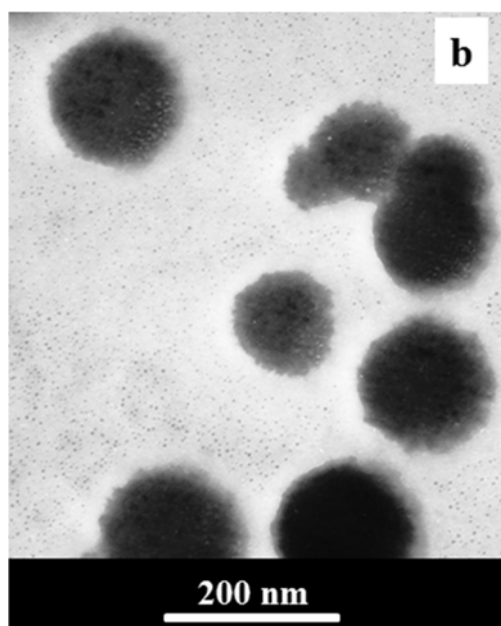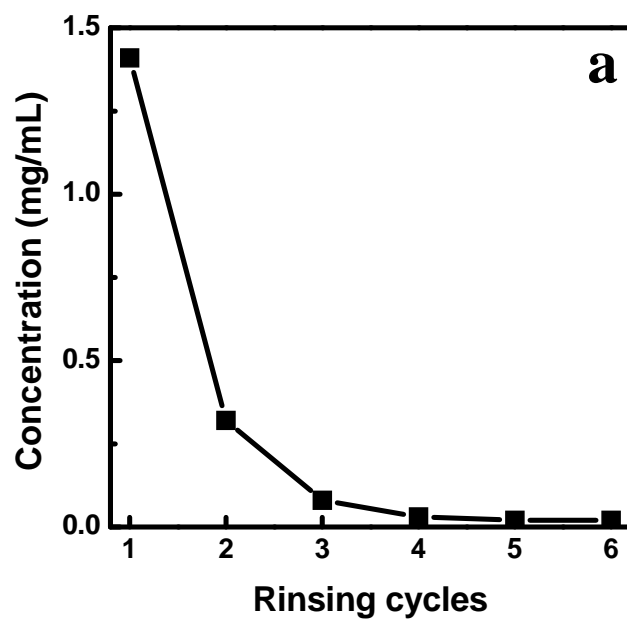
Figure 3.13 (a) Decrease in [PEO$_{45}$-Py] in the aqueous pH = 2.85 rinsing liquid as a function of the number of rinsing cycles for a sample of PEO$_{45}$-Py-loaded capsules. (b) TEM image of OsO$_4$-stained capsules after they had been loaded with PEO$_{45}$-Py to a weight fraction of 31 wt%.

In contrast, the rhodamine-B-loaded capsules behaved in a completely different manner. The rinsing liquid always had a red color of the dye until the capsules eventually

lost the dye color. This behavior was probably caused by the high release rate of rhodamine B from the capsules and provided anecdotal evidence for the size-selective release through the nanochannels of rhodamine B over PEO_{45}-Py. Because of the fast release of rhodamine B even at pH = 2.85, we did not compare their release kinetics under different pH conditions.

We determined the amount of PEO_{45}-Py that remained in a capsular sample after it had been rinsed five times with aqueous HCl (pH = 2.85). This task involved drying the PEO_{45}-Py-loaded capsule sample, weighing it, re-dispersing it overnight into a basic aqueous solution to give a final dispersion pH of 11.23, and then determining its absorbance at 342 nm. As will be discussed later, the high pH of the re-dispersing medium and the long re-dispersal time ensured that the loaded PEO_{45}-Py was mostly released from the capsules. Thus, the molar extinction coefficient ε of 3.5×10^4 $M^{-1} \cdot cm^{-1}$ that we had determined for dilute aqueous PEO_{45}-Py solutions was used to calculate $[PEO_{45}$-Py] in the re-dispersing medium and then used to determine the amount of PEO_{45}-Py that was originally in the capsules. This experiment yielded in the capsule and dye mixture a high PEO_{45}-Py loading density of 31 wt%, suggesting the effectiveness of the capsule loading method.

This PEO_{45}-Py-loaded capsule sample was then re-dispersed into water, immediately aero-sprayed onto a nitrocellulose-coated TEM grid, and stained with OsO_4 vapor for analysis. Figure 3.13b shows a TEM image of a capsule specimen that was prepared in this manner. The TEM image of Figure 3.13b appears clearly different from those shown in Figure 3.7. While the internal structures of the capsules could be observed in Figure 3.7, the capsules shown in Figure 3.13b were too dark to allow viewing of their internal

structures. Moreover, the darkness increased as one moved from the outer edge to the center of the particles, giving the impression that the particles were solid rather than hollow. Thus, the TEM image suggests that the capsules were indeed heavily loaded with PEO$_{45}$-Py.

We established the necessity of the nanochannels to allow the uptake of PEO45-Py from a control experiment. In this experiment, we prepared micelles from a PCEMA-*b*-PAA diblock copolymer consisting of 600 CEMA units and 55 AA units and the micelles were then photolyzed to crosslink the PCEMA core.[64] After the solid nanoparticles had been loaded with PEO$_{45}$-Py and subjected to four rinsing cycles, the loaded PEO$_{45}$-Py content was determined to be 1.3 wt%. This value was essentially zero or much lower than the PEO$_{45}$-Py loading density of 31wt% in the μ-(P*t*BA)(PCEMA)(PEO)$_{1.14}$ nanocapsules.

3.3.9 pH-Gated PEO$_{45}$-Py Release

PEO$_{53}$-Py, which has a slightly longer PEO block than the 45 repeat units for our PEO chain, has been previously shown to exhibit a normal monomeric Py emission spectrum at concentrations < 0.1 mg/mL in aqueous solution.[65-67] Above this concentration, a broad featureless excimer emission centered at ~490 nm emerged and the excimer fluorescence intensity increased with [PEO$_{53}$-Py] at the cost of the monomer emission. Since the [PEO$_{45}$-Py] in our capsular cores was some three orders of magnitude higher than 0.1 mg/mL, the monomeric fluorescence intensity of PEO$_{45}$-Py should be low in the capsules due to Py excimer formation. After the release of PEO$_{45}$-Py into the surrounding aqueous solution, the Py monomeric fluorescence intensity should increase initially with time until the concentration of the released PEO$_{45}$-Py in the aqueous phase

was high enough to produce Py excimers again. Therefore, this increase in Py monomeric fluorescence intensity as a function of time should allow us to monitor the PEO$_{45}$-Py release kinetics.
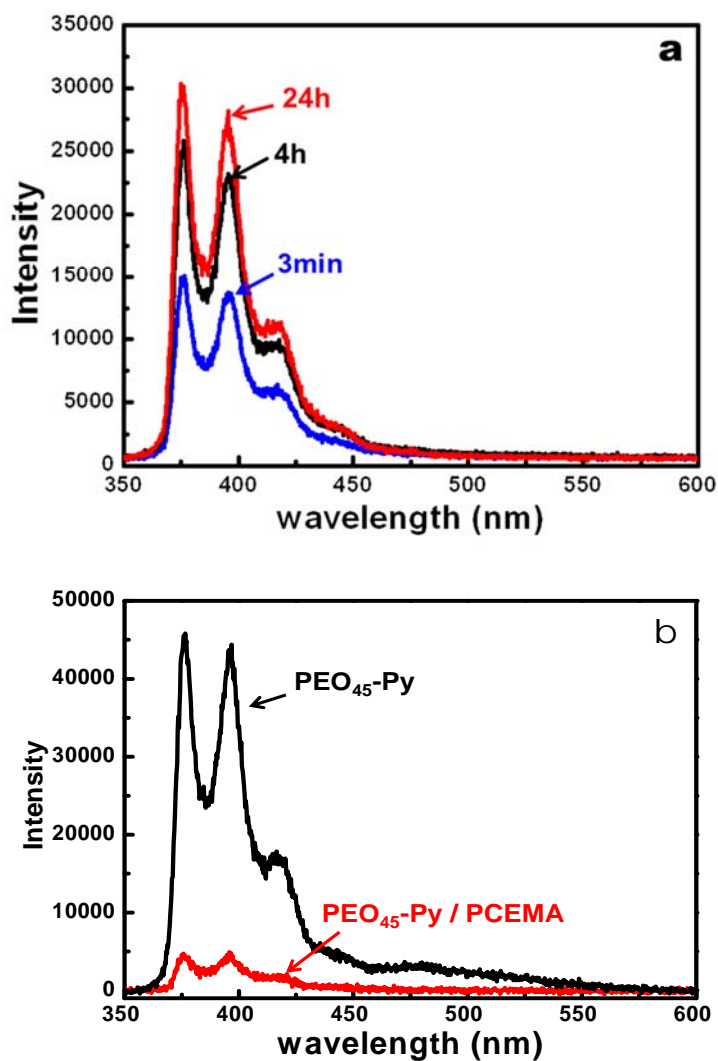
Figure 3.14 (a) Fluorescence spectra of a PEO$_{45}$-Py-loaded capsular sample 3 min, 4 h, and 24 h after its dispersion into an aqueous HCl solution that gave a final pH of 2.85 after capsule dispersion. (b) Fluorescence spectra of PEO$_{45}$-Py at 0.20 mg/mL in THF in the presence or absence of PCEMA at an EO/CEMA molar ratio of 1/1.

We excited PEO$_{45}$-Py at 342 nm where the capsules scattered some light but exhibited negligible absorbance and measured the fluorescence spectra of PEO$_{45}$-Py 3 min, 4 h, and 24 h after a freshly-rinsed clay-like sample of PEO$_{45}$-Py-loaded capsules was dispersed into an aqueous HCl solution that gave a final pH of 2.85. The resultant spectra are compared in Figure 3.14a. As expected, the monomeric fluorescence intensity increased with time. A remarkable surprise was that the excimer emission peak at ~490 nm was missing from all of the spectra shown in Figure 3.14a.

The excimer emission was absent even only 3 min after the PEO$_{45}$-Py-loaded capsules had been dispersed in the acidic water, a point when much of the loaded PEO$_{45}$-Py chains had not been released yet. The lack of an excimer signal at this point suggested that the excimer emission was quenched by the capsules. To indentify the quencher, we then compared the fluorescence behavior of PEO$_{45}$-Py at 0.20 mg/mL with or without PAA or PCEMA, where PAA and PCEMA were derived from PtBA and P(HEMA-TMS) chains that were prepared via anionic polymerization. In water at [EO]/[AA] = 1.00/1.00, PAA chains with 100 repeat units exhibited negligible effect on the monomeric or excimer fluorescence of PEO$_{45}$-Py. On the other hand, the intensity of the monomer and the excimer fluorescence of PEO$_{45}$-Py drastically decreased in the presence of 150-unit-long PCEMA chains at [CEMA]/[EO] = 1.00/1.00 (Figure 3.14b). Therefore, PCEMA effectively quenched the fluorescence of Py monomers and excimers, a conclusion resonated by a report on the quenching of pyrene monomer and excimer fluorescence by methyl cinnamate.[68] This quenching was still efficient in the capsules despite the low mobility of wall-forming PCEMA chains for two possible reasons. First, Py monomers and excimers still had sufficient mobility to facilitate dynamic fluorescence quenching.

Second, the Py end-groups might even form ground-state complexes with CEMA due to the strong hydrophobicity of Py and CEMA and some static quenching could also have occurred.

The monomer emission for the encapsulated PEO_{45}-Py should be low not only due to Py excimer formation but also due to quenching by the capsules. We excited PEO_{45}-Py at 342 nm and monitored changes in the monomer emission intensity at 375 nm as a function of time for several sets of the loaded capsules after they had been dispersed into dilute HCl or NaOH solutions that gave final pH values of 2.85, 6.76, and 9.98, respectively. The results are shown in Figure 3.15a. In every case, the PEO_{45}-Py monomeric fluorescence intensity initially increased rapidly with time and then gradually plateaued. The plateaued-to-initial intensity ratio was 13.6 for the sample studied at pH = 9.98. While this number was large, the true ratio could be even larger because some PEO_{45}-Py was released already when the initial intensity was measured. This pre-release occurred first because the initial loaded capsular sample was not completely dry and the external aqueous phase contained some PEO_{45}-Py already. Subsequently, ~15 s were required to disperse the clay-like sample into water and to begin the data acquisition process. During this time period some further release would have occurred. This high ratio of the final-to-initial PEO_{45}-Py fluorescence intensity suggested that the quantum yield of the released PEO_{45}-Py was indeed much higher than that of the encapsulated PEO_{45}-Py, confirming extensive monomer fluorescence quenching for the encapsulated PEO_{45}-Py.
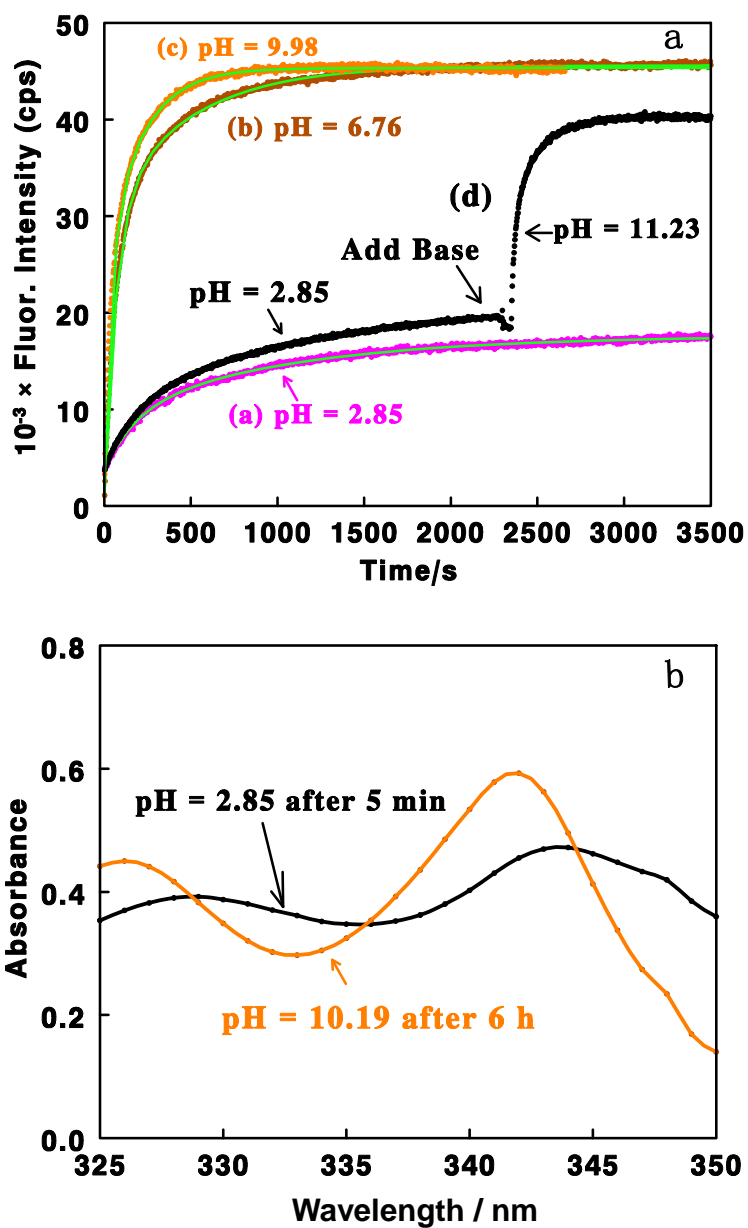
Figure 3.15 (a) Variations in the intensity of Py monomeric fluorescence as a function of time after PEO$_{45}$-Py-loaded capsules had been dispersed into HCl or NaOH solutions that gave final solution pH values of 2.85, 6.76, and 9.98, respectively. Also shown are the data for a sample that was initially at pH = 2.85 and then at 11.23. The solid green curves are the best fit to the experimental data obtained by Equation 3.1. (b) UV-visible absorption spectra of PEO$_{45}$-Py-loaded capsule samples that were recorded 5 min and 6 h after their dispersion into aqueous solutions at pH = 2.85 and 9.98, respectively.

144

The high final-to-initial monomer fluorescence intensity ratio initially solicited us to neglect the fluorescence emission of the encapsulated PEO_{45}-Py and to relate the observed fluorescence intensity directly to the released PEO_{45}-Py concentration. By assuming that the free and encapsulated PEO_{45}-Py had the same molar extinction coefficient at 342 nm, we quantified the total PEO_{45}-Py present in a sample via UV absorption analysis. Combining the UV and the fluorescence data of Figure 3.15a, we calculated the plateaued released PEO_{45}-Py amounts of 35 w%, 76 w%, and 79 w% for the samples studied at pH = 2.85, 6.76, and 9.98, respectively. Unfortunately, our further analysis suggested that these numbers were approximate because our second assumption that the extinction coefficient of the free and the encapsulated PEO_{45}-Py would be similar was incorrect. We recorded an absorption spectrum for a PEO_{45}-Py-loaded capsular sample 5 min after its dispersion at pH = 2.85. To this sample was then added NaOH so that its pH increased to 10.19. After the dispersion had been stirred at this pH for another 6 h, we obtained another absorption spectrum. Figure 3.15b compares the two absorption spectra. The absorbance at 342 nm was not constant because the 342 nm peak in the pH = 10.19 solution appeared narrower, had a greater absorbance, and exhibited a red-shift. These phenomena were observed because PEO_{45}-Py was mostly released in the second but not in the first sample. Aggregated PEO_{53}-Py chains have been shown previously to possess broader absorption peaks and lower extinction coefficients than their free counterparts.[65-67] Thus, these changes in the absorption spectra of Figure 3.15b supported the release of PEO_{45}-Py over time under basic conditions. Unfortunately, they made the accurate quantification of the released PEO45-Py chains difficult.

Despite the challenges in accurately determining the percentage of PEO_{45}-Py released, the data of Figure 3.15a could be used to draw the conclusion that PEO_{45}-Py was released faster and more completely under basic conditions. Our control experiment showed that the PEO_{45}-Py fluorescence intensity at $[PEO_{45}$-Py$] \leq 0.02$ mg/mL, which was the maximum bulk concentration that we ever used in our release experiments, had no pH dependence. Therefore, the more complete release of PEO_{45}-Py was evident from the plateaued-to-initial intensity ratios of 4.5, 13.4, and 13.6 for the samples studied at pH = 2.85, 6.76, and 9.98, respectively. More directly, we monitored the PEO_{45}-Py fluorescence intensity variation with time of a loaded capsule sample that was dispersed initially at pH = 2.85 and then adding base to increase the solution pH to 11.23 (Figure 3.15a). The addition of the basic solution was first followed by a decrease and then another 1.8-fold increase in the fluorescence intensity. The initial decrease in intensity was due to the dilution that had occurred upon the addition of the basic solution. The subsequent increase in the fluorescence intensity was caused by the further release of PEO_{45}-Py from the capsules.

The conclusion of faster PEO_{45}-Py release under basic conditions could be reached by comparing the slope or rate of fluorescence intensity increase at early stages of PEO_{45}-Py release when the PEO_{45}-Py fluorescence intensity increased linearly with time. More quantitatively, we fitted the PEO_{45}-Py fluorescence intensity $I(t)$ for the release data at pH = 2.85, 6.76, and 9.98 using the following phenomenological equation:

$$I(t) = I_\infty - I_1\, exp(-k_1 t) - I_2\, exp(-k_2 t) \qquad\qquad \text{Equation 3.1}$$

where I_∞ is the plateaued fluorescence intensity, k_1 is the rate constant at which the fluorescence intensity component I_1 grows, and k_2 is the rate constant at which the

146

fluorescence intensity component I_2 grows. We further calculated the average rate constant $<k>$ for the fluorescence intensity to grow using:

$$<k> = (I_1 \times k_1 + I_2 \times k_2)/(I_1 + I_2) \qquad \text{Equation 3.2}$$

The $<k>$ values were 2.37×10^{-3}, 1.03×10^{-2}, and 1.67×10^{-2} s^{-1} at pH = 2.85, 6.76, and 9.98, respectively. Thus, $<k>$ increased with pH and the $<k>$ value at pH = 9.98 was 7.04 times larger than that at pH = 2.85.

The higher release rate and more complete release of PEO$_{45}$-Py under more basic conditions was most likely due to the gating effect of the PAA chains under acidic conditions.   At low pH values, the PAA chains underwent hydrogen bonding[69] and probably formed a compact structure resembling "gelled PAA rings" that guarded or partially blocked the nanochannels (Structure 4a, Scheme 3.3). Partial channel blocking should slow down PEO$_{45}$-Py release in general.   More importantly, it might completely stop the release of the high-molecular-weight fraction of the PEO$_{45}$-Py chains, reducing the extent of PEO$_{45}$-Py release. These gates were opened in highly basic media, leading to faster and more complete release of PEO$_{45}$-Py.

3.4 Conclusions

PtBA-b-PCOOH-b-PCEMA has been prepared by derivatizing a triblock terpolymer precursor prepared via anionic polymerization. The repeat unit numbers of the PtBA, PCOOH, and PCEMA blocks were 100, 5, and 130, respectively. On the other hand, PEO-b-PNH$_2$ consisting of 114 EO units and 5 amine group-bearing units were prepared by derivatizing a precursor diblock copolymer that had been synthesized via ATRP. PtBA-b-PCOOH-b-PCEMA and PEO-b-PNH$_2$ were then associated through their complementary

PCOOH and PNH$_2$ blocks and covalently linked via amidization to yield two novel pseudo μ-(PtBA)(PCEMA)(PEO)$_x$ triblock terpolymers with $x = 1.14$ and 1.58. This represents the first report on the synthesis of pseudo miktoarm triblock terpolymers using this method. The copolymers were significant because they contained blocks that could be readily modified via crosslinking and hydrolysis treatment. Additionally, the preparation protocol was general and should be useful for the preparation of other functional pseudo miktoarm copolymers.

The prepared μ-(PtBA)(PCEMA)(PEO)$_x$ self-assembled in THF/water at $f_{H2O} = 80\%$ into vesicles with the PtBA and PCEMA blocks forming the vesicular wall. Since the volume fraction of PtBA was 30% among the PtBA and PCEMA blocks, PtBA formed a hexagonally-packed cylindrical phase that was embedded in the PCEMA wall. This vesicular structure was confirmed via TEM, DLS, and AFM analyses. While the capsular morphology did not change with x, the average diameter of the vesicles increased as x decreased. Therefore, varying in a certain range the average number x of PEO-b-PNH$_2$ chains that reacted with each PtBA-b-PCOOH-b-PCEMA chain did not affect the morphology of the micellar aggregates formed. Rather, tuning x offered a unique route to fine-tuning the average size of the vesicles.

The PCEMA phase in the vesicular walls was then photocrosslinked and the PtBA domains were hydrolyzed to yield an unprecedented nanostructure, capsules that were permeated by PAA-gated nanochannels. After PEO$_{45}$-Py was loaded into the capsules, we made the surprising discovery that both the monomer and excimer fluorescence of the terminal pyrene groups of PEO$_{45}$-Py was quenched by PCEMA. Thus, the fluorescence intensity of PEO$_{45}$-Py was very low within the capsules but increased drastically after their

release. This increase in the pyrene monomer fluorescence intensity with time allowed us to monitor the PEO$_{45}$-Py release kinetics under different conditions. The rate and total amount of PEO$_{45}$-Py released could be regulated by changing the aqueous pH and increased under basic conditions. While the quenching of the Py fluorescence by PCEMA represents a fascinating photochemical and photophysical behavior of PCEMA, future generations of these capsules may find applications in controlled release applications.

3.5 **Note and** References

Part of the work described in this chapter includes contributions from the following publications:

Hu, H.; Liu, G. Miktoarm Star Copolymer Capsules Bearing pH-Responsive Nanochannels. *Macromolecules*, **2014**, *47*, 5096–5103

References

1.   Maurer, K. H. Detergent proteases. *Curr. Opin. Biotechnol.* **2004**, *15*, 330-334.

2.   Kost, J.; Langer, R. Responsive polymeric delivery systems. *Adv. Drug Delivery Rev.* **2012**, *64*, 327-341.

3.   De Oliveira, H.; Thevenot, J.; Lecommandoux, S. Smart polymersomes for therapy and diagnosis: fast progress toward multifunctional biomimetic nanomedicines. *Wiley Interdisciplinary Reviews-Nanomedicine And Nanobiotechnology* **2012**, *4*, 525-546.

4.   Lee, J. S.; Feijen, J. Polymersomes for drug delivery: Design, formation and characterization. *J. Controlled Release* **2012**, *161*, 473-483.

5.   Keating, C. D. INORGANIC PROTOCELLS Gated access to microreactors. *Nat. Chem.* **2013**, *5*, 449-451.

6.   Thompson, K. L.; Chambon, P.; Verber, R.; Armes, S. P. Can Polymersomes Form Colloidosomes? *J. Am. Chem. Soc.* **2012**

134, 12450-12453.

7.   Li, M.; Harbron, R. L.; Weaver, J. V. M.; Binks, B. P.; Mann, S. Electrostatically gated membrane permeability in inorganic protocells. *Nat. Chem.* **2013**

5, 529-536.

8.   Wolosiuk, A.; Armagan, O.; Braun, P. V. Double direct templating of periodically nanostructured ZnS hollow microspheres. *J. Am. Chem. Soc.* **2005**, *127*, 16356-16357.

9.   Rosenbauer, E. M.; Wagner, M.; Musyanovych, A.; Landfester, K. Controlled Release from Polyurethane Nanocapsules via pH-, UV-Light- or Temperature-Induced Stimuli. *Macromolecules* **2010**, *43*, 5083-5093.

10.   Landfester, K.; Musyanovych, A.; Mailander, V. From Polymeric Particles to Multifunctional Nanocapsules for Biomedical Applications Using the Miniemulsion Process. *J. Polym. Sci., Part A: Polym. Chem.* **2010**, *48*, 493-515.

11.   Zheng, R. H.; Liu, G. J. Water-dispersible oil-filled ABC triblock copolymer vesicles and nanocapsules. *Macromolecules* **2007**, *40*, 5116-5121.

12.   Liu, F.; Hu, J. W.; Liu, G. J.; Hou, C. M.; Lin, S. D.; Zou, H. L.; Zhang, G. W.; Sun, J. P.; Luo, H. S.; Tu, Y. Y. Ternary Graft Copolymers and Their Use in Nanocapsule Preparation. *Macromolecules* **2013**, *46*, 2646-2657.

13.   Discher, D. E.; Eisenberg, A. Polymer vesicles. *Science* **2002**, *297*, 967-973.

14.   Zhang, L. F.; Eisenberg, A. Multiple Morphologies of Crew-cut Aggregates of Polystyrene-b-Poly(Acrylic Acid) Block Copolymers. *Science* **1995**, *268*, 1728-1731.

15.   Ding, J. F.; Liu, G. J. Polyisoprene-*block*-poly(2-cinnamoylethyl methacrylate) vesicles and their aggregates. *Macromolecules* **1997**, *30*, 655-657.

16.   Ding, J. F.; Liu, G. J.; Yang, M. L. Multiple morphologies of polyisoprene-*block*-poly(2-cinnamoylethyl methacrylate) and polystyrene-*block*-poly(2-cinnamoylethyl methacrylate) micelles in organic solvents. *Polymer* **1997**, *38*, 5497-5501.

17.   Battaglia, G.; Ryan, A. J. Bilayers and interdigitation in block copolymer vesicles. *J. Am. Chem. Soc.* **2005**, *127*, 8757-8764.

18. Al-Jamal, W. T.; Kostarelos, K. Liposomes: From a Clinically Established Drug Delivery System to a Nanoparticle Platform for Theranostic Nanomedicine. *Acc. Chem. Res.* **2011**, *44*, 1094-1104.

19. Nardin, C.; Thoeni, S.; Widmer, J.; Winterhalter, M.; Meier, W. Nanoreactors based on (polymerized) ABA-triblock copolymer vesicles. *Chem. Commun.* **2000**, 1433-1434.

20. Onaca, O.; Enea, R.; Hughes, D. W.; Meier, W. Stimuli-Responsive Polymersomes as Nanocarriers for Drug and Gene Delivery. *Macromol. Biosci.* **2009**, *9*, 129-139.

21. Fuks, G.; Talom, R. M.; Gauffre, F. Biohybrid block copolymers: towards functional micelles and vesicles. *Chem. Soc. Rev.* **2011**, *40*, 2475-2493.

22. Gaitzsch, J.; Appelhans, D.; Wang, L. G.; Battaglia, G.; Voit, B. Synthetic Bio-nanoreactor: Mechanical and Chemical Control of Polymersome Membrane Permeability. *Angew. Chem., Int. Ed.* **2012**, *51*, 4448-4451.

23. Amstad, E.; Kim, S. H.; Weitz, D. A. Photo- and Thermoresponsive Polymersomes for Triggered Release. *Angew. Chem., Int. Ed.* **2012**, *51*, 12499-12503.

24. Yan, B.; Tong, X.; Ayotte, P.; Zhao, Y. Light-responsive block copolymer vesicles based on a photo-softening effect. *Soft Matter* **2011**, *7*, 10001-10009.

25. Cheng, Z. L.; Tsourkas, A. Paramagnetic porous polymersomes. *Langmuir* **2008**, *24*, 8169-8173.

26. Van Gough, D.; Defino, J. L.; Braun, P. V. Programmed size-selected permeation of ssDNA into ZnS mesoporous hollow spheres. *Soft Matter* **2012**, *8*, 4396-4401.

27.   Hadjichristidis, N.; Iatrou, H.; Pitsikalis, M.; Pispas, S.; Avgeropoulos, A. Linear and non-linear triblock terpolymers. Synthesis, self-assembly in selective solvents and in bulk. *Progr. Polym. Sci.* **2005**, *30*, 725-782.

28.   Moughton, A. O.; Hillmyer, M. A.; Lodge, T. P. Multicompartment Block Polymer Micelles. *Macromolecules* **2012**, *45*, 2-19.

29.   Wyman, I. W.; Liu, G. J. Micellar structures of linear triblock terpolymers: Three blocks but many possibilities. *Polymer* **2013**, *54*, 1950-1978.

30.   Pispas, S.; Hadjichristidis, N.; Potemkin, I.; Khokhlov, A. Effect of architecture on the micellization properties of block copolymers: A(2)B miktoarm stars vs AB diblocks. *Macromolecules* **2000**, *33*, 1741-1746.

31.   Li, Z. B.; Hillmyer, M. A.; Lodge, T. P. Morphologies of multicompartment micelles formed by ABC miktoarm star terpolymers. *Langmuir* **2006**, *22*, 9409-9417.

32.   Li, Z. B.; Kesselman, E.; Talmon, Y.; Hillmyer, M. A.; Lodge, T. P. Multicompartment micelles from ABC miktoarm stars in water. *Science* **2004**, *306*, 98-101.

33.   Tian, Y.; He, Q.; Tao, C.; Li, J. B. Fabrication of fluorescent nanotubes basel on layer-by-layer assembly via covalent bond. *Langmuir* **2006**, *22*, 360-362.

34.   Kong, W. X.; Li, B. H.; Jin, Q. H.; Ding, D. T.; Shi, A. C. Helical Vesicles, Segmented Semivesicles, and Noncircular Bilayer Sheets from Solution-State Self-Assembly of ABC Miktoarm Star Terpolymers. *J. Am. Chem. Soc.* **2009**, *131*, 8503-8512.

35.   Wyman, I.; Liu, G. J. Self-assembly and chemical processing of block copolymers: A roadmap towards a diverse array of block copolymer nanostructures. *Sci. China Chem.* **2013**, *56*, 1040-1066.

36.   Chen, Y. M. Shaped Hairy Polymer Nanoobjects. *Macromolecules* **2012**, *45*, 2619-2631.

37.   Thurmond, K. B.; Kowalewski, T.; Wooley, K. L. Water-soluble knedel-like structures: The preparation of shell-cross-linked small particles. *J. Am. Chem. Soc.* **1996**, *118*, 7239-7240.

38.   Liu, G. J.; Qiao, L. J.; Guo, A. Diblock copolymer nanofibers. *Macromolecules* **1996**, *29*, 5508-5510.

39.   Liu, G. J.; Ding, J. F.; Qiao, L. J.; Guo, A.; Dymov, B. P.; Gleeson, J. T.; Hashimoto, T.; Saijo, K. Polystyrene-block-poly (2-cinnamoylethyl methacrylate) nanofibers - Preparation, characterization, and liquid crystalline properties. *Chem. Eur. J.* **1999**, *5*, 2740-2749.

40.   Stewart, S.; Liu, G. Block copolymer nanotubes. *Angew. Chem., Int. Ed.* **2000**, *39*, 340-344.

41.   Yan, X. H.; Liu, G. J.; Liu, F. T.; Tang, B. Z.; Peng, H.; Pakhomov, A. B.; Wong, C. Y. Superparamagnetic triblock copolymer/Fe2O3 hybrid nanofibers. *Angew. Chem., Int. Ed.* **2001**, *40*, 3593-97.

42.   Liu, G. J.; Ding, J. F.; Guo, A.; Herfort, M.; Bazett-Jones, D. Potential skin layers for membranes with tunable nanochannels. *Macromolecules* **1997**, *30*, 1851-1853.

43.   Liu, G. J.; Ding, J. F.; Hashimoto, T.; Kimishima, K.; Winnik, F. M.; Nigam, S. Thin films with densely, regularly packed nanochannels: Preparation, characterization, and applications. *Chem. Mater.* **1999**, *11*, 2233-2240.

44.   Khanna, K.; Varshney, S.; Kakkar, A. Miktoarm star polymers: advances in synthesis, self-assembly, and applications. *Polym. Chem.* **2010**, *1*, 1171-1185.

45.   Hirao, A.; Hayashi, M.; Loykulnant, S.; Sugiyama, K. Precise syntheses of chain-multi-functionalized polymers, star-branched polymers, star-linear block polymers, densely branched polymers, and dendritic branched polymers based on iterative approach using functionalized 1,1-diphenylethylene derivatives. *Prog. Polym. Sci.* **2005**, *30*, 111-182.

46.   Dou, H. J.; Hong, L. Z.; Liu, G. J. Miktoarm Star Copolymers from the Chemical Stitching of Associating Block Copolymers. *Macromolecules* **2010**, *43*, 4629-4637.

47.   Simon, R. H. M. Anionic-POlymerization - Principles and Practice. *American Scientist* **1984**, *72*, 413-414.

48.   Hirao, A.; Kato, H.; Yamaguchi, K.; Nakahama, S. Polymerization Of Monomers Containing Functional-Groups Protected By Trialkylsilyl Groups. 5. Synthesis Of Poly(2-Hydroxyethyl Methacrylate) With A Narrow Molecular-Weight Distribution By Means Of Anionic Living Polymerization. *Macromolecules* **1986**, *19*, 1294-1299.

49.   Mori, H.; Wakisaka, O.; Hirao, A.; Nakahama, S. Protection and Polymerization of Functional Monomers 23. Synthesis of Well-defined Poly(2-Hyroxyethel Methacrylate) by Means of Anionic Living Polymerization of Protected Monomers. *Macromol. Chem. Phys.* **1994**, *195*, 3213-3224.

50.   Tsarevsky, N. V.; Sarbu, T.; Gobelt, B.; Matyjaszewski, K. Synthesis of styrene-acrylonitrile copolymers and related block copolymers by atom transfer radical polymerization. *Macromolecules* **2002**, *35*, 6142-6148.

51.   Muhlebach, A.; Gaynor, S. G.; Matyjaszewski, K. Synthesis of amphiphilic block copolymers by atom transfer radical polymerization (ATRP). *Macromolecules* **1998**, *31*, 6046-6052.

52.   Berne, B. J.; Pecora, R. *Dynamic Light Scattering: With Applications to Chemistry, Biology, and Physics*. Dover Publications, Inc.: Mineola, N.Y., **2000**.

53.   Bates, F. S.; Fredrickson, G. H. Block copolymers - Designer soft materials. *Phys. Today* **1999**, *52*, 32-38.

54.   Huglin, M. B. *Light Scattering from Polymer Solutions*. Academic Press: London, 1972; p p34.

55.   Matyjaszewski, K.; Xia, J. H. Atom transfer radical polymerization. *Chem. Rev.* **2001**, *101*, 2921-2990.

56.   Bald, E.; Saigo, K.; Mukaiyama, T. Facile Synthesis of Carboxamides by Using 1-Methyl-2-Halopyridinium Iodides as Coupling Reagents. *Chem. Lett.* **1975**, 1163-1166.

57.   Kubo, M.; Hayashi, T.; Kobayashi, H.; Itoh, T. Syntheses of tadpole- and eight-shaped polystyrenes using cyclic polystyrene as a building block. *Macromolecules* **1998**, *31*, 1053-1057.

58.   Ding, J. F.; Liu, G. J. Growth and morphology change of polystyrene-block-poly(2-cinnamoylethyl methacrylate) particles in solvent-nonsolvent mixtures before precipitation. *Macromolecules* **1999**, *32*, 8413-8420.

59.   Tao, J.; Stewart, S.; Liu, G. J.; Yang, M. L. Star and cylindrical micelles of polystyrene-block-poly(2-cinnamoylethyl methacrylate) in cyclopentane. *Macromolecules* **1997**, *30*, 2738-2745.

60.   Choucair, A. A.; Kycia, A. H.; Eisenberg, A. Kinetics of fusion of polystyrene-b-poly(acrylic acid) vesicles in solution. *Langmuir* **2003**, *19*, 1001-1008.

61.   Guo, A.; Liu, G. J.; Tao, J. Star polymers and nanospheres from cross-linkable diblock copolymers. *Macromolecules* **1996**, *29*, 2487-2493.

62. Hoppenbrouwers, E.; Li, Z.; Liu, G. J. Triblock nanospheres with amphiphilic coronal chains. *Macromolecules* **2003**, *36*, 876-881.

63. Lu, Z. H.; Liu, G. J.; Duncan, S. Morphology and permeability of membranes of polysulfone-*graft*-poly(*tert*-butyl acrylate) and derivatives. *J. Membr. Sci.* **2005**, *250*, 17-28.

64. Henselwood, F.; Liu, G. J. Water-soluble nanospheres of poly(2-cinnamoylethyl methacrylate)-*block*-poly(acrylic acid). *Macromolecules* **1997**, *30*, 488-493.

65. Siu, H.; Prazeres, T. J. V.; Duhamel, J.; Olesen, K.; Shay, G. Characterization of the aggregates made by short poly(ethylene oxide) chains labeled at one end with pyrene. *Macromolecules* **2005**, *38*, 2865-2875.

66. Siu, H.; Duhamel, J. Molar Absorption Coefficient of Pyrene Aggregates in Water. *J. Phys. Chem. B* **2008**, *112*, 15301-15312.

67. Siu, H.; Duhamel, J. Molar Absorbance Coefficient of Pyrene Aggregates in Water Generated by a Poly(ethylene oxide) Capped at a Single End with Pyrene. *J. Phys. Chem. B* **2012**, *116*, 1226-1233.

68. Mizuno, K.; Maeda, H.; Inoue, Y.; Sugimoto, A.; Vo, L. P.; Caldwell, R. A. Stereospecific (2 pi+2 pi) photocycloaddition of arylalkenes to pyrene via exciplex: formation of 1 : 1-and 2 : 1-cycloadducts. *Tetrahedron Lett.* **2000**, *41*, 4913-4916.

69. Gupta, P.; Vermani, K.; Garg, S. Hydrogels: from controlled release to pH-responsive drug delivery. *Drug Discovery Today* **2002**, *7*, 569-579.

Chapter 4

Summary, Conclusions, and Future Work

4.1 Summary and Conclusions

In this work, we prepared μ-ABC miktoarm copolymers and μ-ABC$_x$ pseudo miktoarm copolymers with low polydispersities through a novel "assembly-and-reaction" method. In this method, a triblock copolymer precursor incorporating a short central carboxyl group-bearing block and a diblock copolymer precursor containing a short amine group-bearing block were synthesized in advance. These copolymers were subsequently associated via electrostatic interactions between their amine group- and carboxyl group-bearing blocks and were covalently linked via amidization to yield pseudo miktoarm copolymers. By controlling the feed ratios between the two precursors and the purification process, we successfully prepared the μ-ABC miktoarm copolymers μ-(PtBA$_{100}$)(PSMA$_{66}$)(PCEMA$_{120}$) and μ-(PtBA$_{100}$)(PGMA$_{200}$)(PCEMA$_{120}$). In addition, we also applied this strategy to prepare μ-(PtBA$_{100}$)(PCEMA$_{130}$)(PEO$_{113}$)$_x$ ($x = 1.14$ and 1.58), which are examples of μ-ABC$_x$ pseudo miktoarm copolymers. This represents the first report describing the synthesis of μ-ABC miktoarm and μ-ABC$_x$ pseudo miktoarm triblock terpolymers using this method. These copolymers were also significant because they contained blocks that could readily undergo crosslinking and hydrolysis reactions, thus providing routes for further modification of these copolymers or processing of their nanostructures.

Factors affecting the yield of the product and whether the product exhibited the desired or mismatches in the stoichiometry were investigated. These factors included the concentration effect, the solvent effect, and the feed ratios. Careful tuning of these

158

parameters provided optimized conditions that improved the efficiency and selectivity of the synthesis. A relatively facile and effective purification method was developed and is described in this thesis as well.

Our method has numerous advantages. Firstly, this method has a modular format. We can thus synthesize different diblock and triblock precursors in advance, and store them for an extended time (at least months). Subsequently, the "assembly-and-reaction" strategy can be used to bind different combinations of the synthesized precursors together, thus providing a wide variety of miktoarm copolymers. Secondly, the reaction conditions are relatively mild. The "assembly-and-reaction" process can be performed in vials or in round bottom flasks at room temperature. In addition, this process is not adversely affected by water or O_2, and only requires hours to complete. Moreover, the reaction can be performed under neutral conditions, thus facilitating the use of pH-sensitive polymers such as PSMA. Therefore, this method can be applied to a wide variety of functional polymers even if they are somewhat unstable. Thirdly, the "assembly-and-reaction" preparation protocol can potentially be expanded as a general methodology to synthesize various classes of miktoarm copolymers, such as μ-ABC$_2$, μ-ABCD or μ-AB(CD) copolymers. For example, if our diblock precursor is replaced with a PNH$_2$-b-C-b-D triblock precursor, a μ-AB(CD) miktoarm copolymer can be obtained.

In this thesis, we have prepared vesicles via a double assembly strategy. At the tier I level, we assembled PtBA-b-PCOOH-b-PCEMA and PEO-b-PNH$_2$ and performed a linkage reaction to the assembled molecular architectures to yield μ-(PtBA)(PCEMA)(PEO)$_x$. The resultant architectural copolymer were then self-assembled again at the tier 2 level, thus yielding vesicles. The prepared μ-(PtBA)(PCEMA)(PEO)$_x$

copolymer self-assembled in THF/water at f_{H2O} = 80% to form vesicles bearing a PCEMA wall that was permeated by PtBA cylinders. The PCEMA domain in the vesicular walls was then photocrosslinked and the PtBA domains were subsequently hydrolyzed to yield an unprecedented nanostructure, capsules that were permeated by PAA-gated nanochannels, as far as we can reach. The nanochannels allowed the capsules to be loaded with PEO$_{45}$-Py up to a weight fraction of 31 %. The loaded PEO$_{45}$-Py chains exhibited weak monomer fluorescence emission due to excimer formation and quenching by the PCEMA domains. However, their emission intensity increased after release. This increase in the pyrene monomer fluorescence intensity with time allowed us to monitor the PEO$_{45}$-Py release profile under various conditions. The rate and extent of PEO$_{45}$-Py release could be regulated by changing the pH of the surrounding aqueous media and the release was enhanced under basic conditions. A future generation of these novel capsules would provide promising candidates for controlled release applications. To the best of our knowledge, these vesicles represent the first examples of nanocapsules bearing walls that are permeated by channels that are both uniformly-sized and pH-responsive.

Only the μ-(PtBA)(PCEMA)(PEO)$_{1.14}$ vesicles were used as test capsules for the release kinetics investigations described in this thesis. However, we also found that the diameters of the μ-(PtBA)(PCEMA)(PEO)$_x$ vesicles could be tuned by adjusting the x value. In particular, a smaller x value yielded larger bigger vesicles. However, the PtBA phase, which affects the size of the channels, did not change with the x value. These results may allow us to prepare nanocapsules with various sizes and loading capacities, without significantly changing the release kinetics.

There have traditionally been fewer morphological investigations focusing on miktoarm copolymers than on linear block copolymers due to the difficulties encountered in the synthesis of miktoarm copolymers. We believe our method provides an easier route for synthesizing miktoarm copolymers, which may thus open the doorway to further investigations on the morphological behaviour of miktoarm copolymers. Existing morphological studies have demonstrated that miktoarm copolymers can yield a diverse array of intricate morphologies, and this field thus has significant room for growth. The "assembly-and-reaction" strategy described in this thesis may facilitate this growth further and allow the existing morphological library to be extended even further.

4.2 Future Work

4.2.1 Future Synthesis

The synthetic methodology that is described in this thesis is a general strategy and thus should be useful for the preparation of not only μ-ABC miktoarm copolymers, but also various other types of miktoarm polymers, such as μ-ABCD and μ-AB(CD) copolymers. An example of the proposed preparation of a μ-ABCD copolymer is illustrated in Scheme 4.1. In this case, two triblock copolymer precursors incorporating short carboxyl group- and amino group-bearing short complementary blocks could be respectively synthesized. In this example, each copolymer bears longer terminal non-stitching blocks, and each of these terminal blocks have a different chemical composition. The same "assembly-and-reaction" strategy that has been described in this thesis could thus be applied to these precursors in order to prepare μ-ABCD copolymers.

Mixed Precursors   **Associated Precursors**   **Miktoarm Polymer**
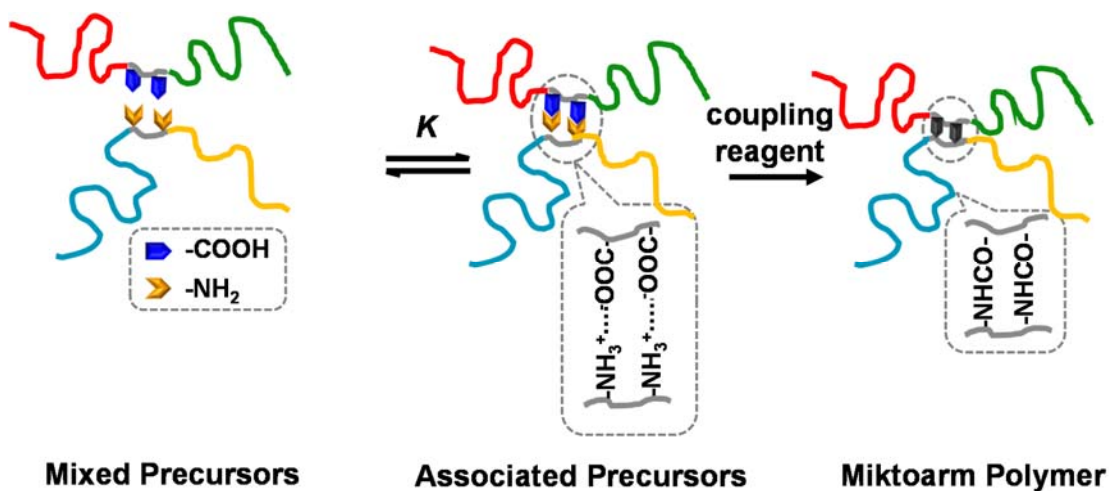
Scheme 4.1 Illustration depicting the preparation of a μ-ABCD miktoarm copolymer via the "assembly-and-reaction" method.

As illustrated in Scheme 4.2, the same strategy can be applied to react a triblock copolymer precursor bearing a short central carboxyl group-bearing stitching block with a triblock copolymer precursor bearing a terminal amino group-bearing stitching block, thus yielding a μ-AB(CD) miktoarm polymer. There are various possibilities for preparing miktoarm polymers through this method, and Schemes 4.1 and 4.2 are only meant to highlight two such examples. Due to the versatility of this strategy, the combinations may be wide ranging, and one could envision the use of tetrablock copolymers (or even those with higher block orders) as precursors for elaborate miktoarm copolymers. In addition, this modular approach allows the preparation of a series of new miktoarm polymers without requiring the synthesis of unique precursors to prepare each novel miktoarm copolymer. Unique miktoarm copolymers can instead be prepared from different combinations of previously-prepared precursors.

Mixed Precursors   **Associated Precursors**   **Miktoarm Polymer**
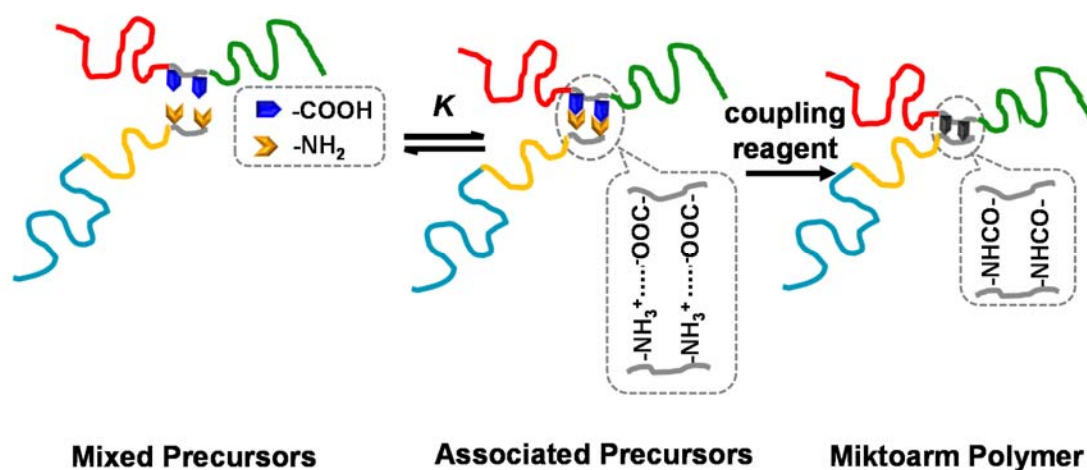
Scheme 4.2 Illustration depicting the preparation of a μ-AB(CD) miktoarm copolymer via the "assembly-and-reaction" method.

4.2.2 Future Morphological Studies

Morphological studies of the novel miktoarm polymers reported in Chapter 2 are currently in progress. Some of the preliminary results from these investigations are described in Appendix A, B, and C. The self-assembled structures of these μ-(P*t*BA)(PGMA)(PCEMA) copolymers with be systematically investigated, both in solution and in bulk. The influence of the copolymer composition on the morphologies will be investigated, and these results will be compared with experimental investigations as well as computer simulations that have been reported in the literature.

In Chapter 3, we reported the formation of vesicles bearing walls composed of a PCEMA matrix that was perforated by P*t*BA cylinders from μ-(P*t*BA)(PCEMA)(PEO)$_x$ miktoarm polymers. In particular, these vesicles were observed among copolymers with a P*t*BA/PCEMA volume ratio of 3/7. In the future, if we intend to reverse the P*t*BA/PCEMA volume ratio to 7/3, we anticipate that this reversed volume ratio will yield vesicles bearing

walls that consist of a continuous P*t*BA matrix that is perforated by regularly packed PCEMA cylinders. Subsequent photo-crosslinking of the PCEMA domains and dissolution of the copolymer in THF, a good solvent for P*t*BA and PEO, may yield short PCEMA cylinders that are stabilized by the PEO and P*t*BA chains. If a selective solvent, such as water (which is a good solvent for PEO but a poor solvent for P*t*BA) was added, these cylindrical units may undergo hierarchical self-assembly to form fascinating structures at the sub-micrometer scale.
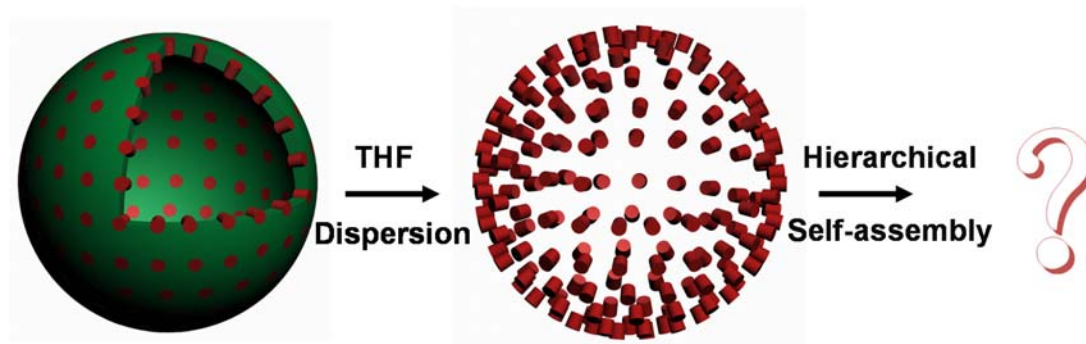
Scheme 4.3 Illustration of the preparation of short PCEMA cylinders, in which green and red denote solid P*t*BA and crosslinked PCEMA domains. The soluble PEO and P*t*BA chains anticipated after dispersion in THF are not shown for clarity. The crosslinked PCEMA cylinders in the middle are drawn in regular packed manner to illustrate they are derived from the regular packed cylinders in vesicles' wall. In THF, the crosslinked PCEMA cylinders should be randomly dispersed.

4.2.3 Future Drug Delivery Studies

The vesicular structure with perforated cylinders reported in Chapter 3, is also a good precursor for control releasing studies. For example, if P*t*BA/PAA are replaced with other stimuli responsive polymerd, eg. a temperature responsive polymer poly(N-isopropylacrylamide), the releasing kinetics could be tuned by other stimuli. Further drug

delivery investigations could also possibly be performed with the vesicles or with variations of the vesicles, using different drug molecules as guests. Possibly collaboration with biology or medical departments could lead to in vivo testing of these with laboratory rats, etc. Or alternatively testing in assays may be possibly performed.

Appendix A

Preliminary Investigation on the Self-Assembly of μ-$(PtBA_{100})(PGMA_{200})(PCEMA_{120})$ in Solution

A1 Preparation of Micelles and TEM Samples

The synthesis of μ-$(PtBA_{100})(PGMA_{200})(PCEMA_{120})$ is described in Chapter 2. In order to prepare micelles from μ-$(PtBA_{100})(PGMA_{200})(PCEMA_{120})$, typically ~2 mg of the terpolymer was stirred in 200 µL of THF for 1 h. Subsequently, ~2 mL of deionized water was slowly added to this solution over a ~30 min period. This solution was kept in vigorously stirred for three weeks before it was dialyzed against water in a dialysis membrane (cut off M_w = 10 000) for one day. The micellar solution was diluted by ~10-fold in water, and was aero spayed onto nitrocellulose film-covered TEM grids. TEM samples were stained with OsO_4 vapor for 2 h, or alternatively with RuO_4 vapour for 30 min. A description of the TEM microscope and the measurement parameters is provided in Chapter 3.

A2 Results and Discussion

Figure A1a and b show representative TEM images of the micelles formed by μ-$(PtBA_{100})(PGMA_{200})(PCEMA_{120})$, which had been selectively stained by OsO_4 (a) and by RuO_4 (b). OsO_4 can selectively stain PCEMA domains, while RuO_4 can introduce contrast to both PCEMA and PGMA to different degrees. Therefore, the dark domains observed in Figure A1a correspond to PCEMA domains. Meanwhile, the central dark domain observed in Figure A1b corresponds to PCEMA, while the surrounding grey domain corresponds to PGMA chains, and the lighter domain represents PtBA chains. Generally speaking, three

types of morphologies were observed in Figure A1, including hamburger micelles, three-lobed micelles (marked by arrows) and Janus micelles (circled).
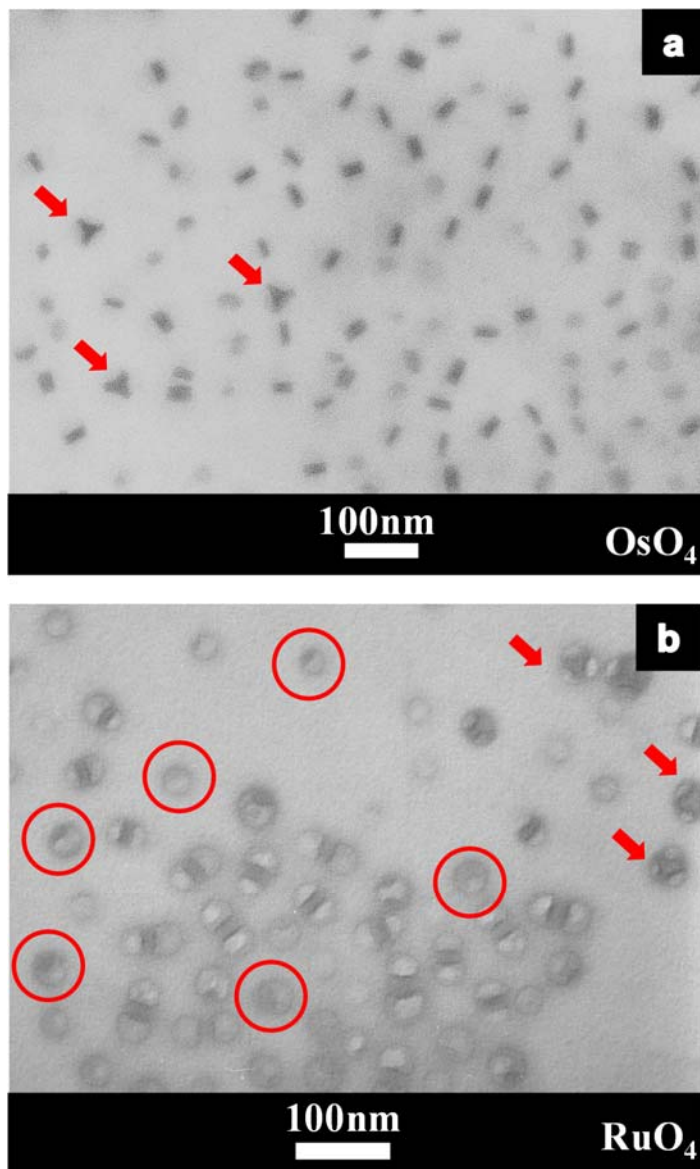
Figure A.1 Representative TEM images of the micelles formed by μ-(PtBA$_{100}$)(PGMA$_{200}$)(PCEMA$_{120}$), which were selectively stained by OsO$_4$ (a) and RuO$_4$ (b).

Figure A.2 Selected RuO₄ stainedTEM images depicting hamburger micelles (a), three-lobed micelles (marked by arrows in c) and Janus micelles (marked by arrows in e). Images (b), (d), and (f) show chain packing illustrations of hamburger, three-lobed, and Janus micelles, respectively.
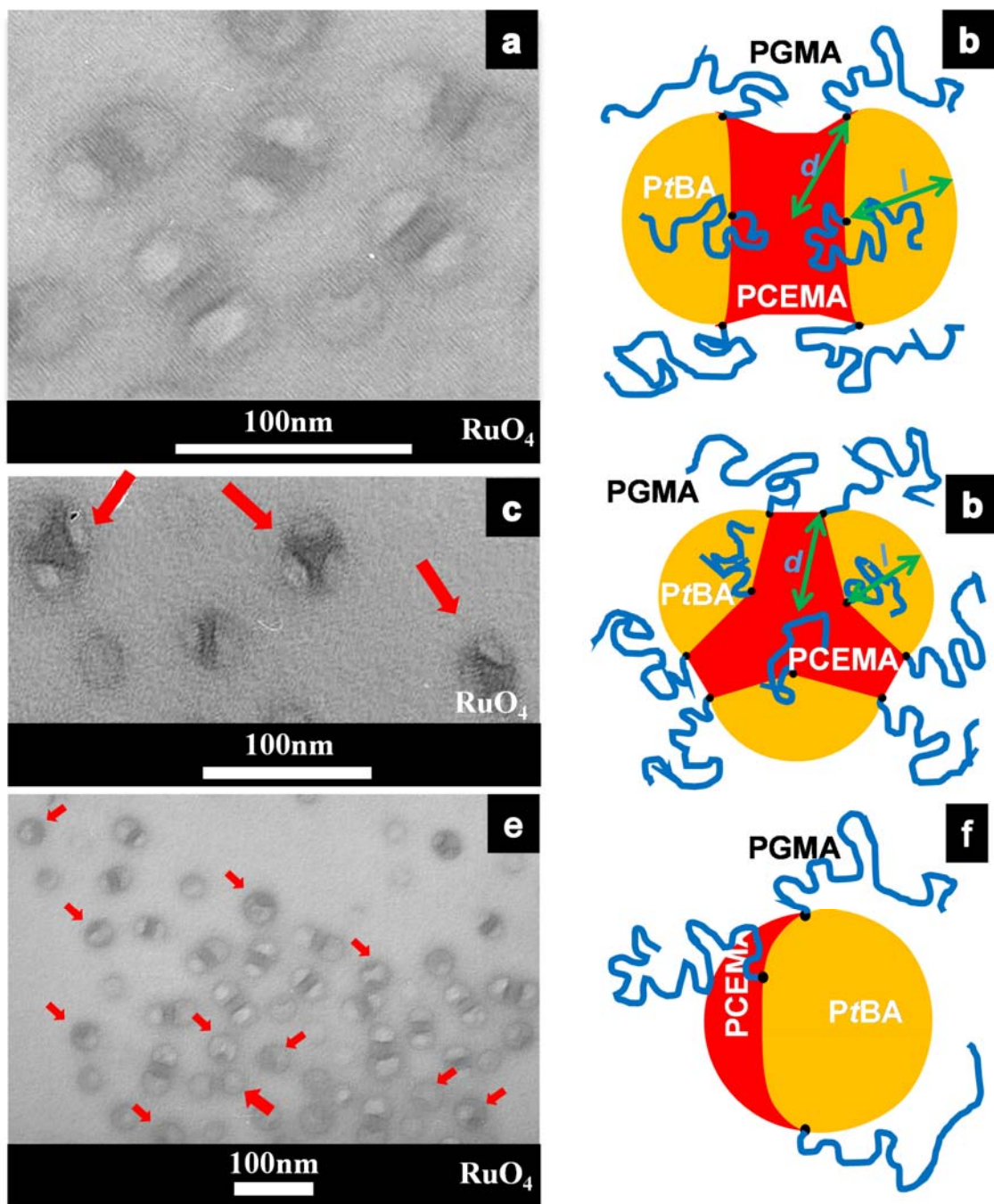
TEM images depicting hamburger micelles, three-lobed micelles, and Janus micelles are shown in Figure A2a, c and e, respectively. The chain packing structures of these nanostructures are illustrated in Figure A2b, d and f, respectively, in which the red, yellow, and blue colors respectively depict PCEMA, PtBA, and PGMA domains. Upon viewing more than twenty large-scale TEM images, it became apparent that the hamburger micelles represented the predominant morphology, while the three-lobed micelles and Janus micelles were in the minority.

In the case of the major morphology, μ-(PtBA$_{100}$)(PGMA$_{200}$)(PCEMA$_{120}$) self-assembled to form "hamburger" micelles, in which the extremely hydrophobic PCEMA domain was sandwiched between two PtBA half-sphere domains, which formed the "buns". The water soluble PGMA chains emanated from the interfaces between the PCEMA and the PtBA domains, and helped to shield these hydrophobic domains against water. This proposed chain packing motif is shown in Figure A2b. The radii of both the PCEMA$_{120}$ core and PtBA$_{100}$ half-sphere were ~15 nm. Meanwhile, from the point of view of relative interfacial tensions, the proposed structure is still the preferable chain packing motif. From our previous experience, the relative interfacial tensions γ between the polymers and solvent (water) are expected to be $\gamma_{PCEMA/W} > \gamma_{PtBA/W} > \gamma_{PGMA/W}$. When the oblate disk-like PCEMA core is sandwiched between two PtBA domains as depicted in the proposed hamburger-like motif, the interfacial contact between the PCEMA$_{120}$ and the solvated PGMA$_{200}$ domains is minimized.

The extreme hydrophobicity of the PCEMA block places this system in the superstrong segregation regime (SSSR).[1-3] In this regime, the chains of the core-forming block are nearly fully extended and the interfacial area per chain (between the solvent and

the core block) is minimized, since the interfacial tension is so large. In the case of the core-forming PCEMA$_{120}$ block, the unperturbed R_g can be estimated by $N^{1/2} \times 0.154$ nm = 2.4 nm.[4] Meanwhile, the fully stretched chain length L roughly equals cos(54.5°) $\times N \times 0.154$ nm = 21.5 nm.[4] Here N denotes the number of the C-C bonds in the main chain, which is 240 in the case of PCEMA$_{120}$. From the TEM image, the radius of the PCEMA$_{120}$ disk-like layer in the hamburger micelles is ~15 nm. This value is close to L and much larger than R_g, which is consistent with the SSSR.[2,3] For PtBA$_{100}$, R_g and L equal 2.2 and 17.8 nm, respectively Meanwhile in the TEM images, the half-width of each PtBA$_{100}$ domain ($W/2$) is ~15 nm, which is also close to L. Thus the PtBA$_{100}$ chains in the "bun" domains are highly stretched, which would also be anticipated in the SSSR.

A small fraction of the three-lobed micellar structure were also visible in the TEM images, as shown in Figure A2c. Utilizing the same analytical techniques that had been used for the hamburger micelles, we proposed the chain packing motif shown in Figure A2d, which is a three-lobed compartment micelle. Based on the TEM images that were recorded using the different staining techniques, it was apparent that the PCEMA block occupied the majority of the micellar core. Once again, this motif would provide a reduced interfacial contact with surrounding PGMA corona chains, while the PtBA domain filled the interstitial space between the PCEMA domains. In comparison with the water contact experienced by the PCEMA domains, the PtBA domains have a relatively larger interfacial contact with the surrounding water. The half-width of the PCEMA$_{120}$ lobe ($W/2$) is ~9 nm. When this value is compared with L = 21.5 nm and R_g = 2.4 nm, it is apparent that the PCEMA$_{120}$ chains are stretched, to a lower extent than those in the hamburger micelles. The half-width of each PtBA$_{100}$ domain ($W/2$) is ~12 nm, in comparison with R_g and L

values equaling 2.2 and 17.8 nm, respectively, for $PtBA_{100}$. Thus the $PtBA$ chains are also stretched, but this stretching is also to a lower extent than that observed in the hamburger micelles.

The Janus micelles (marked by arrows in Figure A2e) are more interesting. The elliptical core of a Janus micelle consists of $PtBA$ and PCEMA domains that are separated into two hemispheres, as shown in Figure A2f. As can be seen from the RuO_4-stained TEM samples, this structure is very distinct. The TEM images of the OsO_4 stained samples exhibited three types of images in Figure A3, depending on the orientation and projections of electron beam. When the Janus micelles were aligned horizontally the TEM grid (marked by arrows as Type 1), the pathlength of the electron beam was the longest, and the Janus micelles appeared as dark bands. When the Janus micelles were aligned vertically with the TEM grid (marked by arrows as Type 2), the pathlength of the electron beam was the shortest, and the Janus micelles appeared as pale circles. In the third situation the Janus micelles were tilted with respect to the TEM grid. In this case the Janus micelles appeared as circular structures with intermediate darkness as marked by the arrow as Type 3 in Figure A3. Janus micelles are very similar in structure to the basic subunits of multicompartment micelles, as illustrated in Figure 1.13. In fact, μ-ABC miktoarm polymers are known for their ability to form multicompartment micelles, as described in Chapter 1.[1] To the best of our knowledge however, there have been no reports of miktoarm-based Janus micelles. We believe the observation of Janus micelles in our case may be attributed to the fact that the water soluble PGMA chains were very long. These corona-forming chains could effectively shield the Janus micelles, and thus prevent them from stacking together to form multicompartment micelles.
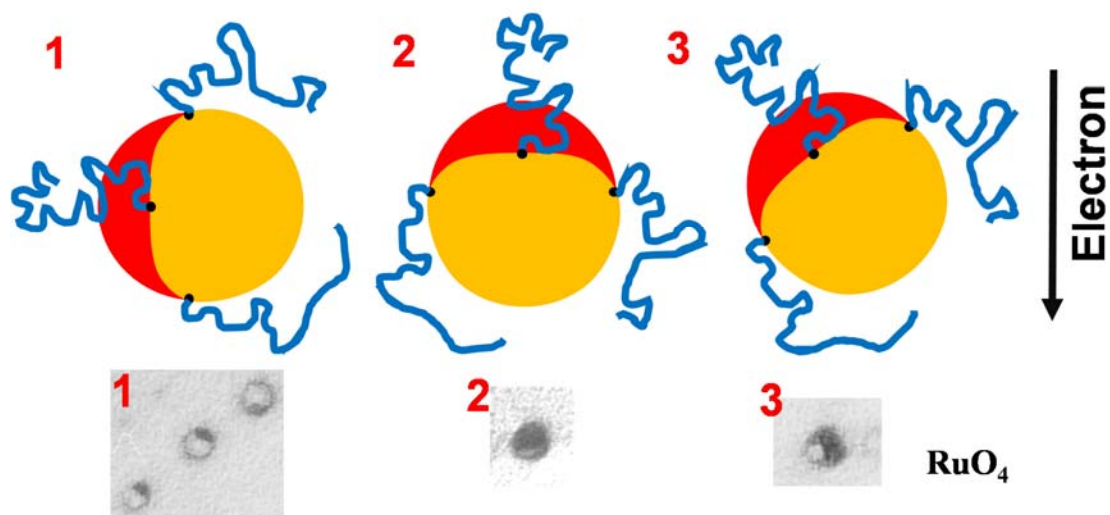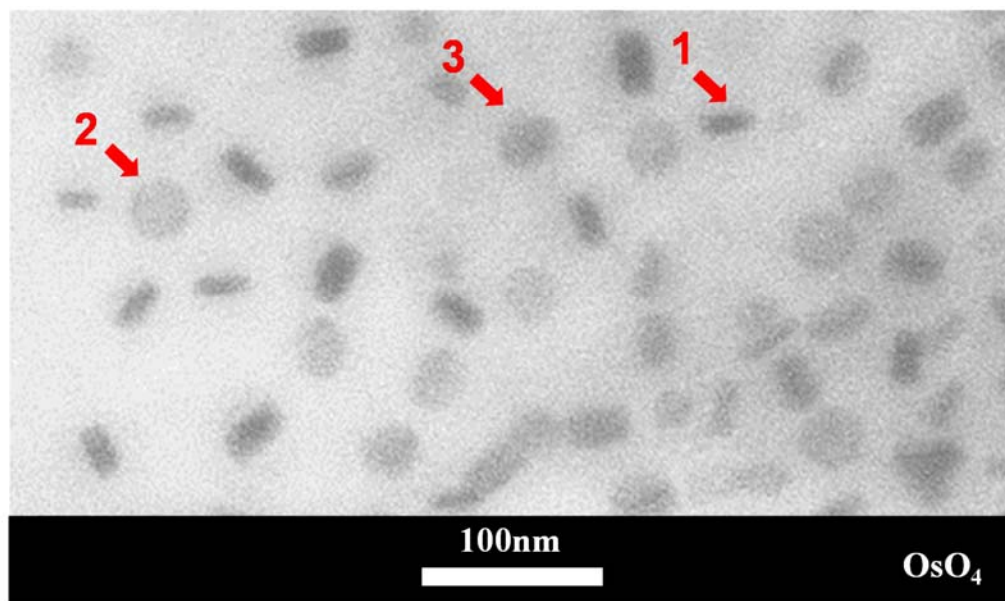
Figure A.3 TEM images of Janus micelles of from μ-(PtBA$_{100}$)(PGMA$_{200}$)(PCEMA$_{120}$) at different projections. The samples were stained with OsO$_4$ (upper) and RuO$_4$ (lower). Also shown are the chain packing motifs of these structures, in which the yellow, blue, and red colors correspond to PCEMA, PtBA and PGMA domains respectively.

Figure A4 provides a comparison between a hamburger micelle, a three-lobed micelle and a Janus micelle within one enlarged TEM image. The chain packing motifs of these structures are also shown. Interestingly, the thickness of the PCEMA "meat" of a hamburger micelle is almost twice of the thickness of the PCEMA domain in a Janus micelle. Meanwhile, the thickness of the PCEMA domain in the center of a three-lobed micelle is very close to that of the PCEMA domain of a hamburger micelle. In addition, the thickness of the PCEMA domain at the edge of the three-lobed micelle is very close to that of the PCEMA domain in a Janus micelle. The thicker arrow in Figure A2e appears to show the formation of two Janus micelles through the fission of a hamburger micelle. Based on these results, we propose a "fusion-fission" mechanism to explain why these three structures were observed from one terpolymer. In our system, the PGMA block was long, which facilitated the formation of Janus micelles. However, the PGMA block was not sufficiently long to keep all of the micelles in Janus form. Some of the Janus micelles became fused or stacked together to minimize their PCEMA/water interactions. In this manner, hamburger micelles may have formed through the fusion of two Janus micelles, while three-lobed micelles may have formed due to the fusion of three Janus micelles (Figure A5). An equilibrium may have existed in solution between these three types of micelles, in which both fusion and fission processes took place.
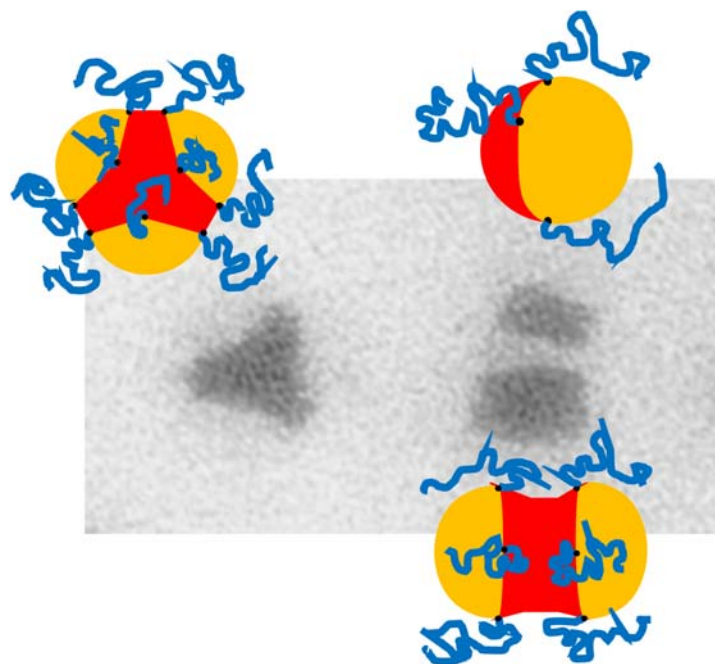
Figure A.4 Enlarged OsO$_4$ stained TEM image showing hamburger, three-lobed, and Janus micelles. The packing motifs of these structures are also shown.
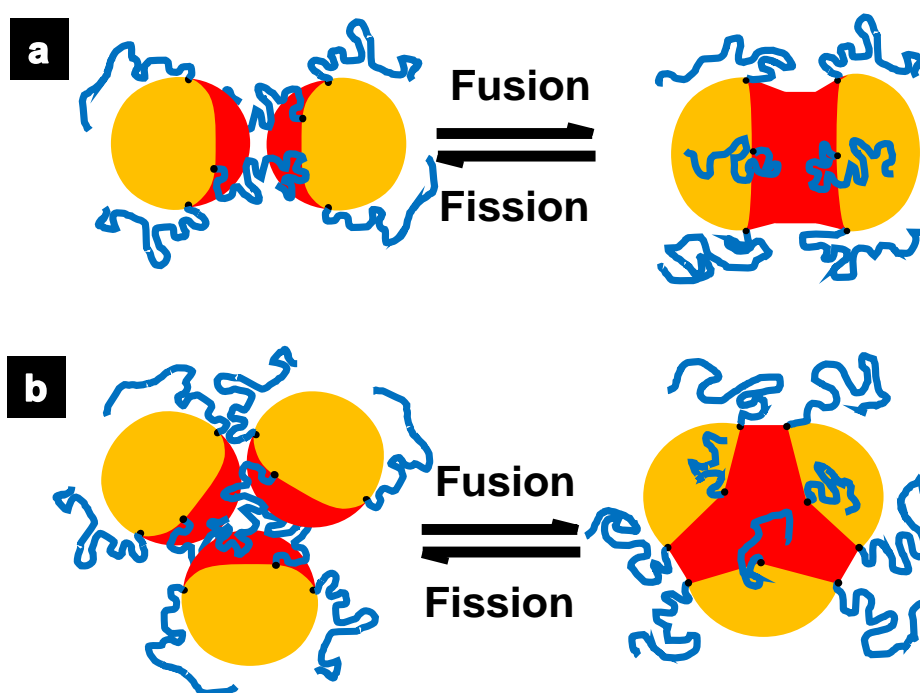

Figure A.5 Illustration of the proposed "Fission-Fusion" equilibrium between the hamburger, three-lobed, and Janus micelles in water.

A3 References

1.   Li, Z. B.; Kesselman, E.; Talmon, Y.; Hillmyer, M. A.; Lodge, T. P. Multicompartment micelles from ABC miktoarm stars in water. *Science* **2004**, *306*, 98-101.

2.   Semenov, A. N.; Nyrkova, I. A.; Khokhlov, A. R. Polymers With Strongly Interacting Groups - Theory For Nonspherical Multiplets. *Macromolecules* **1995**, *28*, 7491-7500.

3.   Lodge, T. P.; Hillmyer, M. A.; Zhou, Z. L.; Talmon, Y. Access to the superstrong segregation regime with nonionic ABC copolymers. *Macromolecules* **2004**, *37*, 6680-6682.

4.   Sperling, L. H.; *Introduction to Physical Polymer Science*. 4th Edition ed.; Wiley-Interscience: Bethlehem: Pennsylvania, **2005**; p 880.

Appendix B

Preliminary Investigation on the Self-Assembly of μ-(PtBA$_{100}$) (PGMA$_{200}$)(PCEMA$_{120}$) in the Solid State

B1 Experimental

B1.1 Preparation of μ-(PtBA$_{100}$)(PGMA$_{200}$)(PCEMA$_{120}$) Film

The synthesis of μ-(P*t*BA$_{100}$)(PGMA$_{200}$)(PCEMA$_{120}$) is described in Chapter 2. Films of μ-(P*t*BA$_{100}$)(PGMA$_{200}$)(PCEMA$_{120}$) (~0.2 mm in thickness) were prepared by evaporating a pyridine solution containing ~10 vol% (by volume) of the copolymer over two weeks. The polymer solution was kept in a glass vial during this two week period. The film was subsequently photo-crosslinked for 1 h on each side.

B1.2 Preparation of the TEM and AFM Samples

A small piece of the copolymer film was sandwiched between two pieces of polystyrene, which were pre-heated to ~120 $^{\circ}$C. The embedded sample was microtomed to films with a thickness of ~100 nm. These thin films were placed on TEM grids and subsequently stained by OsO$_4$ vapour for 2 h. Alternatively, these films were stained with RuO$_4$ vapour for 30 min. These samples were subsequently characterized via TEM.

Another small piece of the crosslinked film was vigorously stirred in ~2 mL of trifluoroacetic acid (TFA) for 2 h to hydrolyze P*t*BA into PAA. The TFA was then removed under vacuum, and the solid residue was vigorously stirred in ~2 mL MeOH for various time spans ranging between 1 h up to two weeks. The solution was diluted by ~10-fold in MeOH, and aero-spayed onto carbon- covered TEM grids. The samples were stained by OsO$_4$ vapour for 2 h prior to TEM analysis. Solutions were also aero-spayed

onto mica and air-dried for 2 h prior to AFM analysis. Descriptions of the TEM and AFM

systems and the measurement parameters are provided in Section 3.2 of Chapter 3 .
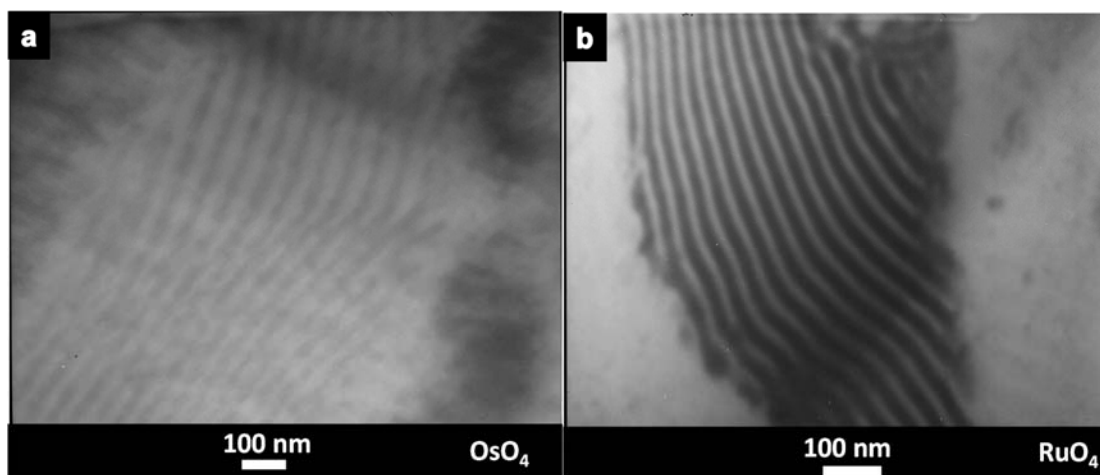
B2 Results and Discussion

Figure B.1 TEM images of μ-(PtBA$_{100}$)(PGMA$_{200}$)(PCEMA$_{120}$) microtomed thin films stained by (a) OsO$_4$ and (b) RuO$_4$.

The TEM images of the microtomed thin film samples are shown in Figure B1. Since

OsO$_4$ selectively reacts with the double bonds of PCEMA, the dark regions correspond to

PCEMA domains. RuO$_4$ stained the PCEMA and PGMA domains by different degrees,

and the dark regions observed in these images also corresponded to PCEMA domains.

Both the OsO$_4$ and RuO$_4$ stained samples exhibit lamellar structures, but the distances

between repeating domains are different. Since the orientation of the microtome slices

would affect the distances between repeating domains observed in the TEM images, the

smallest repeating distances measured from all TEM images should represent the actual

repeating distance in the lamellar structure, which is 30 nm. From the microtomed samples,

only the PCEMA domain could be located, while the locations of the PGMA and PtBA

domains could not be determined for these samples. In addition, these images did not provide details on the nature of the phase separation within the lamellae.

In order to gain insight into the internal structure of the lamellae, the following process was done to separate the different layers. A small sample of μ-(PtBA$_{100}$)(PGMA$_{200}$)(PCEMA$_{120}$) bulk film was photocrosslinked in order to permanently lock its structure, before hydrolysis was performed to convert the PtBA domains into PAA domains. The sample was then vigorously stirred in MeOH, which is a good solvent for both PGMA and PAA, in order to separate and disperse the layers. After 1 h of dispersal, the sample was characterized via AFM. The topography image (Figure B2a) confirmed that the film exhibited an overall lamellar structure, and also demonstrated these lamellae were perforated by channels. These channels appeared as the darker and depressions in the film. The repeating distance between the lamellae was 65 nm based on the AFM images, in comparison with 30 nm based on TEM characterization. This difference can be attributed to the fact that the AFM sample had become swollen with the solvent. The sample was also dispersed in MeOH for a longer time of up to two weeks before AFM (Figure B2b,c) and TEM (Figure B2d) characterizations were performed after this dispersion period. As shown by the AFM phase image in Figure B2b, the lamellae had assumed a staggered arrangement, which was quite different from the stacked arrangement observed after only 1 h of dispersion. This effect of the dispersion time on the resultant AFM images is illustrated in Figure B3. After a longer time in solution, the layers became staggered, which allowed AFM tip to scan individual layers. In contrast, the AFM tip is shown in Figure B3 facing the edges of the layers of a sample that had been dispersed for only 1 h, to give a cross-sectional view of the stacked layers.

178

As shown in Figure B2b, the side of each layer exhibits regularly packed domains. When the top layer of one sample was scanned with the AFM tip, these dispersed domains became more clearly visible. The topography image (Figure B2c, left) indicates that these regularly packed domains were channels. It was apparent from the edges of the layer that it was perforated by these channels, which is consistent with the structure of the channels observed in Figure B2a. This structure can also be visualized by considering postage stamps. A sheet of postage stamps is perforated by holes at the edges of each individual stamp, thus causing an individual stamp to possess ragged edges after it has been torn from this sheet due to the remnants of these holes. In a similar manner, when the strong stirring force causes a larger section of a layer to break down into smaller sections, the cross-sections of these channels are visible at the edges of the layers, as highlighted in Figure B2a and c. The diameter of these channels as measured via AFM was ~8 nm, which perfectly matched the diameter of the channels that perforated the walls of the μ-$(PtBA_{100})(PCEMA_{120})(PEO_{114})_x$ capsules described in Chapter 3. The staggered layers observed after two weeks of dispersion were also visible via TEM (Figure B2d). However, after heavy crosslinking treatment, the PCEMA domains lost most of their double bonds, and these domains exhibited poor contrast against the channels.
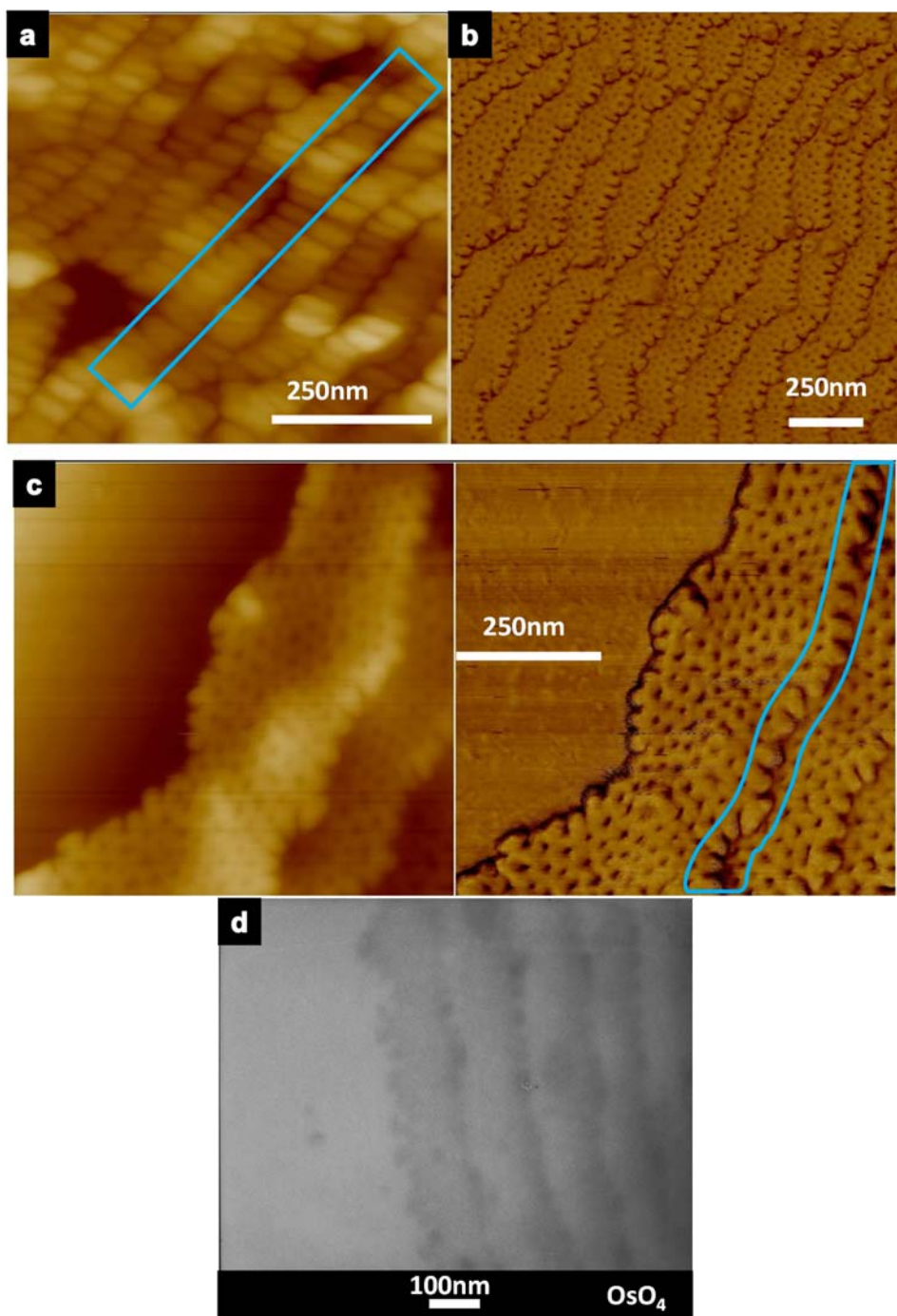
Figure B.2 AFM images of the dispersed samples, including: (a) a topography image of a sample dispersed for 1 h, (b) a phase image of a sample dispersed for two weeks, and (c) topography (left) and phase (right) images of a sample that had been dispersed for two weeks. Also shown is a (d) TEM image of a sample that had been dispersed for two weeks.
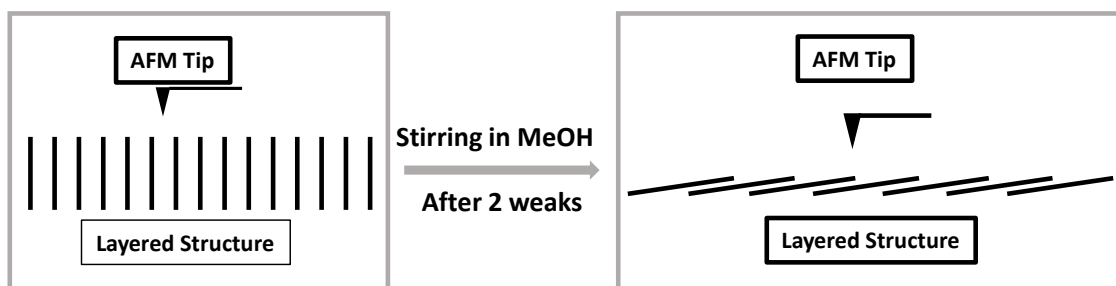
Figure B.3 Illustration of the effect of a longer dispersion time on the structures of the layers. After prolonged dispersion, the layers became staggered. In the former case, the AFM tip is shown facing the edges of the layers to provide a cross-sectional view, while the AFM tip is able to view the profiles of the individual staggered layers in the latter case.

Based on all of these observations, we propose that μ-$(PtBA_{100})(PGMA_{200})(PCEMA_{120})$ underwent self-assembly in the solid state to form a cylinder-in-lamellae structure, as shown in Figure B4. This morphology consists of alternating PCEMA and PGMA lamellae, in which the former PCEMA layers are perforated by PtBA cylinders. This pattern was proposed based on a number of facts regarding this copolymer. Firstly, both the PCEMA and PtBA domains are hydrophobic, while PGMA is hydrophilic. In addition, PGMA should be less compatible with either PCEMA or PtBA, than PCEMA would be with PtBA. Meanwhile, the volume ratio $f_{(PCEMA+PtBA)}/f_{PGMA} \approx 1/0.7$. However, considering that PGMA is hydrophilic, and could become swollen by pyridine or by moisture during the casting of the film, the actual $f_{(PCEMA+PtBA)}/f_{PGMA}$ ratio in the bulk film could be close to 1/1, which is supported by the formation of the lamellar structures described in Chapter 1.[1,2] Moreover, $f_{PCEMA}/f_{PtBA} = 7/3$, so that PtBA should form cylinders within a PCEMA matrix.[1] In addition, the diameter of the $PtBA_{100}$ cylinders perforating the $PCEMA_{120}$ matrix perfectly matched the diameter of the channels that penetrated the vesicular walls described in Chapter 3. Interestingly,

those vesicular walls were based on the same copolymer blocks with very similar block lengths (PCEMA$_{130}$ and PtBA$_{100}$ in Chapter 3). Taken together, these results provide compelling evidence supporting the proposed morphology.
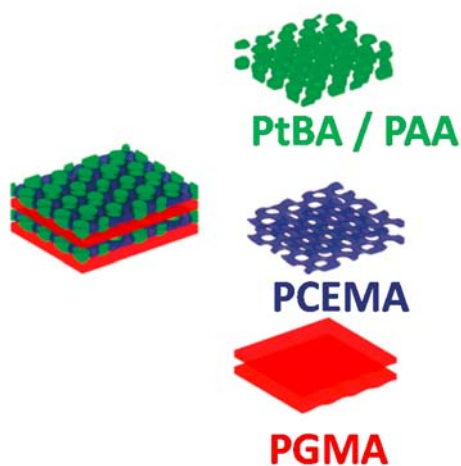

Figure B.4 Illustration of the proposed cylinder-in-lamellae structure formed by μ-(PtBA$_{100}$)(PGMA$_{200}$)(PCEMA$_{120}$) in the solid state.

B3 References

1.   Bates, F. S.; Fredrickson, G. H. Block copolymers - Designer soft materials. *Phys. Today* **1999**, *52*, 32-38.

2.   Abetz, V.; Goldacker, T. Formation of superlattices via blending of block copolymers. *Macromol. Rapid Commun.* **2000**, *21*, 16-34.

Appendix C

Preliminary Investigation on the Self-Assembly of μ-$(PtBA_{100})(PGMA_{66})(PCEMA_{120})$ in Solution

C1 Experimental

C1.1 Synthesis of μ-$(PtBA_{100})(PGMA_{66})(PCEMA_{120})$

The synthesis of μ-$(PtBA_{100})(PSMA_{66})(PCEMA_{120})$ is described in Chapter 2. In order to convert the PSMA chains into PGMA chains via hydrolysis, 10 mg of μ-$(PtBA_{100})(PSMA_{66})(PCEMA_{120})$ was dissolved in 2 mL of THF, and 0.2 mL of a THF solution containing 1 M HCl was added. After 1 h, the solvent and HCl were removed via evaporation under a N_2 flow.

C1.2 Micellization of μ-$(PtBA_{100})(PGMA_{66})(PCEMA_{120})$ and Preparation of the TEM and AFM Samples

The solid residue obtained from the last step of the preparation summarized in Section C1.1 was dissolved in 0.2 mL of THF. Subsequently, ~5 mL of deionized water was slowly added to over a ~30 min period. The solution was vigorously stirred for one week, before it was aero-sprayed onto nitrocellulose film covered TEM grids and onto mica substrates for AFM characterization.

In some cases, sample solutions were also photocrosslinked and subjected to hydrolysis before they were aero-sprayed for TEM and AFM analysis. The photo crosslinking procedure refers to Section 3.2 in Chapter 3. Portions of the crosslinked samples were dried under vacuum, before they were mixed with TFA overnight in order to convert the PtBA chains into PAA chains via hydrolysis. The TFA was subsequently

removed via evaporation under a N_2 flow, and the hydrolyzed vesicles were re-dispersed into MeOH. This dispersion was subsequently aero sprayed onto carbon covered TEM grids. The hydrolyzed samples were stained with uranyl acetate (UO_2Ac_2). Descriptions of the TEM and AFM instruments used to perform these characterizations as well as the measurement parameters are provided in Chapter 3. The process for staining, samples with OsO_4 involved exposing grids containing the samples in OsO_4 vapor for 2 h.

C2 Results and Discussion

Initially, we anticipated the micelles of μ-(PtBA$_{100}$)(PGMA$_{66}$)(PCEMA$_{120}$) to exhibit a similar structure in water as had been observed for the μ-(PtBA$_{100}$)(PCEMA$_{130}$)(PEO$_{113}$)$_x$ vesicles described in Chapter 3. This expectation was based on the fact that both copolymers possessed insoluble arms with the same composition (PtBA and PCEMA) and with very similar lengths. Only the soluble arm differed significantly, as the PEO chains employed in Chapter 3 had been replaced with PGMA chains in this case. In addition, the volume ratio between the soluble to insoluble arms ($f_{PGMA}/f_{(PCEMA+PtBA)}$) was ~0.2/1. According to classical theory,[1] this volume ratio should yield vesicles. Moreover, $f_{PCEMA}/f_{PtBA} \approx 7/3$, suggesting that P$t$BA should form cylinders embedded within a PCEMA matrix.[1] The overall structure and chain packing motif is shown in Figure C1.
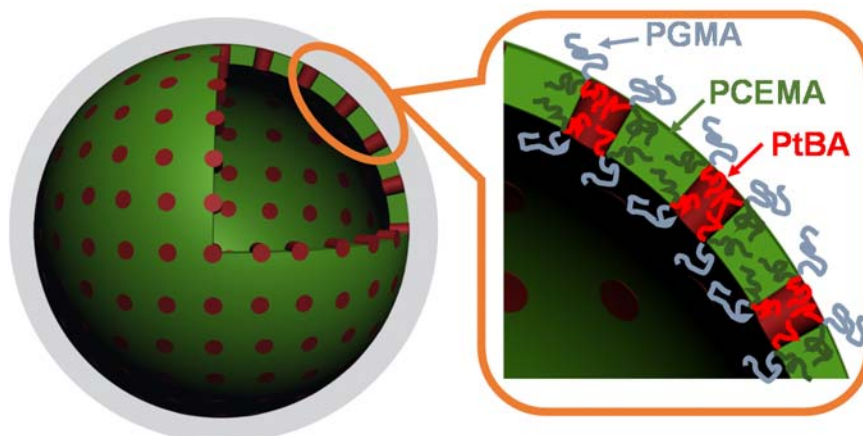
Figure C.1 Illustration of a μ-(PtBA$_{100}$)(PGMA$_{66}$)(PCEMA$_{120}$) vesicle bearing PGMA corona chains, and vesicular walls composed of a PCEMA matrix that is perforated by PtBA cylinders.

The TEM image of the vesicles observed prior to photocrosslinking treatment (Figure C2a) appeared very similar to the TEM image of the vesicles described in Chapter 3 (Figure 3.7a). In particular, they consisted of a dark globular structure along with a discontinuous grey phase. Since the sample was selectively stained by OsO$_4$, the dark continuous phase corresponds to PCEMA domains, while the grey discontinuous regions represent PtBA domains. After heavy crosslinking, the PCEMA domains lost most of their double bonds, so that Figure C2b shows no contrast between the PCEMA and PtBA regions. However, this image reveals that these globular structure have a cavity in their center, suggesting that they are vesicles rather than solid spheres. The thickness of the vesicular wall is ~23 nm, in comparison with 20 nm observed in Chapter 3. Hydrolysis treatment also helped to locate the PtBA domains. The crosslinked vesicles were treated with TFA in order to hydrolyze the PtBA chains into PAA chains. Subsequently, UO$_2$Ac$_2$ was used to selectively stain the carboxyl groups of the PAA chains. As shown in Figure C2c,

discontinuous dark dots were visible in the resultant TEM image, which corresponded to PAA domains. As shown by the arrow, it was apparent that the dark regions penetrated the vesicular wall, thus suggesting that the PtBA/PAA domains perforated the PCEMA-based wall of the vesicles.
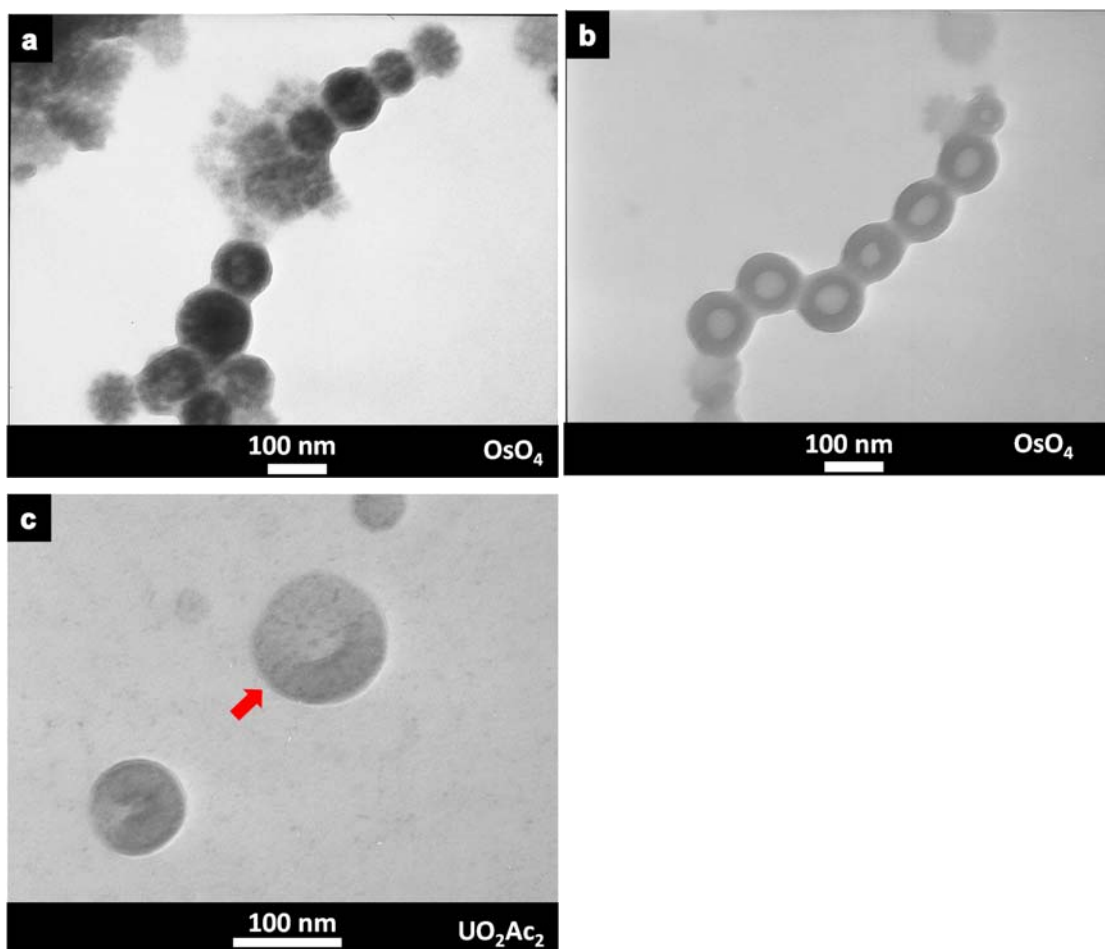

Figure C.2 TEM images of μ-(PtBA$_{100}$)(PGMA$_{66}$)(PCEMA$_{120}$) micelles: (a) an uncrosslinked sample, (b) a heavily crosslinked sample, and c) a heavily crosslinked sample that had also underwent PtBA hydrolysis. The samples shown in (a) and (b) were stained by OsO4, while that shown in (c) was stained by UO$_2$Ac$_2$.

AFM images were recorded before and after the vesicles were photocrosslinked. Figure C3a shows an AFM image of an uncrosslinked sample. It is apparent that some of

the vesicles shown in this image had collapsed, which provided further evidence that these structures were indeed hollow. In addition, the large collapsed vesicle on the lower left corner of this image, exhibited phase separation between the dispersed PtBA cylindrical phase and the continuous PCEMA matrix. The vesicles shown in Figure C3b had underwent crosslinking treatment and were relatively rigid. Despite this rigidity, a few of these vesicles had collapsed, while most of them retained their globular shape. Some phase separation was visible on the surface, but was not as clearly visible as had been observed among samples described in Chapter 3 (Figure 3.8). We believe this relative lack of clarity may be attributed to the PGMA chains covering the surface, which may have affected the ability of the AFM tip to detect this phase separation.
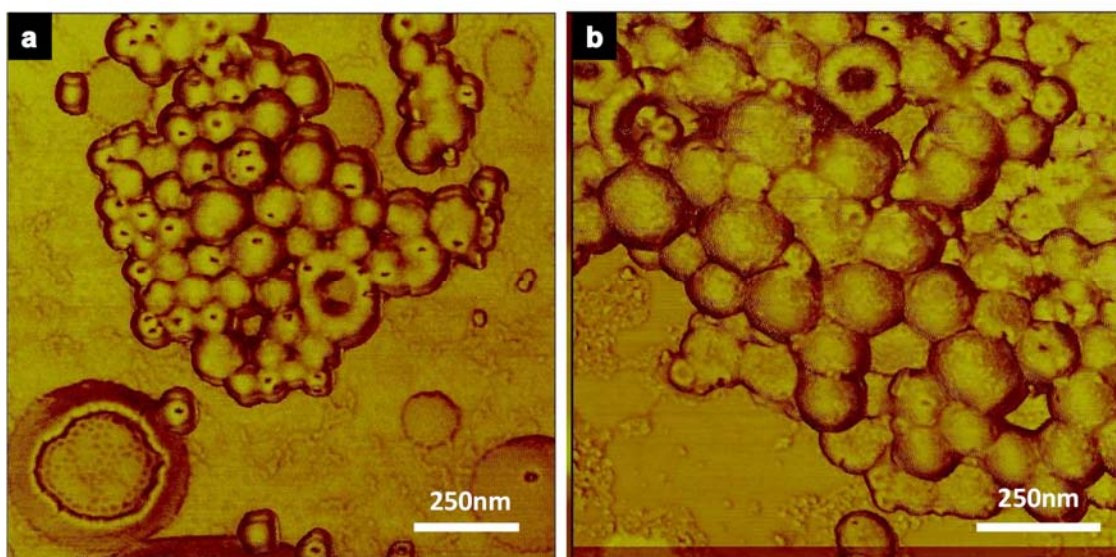

Figure C.3 AFM phase images of μ-(PtBA$_{100}$)(PGMA$_{66}$)(PCEMA$_{120}$) vesicles before (a) and after (b) photo crosslinking treatment.

Both the TEM and AFM results provided evidence supporting the proposal that μ-(PtBA$_{100}$)(PGMA$_{66}$)(PCEMA$_{120}$) self-assembled into the vesicular structure illustrated in Figure C1. We claimed in Chapter 3 that this type of capsule bearing walls that are

perforated by regularly-packed pH-responsive nanochannels represents an unprecedented class of structures prepared from block copolymers. In addition, these vesicles should provide promising candidates for controlled release applications. In this Appendix Section, we have described a second approach for the preparation of these unique structures.

C3 References

1.   Bates, F. S.; Fredrickson, G. H. Block copolymers - Designer soft materials. *Phys. Today* **1999**, *52*, 32-38.